Università degli Studi di Ferrara

DOTTORATO DI RICERCA IN
SCIENZE CHIMICHE

CICLO XXX

COORDINATORE Prof. Carlo Alberto Bignozzi

Mass transfer characteristics and thermodynamic properties of new generation porous particles for ultrafast, high-efficient separations in chiral and achiral liquid chromatography

Settore Scientifico Disciplinare CHIM/01

Dottorando
Dott.ssa Martina Catani

Tutore
Prof. Alberto Cavazzini

Anni 2014/2017

Abstract

During the last years, there has been a continuous evolution in high performance liquid chromatography (HPLC) aimed at developing high efficient, selective and fast separation methods. One of the main factors affecting the efficiency of a separation is the type of adsorbent used to pack the column since both physico-chemical and geometrical characteristics of packing particles play a key role on column performance. The investigation of kinetic and thermodynamic properties of porous materials used as stationary phases in LC is of fundamental importance for future developments in column design and new applications.
It is well known that the efficiency of separation is strongly influenced by kinetic factors while thermodynamics (adsorption equilibria) affects retention and selectivity. Anyhow, these aspects are very often strictly interconnected to each other.
Adsorption equilibria can be investigated through several chromatographic techniques (e.g. frontal analysis, perturbation method). However, new approaches ("Inverse Method") allow to estimate the adsorption isotherm of any analyte on a stationary phase by means of only few experimental overloading measurements.
Kinetic factors have been estimated for a long time through the nonlinear fitting of the experimental van Deemter curve. Recently, this approach has been demonstrated to lead to parameters whose physical meaning is debatable. Accordingly, it has been substituted by a more advanced approach which allows to independently estimate each mass transfer contribution. Experimentally, the effective diffusion coefficient of the analyte in the porous medium is calculated by means of stop-flow techniques (peak parking), where analyte molecules are left free to diffuse in the middle of the column when the flow is switched off. The results of peak parking experiments must be then interpreted in the light of a proper model of diffusion in porous media.
Mass transfer processes in liquid chromatography can be predicted through CFD simulations. These studies accurately mimic the band broadening in specific sections of packed beds. Combined to sophisticated reconstruction of stationary phase structures and the calculation of transport properties in the reconstructed materials, these approaches have permitted to revise some concepts traditionally accepted in the field of diffusion through porous media (such as, for instance, the independence of mass fluxes outside and inside porous particles).
In this thesis, kinetic performance and thermodynamic properties of different types of stationary phases have been explored. Mass transfer kinetics has been firstly investigated in recently introduced sub-2μm monodisperse C_{18} FPPs for reversed-phase separations characterized by a narrow particle size distribution (nPSD). Then, kinetic performance of new chiral stationary phases (CSPs) for ultrafast separations have been studied by comparing columns in-house packed with both SPPs and sub-2μm FPPs functionalized with the same chiral selector. The results reported in this thesis concern two different studies carried out with two different types of chiral selectors (Whelk-O1 and teicoplanin). Sub-second enantioseparations have been obtained with very short columns packed with these CSPs operated at high flow rates, being an extraordinary result in the field of enantioseparations, unimaginable only few years ago.
On the other hand, the adsorption properties of benzene derivatives on a perfluorinated ad-

sorbent have been studied by means of nonlinear chromatography measurements in order to investigate the well-known capacity of perfluorinated stationary phases to selectively recognize perfluorinated molecules ("fluorophilicity"), which is usually referred to be active when the molecule contains at least six sp^3 perfluorinated carbon atoms. The results of this study, however, showed that even a single CF_3 group induce a drastic change in the adsorption properties of molecules.

List of papers

This thesis is based on the following papers. Reprints are appended at the end of the thesis.

I **Experimental evidence of the kinetic performance achievable with columns packed with new 1.9 μm fully porous particles of narrow particle size distribution**, O. H. Ismail, M. Catani, L. Pasti, A. Cavazzini, A. Ciogli, C. Villani, D. Kotoni, F. Gasparrini, D. S. Bell, *J. Chromatogr. A*, 1454, **2016**, 86-92. Reprinted with permission from Elsevier.

II **Rationale behind the optimum efficiency of columns packed with new 1.9 μm fully porous particles of narrow particle size distribution**, M. Catani, O. H. Ismail, A. Cavazzini, A. Ciogli, C. Villani, L. Pasti, C. Bergantin, D. Cabooter, G. Desmet, F. Gasparrini, D. S. Bell, *J. Chromatogr. A*, 1454, **2016**, 78-85. Reprinted with permission from Elsevier.

III **A theoretical study on the advantage of core-shell particles with radially-oriented mesopores**, S. Deridder, M. Catani, A. Cavazzini, G. Desmet, *J. Chromatogr. A*, 1456, **2016**, 137-144. Reprinted with permission from Elsevier.

IV **New frontiers and cutting edge applications in ultra high performance liquid chromatography through latest generation superficially porous particles**, M. Catani, S. Felletti, O. H. Ismail, F. Gasparrini, L. Pasti, N. Marchetti, V. Costa, A. Cavazzini, **2017**, *Anal. Bioanal. Chem.*, DOI 10.1007/s00216-017-0842-4. Reprinted with permission from Springer.

V **Pirkle-type chiral stationary phase on coreshell and fully porous particles: Are superficially porous particles always the better choice toward ultrafast high-performance enantioseparations?**, O. H. Ismail, L. Pasti, A. Ciogli, C. Villani, J. Kocergin, S. Anderson, F. Gasparrini, A. Cavazzini, M. Catani, *J. Chromatogr. A*, 1466, **2016**, 96-104. Reprinted with permission from Elsevier.

VI **Pirkle-type chiral stationary phases for ultra-high performance ultra-fast enantioseparations**, M. Catani, O. H. Ismail, S. Felletti, F. Gasparrini, L. Pasti, V. Costa, A. Cavazzini, *American Pharmaceutical Review*, 20, 4, May-June **2017**

VII **Recent advancements and future directions of superficially porous chiral stationary phases for ultrafast high-performance enantioseparations**, M. Catani, O. H. Ismail, F. Gasparrini, M. Antonelli, L. Pasti, N. Marchetti, S. Felletti, A. Cavazzini, *Analyst*, 142, **2017**, 555-566. Reprinted with permission from the Royal Society of Chemistry.

VIII **Future perspectives in high efficient and ultrafast chiral liquid chromatography through zwitterionic teicoplanin-based 2-μm superficially porous particles**, O. H. Ismail, M. Antonelli, A. Ciogli, C. Villani, A. Cavazzini, M. Catani, S. Felletti, D. S. Bell, F. Gasparrini, *J. Chromatogr. A*, 1520, **2017**, 91-102. Reprinted with permission from Elsevier.

IX **Exploring fluorous affinity by liquid chromatography**, M. Catani, R. Guzzinati, N. Marchetti, L. Pasti, A. Cavazzini, *Anal. Chem.*, 87, **2015**, 6854-6860. Reprinted with permissionn from American Chemical Society.

X **New insights into perfluorinated adsorbents for analytical and bioanalytical applications**, N. Marchetti, R. Guzzinati, M. Catani, A. Massi, L. Pasti, A. Cavazzini, *Anal. Bioanal. Chem*, 407, **2015**, 17-21. Reprinted with permission from Springer.

My contributions to the papers included in this work are described below:

I: I did experiments and wrote the manuscript together with my coauthors; **II**: I did experiments, calculations and wrote the manuscript together with my coauthors; **III**: I did CFD simulations; **IV**: I wrote the manuscript; **V**: I did experiments and wrote the manuscript together with my coauthors; **VI**: I wrote the manuscript; **VII**: I wrote the manuscript; **VIII**: I wrote the manuscript together with my coauthors; **IX**: I did experiments, calculations and wrote part of the manuscript, **X**: I wrote the manuscript together with my coauthors.

Papers not included in this thesis

Expeditious synthesis and biological characterization of enantio-enriched (-)-Nutlin-3, A. Fantinati, S. Bianco, V. Cristofori, A. Cavazzini, M. Catani, V. Zanirato, S. Pacifico, E. Rimondi, D. Milani, R. Voltan, P. Secchiero, C. Trapella, *ChemistrySelect*, 2, **2017**, 8504-8508

Multi-biomarker investigation to assess toxicity induced by two antidepressants on Dreissena polymorpha, S. Magni, M. Parolini, C. Della Torre, L. Fernandes de Oliveira, M. Catani, R. Guzzinati, A. Cavazzini, A. Binelli, *Sci. Total Environ.*, 578, **2017**, 452-459.

Microscopic models of liquid chromatography: From ensemble-averaged information to resolution of fundamental viewpoint at single-molecule level, L. Pasti, N. Marchetti, R. Guzzinati, M. Catani, V. Bosi, F. Dondi, A. Sepsey, A. Felinger, A. Cavazzini, *TrAC*, 81, **2016**, 63-68

(S)-Selectivity in phenylacetyl carbinol synthesis using the wild-type enzyme acetoin:dichlorophenolindophenol oxidoreductase from Bacillus licheniformis, P. P. Giovannini, L. A. Lerin, M. Müller, G. Bernacchia, M. De Bastiani, M. Catani, G. Di Carmine, A. Massi, *Adv. Synth. Catal.* 358, **2016**, 2767-2776

Continuous ion-exchange resin catalysed esterification of eugenol for the optimized production of eugenyl acetate using a packed bed microreactor, L. A. Lerin, M. Catani, D. Oliveira, A. Massi, O. Bortolini, A. Cavazzini, P. P. Giovannini, *RSC Adv.*, 5, **2015**, 76898-76903

Contents

1 Introduction

Liquid Chromatography (LC) allows for the separation of a broad range of compounds including chemicals, pharmaceuticals, biological samples and proteins, to name but a few. It makes use of a liquid mobile phase pumped through a column packed with an adsorbing porous material (stationary phase).
The injected analytes, percolating throughout the column with the stream of mobile phase, distribute to varying extents between the two phases, due to the different physico-chemical interactions occurring with either the mobile or the stationary phase. Therefore, different analytes travel at different velocities, reaching the end of the column at different times.
The development of this technique is attributed to the Russian botanist Mikhail Tswett in 1903, who reported about the separation of different plant pigments into a series of colored bands on a packed column [1, 2]. However, it was in the late 1960s when LC had its real breakthrough, with the introduction of porous particles with reduced diameter and pumps to help pushing the liquid through the packed bed. This technique, named High Performance (or Pressure) Liquid Chromatography (HPLC), has experienced a rapid development during the last 40 years, becoming the most widespread and versatile separation method in use. However, HPLC is still an active research area. Indeed, there is an increasing demand from chemical and pharmaceutical industries for the development of ever faster and more efficient methods for quick, high-troughput analysis. Nowadays, routine chromatographic separations take place in a few minutes, but the trend is to move to the second scale. To this end, column manufacturers have put much effort, during the last decade, to develop stationary phases for high efficient and ultrafast separations. At the same time, new instruments, able to reach up to 1200-1500 bars and very high flow rates, were introduced into the market. This technique, which makes use of very high pressures and high efficient columns, is called Ultra-High Performance Liquid Chromatography (UHPLC).
However, a deep understanding of the factors that affect column performance is fundamental for the future proper improvements in column design. These factors can be essentially collected into two groups: thermodynamic and kinetic factors.
Thermodynamic factors are related to the distribution of the sample molecules between the stationary and the mobile phases, comprehending adsorption equilibria and any other partition mechanism. They intrinsecally regulate the aspects of retention and selectivity. On the other hand, kinetic factors provide an account of the magnitude of mass transfer processes occurring during sample migration. They include diffusion processes, mobile phase dispersion effects, mass transfer resistances. Beside these phenomena, also the type of adsorbent, column hardware and extra-column contributions could affect a chromatographic separation from a kinetic point of view.
In other words, thermodynamics affects retention times while kinetics is responsible for any source of band broadening and loss of efficiency. By considering an "ideal" case with an uniform flow profile and negligible mass transfer kinetics, the eluted bands should have the same

width and height as those injected. In "real" systems, however, kinetic factors are not trivial and they can compromise the efficiency of the separation.
My PhD program has been focused on the study of these factors on stationary phases of current great interest. On the one hand, mass transfer processes and kinetics of columns packed with new generation porous particles for ultrafast achiral and chiral separations has been investigated under different chromatographic conditions. On the other hand, thermodynamic properties of perfluorinated adsorbents have been evaluated through the calculation of adsorption isotherms for a series of benzene derivatives, in order to investigate their well-known capacity of selectively recognize perfluorinated molecules ("fluorophilicity").

1.1 Stationary phases for ultrafast separations

1.1.1 Achiral separations

It is well known that the size of packing particles and packing quality dramatically affect column performance. Indeed, the efficiency of a column (evaluated in terms of height equivalent to a theoretical plate, H) is inversely proportional to the particle diameter, d_p. As a matter of fact, for a long time, the main approach followed by column manufacturer has been to progressively decrease the diameter of particles. Nowadays, fully porous silica particles (FPPs) with sub-2μm dimensions are commonly employed. However, the downside of this approach is that, since pressure drop increases by a square function of the inverse particle size [3], very high pressures (up to 1200-1500 bars or more) are required to push the mobile phase into these columns.
In 2006, Kirkland introduced the so-called second generation superficially porous particles (SPPs) [4, 5], also referred to as core-shell, solid-core, Fused-Core^{TM} or pellicular particles.
These particles, made of a nonporous core surrounded by a porous shell, renewed the concept of pellicular particles developed by Horváth and Lipsky in 1960 [6]. Playing on particle morphology, the contributions to band broadening could be significantly reduced by the presence of the solid core, which decrease the pore volume accessible to the analyte molecules [7–11]. Longitudinal diffusion decreases up to 30% and solid-liquid mass transfer is reduced especially for large molecules. Moreover, columns packed with C_{18} SPPs have been demonstrated to be extremely efficient also thanks to a very low eddy diffusion. Even if the explanation of this remains to a large extent unknown, the most accepted hypothesis is that roughness of core-shell particles limits particle slipping after releasing the high pressure employed for the preparation of the packed bed by slurry packing, therefore reducing radial bed heterogeneity [8, 12]. To further increase the kinetic performance of core-shell particles, their diameter was decreased down to 1.1 μm and their porous layer was diminished [13–15]. Despite their intrinsically high potential, columns packed with these particles suffered from the limitations of current instrumentation in terms of upper pressure limit and extra-column band broadening. Indeed, even at 1200 bar, the minimum plate height value was not reached, due to the low permeability of these column, and the extra-column band broadening could have a great impact on the apparent kinetic performance of short narrow bore columns packed with these particles.
More recently, prototype new core-shell particles with a narrower particle size distribution (PSD) and highly ordered radially oriented mesopores were designed and tested for chromatographic separations. These particles showed enhanced
mass transfer characteristics, pushing further the performance limit of SPPs [16].

1.1.2 Chiral separations

The transition from traditional enantioseparations (usually performed on 3-5 μm FPPs) to ultrafast ones has been slowed down by the lack of complete understanding of the complex mass transfer phenomena in chiral chromatography and by the practical difficulties in functionalizing small particles with chiral selectors. Aggregation phenomena have been often observed and, most importantly, the adaption of traditional techniques of surface modification could be difficult when operating with small particles.
However, pressing requirements especially by pharmaceutical and medicinal industries e.g., for the screening of large libraries of chiral molecules or, in general, for high-throughput analysis have pushed towards the development of increasingly faster and efficient chiral separations methods, which could not be achieved on chiral stationary phases (CSPs) developed on typical 3-5 μm FPPs.
In the last decade the field of chiral separations has been affected by a radical transformation. The attention of scientists and manufacturers has indeed moved from the research of novel CSPs with enhanced enantioselectivity to the preparation of new versions of already known CSPs prepared on kinetically highly efficient silica particles. In 2010, Gasparrini and his group were the first to introduce sub-2μm FPPs functionalized with teicoplanin chiral selector, obtaining very promising results in terms of efficiency and reduced analysis times [17]. In 2011, Lindner and coworkers published the first work in which chiral 2.7 μm SPPs have been employed for the separation of amide type amino acid derivatives [18]. One year later, Chankvetadze et al. compared the kinetic performance of CSPs prepared on polysaccharide-coated FPPs and SPPs, mentioning some of the benefits achievable with chiral SPPs such as enhanced enantioselectivity and a limited dependence on mobile phase flow rate [19]. However, the most sistematic works aimed at evaluating the potential of chiral SPPs over their fully porous counterparts are those published by Armstrong's group since 2014. The study was carried out on columns packed with particles functionalized with different chiral selectors (including macrociclic antibiotics and cyclofructans) and operated in different modes of chromatography (reversed-phase, HILIC, normal
phase). The conclusion driven by these authors is that chiral 2.7 μm SPPs outperformed FPP ones in any operating mode. Moreover, by using 5 cm long columns packed with chiral SPPs operated at very high flow rates, these authors were able to obtain sub-second separations of different pairs of enantiomers [20–26]. A schematic evolution of particle design and separations times is schematically reported in Fig. 1.1.
All of the above-cited works are mainly focused on the comparison of kinetic performance (in terms of efficiency and speed of separation) of both chiral FPPs and SPPs but none of these is devoted to the study of mass transfer processes in these different particle formats.
However, a deep understanding of mass transfer phenomena in chiral chromatography is fundamental for further developments in this field. It is well known that adsorption-desorption kinetics plays a key role in chiral separations [27]. Therefore, the adsorption-desorption process of enantiomers onto the stationary phase must be investigated not only to evaluate its impact on column efficiency but also to determine if there could be a speed limit for ultrafast chiral separations.

1.2 Perfluorinated stationary phases

Perfluorinated (*F*-) adsorbents are generally prepared by bonding perfluoro-functionalized silanes to silica gels. They have the general structure silica-O-Si$(CH_3)_2(CH_2)_n R_f$, where n is either 2 or 3 and R_f is C_6F_{13} or C_8 F_{17} [28].

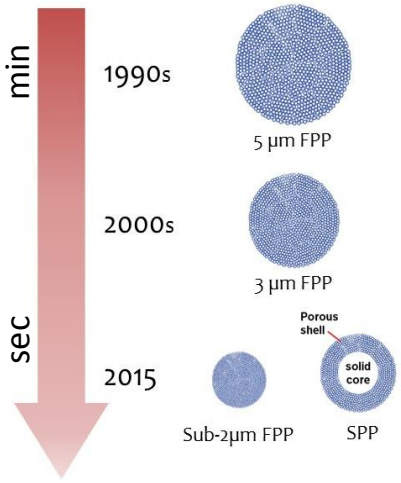

Figure 1.1: Evolution of particles used as stationary phase for chiral columns.

F-silica gels have been introduced in the early 1980s and thanks to their extreme hydrophobicity and low polarity, they were claimed to be ideal candidates as adsorbents for reversed phase separations of large biomolecules under nondenaturating conditions (i.e., with minimum amount of organic modifier in the mobile phase) [29,30]. Actually, this field has not been explored in depth and *F*-silica gels have rather been applied as adsorbents for the separation of fluorous molecules from non-fluorous ones and from each other [31, 32]. The ability of *F*-molecules to recognize other molecules with an *F*-portion is referred to as fluorous affinity or fluorophilicity. It arises from selective, strong noncovalent interactions between the perfluoroalkyl segments of molecules, in a sort of "like dissolves like" interaction. The importance of fluorous-functionalized stationary phases has been increasingly more recognized by the analytical chemistry community for the development of new methods, based on the concept of fluorophilicity, to analyze classes of compounds from very complex matrixes. This is the case, for instance, of the determination of low-abundance proteins in complex biological mixtures, which represents one of the most relevant issues in bioanalytical applications. Another very important application of *F*-adsorbents is the selective determination of perfluorinated compound (PFC) in the environment [33]. PFCs can be found in many products, including Teflon®, GORE-TEX®, water-proof clothing, paint, windshield washer fluid, fast food wrappers, pizza boxes, etc. In addition to the well-known cases of perfluorooctanoic acid (PFOA) and perfluorooctanesulfonic acid (PFOS), recent studies have identified many other potentially dangerous perfluorinated compounds, such as perfluoroalkyl phosphinic and phosphonic acids and fluorotelomers. The carbon-fluorine bond of these chemicals is incredibly strong, therefore they can persist in the environment and bioaccumulate in food chains, representing a risk to human health and ecosystem.

2 Theory

In this chapter, a brief review of theoretical principles of chromatography will be presented. The most relevant models used to describe chromatographic separations will be discussed. Then, the basis of adsorption equilibria and mass transfer kinetics in LC will be summarized.

2.1 Models of chromatography

Chromatographic separations could be modeled through either equilibrium or kinetic theories. The first ones could be employed when an instantaneous equilibrium is achieved between the mobile and the stationary phases. This happens when mass transfer and adsorption processes are considerably fast, so that their contribution could be neglected. However, this is not usually possible in a real chromatographic system, where non-equilibrium effects take place due to slow mass transfer or adsorption processes. For this reason, kinetic theories better describe a chromatographic process, taking into account each contributions to band broadening. [34]
There is one parameters that is conserved throughout any chromatographic process, which is the mass of each injected component. Since it is assumed that components do not react between them inside the column, a mass balance equation can be written for each component and a set of initial boundary conditions could be determined in order to account for a wide variety of experimental situations. These types of models can describe both linear and non-linear chromatographic conditions. In *linear chromatography*, the concentration of the adsorbed solute is directly proportional to the concentration of the solute in the mobile phase, which means that the adsorption isotherm is linear. This is the case of analytical conditions, where the sample is dilute and small amount of solute is injected. Retention times are independent from sample concentration and the peak height is proportional to the amount of each injected component. In *nonlinear chromatography*, on the other hand, adsorption isotherms are not linear. This means that, at the equilibrium, the concentration of the adsorbed solute is no longer directly proportional to the concentration of the solute in the mobile phase and sample concentration influences retention times. This is the case of preparative chromatography where large amount of sample are injected into the column.

2.1.1 Equilibrium-dispersive model

In this model, instantaneous equilibrium between the stationary and the mobile phases is assumed. The mass balance equation includes an apparent lumped dispersion term (D_a) accounting for both the axial dispersion and the finite rate of mass transfer kinetics:

$$\frac{\delta C}{\delta t} + F\frac{\delta q}{\delta t} + u\frac{\delta C}{\delta z} = D_a\frac{\delta^2 C}{\delta z^2} \tag{2.1}$$

where C and q are the concentrations of the analyte in the mobile and stationary phases, respectively, $F = (1-\epsilon_t)/\epsilon_t$ the phase ratio (being $\epsilon_t = V_0/V_{col}$ the total porosity of the bed),

t and z represent the temporal and spatial coordinates, respectively, and u the mobile phase linear velocity.
The apparent dispersion coefficient can be calculated from the number of theoretical plates (N) determined by an analytical injection:

$$D_a = \frac{uL}{2N} \tag{2.2}$$

being L the length of the column.
Due to its simplicity, this model of chromatography can be easily used for the prediction of band broadening in preparative chromatography, even if it completely ignores the causes for the non-equilibrium effects taking place in the chromatographic columns, providing physically meaningless D_a values.

2.1.2 General rate model

The most physically detailed and exhaustive kinetic model is the general rate one [35]. It considers separately the fraction of mobile phase percolating through the column, in the interstitial volume and that stagnant in the pores. A mass balance equation is written for each fraction and the set of equations is solved simultaneously. Diffusion is considered to take place between the percolating eluent and that stagnant within the pores and adsorption-desorption kinetics between the stagnant mobile phase and the surface of the adsorbent. With this approach, all the contributions to band broadening are taken into account. The mass balance equation for the bulk eluent percolating in the interstitial volume is written as:

$$\frac{\delta C}{\delta t} + u_e \frac{\delta C}{\delta z} + \frac{3}{r_p} \frac{1-\epsilon_e}{\epsilon_e} j_s = D_L \frac{\delta^2 C}{\delta z^2} \tag{2.3}$$

where ϵ_e is the external porosity of the column, $u_e = F_v / \pi r_c^2 \epsilon_e$ the interstitial linear velocity (being F_v the flow rate, and r_c the column radius), r_p the particle radius and j_s is the mass flux of the analyte from the mobile phase to the surface of the stationary phase, defined as:

$$j_s = k_f [C - C_p(r = r_p)] = D_p \left(\frac{\delta C_p}{\delta r} \right)_{r=r_p} \tag{2.4}$$

where C_p is the concentration of the analyte within the pores, k_f is the external mass-transfer coefficient, r is the radial distance in the spherical particle, and D_p is the pore diffusivity coefficient.
Additionally, the mass flux from the stagnant mobile phase to the adsorbent surface, j_p, is defined as:

$$j_p = (1-\epsilon_p) \frac{\delta q}{\delta t} = (1-\epsilon_p) k_a \left(C_p - \frac{q}{K_a} \right) \tag{2.5}$$

being ϵ_p the porous zone porosity, k_a the adsorption rate constant and K_a the equilibrium Henry's constant for the adsorption.
This set of partial differential equations can be solved in the Laplace domain. When a linear adsorption isotherm ($q = K_a c$) is considered, the following plate height equation can be derived from the first and second central moments of the resulting peak shape:

$$H = \frac{2D_L}{u_e} + 2\frac{1-\epsilon_e}{\epsilon_e}\left(\frac{k_1}{1+k_1}\right)^2\left[\left(\frac{r_p}{6k_f} + \frac{1}{1-\epsilon_p}\left(\frac{k_p}{1+k_p}\right)^2\frac{1}{k_a} + \right.\right.$$
$$\left.\left. + \frac{r_p^2}{30D_p}\frac{(1+2\rho+3\rho^2-\rho^3-5\rho^4)}{(1+\rho+\rho^2)^2)}\right)u_e \right. \tag{2.6}$$

where ρ is the core-to-particle diameter ratio (r_{core}/r_p), a parameter that takes into account the possible presence of a solid core. It is 0 for fully porous particles, 1 for non-porous ones and it absumes values between 0.6 and 0.8 for SPPs.
k_1 is the zone retention factor defined as:

$$k_1 = \frac{1-\epsilon_e}{\epsilon_e}[\epsilon_p + (1-\epsilon_p)K_a](1-\rho^3) = \frac{t_R - t_e}{t_e} \tag{2.7}$$

being t_R the retention time and t_e the time spent by the analyte in the external volume.
k_p is the particle retention factor:

$$k_p = \frac{1-\epsilon_p}{\epsilon_p}K_a \tag{2.8}$$

In conclusion, the general rate model accounts for any source of band broadening into a chromatographic column: (1) the axial dispersion in the interstitial volume (through the parameter D_L), which comprehend both longitudinal diffusion and eddy dispersion; (2) the mass transfer resistance in the film of eluent on the external surface of the stationary phase (through the kinetic constant k_f); (3) the slow adsorption-desorption kinetics onto the stationary phase (through the kinetic constant k_a) and (4) the sample diffusivity in the porous zone (through D_p).

2.1.3 Stochastic model

The stochastic model is a microscopic kinetic theory of chromatography, originally proposed by Giddings and Eyring in 1955 [36]. They demonstrated that the random migration of a solute along the column could be modeled at a molecular level as a Poisson process and the chromatogram is the result of the probability density functions of the individual retention times of the molecules travelling throughout the column. In this derivation, the effect of axial dispersion was neglected and only one type of sites was considered for the random adsorption-desorption process. Later on, this approach was extended also to the case of two-sites adsorption [37, 38]. McQuarrie used the complex variable theory of Laplace transforms to derive the expression for the peak profile with various input distribution functions [39].
However, it was demonstrated that the best approach to the stochastic model is by means of the characteristic function (CF) method [7, 40]. The CF of a continuous random variable t (for instance, the time spent by a single molecule into the column) is defined as the inverse Fourier transform of its probability density function, $f(t)$ [39]:

$$\Phi(\omega) = \int exp(i\omega t)f(t)dt \tag{2.9}$$

where i is the imaginary unit and ω an auxiliary real variable (frequency). $f(t)dt$ represents the probability that the molecule leaves the column with a retention time between t and $t+dt$. Closed form expressions of the band profiles are obtained in the Fourier domain, from which the statistical moments of the chromatographic peaks can be directly calculated. [40, 41]

The use of the CF method facilitated the extension of the stochastic model to two-site [42] or to generic multiple-site heterogeneous surfaces [43], which are very complex cases to manage otherwise.
For a homogeneous (single-site) surface, if n is the average number of adsorption-desorption steps executed by the molecule along the column and τ_s its residence time onto the stationary phase in a single adsorption-desorption step, the CF is written as [40]:

$$\Phi(\omega) = exp\left\{ n\left[\frac{1}{1 - i\omega\tau_s} - 1 \right] \right\} \tag{2.10}$$

By taking into account only the processes at the stationary phase (therefore ignoring the contribution of the mobile phase), the corrected retention time could be calculated as $t'_R = n\tau_s$. For a multiple-site surface with m different sites the following CF is obtained [43]:

$$\Phi(\omega) = exp\left\{ n\left[-1 + \sum_{j=1}^{m} p_j \frac{1}{1 - i\omega\tau_{s,j}} \right] \right\} \tag{2.11}$$

where p_j is the abundance of site j, and τ_j the residence time on site j. In this case, the corrected retention time is $t'_R = n\sum_{j=1}^{m} p_j\tau_j$. This equation can be rewritten as follows:

$$\Phi(\omega) = \prod_{j=1}^{n} exp\left(\frac{n_j}{1 - i\omega\tau_j} - n_j \right) \tag{2.12}$$

where $n_j = np_j$, demonstrating that the whole band profile could be easily calculated as the convolution of the CFs corresponding to different adsorption sites.
The stochastic theory of chromatography has been extended to include also the effects of axial and mobile phase convection [44] and to different types of chromatography [45] including, for instance, Size Exclusion Chromatography [46–51], ion-exchange chromatography [52] and nonlinear chromatography [53, 54].

2.2 Adsorption equilibria

In order to solve mass balance equations reported in Eq. 2.1, 2.3, a proper adsorption isotherm must be defined. These functions describe the relationship between the concentration of each compound in the stationary and mobile phases, at equilibrium and at constant temperature and pressure. Adsorption isotherms depend on all the possible interactions between the solutes and the two phases and they provide important thermodynamic information to describe chromatographic separations in nonlinear conditions. Their comprehension is fundamental to model preparative or nonlinear processes.
A large number of adsorption model has been proposed in order to efficiently describe different conditions, on the basis of the extent of interactions occurring between adsorbate molecules and on the heterogeneity of the surface. Even if column manufacturers nowadays produce stationary phases as homogeneous as possible, it has been demonstrated that different adsorption isotherm could be used to fit experimental peak profiles, depending on the type of adsorbate. In this section, some of the most useful adsorption isotherm models will be described.

2.2.1 Linear isotherm

This type of isotherm is commonly employed in analytical applications, where small amounts of solute are injected into the column. The concentrations of the analyte in the stationary and mobile phase are considered to be directly proportional:

$$q = K_a C \tag{2.13}$$

The slope of the isotherm, K_a, is related to the retention factor (k') through the following relationship:

$$K_a = \frac{k'}{F} = \frac{k' \epsilon_t}{1 - \epsilon_t} \tag{2.14}$$

being F the phase ratio.
The assumption made in linear applications is that there is no competition between analyte molecules for the adsorption on the stationary phase. This model, however, is not suitable for the description of preparative applications, where the injected components could compete with each others or with the mobile phase for the adsorption.

2.2.2 Langmuir isotherm

This type of isotherm assumes that there is only one type of site where the molecules can be adsorbed, therefore the stationary phase is defined to be homogeneous. The equation correlating q and C is written as:

$$q = \frac{q_s b C}{1 + bC} \tag{2.15}$$

being q_s the saturation capacity (i.e., the maximum concentration of analyte that can be adsorbed on the stationary phase at a fixed temperature) and b the adsorption constant. This adsorption isotherm is convex upward and, by extension, all the isotherms that shows upward convexity are defined "Langmuirian". On the contrary, all the isotherms that are convex downward are usually addressed to as "anti-Langmuirian".
This is also reflected in different peak shapes. Indeed, Langmuirian isotherms lead to overloaded peaks with a shock in the front part and a diffuse boundary on the rear, while anti-Langmuirian peaks have a diffuse boundary in their front and a shock in the rear.
It should be easily demonstrated that, when C tends towards 0, the Langmuir isotherm is reduced to a linear isotherm $q = q_s b C$, where the product $q_s b$ corresponds to the equilibrium Henry's constant, K_a.
Even if the assumptions of this model make it too simple and too far from reality, the Langmuir isotherm is an excellent approximation for single-component adsorption processes in chromatography.

2.2.3 Bilangmuir isotherm

This model is derived from the Langmuir one, but it assumes two different types of independent adsorption sites on the stationary phase. It is the simplest model for a nonhomogeneous surface, covered with two different kinds of chemical groups. A given solute may interact in a very similar way with the two sites while exhibiting different interaction energies or, on the contrary, it may give completely different types of interactions. The equation of the Bilangmuir isotherm is the following:

$$q = \frac{q_{s,1} b_1 C}{1 + b_1 C} + \frac{q_{s,2} b_2 C}{1 + b_2 C} \tag{2.16}$$

where $q_{s,1}$ and $q_{s,2}$ are the saturation capacities of site 1 and 2, while b_1 and b_2 are the adsorption constants of the two sites. Even if the Bilangmuir isotherm is an ideal model (in the sense that real surfaces do not possess the characteristics at the heart of this model) it can be

successfully applied to fit the adsorption behavior of enantiomers on chiral stationary phases. Indeed, due to the physico-chemical characteristics of enantiomers, it is assumed that one type of site (enantioselective one) is much stronger than the other, that accounts for all the possible nonselective interactions.

2.2.4 Tóth isotherm

The Tóth isotherm accounts for a continuous and wide adsorption energy distribution. It contains an heterogeneity parameter, ν:

$$q = \frac{q_s b C}{(1 + (bC)^{\nu})^{1/\nu}} \tag{2.17}$$

when ν tends towards 1, the Tóth isotherm coincides with the Langmuir one.

2.2.5 Extended solid-liquid BET isotherm

This isotherm model account for the existance of multilayer adsorption. The solute molecules, indeed, can adsorb onto the surface of the bare silica or, alternatively, onto a layer of solute already adsorbed. The equation is written as:

$$q = \frac{q_s b C}{(1 - b_l C)(1 - b_l C + b_s C)} \tag{2.18}$$

where b_l and b_s are the equilibrium constants of adsorption of the compound on a layer of adsorbate previously adsorbed and on the bare surface, respectively. If $b_l C < 1$, the system can be described by a simple adsorbed monolayer, that is, by the classical convex upward Langmuir isotherm model. When b_l becomes large (meaning that the strength of the interactions between two adsorbate molecules increases), a reversal in the direction of the isotherm curvature takes place. At high concentrations, when the amount of adsorbed molecules increases further, the effect of the finite surface area of the adsorbent may be felt and the isotherm tends toward saturation (convex upward).

2.3 Mass transfer kinetics in liquid chromatography

In this section, the fundamentals of mass transfer in chiral chromatography are shortly revised. The equation from which this discussion starts from is the well-known van Deemter equation [55], which correlates the height equivalent to a theoretical plate, H (or its adimensional form, $h = H/d_p$, where d_p is the particle diameter) to the mobile phase velocity. Since there is not flow inside the mesoporous silica employed in LC, the right velocity to refer to is the interstitial velocity, u_e, or, in reduced coordinates:

$$\nu = \frac{u_e d_p}{D_m} \tag{2.19}$$

Under the hypothesis that the different mass transfer phenomena are independent of each other, the van Deemter equation, in reduced coordinates, is written as:

$$h = a(\nu) + \frac{b}{\nu} + c_s \nu + c_{ads} \nu + h_{heat} \tag{2.20}$$

where $a(\nu)$ is the eddy dispersion, b represents the longitudinal diffusion term, c_s is the solid-liquid mass transfer resistance and c_{ads} is a term accounting for a possible slow adsorption-desorption kinetics. This term is usually omitted in achiral RP LC, where the adsorption-desorption process is usually fast (unless in the case of separation of very large molecules,

such as proteins). In chiral LC, on the other hand, the adsorption-desorption kinetics can be significantly slow also for low molecular-weight compounds and, particularly, for the second eluted enantiomer [56]. The term h_{heat} in Eq. 2.20 accounts for the frictional heating due to the stream of the mobile phase against the packed bed under significant pressure. This contribution could have a significant impact on the efficiency of separation especially for columns packed with very fine particles [55].
During the last years, the study of mass transfer has definitely moved on. Nowadays an accurate and independent evaluation of the single mass transfer contributions in LC is possible [55, 57–60]. Conversely, the approach based on nonlinear fitting of experimental h data collected at different flow rates has been demonstrated to lead to physically meaningful parameters [55].

2.3.1 Longitudinal diffusion

The longitudinal (or axial) diffusion b-term describes the band broadening due to the relaxation of axial gradient concentration through the porous particles and the interstitial volume, in absence of flow. Since this is the only contribution to band broadening when the flow is switched off, it could be estimated through peak parking experiments. These consist of: (1) injecting the analyte at a constant linear velocity; (2) when it reaches approximately the middle of the column, suddenly stopping the flow; (3) leaving the band free to diffuse inside the porous media during a certain parking time, t_p; (4) resuming the flow rate at the same linear velocity as the starting one to move the band out of the column. The slope of σ_x^2 (the variance in length units of the eluted peak) *vs.* t_p plot gives an estimate of D_{eff}, the effective diffusion coefficient of the analyte into a porous media [55, 61]:

$$D_{eff} = \frac{1}{2}\frac{\Delta\sigma_x^2}{\Delta t_p} \tag{2.21}$$

Through D_{eff}, the longitudinal diffusion term can be calculated. In reduced coordinates, it is:

$$b = 2(1 + k_1)\frac{D_{eff}}{D_m} \tag{2.22}$$

where D_m is the molecular diffusion coefficient of the analyte in the mobile phase mixture.

2.3.1.1 Models of diffusion in porous media

D_{eff} takes into account all the contributions to diffusion of the sample in the composite material. This consists of the porous zone impregnated by the eluent (whose diffusivity is indicated with D_p) and the bulk mobile phase (diffusion coefficient D_m). There are many models describing diffusion processes in porous media, but only those between the most often used in LC will be reported here.

Time-averaged or parallel model This model of diffusion in porous media was elaborated by Knox [62] and often applied to mass transfer kinetics in LC. It is simply based on the assumption that mass fluxes inside and outside the particles are additives:

$$D_{eff} = \frac{\gamma_e D_m + \dfrac{1 - \epsilon_e}{\epsilon_e}(1 - \rho^3)D_p}{1 + k_1} \tag{2.23}$$

being γ_e the so-called obstructive geometrical factor. For a randomly packed column of impermeable spheres with a porosity of about 0.4, γ_e is approximatively 0.65 [63] (otherwise γ_e

can be experimentally estimated through pore blocking [64]). The distribution of the sample between the different phases (external eluent, porous zone and solid cores) is not as simple as that considers in this model. However, the interpretation of D_{eff} through the parallel model leads to acceptable values, not so far from those provided by more elaborated and realistic models, such as the Effective Medium Theory (EMT).

Effective Medium Theory Using the permeability analogue of diffusion and partitioning processes occurring into a chromatographic column, the different EMT models used in many other fields of science and technology have been transformed into expressions that accurately describe the band broadening due to longitudinal diffusion in chromatographic columns. Chemical potential is considered the correct driving force for diffusion in the presence of a preferential solubility and the correct property that obeys the EMT-rules is the permeability [58]. The most simple between the EMT model is the Maxwell-based one, where the expression for D_{eff} is written as:

$$D_{eff} = \frac{1}{\epsilon_e(1+k_1)}\left[\frac{1+2(1-\epsilon_e)\beta}{1-(1-\epsilon_e)\beta}\right]D_m \tag{2.24}$$

where β is:

$$\beta = \frac{\frac{2(1-\rho^3)}{2+\rho^3}\frac{D_p}{D_m}-1}{\frac{2(1-\rho^3)}{2+\rho^3}\frac{D_p}{D_m}+2} \tag{2.25}$$

Even more accurate results are predicted by the Torquato EMT model, where both geometry, spatial distribution of the particles and packing microstructure are taken into account:

$$D_{eff} = \frac{1}{\epsilon_e(1+k_1)}\left[\frac{1+2(1-\epsilon_e)\beta-2\epsilon_e\xi_2\beta^2}{1-(1-\epsilon_e)\beta-2\epsilon_e\xi_2\beta^2}\right]D_m \tag{2.26}$$

with $\xi_2 = 0.3277$ when using SPPs in physical contact [65].

2.3.2 Solid-liquid mass transfer resistance

The c_s term appearing in Eq. 2.20 describes the solid-liquid mass transfer resistance due to the diffusion across the particles. Since there is absence of flow inside particles, this term is velocity-independent. Following Kaczmarski [66], for superficially porous spherical particles this term can be written as:

$$c_s = \frac{1}{30}\frac{\epsilon_e}{1-\epsilon_e}\left[\frac{k_1}{1+k_1}\right]^2\frac{1+2\rho+3\rho^2-\rho^3-5\rho^4}{(1+\rho+\rho^2)^2}\frac{D_m}{D_p} \tag{2.27}$$

being D_p, the pore diffusivity coefficient, estimable from D_{eff}, once a model of diffusion through the porous medium has been defined.

2.3.3 Adsorption-desorption kinetics

The expression of the term associated with a slow adsorption-desorption kinetics obtained by the Laplace transform of the general rate model of chromatography [7, 67], is written in the case of superfially porous particles [56, 66, 68, 69]:

$$c_{ads} = 2\frac{\epsilon_e}{1-\epsilon_e}\frac{1}{1-\epsilon_p}\frac{1}{1-\rho^3}\left(\frac{k_1}{1+k_1}\right)^2\left(\frac{k_p}{1+k_p}\right)^2\frac{D_m}{k_{ads}d_p^2} \tag{2.28}$$

where k_{ads} is the kinetic adsorption constant.

2.3.4 Eddy dispersion

The eddy dispersion term, $a(\nu)$ in Eq. 2.20, is caused by the erratic flow profile in the through-pores of the packed bed. It includes trans-channel eddy dispersion, short-range inter-channel eddy dispersion, trans-column eddy dispersion. Despite the fundamental work of Giddings culminated in the well-known coupling theory [70], there is still considerable debate in literature regarding the values of the geometrical parameters needed to describe the complex structures of packed beds. Much work in this direction has been done by Tallarek and coworkers, who proposed a sophisticated approach based on the morphology reconstruction of the stationary phase structure and the calculation of transport properties in the reconstructed materials [59, 60].
In achiral systems, where the contribution of c_{ads} is negligible, the experimental estimation of $a(\nu)$ can be achieved by ignoring the contribution of h_{heat} and subtracting both the b and c_s terms (estimated by Eqs. 2.22 and 2.27, respectively) to accurately measured h values (Eq. 2.20) [55].

$$a(\nu) = h - \frac{b}{\nu} - c_s\nu \tag{2.29}$$

In chiral systems, on the contrary, this approach cannot be applied since c_{ads} cannot be neglected. By ignoring frictional heating, indeed, the subtraction of b and c_s terms from h values, leads to:

$$a(\nu) + c_{ads}\nu = h - \frac{b}{\nu} - c_s\nu \tag{2.30}$$

showing that an independent evaluation of the $a(\nu)$ and c_{ads} terms is not possible with this approach. Either $a(\nu)$ or c_{ads} must be estimated by different routes.

3 Results and Discussion

This chapter enclose the results of published papers or already submitted for publication at the time of writing this thesis, listed at page iii. To avoid repetition and overlaps, this chapter is organized in different sections containing a summary of the results for each different argument, referring to papers cited in the section header. For further details, the reader is referred to reprints of the full papers appended at the end of the thesis.

3.1 Mass transfer kinetics in new generation porous particles for ultrafast high-efficient separations

3.1.1 Achiral separations (Papers I - III)

3.1.1.1 Sub-2μm C_{18} FPPs with a narrow particle size distribution (Papers I, II)

The kinetic performance and mass transfer kinetics of Titan^{TM} columns packed with 1.9 μm C_{18} FPPs have been investigated under typical reversed-phase (RP) conditions. This type of particles, commercialized about three years ago, is characterized by a narrow particle size distribution (nPSD). The benefit of a nPSD on chromatographic performance is still under debate [55]. The past literature is substantially unanimous on the statement that a very nPSD is not essential for the achievement of efficient columns. However, the introduction of SPPs in 2006, characterized by a very nPSDs (with RSD of roughly 5%), re-opened the debate about its impact on kinetic performance of packed columns. PSD of Titan particles resulted to be very similar to that of SPPs, as it can be evinced from Fig. 3.1

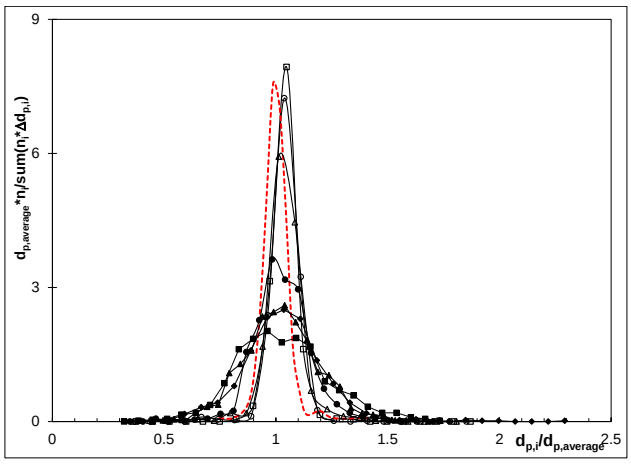

Figure 3.1: Normalized particle size distributions (from SEM images) of the Titan C_{18} material (d_p = 1.9 μm) (red dotted line), compared to that of some common fully porous and superficially porous particles: XBridge C_{18} (d_p = 3.5 μm) (■), ACE3 C_{18} (d_p = 3.0 μm) (●), Gemini NX C_{18} (d_p = 3.0 μm) (♦), Hypersil GOLD C_{18} (d_p = 3.0 μm) (▲), Kinetex Fused Core C_{18} (d_p = 2.6 μm) (□), HALO Fused Core C_{18} (d_p = 2.7 μm) (△) and Poroshell C_{18} (d_p = 2.7 μm) (○). Data adapted from [71]. Reprinted from **II** with permission from Elsevier.

The kinetic performance of Titan columns were evaluated from a kinetic viewpoint on six columns with different length (100, 75 and 50 mm) and internal diameter (3.0 and 2.1 mm). These columns have been characterized from a geometrical viewpoint through Inverse Size Exclusion Chromatography (ISEC) experiments to determine porosities. The estimated values of ϵ_t, ϵ_e and ϵ_p were found to be consistent with each other.
Then, van Deemter curves of a series of benzene derivatives were calculated on the six columns, showing good kinetic performance under RP conditions. At their optimal flow rates, indeed, these columns were able to generate roughly 300,000 theoretical plates per meter (by using probes with a retention factor of 4) and they were characterized by very flat c-branches, meaning that they could be operated at flow rates higher than the optimal one without substantial loss of efficiency.
This latter conclusion contrasts that published before by Gritti and Guiochon [72,73] who observed, by using a series of phenone derivatives under RP conditions on the same columns, a dramatic loss of performance by increasing the flow rate. They explained this finding on the base of the very low intraparticle diffusivity that would characterize Titan C_{18} particles.

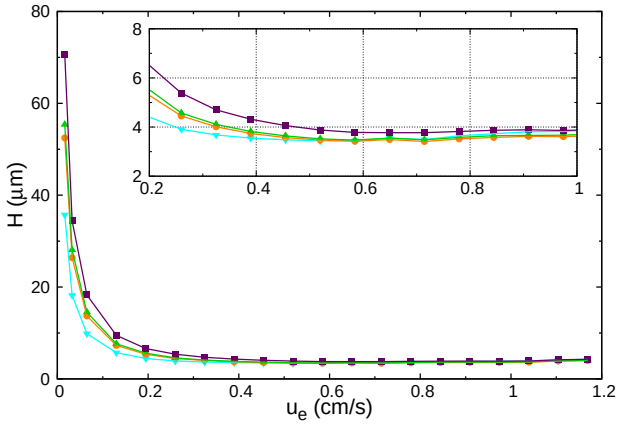

Figure 3.2: Experimental van Deemter plots for the Titan C_{18} 50×2.1 mm. The inset zoom shows the region of interstitial velocity between 0.2 and 1.4. Experimental points: nitrobenzene (cyan), toluene (orange), ethylbenzene (green), butylbenzene (purple). Reprinted from **I** with permission from Elsevier.

In order to give an explanation of this different result, each contribution to band broadening was independently estimated by applying a well-established protocol which consists in few experimental measurements (van Deemter curves and peak parking) and interpretation of D_{eff} with a proper model of diffusion in porous media. The study was carried out on two 100×3.0 mm columns packed with 1.9 μm C_{18} Titan particles with different pore size (80Å and 120Å), by considering four different compounds (nitrobenzene, toluene, ethylbenzene and butylbenzene) covering a wide range of retention factors ranging from 1.2 to 12.3. The results of this investigation has revealed that these columns are characterized by an extremely small eddy dispersion, even comparable to those of columns packed with SPPs, suggesting a very good packing "quality" of Titan columns. Indeed, at reduced velocity of $\simeq$10, its value is only 1.2 on the Titan C_{18} 80Å column and even 1.0 on the Titan C_{18} 120Å one (see Table 3.1). On the other hand, contrary to previous conclusions, the b and c_s terms of the van Deemter equation were found to be essentially comparable to those of other columns packed with particles of similar chemistry and characteristics.

Column	d_p	Length×I.D. (mm)	$a(\nu \sim 10)$	Ref.
Symmetry$^{(*)}$	5.0	150×4.6	1.30	JCA, 1355, 2014, 164 [74]
Luna$^{(*)}$	5.0	150×4.6	1.60	JCA, 1355, 2014, 179 [69]
Titan 80Å$^{(*)}$	1.9	100×3.0	1.20	Paper **II**
Titan 120Å$^{(*)}$	1.9	100×3.0	1.00	Paper **II**
Kinetex 1.7$^{(**)}$	1.7	100×4.6	1.80-1.90	JCA, 1355, 2014, 179 [69]
Kinetex 2.6$^{(**)}$	2.6	100×4.6	0.90-1.00	JCA, 1217, 2010, 1589 [75]

Table 3.1: Comparison between eddy dispersion values at $\nu \simeq 10$ between columns of different dimensions and particle diameters (d_p) packed with fully porous$^{(*)}$ (including Titan C_{18} 80Å and 120Å columns) and core-shell$^{(**)}$ particles. The last column reports literature reference from where the information was taken (JCA: Journal of Chromatography A). Reproduced from Paper **II** with permission from Elsevier.

These results suggest that the impact of a nPSD on the efficiency of HPLC separations is still an open and controversial point requiring the collection of accurate and reproducible experimental data in order to be solved.

3.1.1.2 Morphological new SPPs with highly ordered radially oriented mesopores (Papers III, IV)

SPPs have represented a revolution in the field of chromatographic separations and they have become the preferred choice for many applications in liquid chromatography, when high efficiency and fast separations are required. Recently, Wei et al. [16] have proposed a new prototype SPP that has the potential to make another leap in efficiency and speed of chromatographic separation. Thanks to an innovative approach named pseudomorphic transformation (PMT) micelle templating, Wei and coworkers produced a completely new type of particle characterized by:

- narrower particle size distribution
- thinner porous layer with high surface area
- a pore network made of highly ordered radially oriented mesopores (ROMs)

Fig. 3.3 reports SEM images of ROM-SPPs (squares a and c) and traditional SPPs (squares b and d). Cross-section views (Fig. 3c and 3d) show how the presence of ROM limits diffusion only to the radial direction.

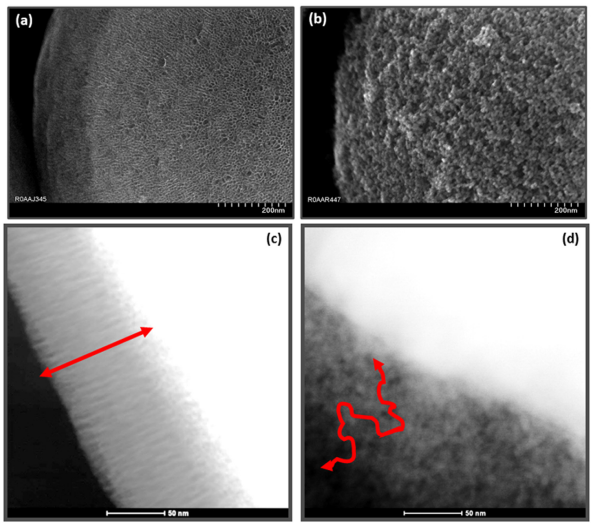

Figure 3.3: High resolution SEM images of a ROM-SPP (squares a and c) and a traditional SPP (squares b and d). Pictures (c) and (d) shows the differences between the diffusion pathways in the two types of particles. Reprinted from [16] with permission from Elsevier.

Prototype columns packed with these new material reached the lowest plate height value ever reported for analytical columns (h_{min} = 1.0).
To further support these findings from a theoretical viewpoint, in collaboration with the group of Prof. G. Desmet (Vrije University of Brussels, Belgium), we investigated the diffusion process in a perfectly ordered packed bed made of these particles thanks to the use of computational fluid dynamics (CFD) simulations. The results of these simulations were compared with data sets previously obtained for FPPs and traditional SPPs. To allow for a fair comparison, the same particle arrangement, the same values for the mobile zone and porous zone diffusion coefficients (D_{pz}/D_{mol} = 0.1 and 0.5, being D_{pz} the diffusion coefficient in the porous zone), as well as the same retention factors have been used to simulate diffusion in the three particle types. Each numerical simulation led to different independent D_{eff} values, efficiently fitted with EMT expressions [65]. Plate heights were determined by following the variance

of a tracer band migrating through the flow domain. As is evident from Fig. 3.4, ROM-SPPs outperformed the other in terms of kinetic performance and the three curves mostly differs in the region at low eluent velocities, where mass transfer is dominated by longitudinal diffusion. Moreover, it was found that longitudinal diffusion is independent of the retention factor. It remained at its minimal value (corresponding to that of unretained molecules) instead of increasing with retention, as it happens for particles with isotropic internal diffusion. This depends from the fact that diffusion in the circumferential direction of the porous shell is completely blocked by the presence of ROMs. On the other hand, the only remaining route for diffusion is in the interstitial volume between particles. This reduction in b-term should be expected to be accompanied by an increase in the c_s-term, as it happens for particles with traditional isotropic internal diffusion. However, it has been demonstrated that any packed bed made of ROM-SPP produces lower b-term without affecting the c_s-term. Moreover, it can be supposed that the straight running mesopores of the CS-ROM particles will lead to higher D_{pz}-values than those that can be expected in the random pore networks of traditional particles.
These large differences observed between the three different types of particles under identical packing conditions suggest that intraparticle diffusivity and porous zone morphology have a strong impact on the efficiency of mass transfer kinetics.

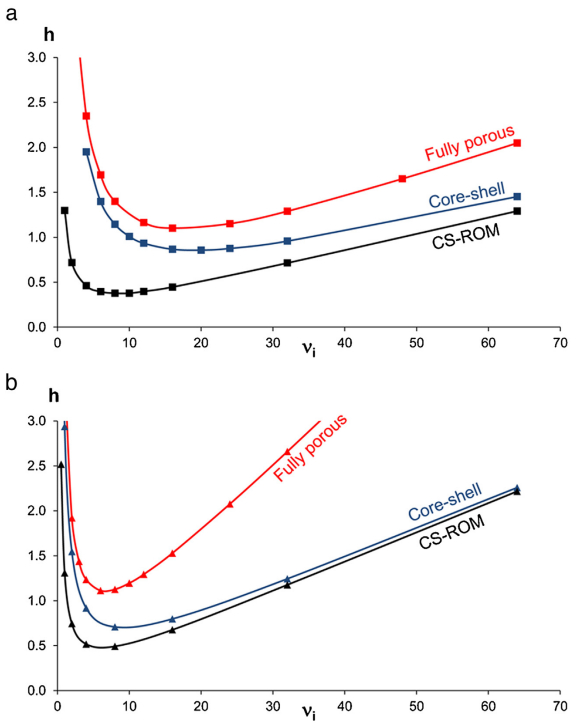

Figure 3.4: Plate height curves for the three particle arrangements with D_{pz}/D_{mol} = 0.1 (a) and 0.5 (b). Reprinted from **III** with permission from Elsevier.

As a side remark, in spite of the high potential of this particle format, the development of ROM-SPPs is apparently not any longer supported, due to both chemical stability problems and low mechanical resistance of packed bed made of these particles (**IV**).

3.1.2 Chiral separations (Papers IV-VIII)

Chromatographic behavior of prototype chiral columns packed with new CSPs designed for ultrafast high performance separations has been investigated on both sub-2μm FPPs and SPPs functionalized with the same chiral selector.
The first study has been carried out on 2.6 μm SPPs functionalized with Whelk-O1 chiral selector. Thermodynamics and kinetics of the column packed with this new CSP have been compared with those of other two columns of similar geometry packed with Whelk-O1 1.8 μm and 2.5 μm FPPs (**V**).
Whelk-O1 chiral selector belongs to the so-called Pirkle type class, even referred to generically as brush-type. This class of selectors is considered one of the best candidates for the transition from traditional enantioseparations to ultrafast ones. This finds its rationale in the ease to prepare sub-2 μm particles (absence of particle aggregation and clogging during their synthesis) and on the supposed fast mass transfer kinetics properties of CSPs based on this class of selectors. The first sub-2μm FPP CSP was, indeed, functionalized with a Pirkle type chiral selector (**VI**).
The preparation of both Whelk-O1 FPPs and SPPs has been carried out by following the same identical procedure adopted before for the functionalization of sub-2μm FPPs [76,77], however a larger surface density of chiral selector (roughly + 20%) was observed for SPPs with respect of the two FPPs. Columns packed with the new Whelk-O1 CSPs have been characterized in normal phase conditions for the separation of *trans*-stilbene oxide (TSO) enantiomers.
In Fig. 3.5, chromatograms recorded at the minimum of the van Deemter curve are reported. For the sake of comparison, they are reported as a function of k. Retention factors of TSO were the same on the two FPPs, with selectivity (α) equal to 2.49. On the other hand, on the column packed with 2.6 μm SPPs, retention of both enantiomers is smaller but α is slightly larger (2.54). In this figure, also the efficiencies for each peak, reported in N/m, are indicated. As it can be evinced, the three columns are characterized by very high performances, even comparable with those usually reported for RPLC.

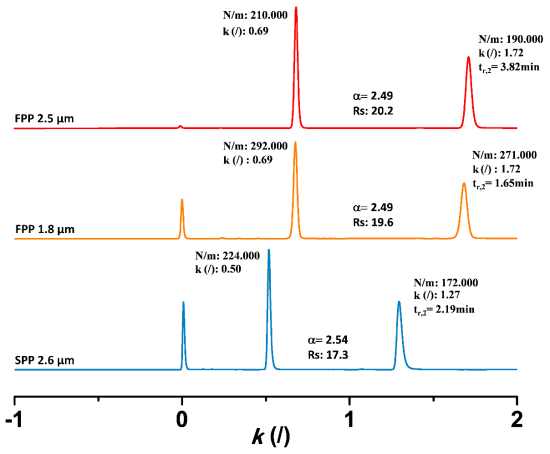

Figure 3.5: Chromatograms showing the separation of TSO enantiomers on the three Whelk-O1 columns. Reprinted from **V** with permission from Elsevier.

Turning to van Deemter curves, the first thing that can be observed from Fig. 3.6, is that the three columns behave practically identically as regards the elution of the first enantiomer. Conversely, by looking at the van Deemter curves for the second enantiomer, it can be evinced that the performance of the 2.6 μm SPP column is worse than that of the sub-2μm one and quasi-

comparable to that of the 2.5 μm FPP. The explanation of this could lay in two possible facts. The first one is about a probable remarkable contribution of eddy dispersion on the performance of the 2.6 μm SPPs. This could be due to some experimental issues encounterd during the slurry packing process of this CSP. Indeed, not only the achievement of a stable slurry suspensions was difficult but also the time needed to compress the bed (by high-pressure flushing) did not follow any expected trend. This could suggest that the ability to generate very efficient packed beds (which is one of the main and well-documented characteristics of hydrophobic SPP) could not be easily reproducible with polar Whelk-O1 SPPs. Further investigation is needed to assess this point, in particular on rheological characteristics of Whelk-O1 SPPs. The second issue that could be responsible of the poor performance of the Whelk-O1 SPP columns is a possible slow adsorption-desorption kinetics on the second eluted enantiomer, which could be related to the largest surface density of chiral selector found on the SP silica. However, also this point needs further investigations, since the impact of surface density on the adsorption-desorption kinetics represent a field which is practically unexplored yet (**V**,**VII**).

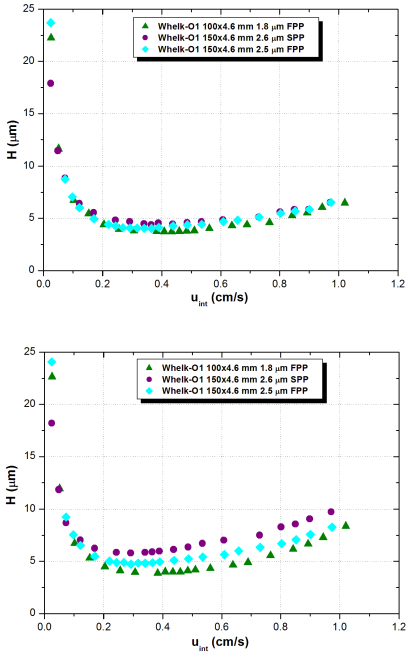

Figure 3.6: van Deemter curves recorded for the first (top) and second (bottom) eluted enantiomer on the three Whelk-O1 columns. Reprinted from **V** with permission from Elsevier.

In order to demonstrate the potential and the applicability of these new CSPs towards ultrafast enantioseparations, very short columns (1 cm long) were packed with the sub-2 μm FPPs and the 2.6 μm SPPs CSPs. The two TSO enantiomers were baseline resolved in less than one second by using a very high flow rate (8 mL/min) as reported in Fig. 3.7.

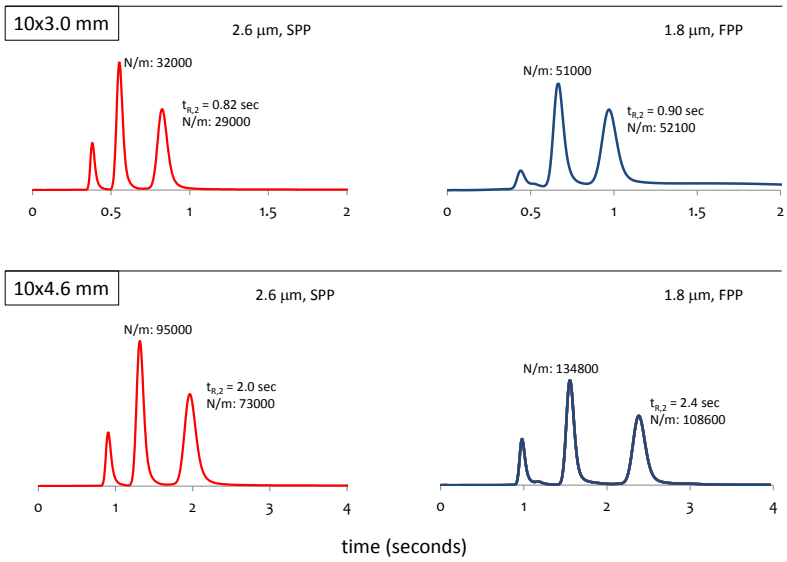

Figure 3.7: Ultrafast enantioseparations of TSO enantiomers on 10×3.0 and 10×4.6 mm columns packed with both 2.6 μm SPP and 1.8 μm FPP Whelk-O1 CSPs. Reprinted from **VII** with permission from the Royal Society of Chemistry.

In a very recent publication (**VIII**), we have prepared and tested the first CSP based on 2.0 μm Halo SPPs functionalized with teicoplanin chiral selector. The kinetic performance of the column packed with this new CSP has been compared to that of other two columns packed with 1.9 μm monodisperse FP Titan particles and 2.7 μm SPPs in HILIC conditions (eluent: acetonitrile/water 85:15 + 20 mM ammonium formate). An already validated bonding protocol has been used to functionalize both SPPs and FPPs with this chiral selector. Also in this case, even if experimental conditions have been kept identical for the three particle types, a larger surface density has been found on the two SPPs with respect of Titan FPPs. This could suggest a larger accessibility of the external layers of SPPs with respect of FPPs.
These CSPs has been in-house packed into 100×4.6 mm columns. The kinetic performance of these columns has been compared through both van Deemter curves and kinetic plots by using achiral and chiral compounds. The columns packed with 2.0 μm SPPs outperformed the other two, reaching efficiencies as high as 300 000 N/m. Their van Deemter curves are characterized by a flat c-branch, meaning that they could be operated at flow rates higher than the optimal one without remarkable loss of efficiency (see Fig. 3.8). This is a very important feature for ultrafast high-throughput separations, which are usually carried out at very high eluent velocities.

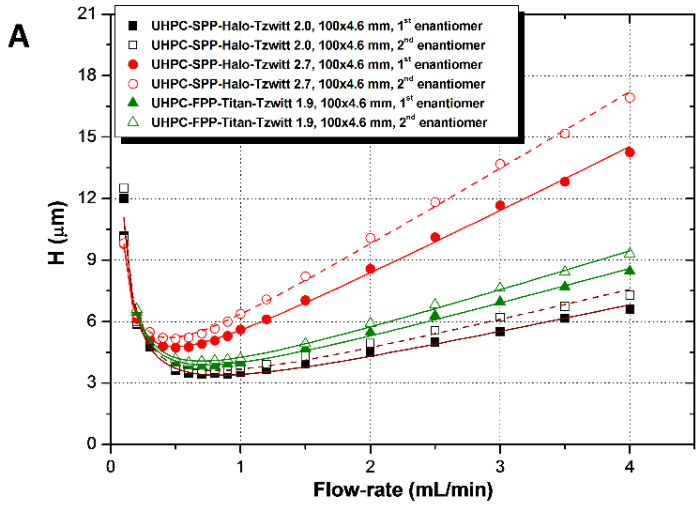

Figure 3.8: van Deemter curves of the first (solid lines) and the second (dashed lines) eluted enantiomers of 2-(4-chloro-phenoxy)-propionic acid on the three 100×4.6 mm teicoplanin columns. Reprinted from **VIII** with permission from Elsevier.

Then, the three columns have been tested for the separation of a large number of chiral compounds. The 2.0 μm SPPs one showed the highest resolution in almost all cases, as reported in Fig. 3.9 for a flow rate of 1 mL/min.

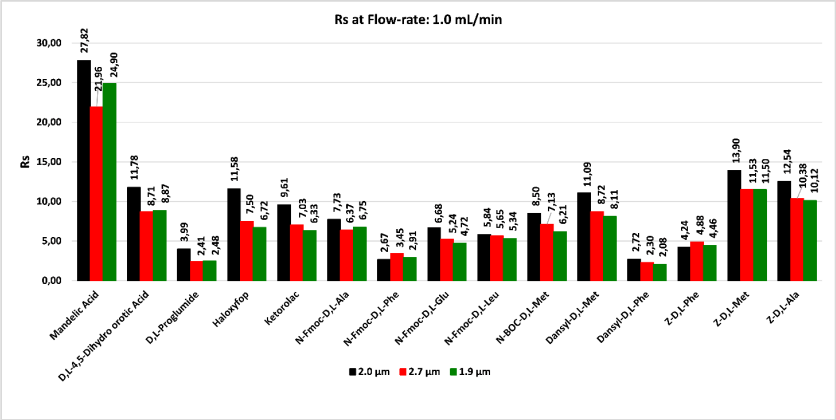

Figure 3.9: Bar plots of resolution values (R_s) obtained on the three 100×4.6 mm columns at a flow rate of 1 mL/min. Reprinted from **VIII** with permission from Elsevier.

In order to test the feasibility of these new CSPs towards ultrafast separations, the column length was firstly decreased to 50 mm and, again, the 2.0 μm SPPs column outperformed the other two, followed by the 1.9 μm Titan FPPs one. Then, these two CSPs have been packed into smaller columns with a length of only 20 mm and operated up to the maximum flow rate reachable by the instrument (8 mL/min) to perform the ultrafast separation of a racemic mixture containing haloxyfop and ketorolac. The enantiomers of the first compound have been separated in 4 and 3.4 seconds on the 1.9 μm FPPs and on the 2.0 μm SPPs, respectively (**IV**,**VIII**).

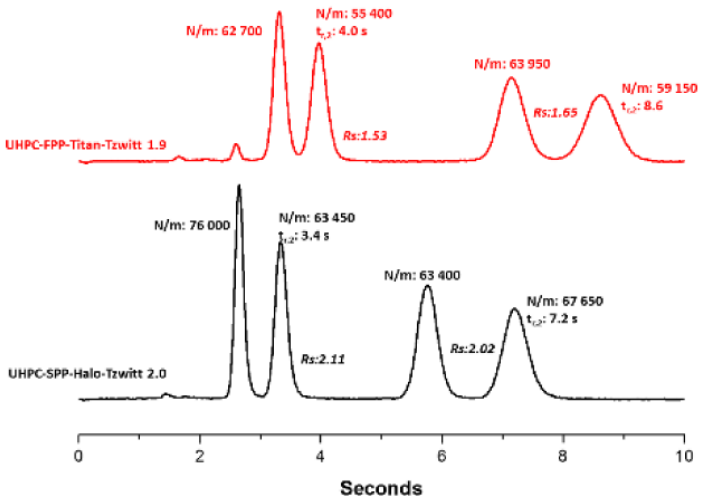

Figure 3.10: Ultrafast enantioseparation of a racemic mixture containing both haloxyfop (firstly eluted pair of peaks) and ketorolac (secondly eluted pair of peaks) on the 1.9 μm Titan FPPs (top) and on the 2.0 μm SPPs (bottom) columns at a flow rate of 8 mL/min. Reprinted from **VIII** with permission from Elsevier.

3.1.3 Closing remarks

The investigation of kinetic performance and mass transfer properties of columns packed with new generation particles for ultrafast high performance separations has increasingly acquired importance for proper future developments of ever better stationary phases.
At present, the mass transfer properties of hydrophobic porous media for reversed phase separations have been thoroughly investigated by means of validated experimental protocols reported in literature by several authors. Ever and ever smaller particles have been commercialized (down to 1.1 μm prototype SPPs) and new morphological porous particles, such as prototype ROM-SPPs (**III**), able to produce the highest efficiencies ever reported in analytical applications have been designed and theoretically studied.
However, even if giant steps have been done also for the separation of enantiomers, the field of chiral chromatography needs further theoretical investigations yet. According to the results discussed in this thesis, the main requirement is to understand if and how particle format and surface density could have an effective impact on the adsorption-desorption kinetics and, consequently, on column efficiency and speed of separation. Another open point that concerns both the two particle formats is the impact of PSD and, more in general, packing "quality" on the efficiency of LC columns. According to results described in this thesis, packing apolar or polar particles (such as chiral ones), be they FPPs or SPPs, can be intrinsically different. However, even the most advanced approaches to study mass transfer in chiral chromatography cannot provide independent estimations of contributions to band broadening coming from eddy dispersion and adsorption-desorption kinetics (**IV**,**VII**). One of the approach that could be adopted in order to understand the impact of adsorption-desorption kinetics is the application of stochastic theory (see Section 2.1.3), which allows to get important information starting from the peak shape. These information at a molecular level could be also crossed with data acquired by means of overloading studies, in order to investigate a possible effect of surface heterogeneity on the adsorption-desorption kinetics.

3.2 Investigation of fluorous affinity through nonlinear chromatography

3.2.1 Adsorption equilibria of benzene derivatives on a perfluorinated adsorbent (Papers IX, X)

Perfluorinated stationary phases exhibit similar features of traditional C_{18} reversed-phase stationary phases when they are used with acetonitrile/water binary eluents, such as the linear dependence of the logarithm of retention factor on the volume fraction of the organic modifier and the preferential adsorption of acetonitrile from acetonitrile/water binary mixtures (**X**). What differentiates perfluorinated and reversed phase stationary phases is their ability to discriminate between molecules differing by one single CH_3 or CF_3 group [78,79].
Paper **IX** reports the results of an investigation carried out on a series of benzene derivatives to study the effect of one single perfluorinated carbon on the chromatographic behavior and adsorption properties of molecules on a perfluorinated stationary phase (Fluophase RP, 150×2.1 mm, 5 μm particle size, bonding phase C_6F_{13}). To this end, the adsorption equilibria of toluene and α,α,α-trifluorotoluene have been studied and, to assess if the alkyl-chain length could have a possible effect on the adsorption process, also linear alkylbenzenes with alkyl chain lengths ranging from C_2 to C_6 have been considered.
Firstly, the excess adsorption isotherm of acetonitrile from the binary mixture of eluent has been determined in order to assess the region where the excess of acetonitrile on the stationary phase decreases linearly with the fraction of acetonitrile in the mobile phase (θ^M_{ACN}). The region ranged between $0.5 < \theta^M_{ACN} < 0.9$, therefore all the measurements have been performed within this zone. The dependence of logarithm of retention factor (ln$k$) on θ^M_{ACN} for the six alkylbenzenes (toluene, ethylbenzene, propylbenzene, butylbenzene, pentylbenzene, and hexylbenzene) has been investigated. For all the compounds, ln$k$ decreases linearly with θ^M_{ACN}, as it happens in reversed-phase chromatography.
Then, lnk of α,α,α-trifluorotoluene was added on the same graph. Some interesting considerations have been made by comparing its behavior with those of toluene and butylbenzene, as reported in Fig. 3.11.

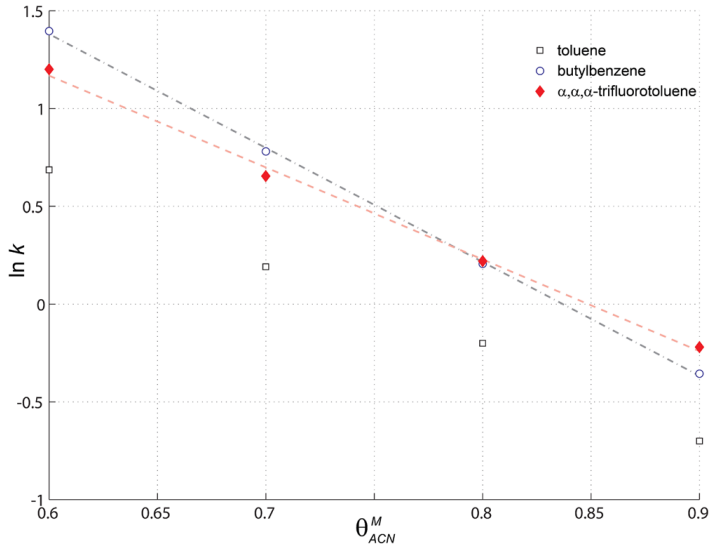

Figure 3.11: Dependence of the ln$k$ on θ^M_{ACN}: toluene (empty squares); butylbenzene (empty circles); α,α,α-trifluorotoluene (full diamond). Reprinted from **IX** with permission from American Chemical Society.

The first thing that can be observed is that the presence of one CF_3 group provokes a drastic

change in the retention behavior of the molecule inducing an increase in retention of roughly 60% if compared with toluene. This could be explained by taking into account that, from a thermodynamic point of view, transferring a single CF_3 group from the mobile phase to the perfluorinated stationary phase is more favorable than one CH_3 unit. Moreover, retention of α,α,α-trifluorotoluene is comparable to that of butylbenzene. This means that, in terms of energy transfer change, four methylene units should correspond to one single CF_3 group.
However, from a more fundamental point of view, the most relevant thing that can be observed from Fig. 3.11 is the inversion of the elution order between toluene and α,α,α-trifluorotoluene by changing the mobile phase composition.
To further investigate this aspect, the adsorption isotherms of the three benzene derivatives has been calculated through the inverse method at mobile phase compositions containing 60% and 70% (%v/v) of acetonitrile.
The results of nonlinear measurements demonstrated that the adsorption behavior of these compound is completely different. Indeed, as shown in Fig. 3.12, alkylbenzene derivatives overloaded profiles have a diffuse boundary in their front and a shock in the rear. On the opposite, α,α,α-trifluorotoluene profile is characterized by a shock in the front part and a diffuse boundary on the rear.

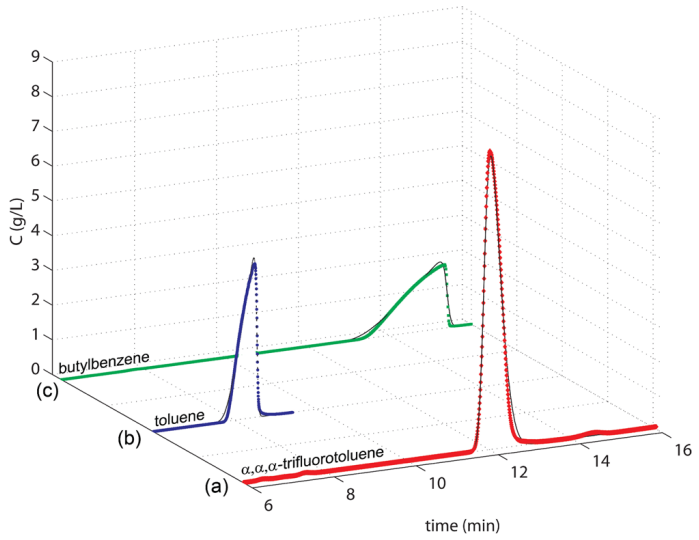

Figure 3.12: Overloaded band profiles recorded for α,α,α-trifluorotoluene, toluene and butylbenzene at a mobile phase composition of acetonitrile/water 60:40 (%v/v). Colored points: experimental, black lines: simulated. Reprinted from **IX** with permission from American Chemical Society.

The solid-liquid BET isotherm has been used to fit experimental peaks of toluene and butylbenzene, while the Tóth isotherm has been adopted for α,α,α-trifluorotoluene (see Section 2.2). Accordingly, α,α,α-trifluorotoluene adsorbs on the stationary phase as a Langmuir monolayers while, alkylbenzenes, tends to form multilayer stack structures. This means that the adsorption nature of benzene derivatives on highly fluorinated stationary phases changes radically depending on the presence of even a single perfluorinated carbon.

3.2.2 Closing remarks

The investigation of adsorption equilibria of benzene derivatives on a perfluorinated adsorbent lead to an important result, showing that even a single CF_3 group could have an impact on the adsorption behavior of molecules. This is surprising by considering that, in fluorous literature, six fully fluorinated sp^3 carbons are considered to be the minimum perfluorinated

portion to exert a primary control over the separability characteristics of a molecule. As it has pointed out by some authors [80], the majority of models used to describe retention involve linear chromatographic measurements, but this approach could have some limitations, primarily due to the fact that the effects of different possible interactions between molecule and stationary phase are lumped in one single parameter (the retention factor). This may cause a loss of fundamental information about the chromatographic process, for example about the existance of energetically different sites on the stationary phase or multilayer adsorption processes. These information, being fundamental to help understanding retention mechanism from a molecular point of view, can only be gathered through nonlinear chromatography.
The approach proposed in this study might be useful for a better understanding not only of the specificity of the FF interaction but also of other properties of highly perfluorinated materials, such as the fact that they do not mix with most organic solvents or their tendency to bioaccumulate in body compartments high in protein content (e.g. liver, kidney, and blood).

References

[1] M. S. Tswett and Tr. Protok. Varshav. obshch. estestvoistpyt. *Otd. Biol.*, 20, 1903, publ. 1905.

[2] M. Verzele and C. Dewaele. *Preparative High Performance Liquid Chromatography, A Parctical Guideline*, chapter 1. College Publishing, TEC Dent, Belgium, 1992.

[3] U. D. Neue. *HPLC Columns: Theory, Technology and Practice*. Wiley-VCH, 1997.

[4] J. J. Kirkland, J. J. DeStefano, and T. J. Langlois. Fused-core particles for HPLC columns. *Am. Lab*, February(39):18–21, 2007.

[5] J. J. DeStefano, S. A. Schuster, J. M. Lawhorn, and J. J. Kirkland. Performance characteristics of new superficially porous particles. *J. Chromatogr. A*, 1258:76–83, 2012.

[6] C. G. Horváth, B. A. Preiss, and S. R. Lipsky. Fast liquid chromatogrpahy: an investigation of operating parameters and the separation of nucleotides on pellicular ion exchangers. *Anal. Chem.*, 39:1422–1428, 1967.

[7] G. Guiochon, A. Felinger, D. G. Shirazi, and A. M. Katti. *Fundamentals of Preparative and Nonlinear Chromatography*. Academic Press, Elsevier, Second Edition, 2006.

[8] G. Guiochon and F. Gritti. Shell particles, trials, tribulations and triumphs. *J. Chromatogr. A*, 1218:1915–1938, 2011.

[9] F. Gritti, A. Cavazzini, N. Marchetti, and G. Guiochon. Comparison between the efficiencies of columns packed with fully and partially porous C18-bonded silica materials. *J. Chromatogr. A*, 1157:289–303, 2007.

[10] F. J. Zuiderweg J. J. Van Deemter and A. Klinkenberg. Longitudinal diffusion and resistance to mass transfer as causes of nonideality in chromatography. *Chem. Eng. Sci.*, 5:271–289, 1956.

[11] F. Gritti, I. Leonardis, J. Abia, and G. Guiochon. Physical properties and structure of fine core-shell particles used as packing materials for chromatography: Relationships between particle characteristics and column performance. *J. Chromatogr. A*, 1217:3819–3843, 2010.

[12] R. Hayes, A. Ahmed, T. Edge, and H. Zhang. Core-shell particles: preparation, fundamentals and applications in high performance liquid chromatography. *J. Chromatogr. A*, 1357:36–52, 2014.

[13] A. C. Sanchez, G. Friedlander, S. Fekete, J. Anspach, D. Guillarme, M. Chitty, and T. Farkas. Pushing the performance limits of reversed-phase ultra high performance liquid chromatography with 1.3 μm core-shell particles. *J. Chromatogr. A*, 1311:90–97, 2013.

[14] S. Fekete and D. Guillarme. Kinetic evaluation of new generation of column packed with 1.3 μm core-shell particles. *J. Chromatogr. A*, 1308:104–113, 2013.

[15] L. E. Blue and J. W. Jorgenson. 1.1 μm superficially porous particles for liquid chromatography. Part II: Column packing and chromatographic performance. *J. Chromatogr. A*, 1380:71–80, 2015.

[16] T. C. Wei, A. Mack, W. Chen, J. Liu, M. Dittmann, X. Wang, and W. E. Barber. Synthesis, characterization and evaluation of a superficially porous particle with unique, elongated pore channels normal to the surface. *J. Chromatogr. A*, 1440:55–65, 2016.

[17] G. Cancelliere, A. Ciogli, I. D'Acquarica, F. Gasparrini, J. Kocergin, D. Misiti, M. Pierini, H. Ritchie, P. Simone, and C. Villani. Transition from enantioselective high performance to ultra-high performance liquid chromatography: A case study of a brush-type chiral stationary phase based on sub-5-micron to sub-2-micron silica particles. *J. Chromatogr. A*, 1217:990–999, 2010.

[18] R. J. Reischl, L. Hartmanova, M. Carrozzo, M. Huszar, P. Frühauf, and W. Lindner. Chemoselective and enantioselective analysis of proteinogenic ammino acids utilizing N-derivatization and 1-D enantioselective anion-exchange chromatography in combination with tandem mass spectrometry. *J. Chromatogr. A*, 1218:8379–8387, 2011.

[19] K. Lomsadze, G. Jibuti, T. Farkas, and B. Chankvetadze. Comparative high-performance liquid chromatography enantioseparations on polysaccharide based chiral stationary phases prepared by coating totally porous and core-shell silica particles. *J. Chromatogr. A*, 1234:50–55, 2012.

[20] D. C. Patel, Z. S. Breitbach, M. F. Wahab, C. L. Barhate, and D. W. Armstrong. Gone in seconds: praxis, performance and peculiarities of ultrafast chiral liquid chromatography with superficially porous particles. *Anal. Chem.*, 87:9137–9148, 2015.

[21] D. A. Spudeit, M. D. Dolzan, Z. S. Breitbach, W. E. Barber, G. A. Micke, and D. W. Armstrong. Superficially porous particles vs. fully porous particles for bonded high performance liquid chromatographic chiral stationary phases: Isopropyl cyclofructan 6. *J. Chromatogr. A*, 1363:89–95, 2014.

[22] C. L. Barhate, Z. S. Breitbach, E. Costa Pinto, E. L. Regalado, C. J. Welch, and D. W. Armstrong. Ultrafast separation of fluorinated and desfluorinated pharmaceuticals using highly efficient and selective chiral selectors bonded to superficially porous particles. *J. Chromatogr. A*, 1426:241–247, 2015.

[23] D. C. Patel, M. F. Wahab, D. W. Armstrong, and Z. S. Breitbach. Advances in high-throughput and high-efficiency chiral liquidchromatographic separations. *J. Chromatogr. A*, 1467:2–18, 2016.

[24] M. D. Dolzan, D. A. Spudeit, Z. S. Breitbach, W. E. Barber, G. A. Micke, and D. W. Armstrong. Comparison of superficially porous and fully porous silica supports used for a cyclofructan 6 hydrophilic interaction liquid chromatographic stationary phases. *J. Chromatogr. A*, 1365:124–130, 2014.

[25] M. F. Wahab, R. M. Wimalasinghe, Y. Wang, C. L. Barhate, D. C. Patel, and D. W. Armstrong. Salient sub-second separations. *Anal. Chem.*, 88:8821–8826, 2016.

[26] R. M. Wimalasinghe, C. A. Weatherly, Z. S. Breitbach, and D. W. Armstrong. Hydroxypropyl beta cyclodextrin bonded superficially porous particle-based HILIC stationary phases. *J. Liq. Chromatogr. Rel. Tech.*, 39:459–464, 2016.

[27] F. Gritti and G. Guiochon. Mass transfer mechanism in chiral reversed phase liquid chromatography. *J. Chromatogr. A*, 1332:35–45, 2014.

[28] J. A. Gladysz, D. P. Curran, and I. T. Horváth, editors. *Handbook of Fluorous Chemistry*. Wiley-VCH, 2004.

[29] G. E Berendsen, K. A Pikaart, L. de Galan, and C. Olleman. (heptadecafluorodecyl)dimethylsilyl bonded phase for reversed-phase liquid chromatography. *Anal. Chem.*, 52:1990–1993, 1980.

[30] G. Zindu and P. W. Carr. Use of fluorinated bonded phases in reversed-phase high-performance liquid chromatography of proteins. *J. Chromatogr.*, 269:96–102, 1983.

[31] D. P. Curran, S. Hadida, and M. He. Thermal allylations of aldehydes with a fluorous allylstannane. separation of organic and fluorous products by solid phase extraction with fluorous reverse phase silica gel. *J. Org. Chem.*, 62:6714–6715, 1997.

[32] W. Zhang and D. P. Curran. Synthetic applications of fluorous solid-phase extraction (f-spe). *Tetrahedron*, 62:11837–11865, 2006.

[33] N. Marchetti, L. Caciolli, A. Lagan, F. Gasparrini, L. Pasti, F. Dondi, and A. Cavazzini. Fluorous affinity chromatography for enrichment and determination of perfluoroalkyl substances. *Anal. Chem.*, 84:7138–7145, 2012.

[34] A. Cavazzini and A. Felinger. *Liquid Chromatography: Fundamentals and Instrumentation*, volume 1, chapter 2. Elsevier, 2017.

[35] E. Kučera. Contribution to the theory of chromatography: linear non-equilibrium elution chromatography. *J. Chromatogr. A*, 19:237–248, 1965.

[36] J. C. Giddings and H. Eyring. A molecular dynamic theory of chromatography. *J. Phys. Chem.*, 59:416–421, 1955.

[37] J. C. Giddings. Kinetic model for chromatographic dispersion and electrodiffusion. *J. Chem. Phys.*, 26:169–173, 1957.

[38] J. C. Giddings. Kinetic origin of tailing in chromatography. *Anal. Chem.*, 35:1999–2000, 1963.

[39] D. A. McQuarrie. On the stochastic theory of chromatography. *J. Chem. Phys.*, 38:437–445, 1963.

[40] F. Dondi and M. Remelli. The characteristic function method in the stochastic theory of chromatography. *J. Phys. Chem.*, 90:1885–1891, 1986.

[41] P. Jandera, V. Bačkovská, and A. Felinger. Analysis of the band profiles of the enantiomers of phenylglycine in liquid chromatography on bonded teicoplanin columns using the stochastic theory of chromatography. *J. Chromatogr. A*, 919:67–77, 2001.

[42] A. Cavazzini, M. Remelli, and F. Dondi. Stochastic theory of two-site adsorption chromatography by the characteristic function method. *J. Microcol. Sep.*, 9:295–302, 1997.

[43] A. Cavazzini, M. Remelli, F. Dondi, and A. Felinger. Stochastic theory of multiple-site linear adsorption chromatography. *Anal. Chem.*, 7:3453–3462, 1999.

[44] A. Felinger, A. Cavazzini, M. Remelli, and F. Dondi. Stochastic-dispersive theory of chromatography. *Anal. Chem.*, 71:4472–4479, 1999.

[45] L. Pasti, N. Marchetti, R. Guzzinati, M. Catani, V. Bosi, F. Dondi, A. Sepsey, A. Felinger, and A. Cavazzini. Microscopic models of liquid chromatography: From ensemble-averaged information to resolution of fundamental viewpoint at single-molecule level. *TrAC*, 81:63–68, 2016.

[46] F. Dondi, A. Cavazzini, M. Remelli, A. Felinger, and M. Martin. Stochastic theory of size exclusion chromatography by the characteristic function approach. *J. Chromatogr. A*, 943:185–207, 2002.

[47] A. Felinger, L. Pasti, F. Dondi, M. van Hulst, P. J. Schoenmakers, and M. Martin. Stochastic theory of size exclusion chromatography: peak shape analysis on sinlge columns. *Anal. Chem.*, 77:3138–3148, 2005.

[48] A. Sepsey, I. Bacskay, and A. Felinger. Molecular theory of size exclusion chromatography for wide pore size distributions. *J. Chromatogr. A*, 1331:52–60, 2014.

[49] I. Bacskay, A. Sepsey, and A. Felinger. Determination of the pore size distribution of high-performance liquid chromatography stationary phases via inverse size exclusion chromatography. *J. Chromatogr. A*, 1339:110–117, 2014.

[50] I. Bacskay, A. Sepsey, and A. Felinger. The pore size distribution of the first and the second generation of silica monolithic stationary phases. *J. Chromatogr. A*, 1359:112–116, 2014.

[51] A. Sepsey, I. Backsay, and A. Felinger. Polydispersity in size-exclusion chromatography: a stochastic approach. *J. Chromatogr. A*, 1365:156–163, 2014.

[52] K. Horváth, M. Olajos, A. Felinger, and P. Haós. Retention controlling and peak shape simulation in anion chromatography using multiple equilibrium model and stochastic theory. *J. Chromatogr. A*, 1189:42–51, 2008.

[53] F. Dondi, P. Munari, M. Remelli, and A. Cavazzini. Monte carlo model of nonlinear chromatography. *Anal. Chem.*, 72:4353–4362, 2000.

[54] A. Cavazzini, F. Dondi, A. Jaulmes, C. Vidal-Madjar, and A. Felinger. Monte carlo model of nonlinear chromatography: correspondence between the microscopic stochastic model and the microscopic thomas kinetic model. *Anal. Chem.*, 74:6269–6278, 2002.

[55] F. Gritti and G. Guiochon. Mass transfer kinetics, band broadening and column efficiency. *J. Chromatogr. A*, 1221:2–40, 2012.

[56] F. Gritti and G. Guiochon. Mass transfer mechanism in chiral reversed phase liquid chromatography. *J. Chromatogr. A*, 1332:35–45, 2014.

[57] G. Desmet, K. Broeckhoven, J. De Smet, S. Deridder, G. V. Baron, and P. Gzil. Errors involved in the existing B-term expressions for the longitudinal diffusion in fully porous chromatographic media. Part I: Computational data in ordered pillar arrays and effective medium theory. *J. Chromatogr. A*, 1188:171–188, 2008.

[58] G. Desmet and S. Deridder. Effective medium theory expressions for the effective diffusion in chromatographic beds filled with porous, non-porous and porous-shell particles and cylinders. Part I: Theory. *J. Chromatogr. A*, 1218:32–45, 2011.

[59] S. Bruns, T. Müllner, M. Kollmann, J. Schachtner, A. Höltzel, and U. Tallarek. Confocal laser scanning microscopy method for quantitative characterization of silica monolith morphology. *Anal. Chem.*, 82:6569–6575, 2010.

[60] S. Bruns and U. Tallarek. Physical reconstruction of packed beds and their morphological analysis: Core-shell packings as an example. *J. Chromatogr. A*, 1218:1849–1860, 2011.

[61] K. Miyabe, Y. Matsumoto, and G. Guiochon. Peak parking-moment analysis. A strategy for the study of the mass-transfer kinetics in the stationary phase. *Anal. Chem.*, 79:1970–1982, 2007.

[62] J. H. Knox and H. P. Scott. B and C terms in the van Deemter equation for liquid chromatography. 282:297–313, 1983.

[63] J. H. Knox and L. McLaren. New gas chromatographic method for measuring gaseous diffusion coefficients and obstructive factors. *Anal. Chem.*, 36:1477–1482, 1964.

[64] D. Cabooter, F. Lynen, P. Sandra, and G. Desmet. Total pore blocking as an alternative method for the on-column determination of the external porosity of packed and monolithic reversed-phase columns. *J. Chromatogr. A*, 1157:131–141, 2007.

[65] S. Torquato. Effective electrical conductivity of twophase disordered composite media. *J. Appl. Phys.*, 58:3790–3797, 1985.

[66] K Kaczmarski. On the optimization of the solid core radius of superficially porous particles for finite adsorption rate. *J. Chromatogr. A*, 1218:951–958, 2011.

[67] K Kaczmarski, A Cavazzini, P Szabełski, D Zhou, X Liu, and G Guiochon. Application of the general rate model and the generalized maxwellstefan equation to the study of the mass transfer kinetics of a pair of enantiomers. *J. Chromatogr. A*, 962:57–67, 2002.

[68] K Miyabe. Moment equations for chromatography using superficially porous spherical particles. *Anal. Sci.*, 27:1007–1017, 2011.

[69] F Gritti and G Guiochon. Possible resolution gain in enantioseparations afforded by core-shell particle technology. *J. Chromatogr. A*, 1348:87–96, 2014.

[70] J C Giddings. *Dynamics of Chromatography*. Marcel Dekker, New York, 1965.

[71] D. Cabooter, A. Fanigliulo, G. Bellazzi, B. Allieri, A. Rottigni, and G. Desmet. Relationship between the particle size distribution of commercial fully porous and superficially porous high-performance liquid chromatography column packings and their chromatographic performance. *J. Chromatogr. A*, 1217:7074–7081, 2010.

[72] F Gritti and G Guiochon. The quantitative impact of the mesopore size on the mass transfer mechanism of the new 1.9 m fully porous Titan-C_{18} particles. I: Analysis of small molecules. *J. Chromatogr. A*, 1384:76–87, 2015.

[73] F Gritti and G Guiochon. The quantitative impact of the mesopore size on the mass transfer mechanism of the new 1.9 m fully porous titan-c_{18} particles. ii: Analysis of biomolecules. *J. Chromatogr. A*, 1392:10–19, 2015.

[74] Fabrice Gritti and Georges Guiochon. The rationale for the optimum efficiency of columns packed with new 1.9μm fully porous Titan-C_{18} particles. A detailed investigation of the intra-particle diffusivity. *J. Chromatogr. A*, 1355:164–178, 2014.

[75] F Gritti, I Leonardis, D Shock, P Stevenson, A Shalliker, and G Guiochon. Performance of columns packed with the new shell particles Kinetex-C_{18}. *J. Chromatogr. A*, 1217:1589–1603, 2010.

[76] D Kotoni, A Ciogli, C Molinaro, I D'Acquarica, J Kocergin, T Szczerba, H Ritchie, C Villani, and F Gasparrini. Introducing enantioselective Ultrahigh-Pressure Liquid Chromatography (eUHPLC): theoretical inspections and ultrafast separations on a new sub-2-μm Whelk-O1 stationary phase. *Anal. Chem.*, 84:6805–6813, 2012.

[77] D Kotoni, A Ciogli, I D'Acquarica, J Kocergin, T Szczerba, H Ritchie, C Villani, and F Gasparrini. Enantioselective ultra-high and high performance liquid chromatography: a comparative study of columns based on the Whelk-O1 selector. *J. Chromatogr. A*, 1269:226–241, 2012.

[78] A Cavazzini, L Pasti, R Greco, V Costa, D Solera, F Dondi, N Marchetti A Laganà, and F Gasparrini. Geometric characterization of straight-chain perfluorohexylpropyl adsorbents for high performance liquid chromatography. *J. Chromatogr. A*, 1286:47–54, 2013.

[79] A Cavazzini, N Marchetti, L Pasti, R Greco, F Dondi, A Laganà, A Ciogli, and F Gasparrini. Understanding mixed-mode retention mechanisms in liquid chromatography with hydrophobic stationary phases. *Anal. Chem.*, 86:4919–4926, 2014.

[80] A Cavazzini, L Pasti, R Greco, V Costa, D Solera, F Dondi, N Marchetti A Laganà, and F Gasparrini. Evaluation of a combined linearnonlinear approach for column characterization using modern alkaline-stable columns as model. *J. Sep. Sci.*, 36:1753–1761, 2013.

Acknowledgements

I would never have arrived here without help, support and simple presence of some people who I had the pleasure to meet and work with during these three years.

First of all, I would like to express my deepest gratitude to the supervisor that everyone wants to work for, **Prof. Alberto Cavazzini**, for his patience, his constant presence and for our fuitful discussions on science and on everyday life. I will always be grateful to him for having placed so many times in front of me the keys to open new doors and opportunities.

A special thanks goes to **Dr. Omar H. Ismail** and **Prof. Francesco Gasparrini** for the fruitful and healthy collaboration. It has been a great pleasure for me to work with them.

I am grateful to **Prof. Attila Felinger**, **Prof. Gert Desmet** and their groups to gave me the opportunity to work in their labs for some months. I have learned much new things when I was there and I got more independent under many points of view.

I thank past and present colleagues, in particular **Simona, Chiara, Elena, Marco, Gelsomina, Claudia, Francesco, Tatiana, Denise, Mara, Valentina, Roberta, Caterina** who have made every working day fun and exciting and with whom I have always shared ideas.

I would like to acknowledge all the other colleagues and professors of the **group of Analytical Chemistry** for their constant help, tips and good humour.

Finally and most importantly, words will never be enough to express how much I am grateful to **Federico** and **my family**, who have always put their faith in me. I feel indebted with them for their patience and all the sacrifices they made to support me in every moment and in every way possible.

PAPER I

Journal of Chromatography A, 1454 (2016) 86–92

Contents lists available at ScienceDirect

Journal of Chromatography A

journal homepage: www.elsevier.com/locate/chroma

Experimental evidence of the kinetic performance achievable with columns packed with new 1.9 μm fully porous particles of narrow particle size distribution

Omar H. Ismail[a], Martina Catani[b], Luisa Pasti[b], Alberto Cavazzini[b,*], Alessia Ciogli[a], Claudio Villani[a], Dorina Kotoni[a,1], Francesco Gasparrini[a,*], David S. Bell[c]

[a] Dept. of Drug Chemistry and Technology, "Sapienza" Università di Roma, P.le A. Moro 5, 00185 Roma, Italy
[b] Dept. of Chemistry and Pharmaceutical Sciences, University of Ferrara, via L. Borsari 46, 44121 Ferrara, Italy
[c] Applied Research and Development, Millipore Sigma, 595 North Harrison Road, Bellefonte, PA 16823, USA

ARTICLE INFO

Article history:
Received 6 March 2016
Received in revised form 7 May 2016
Accepted 10 May 2016
Available online 12 May 2016

Keywords:
Column efficiency
Sub-2 μm fully porous particles
Ultra high performance liquid chromatography (UHPLC)
Narrow particle size distribution (nPSD)

ABSTRACT

Fully porous particles of narrow particle size distribution (nPSD) are now commercially available. In this paper, the kinetic performance of columns packed with these particles (1.9 μm, 80 Å pore size) has been investigated under typical reversed phase conditions by using a mixture of benzene derivatives as probes. The columns exhibited remarkably high efficiency (in the order of 300,000 theoretical plates per meter) and the possibility to be used at relatively high flow rates without loss of performance.

These results contrast with previous studies on the same columns. Indeed we have found column efficiency comparable to that reported in previous work but, on the other hand, we could not observe the same dramatic loss of performance when columns were operated at high flow rates. The results presented in this paper, based on a set of six columns with different geometries (2.1 and 3.0 internal diameter × 50, 75 and 100 mm length), are not consistent with the previously proposed hypothesis that the unusually low intraparticle diffusion, which would characterize these particles, is the origin of the high efficiency of the columns. In a companion paper [1], a detailed investigation of the different terms leading to band broadening will be performed to point out the major contribution to plate height on nPSD columns.

1. Introduction

During the last several years, many efforts have been made to prepare high efficiency chromatographic columns. This trend has led column manufacturers to produce shorter, narrower columns packed with smaller (sub-2 μm) particles. The use of sub-2 μm fully porous particles essentially reflects the need to improve mass transfer inside the column by reducing intraparticle diffusion (less steep *C*-term in the van Deemter equation), albeit at cost of increased back pressure [2,3]. However, the availability of fine particles is not enough for the preparation of columns suitable for high or ultra-high performance liquid chromatography (HPLC, UHPLC). The packing procedure and the column bed consolidation (shortly, the packing protocol) are indeed of utmost importance for column performance. Pressurized slurry column packing is in fact influenced by many variables (e.g., filling pressure; slurry composition and concentration; particle roughness, density, etc.), which dramatically affect column efficiency and stability [4,5]. Recently, columns packed with new 1.9 μm fully porous spherical particles (nominal pore size 80 Å) have been introduced into the market (commercial name: Titan C_{18} particles, from Supelco). Titan C_{18} particles are characterized by an unusually narrow particle size distribution (nPSD) for fully porous particles, with a relative standard deviation (RSD) smaller than 10%. This is due to an innovative and proprietary process for synthesizing fully porous spherical particles that, in addition, does not require secondary sizing operation [6]. Usually, fully porous sub 2-μm particles come in broader PSD, with RSD in the order of 15–30% [2,7].

The benefit of a nPSD on chromatographic performance is still under debate [8]. The past literature is substantially unanimous on the statement that a nPSD is not essential for the achievement of efficient columns. In the late 60s-early 70s, Snyder [9], Done and Knox [10], Halász and Naefe [11] and Endele et al. [12]

* Corresponding authors.
E-mail addresses: cvz@unife.it (A. Cavazzini), francesco.gasparrini@uniroma1.it (F. Gasparrini).
[1] Current address: Chemical and Analytical Devel., Novartis Pharma AG, St. Johann Campus, 4102 Basel, Switzerland.

http://dx.doi.org/10.1016/j.chroma.2016.05.038
0021-9673/

independently concluded that, unless the PSD is wider than 40% around the mean, the influence of PSD on the plate height and column permeability is essentially negligible. Some ten years later, Dewaele and Verzele [13] performed a systematic study on the influence of PSD on the column efficiency, by employing a series of packing media prepared by accurately mixing different portions of spherical fully porous silica particles with average sizes included between 3 and 10 μm. This study confirmed that, as long as the PSD is sufficiently narrow ($d_{90}/d_{10} < 2$, being d_{90} and d_{10} respectively the particle diameter at 90%- and 10%-point of the cumulative distribution function), the reduced plate height is independent on the width of the PSD, provided that the solvent flow-rate is close to its optimum value. Since 2007, following the introduction of core–shell particles characterized by very nPSDs (with RSD of roughly 5%) [14], the debate about PSD as a possible route to improve performance of packed HPLC columns has been rekindled. Core–shell particles are able to produce more efficient columns than classical fully porous particles [15–17]. However, to conclude from this that there is a relationship between PSD and column efficiency is all but obvious. In fact, reconstruction of packed bed [18,19] and numerical calculations [20] have shown that the most likely explanation of the enhanced performance of core–shell particles is their roughness. Thus, during the packing, core–shell particles slip against each others and against the wall of the column less easily than smooth fully porous particles with the formation of more radially uniform packed structures. Based on this model, accordingly, it is the shear stress originating between core–shell particles that explains the performance gain, not their tight PSD [21]. In support of this, there is evidence that short-range eddy dispersion is larger for core–shell particles than for conventional ones (due to the larger interstitial porosity), while the long-range eddy dispersion is significantly lower [8].

The most advanced study aimed at investigating the influence of PSD on column performance are those based on the simulation of fluid flow and advective-diffusive mass transport in the packing interparticle void space of computer-reconstructed bulk packings (as to avoid the effect of different packing protocols on the final bed structure), performed by Tallarek and coworkers [20,22–24]. They have shown that, as long as the PSD is reasonably narrow (RSD < 25%), the effect of PSD on chromatographic bulk dispersion is negligible, especially if compared to that of the interstitial bed porosity [20,22]. The morphological analysis of physically reconstructed packings has shown indeed that the actual disorder in the bulk of beds made of particles with nPSD is essentially the same as that found in beds packed with particles of wide PSD [23,24]. On the other hand, what makes the difference in terms of kinetic performance in confined packings (e.g., chromatographic columns) are the wall effects, which depend on the packing protocol and on the particle properties (including thus their PSD).

The first detailed reports on the use of Titan C_{18} columns in reversed phase liquid chromatography (RPLC) evidenced their excellent kinetic performance [25,26]. Extremely low reduced plate heights, h_{min}, were found for retained compounds with values as small as 1.7–1.9 [25,26] (thus very close to h_{min} values typical of core–shell particles [2,27,28,24,8]). Gritti and Guiochon [25,26] employed a series of phenone derivatives under RP conditions as probe compounds to investigate in detail all the terms of the van Deemter equation. According to their study, Titan C_{18} columns are characterized by an extremely small *B*-term, due to the very small intra-particle diffusivity across the Titan C_{18} particles [26]. The internal obstruction factor, which accounts for the overall diffusion hindrance in the confined pore geometry [29], was indeed found to be roughly 1.6 times smaller (for a retention factor of about 2) than for typical fully porous particles of similar chemistry. This was used to explain why the reduced optimum flow rate, ν_{opt}, was found at only around 4–5, while in RPLC it is usually around 10. The downside of a small *B* term is indeed a large *C* term in the van Deemter equation. It was concluded in these studies that there is no effect of PSD on column efficiency.

In this work, we report on the experimental evaluation of the kinetic behavior of 1.9 μm C_{18} Titan columns. Essentially, we have measured van Deemter curves of a series of benzene derivatives up to the maximum back pressure allowed by our equipment (roughly 1000 bar or 14,500 psi) on six columns with different geometrical characteristics. This is, in our opinion, a significant number of case studies to draw reliable conclusions. The experimental data collected in this work show that these columns are very efficient at their optimal reduced velocities ($h_{min} \simeq 1.7$ were measured at optimal reduced velocities of 8–10). In addition, they also reveal that the van Deemter curve remains remarkably flat up to the maximum flow rate achievable with our equipment (for instance at $\nu = 22.5$, $h = 2.85$). This experimental finding, which represents a significant difference from the observations reported in [25,26], will be discussed again in connection with further results in the companion paper [1], where we present a detailed study of the single terms of the van Deemter equation for the compounds used in this work.

2. Experimental section

2.1. Columns and materials

The six stainless steel Titan C_{18} columns packed with 1.9 μm particles (80 Å pore size; C_{18} ligand density: 2 μmol/m^2; specific surface area: 400 m^2/g) were generously donated by Supelco Analytical (USA). Their dimensions (length × internal-diameter, i.d.) were: 100 mm × 2.1 mm, 75 mm × 2.1 mm, 50 mm × 2.1 mm, 100 mm × 3.0 mm, 75 mm × 3.0 mm and 50 mm × 3.0 mm. A 33 mm × 4.6 mm Micra column (Eprogen, Inc., USA) packed with 1.5 μm non-porous silica particles was purchased by DBA Italia s.r.l. (Italy). This column was employed for the estimation of bulk molecular diffusion coefficients. Uracil, phenol, nitrobenzene, benzaldehyde, benzene, toluene, ethylbenzene, butylbenzene, propylbenzene, pentylbenzene and tetrahydrofuran were purchased from Sigma–Aldrich. The fourteen polystyrene standards (molecular weights 500, 2000, 2500, 5000, 9000, 17,500, 30,000, 50,000, 156,000, 330,000, 565,000, 1,030,000, 1,570,000, 2,310,000), employed for inverse size exclusion chromatography, were from Supelco. Acetonitrile (ACN) was from VWR International and ultra-high quality Milli-Q water was obtained by a Milli-Q water purification system (Millipore).

2.2. Equipment

A Waters Acquity UPLC, controlled by Empower 3 software and equipped with a binary solvent delivery system, an autosampler, a column thermostat, a photodiode array detector with a 500 nL cell, was used for the construction of the van Deemter curves. The equipment was operated under still-air, quasi-adiabatic conditions [30,31]. The maximum back pressure reachable by the system is 1000 bar. To reduce the extra-column contributions, two 250 mm × 0.075 mm nano-Viper capillary tubes (Thermo Scientific) were used to connect the injector to the column and the column to the detector. The extra column peak variance, measured from the injector needle port to the detector cell (by using uracil as marker), was 1.2 μL^2 (calculated through peak moments) at a flow rate of 1 mL/min (more details can be found as Supplementary Material). Inverse size exclusion chromatography (ISEC) experiments were carried out on an Agilent 1100 Series Capillary LC system equipped with a binary pump system, an autosampler, a column thermostat and a photodiode array detector. This equipment was also employed for peak parking experiments.

2.3. Inverse size exclusion chromatography (ISEC)

ISEC measurements were performed by using tetrahydrofuran as the mobile phase [32]. Injection volume, flow rate and detection wavelength were, respectively, 2 μL, 0.1 mL/min and 254 nm. For ISEC plots (see Section 3), retention volumes were corrected for the extra-column contribution before being plotted against the cubic root of the molecular weight (*MW*).

2.4. Peak parking measurements

The flow rate used for peak parking measurements was 0.1 mL/min. Parking times were 0, 120, 600, 1200 and 1800 s. For the calculation of the spatial peak variance σ_x^2, the following equation was used:

$$\sigma_x^2 = \frac{L^2}{N} \quad (1)$$

where L is the column length and N is the number of theoretical plates. For the calculation of N, peak width was that returned by the software and the retention time was corrected by the parking time. All the data were corrected for the extra-column peak variance.

2.5. van Deemter curve measurements

For all columns, the data to construct the van Deemter curves for nitrobenzene, toluene, ethylbenzene and butylbenzene were measured at 35.0 ± 0.1 °C. The mobile phase was a binary mixture of ACN/water 60:40 (v/v). The injection volume was 0.5 μL. Injection mode was partial loop with needle overfill. Retention time and column efficiency of eluted peaks were automatically calculated through the Empower software (v. 3). The detection wavelength was 214 nm; sampling rate was 80 points/s. Due to the very reduced extra-column volume of the modified Waters UPLC employed in this work, no correction was applied to compensate for the extra-column contribution. Only in the case of the less retained compound (nitrobenzene, retention factor about 1.5) and with the 50 mm × 2.1 mm column the extra-column contribution is significant, representing some 20% of the column variance. The flow rates employed for studying the dependence of H on the mobile phase velocity were 0.025, 0.05, 0.1 mL/min and then, from 0.1 mL/min to the maximum reachable flow rate, step increments of 0.1 mL/min were applied (see figure captions for more details).

3. Discussion

A detailed characterization of geometrical and physico-chemical characteristics of all the columns used in this work has been achieved through a series of measurements combining ISEC, pycnometry, peak parking and the traditional study of the dependence of the efficiency on the flow rate (van Deemter curves) [33,34].

3.1. ISEC experiments

Fig. 1 reports the ISEC plot for the estimation of interstitial and thermodynamic void volumes [35], measured on the 75 mm × 3.0 mm Titan C_{18} column. The interstitial volume, V_e, was derived from the extrapolation to $MW = 0$ of the linear regression calculated for the volumes of the totally excluded polystyrene samples. From this, the estimation of external column porosity, ϵ_e, is straightforward (being $\epsilon_e = V_e/V_{col}$, with V_{col} the geometric volume of the column). The ISEC estimation of the thermodynamic void volume, V_0, was based on the retention volume of benzene. Through

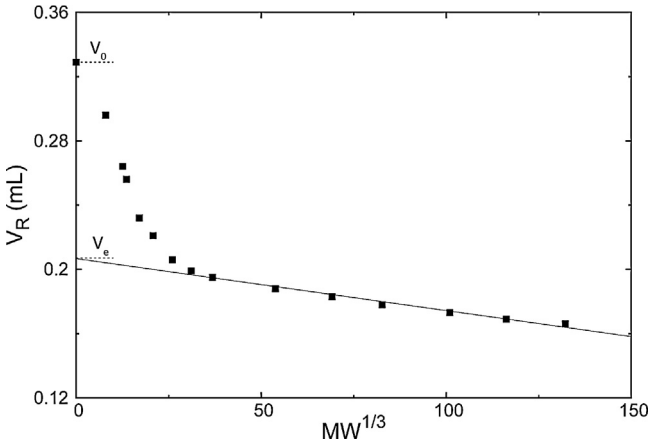

Fig. 1. ISEC plot. Retention volume (V_R) of polystyrene standards are plotted as a function of the cubic root of their molecular weight ($MW^{1/3}$). Column: Titan C_{18} 75 mm × 3.0 mm. V_e: interstitial volume; V_0: thermodynamic void volume. See text for more details.

this, the total porosity ϵ_t can be calculated ($\epsilon_t = V_0/V_{col}$). Thus the particle porosity, ϵ_p, is given by [36]:

$$\epsilon_p = \frac{\epsilon_t - \epsilon_e}{1 - \epsilon_e} \quad (2)$$

The porosities (ϵ_t, ϵ_e, ϵ_p) for the six Titan C_{18} columns are reported in Table 1. As it can be noticed, the estimates of ϵ_t, ϵ_e, ϵ_p from the six columns are remarkably consistent with each other. Their average values are $\epsilon_t = 0.603 \pm 0.009$, $\epsilon_e = 0.371 \pm 0.009$ and $\epsilon_p = 0.368 \pm 0.007$ (errors are reported as plus/minus one standard deviation). For all columns, the thermodynamic void volume was also estimated by pycnometry. The agreement between void volumes estimated by ISEC and pycnometry was reasonably satisfactory in all cases (with differences in the order of roughly ±5%). The pycnometric procedure and obtained void volumes are reported as Supplementary Material.

3.2. Estimation of molecular diffusion coefficients

Molecular diffusion coefficients, D_m, were evaluated through the peak parking technique by employing a column packed with nonporous particles (Micra column) [37,38,8]. The peak parking method permits the empirical estimation of the apparent (or effective) axial diffusion coefficient in the composite material made of porous particles in contact and dispersed in the eluent matrix, D_{eff}. For columns packed with nonporous particles:

$$D_{eff} = \gamma_e D_m \quad (3)$$

Table 1
Geometrical characteristics and physico-chemical properties of the Titan C_{18} columns: total (ϵ_t), interstitial (ϵ_e) and particle (ϵ_p) porosities; specific permeability (k_0); Kozeny–Carman constants (K_c). Batch: number of silica batch. Calculation of K_c (Eq. (7)) for the Titan C_{18} columns was based on d_{Sauter}. See text for further details.

$L \times$ I.D. (mm)	Batch	ϵ_t	ϵ_e	ϵ_p	$k_0 \times 10^{11}$ (cm^2)	K_c
100 × 3.0	8202	0.593	0.364	0.360	2.77	179
75 × 3.0	8033	0.613	0.381	0.375	3.06	196
50 × 3.0	412,502	0.594	0.363	0.363	3.05	161
100 × 2.1	8033	0.612	0.384	0.370	3.17	196
75 × 2.1	7988	0.600	0.370	0.365	3.38	157
50 × 2.1	412,502	0.605	0.366	0.377	3.05	166

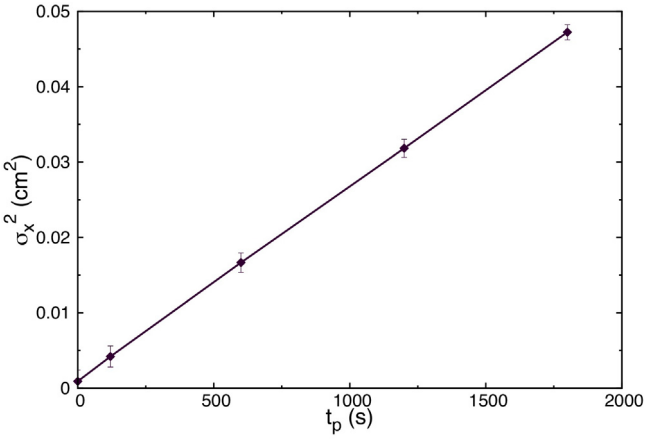

Fig. 2. Peak parking experiments. Plot of band spreading (spatial peak variance, σ_x^2) as a function of the peak parking time, t_p (linear regression coefficient $R^2 > 0.999$). Compound: ethylbenzene; Eluent: ACN/water 60:40 (v/v); $T = 35\,^\circ$C; Column: Micra 33 mm × 4.6 mm, 1.5 μm nonporous silica particles.

where γ_e is the external obstruction factor generated by the tortuosity and constriction of inter-particle channels [29]. Accordingly, if γ_e is known, D_m can be calculated by:

$$D_m = \frac{D_{eff}}{\gamma_e} \tag{4}$$

The value of γ_e (D_{eff}/D_m) was determined by measuring D_{eff} (by means of peak parking) for a molecule of known D_m. In this work, thiourea in pure water at 25 °C was used (under these conditions, D_m of thiourea is 1.33×10^{-5} cm^2/s) [39]. γ_e for the 33 mm × 4.6 mm Micra column was 0.68.

The peak parking method consists of: (1) taking at a constant, arbitrary linear velocity a sample zone somewhere in the middle of the chromatographic column; (2) suddenly stopping the flow; (3) leaving the band free to diffuse during a certain parking time, t_p; (4) resuming the flow rate to move the band out of the column. The variance (in length units) of the eluted peak, σ_x^2, is measured ($\sigma_x^2 = L^2/N$, where L is the column length and N the number of theoretical plates) and the procedure is repeated (keeping constant the flow rate) for different parking times. The slope of σ_x^2 vs. t_p plot gives an estimate of the D_{eff}, being [38,8]:

$$D_{eff} = \frac{1}{2}\frac{\Delta\sigma_x^2}{\Delta t_p} \tag{5}$$

As an example, Fig. 2 shows the σ_x^2 vs. t_p plot, employed for the estimation of D_{eff} (Eq. (5)), obtained for ethylbenzene. D_m of nitrobenzene, toluene, ethylbenzene and butylbenzene in ACN/H_2O 60/40 (v/v) at 35 °C are reported in Table 2. As it can be seen from this table, D_m values of alkyl-benzenes decrease quasi-linearly with increasing the number of methyl groups in the alkyl chain (from one to three), inasmuch as diffusion coefficients decrease with increasing the molecular size [40].

Table 2
Bulk molecular diffusion coefficient, D_m, estimated through peak parking measurements for the four compounds considered in this work. Mobile phase: ACN/water 60/40 (v/v); T: 35 °C.

Compound	$D_m \times 10^5$ (cm^2/s)
Nitrobenzene	1.92
Toluene	2.10
Ethylbenzene	1.88
Butylbenzene	1.76

3.3. Specific permeability and Kozeny–Carman constant

The specific permeability of each column was calculated according to the traditional equation [28,29]:

$$k_0 = \frac{u_s \eta L}{\Delta P} \tag{6}$$

where $u_s = F_v/\pi r_c^2$ is the superficial velocity (being r_c the inner column radius and F_v the flow rate in mL/min) and η the viscosity of the eluent ($\eta = 0.59$ cP for ACN/water 60/40, v/v) at 35 °C. ΔP is the difference between the total pressure drop, P_{tot}, and the extra-column pressure drop, P_{ex} (P_{ex} was measured by replacing the column with a zero-volume connector). Experimentally, k_0 can be estimated by the slope of ΔP vs. u_s plot. Some examples of these plots for the columns used in this work are reported as Supplementary Material.

The Kozeny–Carman constant K_c was estimated by [28]:

$$K_c = \frac{\epsilon_e^3}{(1-\epsilon_e)^2}\frac{d_p^2}{k_0} \tag{7}$$

where d_p is the particle size. For the calculation of K_c for Titan C_{18} columns, the mean Sauter diameter d_{Sauter} was used (in place of the nominal $d_p = 1.9$ μm). d_{Sauter} is indeed considered the most suitable average particle size to investigate sample dispersion along beds packed with non-uniform size distribution [18]. d_{Sauter} is defined by [41]:

$$d_{Sauter} = \frac{\Sigma n_i d_i^3}{\Sigma n_i d_i^2} \tag{8}$$

where d_i and n_i are, respectively, a given particle size and the number of particles with diameter included between d_i and $d_i + \Delta d_i$ (Δd_i was assumed 0.015 μm for d_i values around 1 μm and 0.25 μm for d_i around 15 μm). d_{Sauter} was calculated at Supelco on some 30,000 particles. Its value was 2.04 μm [25]. k_0 and K_c for all the considered columns values are listed in Table 1.

3.4. Kinetic performance of Titan C_{18} columns

Figs. 3 and 4 show the van Deemter plots obtained for the four compounds considered in this work on the two 50 mm Titan C_{18} columns (3.0 and 2.1 mm i.d.). Other examples of van Deemter

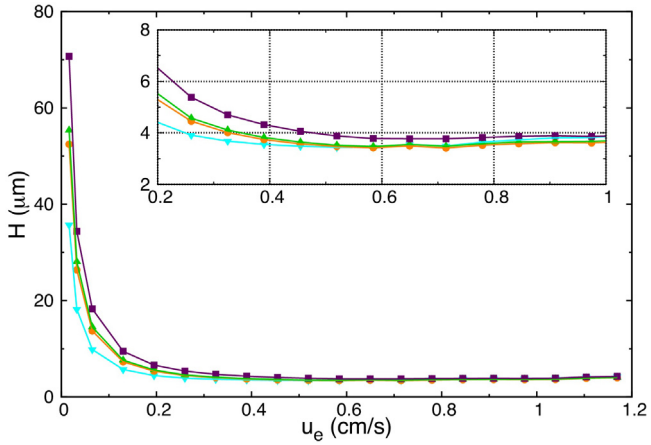

Fig. 3. Van Deemter plots showing the plate height, H, vs. the interstitial linear velocity, u_e, for the Titan C_{18} 50 mm × 3.0 mm. The inset zoom shows the region of interstitial velocity between 0.2 and 1. Experimental points: nitrobenzene (cyan), toluene (orange), ethylbenzene (green), butylbenzene (purple). The maximum u_e corresponds to a flow rate $F_v = 1.8$ mL/min (system back-pressure: 646 bar; column back-pressure: 410 bar). (For interpretation of the references to color in this figure legend, the reader is referred to the web version of this article.)

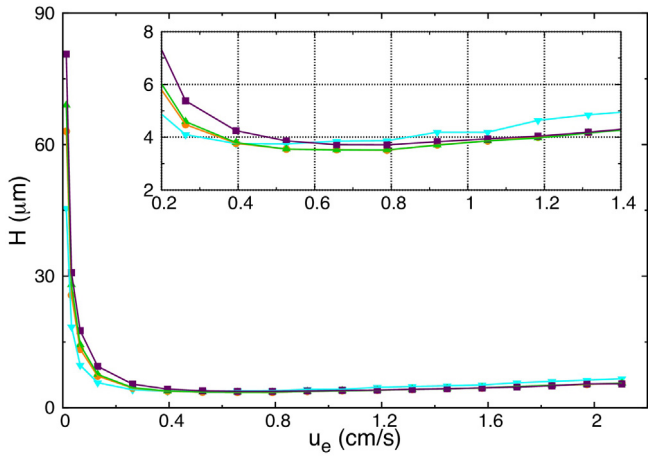

Fig. 4. Van Deemter plots showing the plate height, H, vs. the interstitial linear velocity, u_e, for the Titan C_{18} 50 mm × 2.1 mm. The inset zoom shows the region of interstitial velocity between 0.2 and 1.4. Experimental points: nitrobenzene (cyan), toluene (orange), ethylbenzene (green), butylbenzene (purple). The maximum u_e corresponds to a flow rate F_v = 1.6 mL/min (system back-pressure: 951 bar; column back-pressure: 743 bar). (For interpretation of the references to color in this figure legend, the reader is referred to the web version of this article.)

curves for columns of different geometries are reported as Supplementary Material. In these graphs, H is plotted as a function of the interstitial velocity, u_e:

$$u_e = \frac{F_v}{\pi r_c^2 \epsilon_e} \tag{9}$$

that is the average velocity of the mobile phase that moves between the particles [28]. From these plots, two common features can be evidenced. The first one is the very small value of the minimum H. For example, values as low as H_{min} = 3.5 μm (flow rate 0.6 mL/min, toluene compound) and H_{min} = 3.4 μm (flow rate 0.9 mL/min) were found for the 50 mm × 2.1 mm and the 50 mm × 3.0 mm columns, respectively. The second important aspect is that the so-called C-branch of the van Deemter curve is remarkably flat. For the cases reported in Figs. 3 and 4, for example, at the maximum flow rates, the estimated H values were 4.0 (column 3.0 mm × 50 mm, u_e = 1.2 cm/s, F_v = 1.8 mL/min) and 5.5 μm (column 2.1 mm × 50 mm, u_e = 2.1 cm/s, F_v = 1.6 mL/min). Analogous behavior was observed also for the other Titan C_{18} columns (see Supplementary Material for the van Deemter plots of the other columns).

Switching to reduced (or dimensionless) coordinates is a common way to compare packed beds of spherical particles [29,42,8]. Thus, all the next van Deemter curves are given in reduced coordinates, where the reduced velocity h:

$$h = \frac{H}{d_p} \tag{10}$$

is plotted against the reduced interstitial velocity ν:

$$\nu = \frac{u_e d_p}{D_m} \tag{11}$$

with D_m estimated through peak parking on a nonporous column (see before and Table 2). The reduced van Deemter curves of the 50 mm columns (3.0 and 2.1 mm i.d.) are presented in Fig. 5, where for the sake of comparison we decided to show the plots obtained by using both the nominal particle diameter (d_p = 1.9 μm) and the Sauter diameter (d_{Sauter} = 2.04 μm). By assuming d_p = 1.9 μm, the minimum reduced plate height was found to be h_{min} = 1.86 at ν_{opt} = 7.1 (50 mm × 3.0 mm column) and h_{min} = 1.92 at ν_{opt} = 7.9 (50 mm × 2.1 mm column). On the other hand, if h is

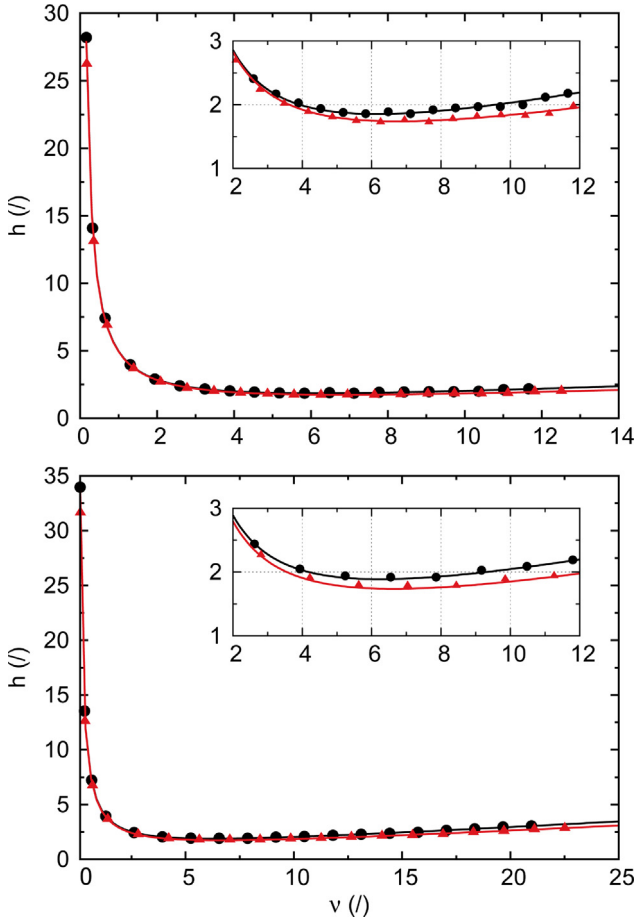

Fig. 5. d_p-based (black points) and d_{Sauter}-based (red triangles) reduced van Deemter plots (h vs. ν) for the Titan C_{18} 50 × 3.0 (top) and 50 × 2.1 (bottom) columns. The inset zoom shows the region of reduced velocity between 2 and 12. Compound: ethylbenzene. (For interpretation of the references to color in this figure legend, the reader is referred to the web version of this article.)

calculated by means of d_{Sauter}, the following values are obtained: h_{min} = 1.73 at ν_{opt} = 7.7 (50 mm × 3.0 mm column) and h_{min} = 1.79 at ν_{opt} = 8.5 (50 mm × 2.1 mm column). Remarkably, at the maximum ν = 12.5 and 22.5, respectively for the 50 mm × 3.0 mm and

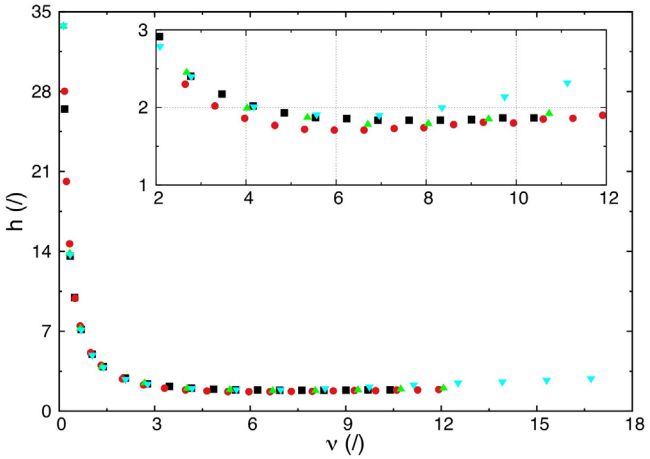

Fig. 6. d_{Sauter}-based reduced van Deemter plots (h vs. ν) for the two 100 mm and the two 75 mm Titan C_{18} columns. Columns: 100 mm × 3.0 mm (black); 75 mm × 3.0 mm (red); 100 mm × 2.1 mm (green); 75 mm × 2.1 mm (cyan). The inset zoom shows the region of reduced velocity between 2 and 12. Compound: ethylbenzene. (For interpretation of the references to color in this figure legend, the reader is referred to the web version of this article.)

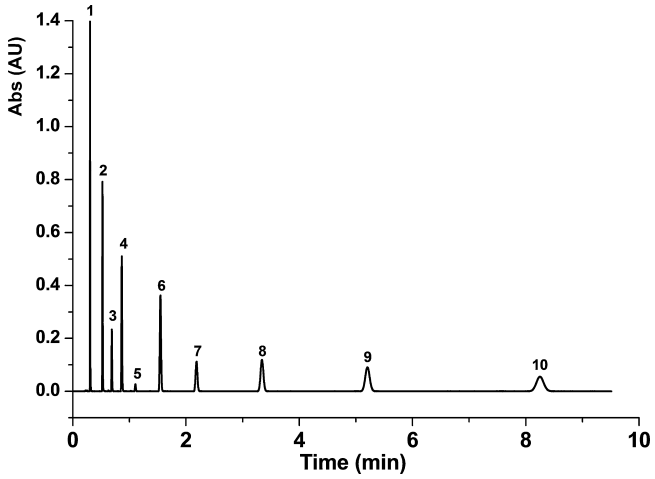

Fig. 7. Chromatogram showing the separation of a mixture of benzene derivatives on the Titan C_{18} 75 mm × 3.0 mm column. Flow rate: 0.9 mL/min. Mobile phase: ACN/water 60:40 (v/v); T = 35 °C. Compounds: (1) Uracil (258,933 N/m); (2) Phenol (300,280, k = 0.8); (3) Benzaldheyde (308,680 N/m, k = 1.3); (4) Nitrobenzene (314,160 N/m, k = 1.9); (5) Benzene (301,000 N/m, k = 2.8); (6) Toluene (296,200 N/m, k = 4.3); (7) Ethylbenzene (286,720 N/m, k = 6.5); (8) Propylbenzene (271,107 N/m, k = 10.6); (9) Butylbenzene (256,733 N/m, k = 17.1); (10) Pentylbenzene (236,920 N/m, k = 27.7). The retention factor k was calculated by using uracil as the void time marker.

the 50 mm × 2.1 mm columns, the d_{Sauter}-based h values were only 2.03 and 2.85, showing how these columns do not dramatically lose efficiency by increasing the flow rate over its optimum value.

The reduced (d_{Sauter}-based) van Deemter plots for the two 75 mm and the two 100 mm columns are given in Fig. 6. As expected, these curves nearly superimpose (so do the reduced van Deemter curves of Fig. 5, not shown in this figure). To demonstrate the great kinetic performance of the Titan C_{18} columns, able to generate some 300,000 N/m at the optimum flow rate, Fig. 7 shows the chromatogram for the separation of a mixture of benzene derivatives (phenol, benzaldehyde, nitrobenzene, benzene, toluene, ethylbenzene, propylbenzene, butylbenzene, pentylbenzene with retention factor k ranging from 1 to almost 28) obtained on the 75 mm × 3.0 mm Titan C_{18} column (see figure caption for details). In the Supplementary Material, a series of chromatograms for the separation of the same mixture of compounds obtained with the other Titan C_{18} columns are reported.

4. Conclusions

This study shows that the Titan C_{18} columns packed with the new 1.9 μm fully porous C_{18} particles are characterized by remarkably good kinetic performance under RP conditions. At their optimal flow rates, indeed, these columns were able to generate some 300,000 theoretical plates per meter (with a retention factor of 4) by using a series of benzene derivatives as test compounds. In addition, we have found that in the high-velocity regime, van Deemter curves remain essentially flat. Therefore, we could not observe the dramatic loss of performance reported in [25,26] when columns were operated at reduced velocity larger than 5.

In this work, we observed that the optimal reduced velocities for the Titan C_{18} column are comparable to those of columns packed with conventional fully porous C_{18} particles used in RP liquid chromatography (ν_{opt} = 8–10), but also that these columns perform very well at reduced velocity as large as 15–18. In the companion paper [1], we present the results of a detailed study on the different contributions to mass transfer within Titan C_{18} columns with the aim of understanding the rationale behind this performance and which factors contribute the more to plate height.

Acknowledgments

The authors thank the Italian University and Scientific Research Ministry (grant PRIN 2012ATMNJ_003) and the Laboratory Terra&Acqua Tech, member of Energy and Environment Cluster, Technopole of Ferrara of Emilia-Romagna High Technology Network. Dr. Valentina Costa from the University of Ferrara is acknowledged for technical support.

Appendix A. Supplementary data

Supplementary data associated with this article can be found, in the online version, at http://dx.doi.org/10.1016/j.chroma.2016.05.038.

References

[1] M. Catani, O.H. Ismail, A. Cavazzini, A. Ciogli, C. Villani, L. Pasti, D. Cabooter, G. Desmet, F. Gasparrini, D.S. Bell, Rationale behind the optimum efficiency of columns packed with the new 1.9 μm fully porous particles Titan c_{18}, J. Chromatogr. A (2016) (submitted for publication).
[2] F. Gritti, G. Guiochon, Perspectives on the evolution of the column efficiency in liquid chromatography, Anal. Chem. 85 (2013) 3017–3035.
[3] K. Broeckhoven, G. Desmet, The future of UHPLC: towards higher pressure and/or smaller particles? Trends Anal. Chem. 63 (2014) 65–75.
[4] J. Kirkland, J. DeStefano, The art and science of forming packed analytical high-performance liquid chromatography columns, J. Chromatogr. A 1126 (2006) 50–57.
[5] A.E. Reising, J.M. Godinho, K. Hormann, J.W. Jorgenson, U. Tallarek, Larger voids in mechanically stable, loose packings of 1.3 μm frictional, cohesive particles: their reconstruction, statistical analysis, and impact on separation efficiency, J. Chromatogr. A 1436 (2016) 118–132.
[6] Development of a New Monodisperse Porous Silica for UHPLC, Poster presented at 38th International Symposium on High Performance Liquid Phase Separations and Related Technique, (HPLC 2012), June 16–21, 2012, Anaheim, CA, USA.
[7] D.S. Bell, R.A. Henry, W. Betz, P. Ross, Advances in liquid chromatography particle technology: perspectives on the development and future of monodispersed silica supports, Chromatogr. today (May/June) (2015) 34–37.
[8] F. Gritti, G. Guiochon, Mass transfer kinetics, band broadening and column efficiency, J. Chromatogr. A 1221 (2012) 2–40.
[9] L.R. Snyder, Column efficiency in liquid–solid adsorption chromatography. H.E.T.P. (height equivalent to a theoretical plate) values as a function of separation conditions, Anal. Chem. 39 (1967) 698–704.
[10] J.N. Done, J.H. Knox, The performance of packings in high speed liquid chromatography II. ZIPAX®. The effect of particle size, J. Chromatogr. Sci. 10 (1972) 606–612.
[11] I. Halász, M. Naefe, Influence of column parameters on peak broadening in high-pressure liquid chromatography, Anal. Chem. 44 (1972) 76–84.
[12] R. Endele, I. Halász, K. Unger, Influence of the particle size (5–35 μm) of spherical silica on column efficiency in HPLC, J. Chromatogr. A 99 (1974) 377–393.
[13] C. Dewaele, M. Verzele, Influence of the particle size distribution of the packing material in reversed-phase high-performance liquid chromatography, J. Chromatogr. A 260 (1983) 13–21.
[14] J.J. Kirkland, J.J. DeStefano, T.J. Langlois, Fused-core particles for HPLC columns, Am. Lab. (February (39)) (2007) 18–21.
[15] A. Cavazzini, F. Gritti, K. Kaczmarski, N. Marchetti, G. Guiochon, Mass-transfer kinetics in a shell packing material for chromatography, Anal. Chem. 79 (2007) 5972–5979.
[16] F. Gritti, A. Cavazzini, N. Marchetti, G. Guiochon, Comparison between the efficiencies of columns packed with fully and partially porous C18-bonded silica materials, J. Chromatogr. A 1157 (2007) 289–303.
[17] N. Marchetti, A. Cavazzini, F. Gritti, G. Guiochon, Gradient elution separation and peak capacity of columns packed with porous shell particles, J. Chromatogr. A 1163 (2007) 203–211.
[18] S. Khirevich, A. Daneyko, A. Höltzel, A. Seidel-Morgenstern, U. Tallarek, Statistical analysis of packed beds, the origin of short-range disorder, and its impact on eddy dispersion, J. Chromatogr. A 1217 (2010) 4713–4722.
[19] K. Khirevich, A. Höltzel, A. Daneyko, U. Tallarek, Structure-transport correlation for the diffusive tortuosity of bulk, monodisperse, random sphere packings, J. Chromatogr. A 1218 (2011) 6489–6497.
[20] A. Daneyko, A. Höltzel, K. Khirevich, U. Tallarek, Influence of the particle size distribution on hydraulic permeability and eddy dispersion in bulk packings, Anal. Chem. 83 (2011) 3903–3910.
[21] F. Gritti, I. Leonardis, D. Shock, P. Stevenson, A. Shalliker, G. Guiochon, Performance of columns packed with the new shell particles Kinetex-C_{18}, J. Chromatogr. A 1217 (2010) 1589–1603.
[22] A. Daneyko, D. Hlushkou, S. Khirevich, U. Tallarek, From random sphere packings to regular pillar arrays: analysis of transverse dispersion, J. Chromatogr. A 1257 (2012) 98–115.

[23] S. Bruns, D. Stoeckel, B.M. Smarsly, U. Tallarek, Influence of particle properties on the wall region in packed capillaries, J. Chromatogr. A 1268 (2012) 53–63.
[24] S. Bruns, E.G. Franklin, J.P. Grinias, J.M. Godinho, J.W. Jorgenson, U. Tallarek, Slurry concentration effects on the bed morphology and separation efficiency of capillaries packed with sub-2 μm particles, J. Chromatogr. A 1318 (2013) 189–197.
[25] F. Gritti, D.S. Bell, G. Guiochon, Particle size distribution and column efficiency. An ongoing debate revived with 1.9 μm Titan-C_{18} particles, J. Chromatogr. A 1355 (2014) 179–192.
[26] F. Gritti, G. Guiochon, The rationale for the optimum efficiency of columns packed with new 1.9 μm fully porous Titan-C_{18} particles. A detailed investigation of the intra-particle diffusivity, J. Chromatogr. A 1355 (2014) 164–178.
[27] J.W. Thompson, R.A. Lieberman, J.W. Jorgenson, Hydrodynamic chromatography for the size classification of micron and sub-micron sized packing materials, J. Chromatogr. A 1216 (2009) 7732–7738.
[28] U.D. Neue, HPLC Columns: Theory, Technology and Practice, Wiley-VCH, 1997.
[29] J.C. Giddings, Dynamics of Chromatography, Marcel Dekker, New York, 1965.
[30] A. de Villiers, H. Lauer, R. Szucs, S. Goodall, P. Sandra, Influence of frictional heating on temperature gradients in ultra-high-pressure liquid chromatography on 2.1 mm i.d. columns, J. Chromatogr. A 1113 (2006) 84–91.
[31] D. Åsberg, J. Samuelsson, M. Lesko, A. Cavazzini, K. Kaczmarski, T. Fornstedt, Method transfer from high-pressure liquid chromatography to ultra-high-pressure liquid chromatography. II. Temperature and pressure effects, J. Chromatogr. A 1401 (2015) 52–59.
[32] I. Halász, K. Martin, Pore size of solids, Angew. Chem. Int. Ed. Engl. 17 (1978) 901–908.
[33] F. Gritti, G. Guiochon, A protocol for the measurement of all the parameters of the mass transfer kinetics in columns used in liquid chromatography, J. Chromatogr. A 1217 (2010) 5137–5151.
[34] D. Cabooter, J. Billen, H. Terryn, F. Lynen, P. Sandra, G. Desmet, Detailed characterisation of the flow resistance of commercial sub-2 μm reversed-phase columns, J. Chromatogr. A 1178 (2008) 108–117.
[35] J.H. Knox, R. Kaliszan, Theory of solvent disturbance peaks and experimental determination of thermodynamic dead-volume in column liquid chromatography, J. Chromatogr. 349 (1985) 211–234.
[36] G. Guiochon, A. Felinger, D.G. Shirazi, A.M. Katti, Fundamentals of Preparative and Nonlinear Chromatography, second ed., Academic Press, Elsevier, 2006.
[37] J.H. Knox, L. McLaren, New gas chromatographic method for measuring gaseous diffusion coefficients and obstructive factors, Anal. Chem. 36 (1964) 1477–1482.
[38] K. Miyabe, Y. Matsumoto, G. Guiochon, Peak parking-moment analysis. A strategy for the study of the mass-transfer kinetics in the stationary phase, Anal. Chem. 79 (2007) 1970–1982.
[39] D. Ludlum, R. Warner, H. Smith, The diffusion of thiourea in water at 25 °C, J. Phys. Chem. 66 (1962) 1540–1542.
[40] M.J. Rosen, J.T. Kunjappu, Surfactants and Interfacial Phenomena, Wiley & Sons, Inc., Hoboken, NJ, USA, 2012.
[41] J.F. Richardson, J.H. Harker, J.R. Backhurst, Coulson and Richardson's Chemical Engineering, vol. 2, fifth ed., Elsevier, Amsterdam, 2002 (Chapter 4).
[42] G. Desmet, D. Clicq, P. Gzil, Geometry-independent plate height representation methods for the direct comparison of the kinetic performance of LC supports with a different size morphology, Anal. Chem. 77 (2005) 4058–4070.

PAPER II

Journal of Chromatography A, 1454 (2016) 78–85

Contents lists available at ScienceDirect

Journal of Chromatography A

journal homepage: www.elsevier.com/locate/chroma

Rationale behind the optimum efficiency of columns packed with new 1.9 μm fully porous particles of narrow particle size distribution

Martina Catani[a], Omar H. Ismail[b], Alberto Cavazzini[a,*], Alessia Ciogli[b], Claudio Villani[b], Luisa Pasti[a], Caterina Bergantin[a], Deirdre Cabooter[c], Gert Desmet[d], Francesco Gasparrini[b], David S. Bell[e]

[a] Dept. of Chemistry and Pharmaceutical Sciences, University of Ferrara, via L. Borsari 46, 44121 Ferrara, Italy
[b] Dept. of Drug Chemistry and Technology, "Sapienza" Università di Roma, P.le A. Moro 5, 00185 Roma, Italy
[c] KU Leuven, Department of Pharmaceutical Sciences, Pharmaceutical Analysis, Herestraat 49, Leuven 3000, Belgium
[d] Vrije Universiteit Brussel (VUB), Department of Chemical Engineering, 1050 Brussels, Belgium
[e] Applied Research and Development, Millipore Sigma, 595 North Harrison Road, Bellefonte, PA 16823, USA

ARTICLE INFO

Article history:
Received 6 March 2016
Received in revised form 7 May 2016
Accepted 10 May 2016
Available online 12 May 2016

Keywords:
Column efficiency
Sub-2 μm fully porous particles of narrow particle size distribution (nPSD)
Mass transfer
Eddy dispersion

ABSTRACT

Columns packed with new commercially available 1.9 fully porous particles of narrow particle size distribution (nPSD) are characterized by extremely high efficiency. Under typical reversed phase conditions, these columns are able to generate very high number of theoretical plates (in the order of 300,000 plates/m and more). In this paper, we investigate the origin of the high performance of these nPSD columns by performing a series of measurements that include, in addition to the traditional determination of the van Deemter curve, peak parking, pore blocking and inverse size exclusion experiments. Two nPSD columns (both 100 × 3.0 mm) have been considered in this study: the first one, packed with particles of 80 Å pore size, is commercially available. The second one is a prototype column packed with 1.9 fully porous particles of 120 Å pore size.

The main conclusion of our study is that these nPSD columns are characterized by extremely low eddy dispersion, while longitudinal diffusion and mass transfer kinetics are substantially equivalent to those of other fully porous particles of similar chemistry.

1. Introduction

In the companion paper to this one [1], the kinetic performance of columns packed with the recently introduced 1.9 μm fully porous particles (average pore diameter 80 Å), known with the commercial name of Titan C_{18}, has been investigated by using a series of benzene derivatives under reversed phase (RP) conditions. The study was performed on a set of 6 columns (length: 50, 75 and 100 mm, internal diameter 2.1 and 3 mm) that represents, in our opinion, a large enough sample to draw reliable conclusions on their kinetic behaviour. The most relevant results from that study confirmed, on the one hand, the excellent kinetic performance of narrow particle size distribution (nPSD) columns already demonstrated in literature [2,3] (with reduced HETP, *h*, as small as 1.7–1.9) but, on the other hand, revealed how these columns can be very efficiently operated even at relatively large flow rates [1]. This latter conclusion thus contrasts those of Gritti and Guiochon [2,3] who observed, by using a series of phenone derivatives under RP conditions, a dramatic loss of performance when the column was operated at velocities slightly larger than the optimum. Gritti and Guiochon explained this finding on the base of the very low intraparticle diffusivity that would characterize the Titan C_{18} particles (about three times smaller, for a retention factor of 2, than for typical fully porous C_{18} particles). Following [2,3], the unusually low intraparticle diffusivity not only explains the very good performance of these columns at relatively low flow rates (thanks to very reduced longitudinal dispersion) but also their scarce performance at high flow rates due to slow mass transfer [2,3]. On the other hand, no effect on eddy dispersion was observed.

In the attempt of giving an explanation for the observed differences, in this study we present a detailed investigation of contributions to band broadening of the individual steps involved in the migration of the compound peaks through heterogeneous porous media. Essentially the same experimental protocol as in [2,3] was employed. It requires peak parking [4–7], total pore-blocking [8,9] and accurate HETP measurements. Combined with

* Corresponding author.
E-mail address: cvz@unife.it (A. Cavazzini).

http://dx.doi.org/10.1016/j.chroma.2016.05.037
0021-9673/

models of effective longitudinal diffusion through the packed bed [10–12], this information permits to achieve a physically-sound interpretation of mass transfer in modern liquid chromatography (LC) columns. The main study was performed by using a series of benzene derivatives as probe compounds, however, for the sake of comparison, the van Deemter curves of phenone derivatives used in [2,3] were also measured.

Finally, besides the Titan C_{18} column packed with 1.9 μm fully porous particles with average pore size 80 Å used in previous works [1–3], a prototype column (supplied by Supelco) was also fully characterized from a kinetic viewpoint. This column is packed with Titan C_{18} 1.9 μm but of average pore size 120 Å

2. Theory

Under the hypothesis of independence of the different contributions leading to peak broadening in LC [13,14], the functional relationship between the reduced plate height $h = H/d_p$ (being H the HETP and d_p the particle diameter) and the interstitial reduced velocity ν is commonly written as the sum of three terms including the eddy dispersion, $a(\nu)$, the longitudinal diffusion, b/ν, and the mass transfer resistance across the stationary phase, $c_s\nu$ [15,16], that is:

$$h = a(\nu) + \frac{b}{\nu} + c_s\nu \tag{1}$$

The interstitial reduced velocity is defined as:

$$\nu = \frac{u_e d_p}{D_m} \tag{2}$$

where D_m is the bulk molecular diffusion coefficient and u_e is the interstitial velocity, i.e. the velocity referred to the mobile phase moving between particles [17]:

$$u_e = \frac{F_v}{\pi r_c^2 \epsilon_e} \tag{3}$$

being F_v the flow rate, r_c the inner column radius and ϵ_e the external column porosity:

$$\epsilon_e = \frac{V_e}{V_{col}} \tag{4}$$

with V_{col} the geometric volume of the column.

For columns packed with very fine particles, usually a term accounting for the frictional heating due to the stream of the mobile phase against the bed under significant pressure must be added to Eq. (1). However, given the quasi-adiabatic conditions under which experiments were performed, it was not necessary to add this term [18–21].

The meaning of the different terms appearing in Eq. (1) is well known. The longitudinal (or axial) diffusion term describes the band broadening due to the diffusion of molecules through the porous particles and the interstitial volume in absence of flow. Since this is the only contribution to band broadening when the flow is switched off, it is best estimated through peak parking experiments [4–7]. In reduced coordinates, the longitudinal diffusion term b is given by [5,13,15,22]:

$$b = 2(1 + k_1)\frac{D_{eff}}{D_m} = 2(1 + k_1)\gamma_{eff} \tag{5}$$

where D_{eff} is the effective longitudinal diffusion coefficient, γ_{eff} ($= D_{eff}/D_m$) is the dimensionless effective diffusion coefficient and k_1 is the zone retention factor, defined as [5,23]:

$$k_1 = \frac{t_R - t_e}{t_e} \tag{6}$$

being t_R the retention time and t_e the time spent by a species molecule in the interstitial volume. k_1 is connected to the more often employed phase retention factor, k, via:

$$k_1 = \frac{(1 + k)\epsilon_{tot}}{\epsilon_e} - 1 \tag{7}$$

where ϵ_{tot} ($= V_0/V_{col}$, being V_0 the thermodynamic void volume) is the total column porosity. In place of the traditional Knox parallel zone model (also referred to as residence time weighted model) very often used in LC for the interpretation of D_{eff} [5,13,24,25], in this work we made use of the more advanced Effective Medium Theory (EMT) [26], which allows for a more physically-sound description of diffusion through complex composite porous media [10,11]. Among the many EMT models available in literature, the simplest Maxwell's expression of the effective longitudinal diffusion in fully porous ordered and random sphere packings is written as [10,11,15,27–30]:

$$D_{eff} = \frac{1}{\epsilon_e(1 + k_1)}\left[\frac{1 + 2(1 - \epsilon_e)\beta}{1 - (1 - \epsilon_e)\beta}\right] D_m \tag{8}$$

where β is the so-called polarizability constant:

$$\beta = \frac{\alpha_{part} - 1}{\alpha_{part} + 2} \tag{9}$$

and α_{part} is the relative permeability:

$$\alpha_{part} = \frac{D_{part} K_p}{D_m} \tag{10}$$

where D_{part} is the overall diffusion coefficient through the porous particles (including diffusion in the stagnant mobile phase and surface diffusion) and K_p is the whole-particle volume (V_{part})-based equilibrium constant, that is:

$$K_p = \frac{m/V_{part}}{C_m} \tag{11}$$

where m and C_m represent the mass of the adsorbed species and the equilibrium concentration in the mobile phase, respectively. Therefore, operatively, K_p can be calculated by:

$$K_p = \frac{k_1 \epsilon_e}{1 - \epsilon_e} \tag{12}$$

Other EMT models, such as for instance the Torquato's one, allows in principle for a more accurate estimation of these parameters. However, under the experimental conditions employed in this work (namely, retention factor always larger than 0.5), it has been demonstrated [12,28,29] that the difference between the simple Eq. (8) and the Torquato's model is negligible (see also later on).

The kinetic c_s term appearing in Eq. (1) describes the mass transfer across the stationary phase. Since there is absence of flow inside particles, the mass transfer coefficient across the stationary phase is velocity-independent, which makes it easier to establish theoretically-sound expression for this contribution [16]. Following Giddings [13], for fully porous spherical particles this term is commonly expressed as [15,22]:

$$c_s = \frac{1}{30}\frac{k_1}{(1 + k_1)^2}\frac{D_m}{D_{part}} \tag{13}$$

Finally, the eddy dispersion term, $a(\nu)$ in Eq. (1), is caused by the erratic flow profile in the through-pores of the packed bed. It includes trans-channel eddy dispersion, short-range inter-channel eddy dispersion, trans-column eddy dispersion. Despite the fundamental work of Giddings culminated in the well-known coupling theory [13], there is still considerable debate in literature regarding the values of the geometrical parameters needed to describe the complex structures of packed beds [31]. Much work in this direction has been done by Tallarek's group with a very sophisticated

approach based on the morphology reconstruction of the actual stationary phase structure and the calculation of transport properties in the reconstructed materials [32–35]. On the other hand, an experimental estimation of $a(\nu)$ can be achieved by subtracting to accurately measured h values (Eq. (1)) both the longitudinal diffusion and the mass transfer terms independently estimated by Eqs. (5) and (13) [15]:

$$a(\nu) = h - \frac{b}{\nu} - c_s\nu \tag{14}$$

3. Experimental

3.1. Columns and materials

Two 100 × 3.0 mm (length × internal-diameter) stainless steel Titan C_{18} columns packed with 1.9 μm particles of respectively 80 Å and 120 Å pore size were employed. C_{18} ligand density was 2 μmol/m^2 for the 80 Å column (specific surface area 400 m^2/g) and 3 μmol/m^2 for the 120 Å one (specific surface area 300 m^2/g). The columns were generously donated by Supelco Analytical (USA). Polystyrene standards (molecular weights 500, 2000, 2500, 5000, 9000, 17,500, 30,000, 50,000, 156,000, 330,000, 565,000, 1,030,000, 1,570,000, 2,310,000) employed for Inverse Size Exclusion measurements were purchased from Supelco. Decane, 2-propanol, tetrahydrofuran, uracil, phenol, nitrobenzene, benzaldehyde, benzene, toluene, ethylbenzene, butylbenzene, propylbenzene, pentylbenzene were from Sigma–Aldrich. Acetonitrile (ACN) was from VWR International. Ultra-high quality Milli-Q water was obtained by a Milli-Q water purification system (Millipore).

3.2. Equipment

A Waters Acquity UPLC, controlled by Empower 3 software and equipped with a binary solvent delivery system, an autosampler, a column thermostat, a photodiode array detector with a 500 nL cell, was used for the determination of the van Deemter curves. The equipment was operated under still-air [21,36] and quasi-adiabatic conditions. The maximum back pressure reachable by the system is 1000 bar. To reduce the extra-column contributions, two 250 × 0.075 mm nano-Viper capillary tubes (Thermo Scientific) were used to connect, respectively, the injector to the column and the column to the detector. The extra column peak variance, measured from the injector needle port to the detector cell, was 1.2 μL^2 (calculated through peak moments) at a flow rate of 1 mL/min. ISEC experiments were carried out on an Agilent 1100 Series Capillary LC system equipped with a binary pump system, an autosampler, a column thermostat and a photodiode array detector. This equipment was also employed for peak parking experiments.

3.3. Inverse size exclusion chromatography (ISEC)

ISEC measurements were performed by using tetrahydrofuran as the mobile phase [37]. Injection volume, flow rate and detection wavelength were, respectively, 2 μL, 0.1 mL/min and 254 nm. Retention volumes were corrected for the extra-column contribution before being plotted against the cubic root of the molecular weight. As shown in [1], the (ISEC estimation of) external column volume, V_e, is calculated by extrapolating the excluded branch of this plot. The thermodynamic void volume, V_0, was calculated from the corrected elution volume of benzene in tetrahydrofuran.

3.4. Total pore blocking

The external column volume was also estimated by using the so-called total pore blocking method [8,38]. In this case, columns were firstly flushed with 100 mL of 2-propanol and then with 60 mL of decane to fill with it the pores of the stationary phase. Finally, pure water was used to remove decane from interstitial space of columns. Complete removal of decane was confirmed by monitoring both DAD signal and column backpressure and by repeatedly injecting an unretained molecule (thiourea dissolved in pure water) until a constant elution volume was achieved, which gives (the total pore blocking estimation of) V_e. Columns were flushed again with 2-propanol to remove the blocking agent from the pores before further use.

3.5. Peak parking measurements

The flow rate used for peak parking measurements was 0.1 mL/min. Parking times were 0, 120, 600, 1800 and 3600 s. The detailed description of peak parking procedure is given in the companion paper [1].

3.6. Van Deemter curve measurements

The van Deemter curves for nitrobenzene, toluene, ethylbenzene and butylbenzene were measured at 35.0 ± 0.1 °C. The mobile phase was a binary mixture of ACN/water 60:40 v/v. The injection volume was 0.5 μL. Retention time and column efficiency (N) of eluted peaks were automatically calculated by the Empower software (v. 3). The detection wavelength was 214 nm; sampling rate was 80 points/s. Due to the very reduced extra-column volume of the modified Waters UPLC employed in this work (see before for details), no correction was applied to compensate for the extra-column contribution. The flow rates employed for studying the dependence of H on the mobile phase velocity were 0.025, 0.05, 0.1 mL/min and then, from 0.1 mL/min to the maximum reachable flow rate, step increments of 0.1 mL/min were applied (see figure captions for more information).

3.7. SEM measurements

SEM images of both bare-silica and C_{18}-functionalized Titan C_{18} particles were obtained with a Zeiss EVO 40. The instrument was operate with an accelerating voltage of 20 kV and with 5000× magnification. Particles were conductive enough to omit the use of carbon coating. Of every particle batch, the diameter of at least 500 particles was measured. To determine particle sizes, SEM pictures were uploaded in a drawing program (Windows Paint) and straight lines, corresponding to the diameter of particles, were manually drawn over them. This manual procedure was preferred because it allowed determining the position of particle circumference with the highest possible degree of precision and certainty. The length of straight lines was determined in an automated way using an in-house written script in Imaq Vision Builder (National Instruments Corporation, Austin, TX, USA). d_{Sauter} was calculated as:

$$d_{Sauter} = \frac{\sum_{i=1}^{n} n_i d_i^3}{\sum_{i=1}^{n} n_i d_i^2} \tag{15}$$

where d_i and n_i are, respectively, a given particle size and the number of particles with diameter included between d_i and $d_i + \Delta d_i$. Δd_i was assumed 0.07.

The particle size distribution of the different supports was subsequently determined from the nominal particle sizes, by

Table 1
Geometrical characteristics and physico-chemical properties of Titan C_{18} columns: total (ϵ_t), interstitial (ϵ_e) and particle (ϵ_p) porosities; specific permeability (k_0); Kozeny–Carman constant (K_c). Batch: number of silica batch. Calculation of K_c for the Titan C_{18} columns was based on d_{Sauter}. See Ref. [1] for further details.

Column	Batch #	ϵ_{tot}	ϵ_e	ϵ_p	$k_0 \times 10^{11}$ (cm^2)	K_C
Titan-C_{18}, 80 Å	7001	0.593	0.364	0.360	2.77	179
Titan-C_{18}, 120 Å	2090	0.597	0.369	0.361	2.70	170

expressing the diameter of at least 500 particles per column batch in a frequency distribution diagram. To properly normalize the graph (surface under curves should be unity), the results were plotted as $(d_{ave} \times n_i)/\sum(n_i \times \Delta d_i)$ vs. d_i/d_{ave}, being d_{ave} the average particle diameter.

4. Results and discussion

Geometric characteristics of Titan columns employed in this work are compared in Table 1 (experimental details on these measurements are given in [1]). ϵ_e was estimated by both ISEC and total pore blocking experiments. The agreement between the two techniques was within about ±3% (in Table 1, only the ISEC-based estimations of ϵ_e have been reported). It is worth to notice how experimental values of ϵ_e (0.364 and 0.369, respectively for the 80 and the 120 Å column) are very close to the theoretical limit (0.36) calculated by Baranau and Tallarek [39] for frictionless random-close packings of particles with a PSD similar to that of the Titan C_{18} columns (about 10%) [1]. This confirms that packing of columns has been extremely efficient. Due to the relationship between ϵ_e and hydraulic permeability, it is not surprising that specific permeabilities of columns (Table 1, sixth column) were also very similar (plots of column backpressure vs. mobile phase velocity needed for the estimation of k_0 are reported under Supporting Information).

The van Deemter curves measured on the two columns are given in Fig. 1 in the form of H vs. u_e. Four compounds were considered in this work, nitrobenzene, toluene, ethylbenzene and butylbenzene. They cover a wide range of retention factors going from 2.7 to more than 20 if given as zone retention factor k_1 (see Table 2, columns 2–3) or from 1.2 to 12.3, if expressed as phase retention factor k (see Table 2, columns 4–5 and Eq. (7)). Two important things can be evidenced by these curves. The first one is the excellent kinetic performance of both columns, with H values at the minimum of the van Deemter curves (H_{min}) significantly lower than twice the particle diameter, traditionally taken as a "reference" value for well-packed fully porous particle columns [17]. This is especially evident for the Titan C_{18} 120 Å column. Calculated as the average of the minimum heights obtained for the four compounds, indeed, H_{min} was 3.7 μm for the Titan C_{18} 80 Å column (at u_e roughly 0.65 cm/s) and only 3.3 μm for the Titan C_{18} 120 Å one (u_e approx. 0.7 cm/s). The second interesting aspect is that, up to maximum achievable velocity (back-pressure reachable by the system is max 1000 bar), van Deemter curves for all compounds on both columns are very flat. Therefore, Titan C_{18} columns can be employed at (relatively) large flow rates, without losing performance. As a visual proof of the excellent performance

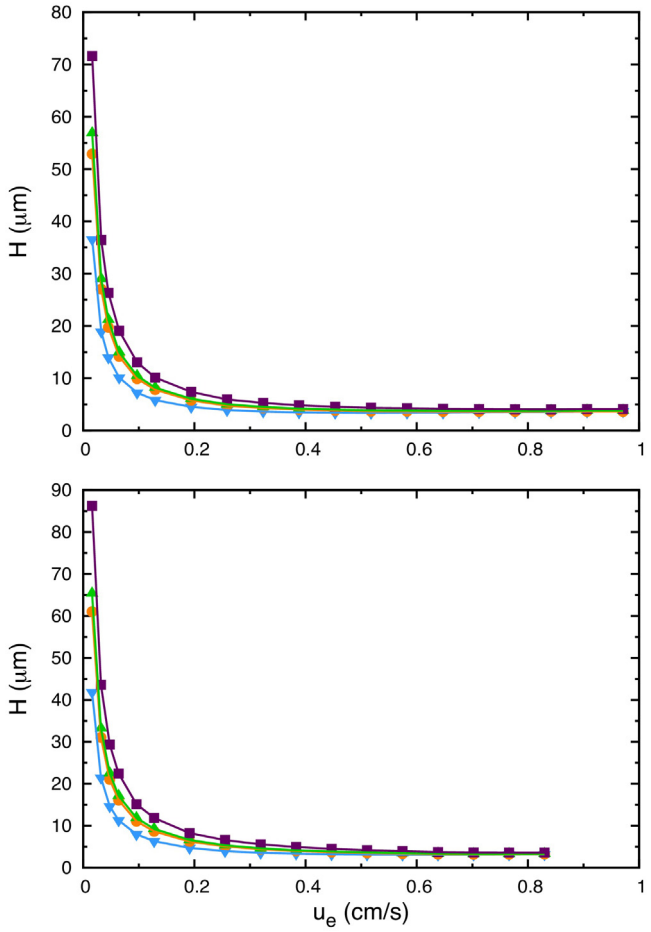

Fig. 1. van Deemter plots showing the plate height, H, vs. the interstitial linear velocity, u_e, for Titan C_{18} 80 Å (top) and 120 Å (bottom) columns. Experimental data: nitrobenzene (cyan), toluene (orange), ethylbenzene (green), butylbenzene (purple). The maximum u_e corresponds to a flow rate $F_v = 1.5$ mL/min for the Titan C_{18} 80 Å column (system back-pressure: 945 bar; column back-pressure: 764 bar) and 1.3 mL/min for the Titan C_{18} 120 Å one (system back-pressure: 829 bar; column back-pressure: 673 bar). (For interpretation of references to colour in this figure, readers are referred to the web version of the article.)

of these columns, in Figs. 2 and 3 the chromatograms for the separation of a mixture of benzene derivatives (including phenol, benzaldehyde, nitrobenzene, benzene, toluene, ethylbenzene, propylbenzene, butylbenzene, pentylbenzene), whose retention factors range from 1 to almost 24, are reported: some 300,000 and 320,000 N/m were measured on the Titan C_{18} 80 Å and the Titan C_{18} 120 Å column, respectively (see figure captions for details).

A more quantitative measure of column performance can be obtained by plotting the van Deemter curves in reduced coordinates. d_{Sauter}-based reduced van Deemter curves are shown in Fig. 4. Following [2], in these plots, d_{Sauter} was assumed equal to 2.04 μm. Impressive reduced h_{min}s were observed. For instance, h_{min} as small as 1.65 (at $\nu_{opt} = 5.5$) and 1.52 (at $\nu_{opt} = 6.1$) was obtained with

Table 2
Zone retention factor (k_1), retention factor (k), optimal reduced velocity (ν_{opt}), minimum reduced plate height (h_{min}) and reduced plate height at the maximum reduced velocity (ν_{max}) for the four compounds on the two Titan C_{18} columns.

	k_1		k		ν_{opt}		h_{min}		h (ν_{max})	
	80 Å	120 Å	80 Å	120 Å	80 Å	120 Å	80 Å	120 Å	80 Å	120 Å
Nitrobenzene	2.7	2.7	1.3	1.3	5.5	6.1	1.65	1.52	1.80 (10.3)	1.57 (8.8)
Toluene	5.6	5.6	3.1	3.1	6.3	6.8	1.78	1.57	1.79 (9.4)	1.59 (8.1)
Ethylbenzene	8.0	8.1	4.5	4.7	8.4	7.6	1.85	1.62	1.87 (10.6)	1.63 (9.0)
Butylbenzene	19.1	20.5	11.3	12.3	9.8	8.9	1.98	1.77	2.00 (11.3)	1.78 (9.6)

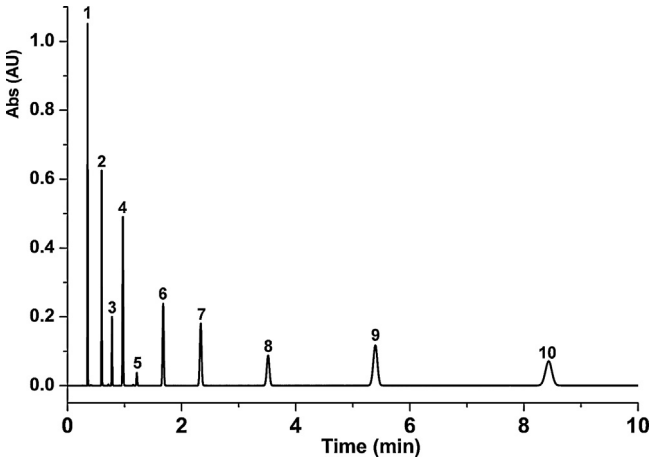

Fig. 2. Chromatogram showing the separation of a mixture of benzene derivatives on the Titan C_{18} 80 Å column. Flow rate: 1.0 mL/min. Mobile phase: ACN/water 60:40, v/v; $T = 35\,^{\circ}C$. Compounds: (1) Uracil (255,980 N/m); (2) Phenol (283,000, $k = 0.7$); (3) Benzaldheyde (289,160 N/m, $k = 1.3$); (4) Nitrobenzene (291,850 N/m, $k = 1.9$); (5) Benzene (280,660 N/m, $k = 2.6$); (6) Toluene (279,800 N/m, $k = 4.0$); (7) Ethylbenzene (264,080 N/m, $k = 5.9$); (8) Propylbenzene (251,060 N/m, $k = 9.4$); (9) Butylbenzene (241,010 N/m, $k = 15.1$); (10) Pentylbenzene (230,270 N/m, $k = 24.1$). The retention factor k was calculated by using uracil as the void time marker.

nitrobenzene ($k = 1.3$), respectively on the Titan C_{18} 80 Å and the Titan C_{18} 120 Å column. h_{min} and ν_{opt} for all the compounds considered in this work are reported in Table 2 (columns 5–8).

From the data reported in the last two columns of this table, one may also appreciate how the efficiency of columns is substantially maintained at the largest velocities reached in this work. For instance, by considering ethylbenzene ($k_1 \simeq 8.0$), h changes by only about 1%, on the Titan C_{18} 80 Å column, going from ν_{opt} (8.4) to the maximum velocity $\nu_{max} = 10.6$ and by less than 1%, on the Titan C_{18} 120 Å one, passing from $\nu_{opt} = 7.6$ to $\nu_{max} = 9$. Even though the compounds employed for measuring column performance are different (benzene- vs. phenone-derivatives), this example allows for a qualitative comparison with the work by Gritti and Guiochon [2,3] who obtained, on a Titan C_{18} 80 Å column (100 × 3 mm) under RP conditions for a compound with comparable retention

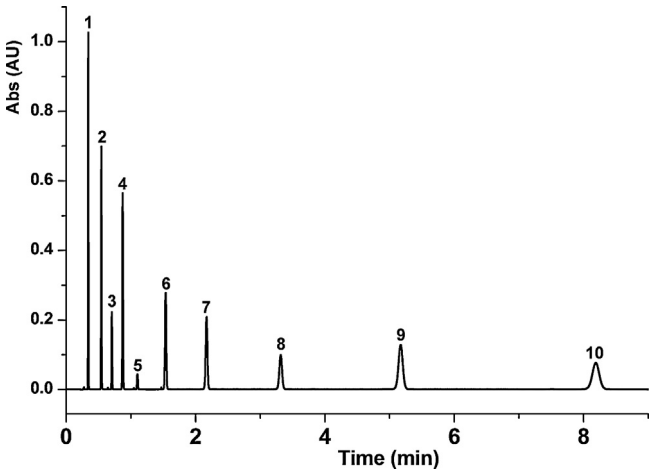

Fig. 3. Chromatogram showing the separation of a mixture of benzene derivatives on the Titan C_{18} 120 Å column. Flow rate: 1.1 mL/min. Mobile phase: ACN/water 60:40, v/v; $T = 35\,^{\circ}C$. Compounds: (1) Uracil (235,310 N/m); (2) Phenol (298,700, $k = 0.4$); (3) Benzaldheyde (310,320 N/m, $k = 1.0$); (4) Nitrobenzene (320,320 N/m, $k = 1.6$); (5) Benzene (306,722 N/m, $k = 2.3$); (6) Toluene (312,330 N/m, $k = 3.7$); (7) Ethylbenzene (302,840 N/m, $k = 5.6$); (8) Propylbenzene (288,995 N/m, $k = 9.1$); (9) Butylbenzene (274,270 N/m, $k = 14.8$); (10) Pentylbenzene (255,640 N/m, $k = 24.0$). The retention factor k was calculated by using uracil as the void time marker.

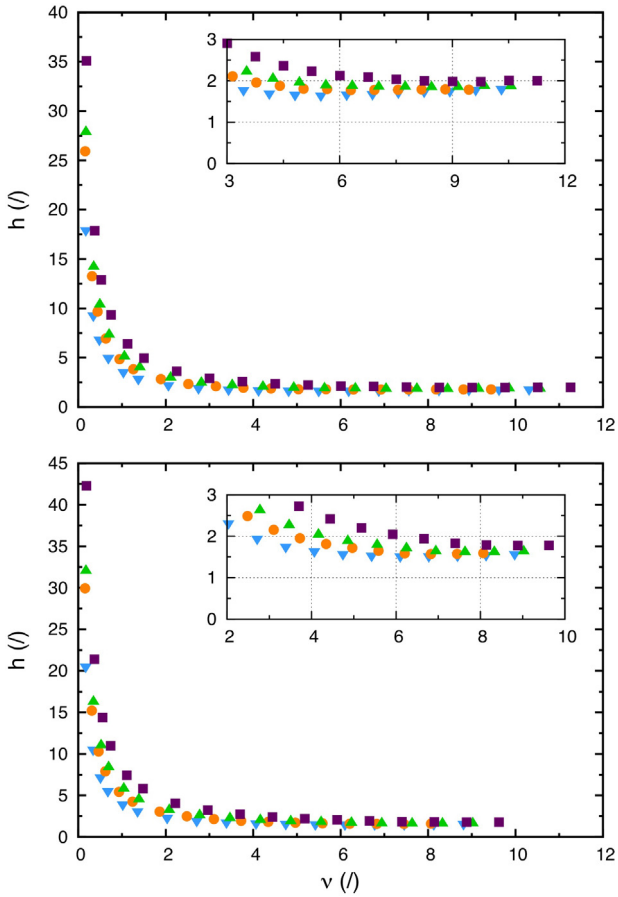

Fig. 4. d_{Sauter}-based ($d_{Sauter} = 2.04$) reduced van Deemter plots (h vs. ν) for Titan C_{18} 80 Å (top) and 120 Å (bottom) columns. Insets: zooms of regions corresponding to reduced interstitial velocity between 3–12 (80 Å column) and 2–10 (120 Å column). Experimental points: nitrobenzene (cyan), toluene (orange), ethylbenzene (green), butylbenzene (purple). (For interpretation of references to colour in this figure, readers are referred to the web version of the article.)

(octaphenone, $k_1 = 10.2$), very similar h_{min} (1.7) but at a significantly lower optimal velocity $\nu_{opt} = 5$. Contrary to us, in addition, they observed a dramatic loss of efficiency by slightly increasing the flow rate over the optimum value. As it was already mentioned before, the explanation proposed by Gritti and Guiochon [3] to explain this behaviour is that C_{18} fully porous Titan particles are characterized by an unusually low (if compared to other particles of similar geometrical characteristics and chemistry) intraparticle diffusivity. To further compare our results with those of Gritti and Guiochon, we therefore performed a series of van Deemter curve measurements by using the same set of phenone derivatives employed in [2,3] (acetophenone, propiophenone, butyrrophenone, valerophenone, hexanophenone) as probe compounds. The detailed results of this study are given as Supplementary Information. The performance of columns with phenones were substantially similar to those with benzene derivatives (e.g., on the Titan C_{18} 80 Å column, the average H_{min} calculated on the five phenones was 3.25 at $u_e = 0.45$ vs. average $H_{min} = 3.7$ at $u_e = 0.65$ for benzene derivatives, see before). In addition, we could not observe the same loss of performance, by increasing the flow rate over its optimum value, as reported in [2,3].

For the sake of comparison between different packing porous particles used in LC, the Titan C_{18} 80 Å column was emptied and particles were subjected to SEM analysis. After elaboration of SEM images (reported under Supplementary Information), PSD and d_{Sauter} of Titan C_{18} 80 Å particles were calculated as described under

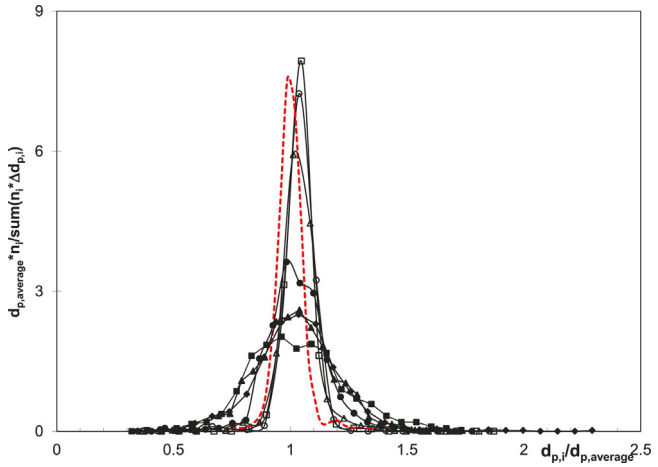

Fig. 5. Normalized particle size distributions (from SEM images) of the Titan C_{18} material (d_p = 1.9 μm) (red dotted line), compared to that of some common fully porous and superficially porous particles: XBridge C_{18} (d_p = 3.5 μm) (■), ACE3 C_{18} (d_p = 3.0 μm) (●), Gemini NX C_{18} (d_p = 3.0 μm) (♦), Hypersil GOLD C_{18} (d_p = 3.0 μm) (▲), Kinetex Fused Core C_{18} (d_p = 2.6 μm) (□), HALO Fused Core C_{18} (d_p = 2.7 μm) (△) and Poroshell C_{18} (d_p = 2.7 μm) (○). (For interpretation of references to colour in this figure, readers are referred to the web version of the article.)
Data adapted from [40].

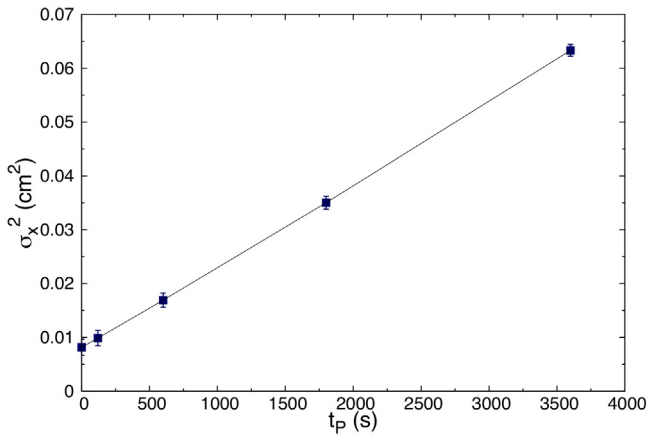

Fig. 6. Band broadening (spatial peak variance, σ_x^2) as a function of parking time, t_p. Compound: toluene; eluent: ACN/water 60:40 v/v%; T = 35 °C; column: Titan C_{18} 80 Å. Linear regression coefficient, $R^2 > 0.999$.

Section 3. In Fig. 5, the normalized PSD of Titan C_{18} 80 Å particles is represented together with those of some common fully porous and superficially porous particles (see figure caption for details), whose PSD was calculated in the same manner in [40]. From this figure, it is evident that Titan particles have an extremely narrow PSD, even comparable to those of superficially porous particles (which are well known for being characterized by nPSDs) and significantly narrower than those of other common fully porous particles. A strong (nearly linear) correlation between the width of the PSD and the *a*-term of the van Deemter equation has been previously observed [40] and could indicate that the excellent performance and low reduced *a*-terms observed for the Titan particles in this study are a consequence of their excellent packing structure. On the other hand, application of Eq. (15) to SEM image of Titan C_{18} 80 Å particles returned d_{Sauter} = 2.4 μm. By recalculating h_{min} and ν_{opt} based on this value, an average h_{min} (calculated on the four compounds) of 1.56 at ν_{opt} = 8.16 was obtained.

In the following, the single terms of the van Deemter equation on Titan C_{18} columns will be independently evaluated by following an approach based on the combination of stop-flow experiments and the EMT-based Maxwell's model (Eq. (8)) for the interpretation of diffusion through porous media. We anticipate that, for the sake of comparison, all parameters were estimated also through the more sophisticated Torquato's model (see before). The results of these calculations are reported as Supporting Information. Essentially, only very small differences were observed between the coefficients calculated by the Maxwell's model and the Torquato's one. For the calculation of the *b*-term, the knowledge of the apparent or effective axial diffusion coefficient D_{eff} is required (Eq. (5)). As it was detailedly described in [1] (but for the estimation of the bulk molecular diffusion D_m), D_{eff} can be estimated by the slope of the plot reporting the variance of the eluted peak against the time the peak was left to diffuse inside the Titan C_{18} columns without flow (parking time). One example of such a plot is given in Fig. 6. D_{eff} and *b* coefficients for the compounds considered in this work are reported in Table 3, while the dependence of b/ν on ν is given graphically in Fig. 7 (red points, right *y*-axis). As it can be seen from these data, in all cases, *b* represents roughly 35–40% of h_{min}, which is the typical value for modern columns packed with fully porous particles [12,41]. On the other hand, *b*-terms estimated in this work are some 15% larger than those reported by Gritti and Guiochon for Titan C_{18} 80 Å columns in [3,42] (at comparable k_1).

According to the EMT, the correct driving force for diffusion in presence of preferential solubility (such as in LC) is the gradient in chemical potential and not the gradient in concentration. Accordingly, the correct property obeying EMT-rules is the permeability and not the diffusivity [10]. The calculation of the relative permeability, α_{part}, can be easily performed from Eqs. (10) and (9) since β can be unequivocally measured from Eq. (8) (being D_{eff}, ϵ_e, k_1 and D_m known). α_{part} values are reported in Table 3. α_{part} corresponds to the so-called sample intraparticle diffusivity, Ω, of [3,42]. Therefore, following what is usually done in literature [12,42], these values can be expressed as a function of k_1 and compared each others. This comparison, whose results are graphically given under Supporting Information, has evidenced that α_{part}s measured in this work are about 30% larger than values given in [42].

The next step is the estimation of D_{part}, which can be done by means of Eq. (10), once K_p (Eq. (12)) is known (see Table 3, columns 8–11). Interestingly, for all benzene derivatives, D_{part} was found about 20% larger on the Titan C_{18} 120 Å column than on the 80 Å one. The faster the intraparticle mass transfer, the smaller the c_s term (Eq. (13)) of the van Deemter equation. Indeed, Table 3 (columns 12–13) shows how c_ss on the Titan 120 Å column are about 20%

Table 3
Effective diffusion coefficient (D_{eff}), reduced longitudinal diffusion coefficient (b), relative permeability (α_{part}), whole-particle volume based equilibrium constant (K_p), overall diffusion coefficient through the porous particles (D_{part}) and mass transfer resistance across the stationary phase coefficient (c_s) for the four compounds in ACN/water 60:40 (v/v) at 35 °C on Titan C_{18} columns.

	$D_{eff} \times 10^6$ (cm^2/s)		b		α_{part}		K_p		$D_{part} \times 10^6$ (cm^2/s)		c_s	
	80 Å	120 Å	80 Å	120 Å	80 Å	120 Å	80 Å	120 Å	80 Å	120 Å	80 Å	120 Å
Nitrobenzene	8.50	9.51	3.32	3.65	0.42	0.51	1.9	1.9	5.31	6.27	0.0244	0.0202
Toluene	6.85	7.64	4.31	4.78	0.67	0.82	4.4	4.5	4.42	5.27	0.0204	0.0171
Ethylbenzene	5.25	5.83	5.03	5.68	0.87	1.08	6.6	6.9	3.57	4.24	0.0173	0.0144
Butylbenzene	2.98	3.27	6.79	7.98	1.39	1.83	16.5	18.2	2.24	2.68	0.0124	0.0097

Table 4
Comparison between eddy dispersion values at $\nu \simeq 10$ between columns of different dimensions and particle diameters (d_p) packed with fully porous(*) (including Titan C_{18} 80 Å and 120 Å columns) and core–shell(**) particles. The last column reports literature reference from where the information was taken (JCA: Journal of Chromatography A).

Column	d_p	Length × I.D. (mm)	a ($\nu \sim 10$)	Ref.
Symmetry(*)	5.0	150 × 4.6	1.30	JCA, 1355, 2014, 164 [3]
Luna(*)	5.0	150 × 4.6	1.60	JCA, 1355, 2014, 179 [2]
Titan 80 Å(*)	1.9	100 × 3.0	1.20	This work
Titan 120 Å(*)	1.9	100 × 3.0	1.00	This work
Kinetex 1.7(**)	1.7	100 × 4.6	1.80–1.90	JCA, 1355, 2014, 179 [2]
Kinetex 2.6(**)	2.6	100 × 4.6	0.90–1.00	JCA, 1217, 2010, 1589 [44]

smaller than those measured on the 80 Å one. Fig. 7 (green triangles, left y-axis) represents as the term $c_s\nu$ changes by changing ν. In terms of c_s coefficient, the comparison between our data and those obtained by Gritti and Guiochon [42] with a similar Titan C_{18} 80 Å column shows that c_s-terms measured in this work are about 25–30% smaller than those obtained for phenones of comparable k_1.

Finally, the information in our possession permits to estimate $a(\nu)$ by difference between h and the independent estimates of b and c_s (Eq. (14)). Fig. 7 (blue squares, left y-axis) shows how $a(\nu)$ changes with ν for the two Titan C_{18} columns. $a(\nu)$ was calculated as the average of the values obtained for the four compounds. As it can be seen, eddy dispersion term presents the typical asymptotic behaviour already reported by other authors, e.g. [15,43].

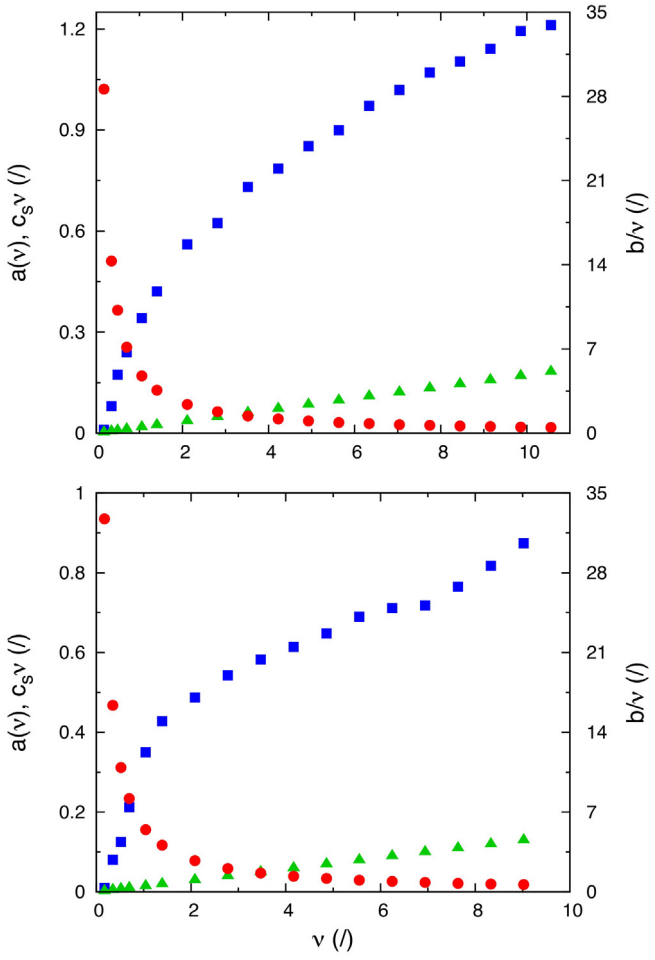

Fig. 7. Plot showing the average contribution of a- b- and c_s-term to h for the Titan C_{18} 80 Å column (top) and the 120 Å one (bottom). $a(\nu)$ (blue squares) and $c_s\nu$ (green triangles): left y-axis. b/ν (red circles): right y-axis. Averages were calculated on the four compounds considered in this work. (For interpretation of references to colour in this figure, readers are referred to the web version of the article.)

However, on the Titan columns, $a(\nu_{max})$ is remarkably small. Indeed at $\nu_{max} \simeq 10$, its value is only 1.2 on the Titan C_{18} 80 Å column and even 1.0 on the Titan C_{18} 120 Å one. In Table 4, eddy dispersion values (at $\nu \simeq 10$) taken from literature for different fully porous and core–shell commercial particles are reported. These data point out the very small eddy dispersion of Titan C_{18} columns, particularly for the Titan C_{18} 120 Å one, whose a-term is very close to that of core–shell Kinetex 2.6 μm particles [44]. Fig. 7 also shows that, by increasing the flow rate, $a(\nu)$ increases less on the 120 Å column than on the 80 Å one, but it is very difficult to provide a physically-sound explanation to these experimental findings. In a recent study, it was observed that the inner particle morphology of a packing also has a significant effect on the dispersion [45]. The combination of nPSD and differences in pore size of the 80 Å and 120 Å could hence provide an explanation for the observed differences in eddy dispersion, that are anyhow very small in both cases.

5. Conclusions

A detailed investigation of mass transfer processes on two nPSD Titan C_{18} columns, by employing a series of benzene derivatives as test compounds, has revealed that these columns are characterized by an extremely small eddy dispersion, even comparable to those of columns packed with core–shell particles. On the other hand, contrary to previous conclusions, the b and c_s terms of the van Deemter equation were found to be essentially comparable to those of other columns packed with particles of similar chemistry and characteristics. Our findings therefore do not confirm the previous hypothesis that the extraordinary efficiency of these nPSD columns is generated by a very small intraparticle diffusion. We observe that the differences in the experimental conditions employed in this work and in [2,3] are too small (namely, about 10 °C in temperature and 15 v/v% in the amount of ACN in the eluent) to explain the observed differences in b and c_s terms. Analogously, equipment characteristics (extra-column volume, etc.) were demonstrated not to significantly contribute (see [1]). Moreover, on the Titan C_{18} 80 Å column employed in this work, the behaviour of phenone derivatives was found to be comparable to that of benzene derivatives (see Supporting Information), so that this variable can be excluded as well. Thus, the only significant difference between the Titan C_{18} 80 Å columns used in this work and those employed in [2,3] is in their external porosity and permeability. In [2,3], indeed, the authors found a permeability about 40% larger than in our case. However, they report about a dramatic loss of performance of columns at high flow rates due to frictional heating that, at comparable flow rates (and column geometries), was not observed in our case. In conclusion, without knowing the individual history of columns, it is very difficult to compare our results with those given in [2,3]. On the other hand, we believe that this work (together with its companion [1]) demonstrates that the value of using nPSD particles in HPLC is a question that is still controversial and open and that requires, to be solved, the collection of accurate (and reproducible) experimental data.

Acknowledgments

The authors thank the Italian University and Scientific Research Ministry (Grant PRIN 2012ATMNJ_003) and the Laboratory Terra&Acqua Tech, Member of Energy and Environment Cluster, Technopole of Ferrara of Emilia-Romagna High Technology Network. Dr. Valentina Costa from the University of Ferrara is acknowledged for technical support. Dr. Daniela Palmeri from the University of Ferrara is acknowledged for SEM measurements.

Appendix A. Supplementary data

Supplementary data associated with this article can be found, in the online version, at http://dx.doi.org/10.1016/j.chroma.2016.05.037.

References

[1] O.H. Ismail, M. Catani, L. Pasti, A. Cavazzini, A. Ciogli, C. Villani, D. Kotoni, F. Gasparrini, D.S. Bell, Experimental evidence of the kinetic performance achievable with columns packed with the new 1.9 μm fully porous particles Titan C_{18}, J. Chromatogr. A (2016), http://dx.doi.org/10.1016/j.chroma.2016.05.038.
[2] F. Gritti, D.S. Bell, G. Guiochon, Particle size distribution and column efficiency. An ongoing debate revived with 1.9 μm Titan-C_{18} particles, J. Chromatogr. A 1355 (2014) 179–192.
[3] F. Gritti, G. Guiochon, The rationale for the optimum efficiency of columns packed with new 1.9 μm fully porous Titan-C_{18} particles. A detailed investigation of the intra-particle diffusivity, J. Chromatogr. A 1355 (2014) 164–178.
[4] J.H. Knox, L. McLaren, New gas chromatographic method for measuring gaseous diffusion coefficients and obstructive factors, Anal. Chem. 36 (1964) 1477–1482.
[5] J.H. Knox, H.P. Scott, B and C terms in the van Deemter equation for liquid chromatography, J. Chromatogr. 282 (1983) 297–313.
[6] K. Miyabe, Y. Matsumoto, G. Guiochon, Peak parking-moment analysis. A strategy for the study of the mass-transfer kinetics in the stationary phase, Anal. Chem. 79 (2007) 1970–1982.
[7] K. Miyabe, N. Ando, G. Guiochon, Peak parking method for measurement of molecular diffusivity in liquid phase systems, J. Chromatogr. A 1216 (2009) 4377–4382.
[8] D. Cabooter, F. Lynen, P. Sandra, G. Desmet, Total pore blocking as an alternative method for the on-column determination of the external porosity of packed and monolithic reversed-phase columns, J. Chromatogr. A 1157 (2007) 131–141.
[9] A. Liekens, D. Cabooter, J. Denayer, G. Desmet, A study of the parameters affecting the accuracy of the total pore blocking method, J. Chromatogr. A 1217 (2010) 6754–6761.
[10] G. Desmet, K. Broeckhoven, J. De Smet, S. Deridder, G.V. Baron, P. Gzil, Errors involved in the existing B-term expressions for the longitudinal diffusion in fully porous chromatographic media. Part I: Computational data in ordered pillar arrays and effective medium theory, J. Chromatogr. A 1188 (2008) 171–188.
[11] K. Broeckhoven, D. Cabooter, F. Lynen, P. Sandra, G. Desmet, Errors involved in the existing B-term expressions for the longitudinal diffusion in fully porous chromatographic media. Part II: Experimental data in packed columns and surface diffusion measurements, J. Chromatogr. A 1188 (2008) 189–198.
[12] A. Liekens, J. Denayer, G. Desmet, Experimental investigation of the difference in b-term dominated band broadening between fully porous and porous-shell particles for liquid chromatography using the effective medium theory, J. Chromatogr. A 1218 (2011) 4406–4416.
[13] J.C. Giddings, Dynamics of Chromatography, Marcel Dekker, New York, 1965.
[14] D. De Wilde, F. Detobel, J. Deconinck, G. Desmet, A numerical study of the assumptions underlying the calculation of the stationary zone mass transfer coefficient in the general plate height model of chromatography in two-dimensional pillar arrays, J. Chromatogr. A 1217 (2010) 1942–1949.
[15] F. Gritti, G. Guiochon, Mass transfer kinetics, band broadening and column efficiency, J. Chromatogr. A 1221 (2012) 2–40.
[16] G. Desmet, K. Broeckhoven, Equivalence of the different Cm- and Cs-term expressions used in liquid chromatography and a geometrical model uniting them, Anal. Chem. 80 (2008) 8076–8088.
[17] U.D. Neue, HPLC Columns: Theory, Technology and Practice, Wiley-VCH, 1997.
[18] C. Horváth, H.J. Lin, Band spreading in liquid chromatography: general plate height equation and a method for the evaluation of the individual plate height contributions, J. Chromatogr. 149 (1978) 43–70.
[19] H. Poppe, J.C. Kraak, J.F.K. Huber, J.H.M.V. Berg, Temperature gradients in HPLC columns due to viscous heat dissipation, Chromatographia 14 (1981) 515–523.
[20] I. Halász, R. Endele, J. Asshauer, Ultimate limits in high-pressure liquid chromatography, J. Chromatogr. 112 (1975) 37–60.
[21] A. de Villiers, H. Lauer, R. Szucs, S. Goodall, P. Sandra, Influence of frictional heating on temperature gradients in ultra-high-pressure liquid chromatography on 2.1 mm i.d. columns, J. Chromatogr. A 1113 (2006) 84–91.
[22] G. Desmet, D. Cabooter, K. Broeckhoven, Graphical data representation methods to assess the quality of LC columns, Anal. Chem. 87 (2015) 8593–8602.
[23] J.H. Knox, Practical aspects of LC theory, J. Chromatogr. Sci. 15 (1977) 352–364.
[24] R.W. Stout, J.J. DeStefano, L.R. Snyder, High-performance liquid chromatographic column efficiency as a function of particle composition and geometry and capacity factor, J. Chromatogr. 282 (1983) 263–286.
[25] F. Gritti, G. Guiochon, General HETP equation for the study of mass-transfer mechanisms in RPLC, Anal. Chem. 78 (2006) 5347–5392.
[26] H.T. Davis, The effective medium theory of diffusion in composite media, J. Am. Ceram. Soc. 60 (1977) 499–501.
[27] M. Barrande, R. Bouchet, R. Denoyel, Tortuosity of porous particles, Anal. Chem. 79 (2007) 9115–9121.
[28] G. Desmet, S. Deridder, Effective medium theory expressions for the effective diffusion in chromatographic beds filled with porous, non-porous and porous-shell particles and cylinders. Part I: Theory, J. Chromatogr. A 1218 (2011) 32–45.
[29] S. Deridder, G. Desmet, Effective medium theory expressions for the effective diffusion in chromatographic beds filled with porous, non-porous and porous-shell particles and cylinders. Part II: Numerical verification and quantitative effect of solid core on expected B-term band broadening, J. Chromatogr. A 1218 (2011) 46–56.
[30] A. Liekens, J. Billen, R. Sherant, H. Ritchie, J. Denayer, G. Desmet, High performance liquid chromatography column packings with deliberately broadened particle size distribution: relation between column performance and packing structure, J. Chromatogr. A 1218 (2011) 6654–6662.
[31] G. Desmet, S. Eeltink, Fundamentals for LC miniaturization, Anal. Chem. 85 (2013) 543–556.
[32] S. Bruns, T. Müllner, M. Kollmann, J. Schachtner, A. Höltzel, U. Tallarek, Confocal laser scanning microscopy method for quantitative characterization of silica monolith morphology, Anal. Chem. 82 (2010) 6569–6575.
[33] S. Bruns, U. Tallarek, Physical reconstruction of packed beds and their morphological analysis: core–shell packings as an example, J. Chromatogr. A 1218 (2011) 1849–1860.
[34] D. Hlushkou, S. Bruns, U. Tallarek, High-performance computing of flow and transport in physically reconstructed silica monoliths, J. Chromatogr. A 1217 (2010) 3674–3682.
[35] S. Bruns, J.P. Grinias, L.E. Blue, J.W. Jorgenson, U. Tallarek, Morphology and separation efficiency of low-aspect-ratio capillary ultrahigh pressure liquid chromatography columns, Anal. Chem. 84 (2012) 4496–4503.
[36] D. Åsberg, J. Samuelsson, M. Lesko, A. Cavazzini, K. Kaczmarski, T. Fornstedt, Method transfer from high-pressure liquid chromatography to ultra-high-pressure liquid chromatography. II. Temperature and pressure effects, J. Chromatogr. A 1401 (2015) 52–59.
[37] I. Halász, K. Martin, Pore size of solids, Angew. Chem. Int. Ed. Engl. 17 (1978) 901–908.
[38] F. Gritti, G. Guiochon, Impact of retention on trans-column velocity biases in packed columns, AIChE J. 56 (2010) 1495–1509.
[39] V. Baranau, U. Tallarek, Random-close packing limits for monodisperse and polydisperse hard spheres, Soft Matter 10 (2014) 3826–3841.
[40] D. Cabooter, A. Fanigliulo, G. Bellazzi, B. Allieri, A. Rottigni, G. Desmet, Relationship between the particle size distribution of commercial fully porous and superficially porous high-performance liquid chromatography column packings and their chromatographic performance, J. Chromatogr. A 1217 (2010) 7074–7081.
[41] F. Gritti, A. Cavazzini, N. Marchetti, G. Guiochon, Comparison between the efficiencies of columns packed with fully and partially porous C_{18}-bonded silica materials, J. Chromatogr. A 1157 (2007) 289–303.
[42] F. Gritti, G. Guiochon, The quantitative impact of the mesopore size on the mass transfer mechanism of the new 1.9 m fully porous Titan-C_{18} particles. I: Analysis of small molecules, J. Chromatogr. A 1384 (2015) 76–87.
[43] A. Andrés, K. Broeckhoven, G. Desmet, Methods for the experimental characterization and analysis of the efficiency and speed of chromatographic columns: a step-by-step tutorial, Anal. Chim. Acta 894 (2015) 20–34.
[44] F. Gritti, I. Leonardis, D. Shock, P. Stevenson, A. Shalliker, G. Guiochon, Performance of columns packed with the new shell particles Kinetex-C_{18}, J. Chromatogr. A 1217 (2010) 1589–1603.
[45] H. Song, G. Desmet, D. Cabooter, Evaluation of the kinetic performance differences between hydrophilic-interaction liquid chromatography and reversed-phase liquid chromatography under conditions of identical packing structure, Anal. Chem. 87 (2015) 12331–12339.

PAPER III

Journal of Chromatography A, 1456 (2016) 137–144

Contents lists available at ScienceDirect

Journal of Chromatography A

journal homepage: www.elsevier.com/locate/chroma

A theoretical study on the advantage of core-shell particles with radially-oriented mesopores

Sander Deridder[a], Martina Catani[b], Alberto Cavazzini[b], Gert Desmet[a,*]

[a] Vrije Universiteit Brussel, Pleinlaan 2, 1050 Brussel, Belgium
[b] University of Ferrara, Via Fossato di Mortara 17, 44121 Ferrara, Italy

ARTICLE INFO

Article history:
Received 13 April 2016
Received in revised form 17 May 2016
Accepted 19 May 2016
Available online 20 May 2016

Keywords:
Core-shell particles
Radially oriented pores
Computational fluid dynamics
Simulations
General plate height model
B-term band broadening

ABSTRACT

We report on a first-principles numerical study explaining the potential advantage of core-shell particles with strictly radially-oriented mesopores. Comparing the efficiency of these particles with fully porous and core-shell particles with a conventional (i.e., randomly oriented) mesopore network, the present numerical study shows a similar strong reduction in minimal reduced plate height (h_{min}) as was very recently observed in an experimental study by Wei et al. (respectively a h_{min}-reduction on the order of about 1 and 0.5 reduced plate height-units). As such, the present work provides a theoretical basis to understand and confirm their experimental findings and quantifies the general advantage of "radial-diffusion-only" particles. Determining the effective longitudinal diffusion (B-term contribution) in a series of dedicated, independent simulations, it was found that this contribution can be described by a very simple, yet fully exact mathematical expression for the case of "radial- diffusion-only" particles. Using this expression, the significant increase in efficiency of these particles can be fully attributed to their much smaller B-term band broadening, while their C-term band broadening (representing the mass transfer resistance) remains unaffected.

1. Introduction

In the past 10 years, core-shell (CS) particles have revolutionized the speed and efficiency of chromatographic separations [1–7]. The introduction of these CS particles, also called superficially porous particles, can be considered as a rejuvenation (and an extension to thicker layers) of the pellicular particle concept proposed by Horvath et al., back in the 1960's [8]. These particles owe their advantage for a small part to the shorter internal diffusion distances, but especially to their significantly lower B-term band broadening [9,10], their lower internal volume (leading to a lower zone retention factor for a given phase retention factor [11]) and to their lower eddy-dispersion [10]. Although the origin of the latter is still under debate, it could be related to the fact that core-shell particles can typically be produced with a much narrower particle size distribution than fully-porous particles [12,13], except for some notable exceptions [14,15]. Because of the aforementioned advantages, core-shell particles rather have a reduced minimal plate height of around $h_{min} = 1.5$ [3,5,12], compared to $h_{min} = 2$ for fully-porous particles. In addition, the lower internal volume also leads to a lower flow resistance, adding further to the kinetic advantage of this particle type [16].

In a very recent publication, Wei et al. [17] have proposed a new type of core-shell particle that has the potential to make another leap in efficiency and speed. This material is of the core-shell type but, being based on pseudomorphic transformation (PMT) micelle templating, has all its mesopores oriented purely radially. Because of this orientation (and the presence of the core), it can be physically expected that the longitudinal diffusion (B-term contribution) will be strongly suppressed, while the C-term mass transfer processes can still go on nearly undisturbed. With this material Wei and coworkers could demonstrate unprecedented reduced minimal plate heights of $h_{min} = 1.0$.

To support these findings from a theoretical point of view and delimit the potential efficiency and kinetic performance limits of core-shell particles with radially-oriented mesopores (CS-ROM), we report here on a series of computational fluid dynamics simulations to accurately simulate the band broadening in simplified, perfectly ordered CS-ROM particle beds. The obtained reduced plate height curves are compared with data sets previously obtained for fully porous and core-shell particles with conventional isotropic internal diffusion. To allow for a fair comparison, the different particle types are compared for the same particle arrangement, the same values for the mobile zone and porous zone

* Corresponding author.
E-mail address: gedesmet@vub.ac.be (G. Desmet).

http://dx.doi.org/10.1016/j.chroma.2016.05.062
0021-9673/

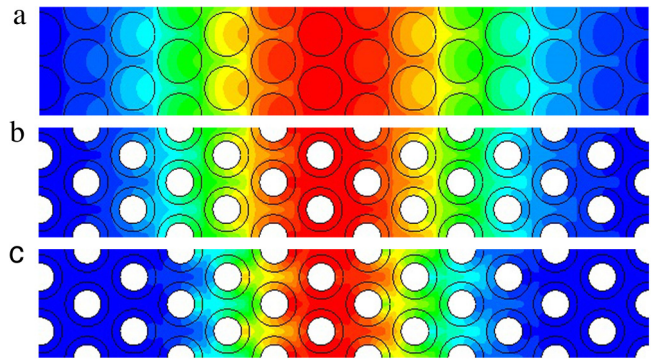

Fig. 1. Bed geometries and computed species distribution for (**a**) fully porous (2D) particles, (**b**) (2D) core-shell particles with conventional (i.e., isotropic) diffusion and (**c**) (2D) CS-ROM particles. Conditions in all cases: $k'' = 8$, $\nu_i = 16$, $D_{pz}/D_{mol} = 0.5$. The color scale varies in a linear way from the highest (red) to the lowest concentration (blue) in the mobile zone. In the stationary zone the same color scale is used, but concentrations are 8 (=k″) times higher. Maximal mobile zone concentration values respectively are: $C_{max} = 0.135$ g/l (a), $C_{max} = 0.152$ g/l (b), $C_{max} = 0.211$ g/l (c). (For interpretation of the references to colour in this figure legend, the reader is referred to the web version of this article.)

diffusion coefficients, as well as the same zone retention factor k″ (defined via the relation $u_R = u_i/(1 + k'')$, wherein u_R is the effective band migration speed and u_i is the interstitial velocity).

The results are analyzed using the general plate height model of packed bed chromatography [18–24], according to which the dimensionless plate height can be written as the sum of 4 different contributions:

$$h = h_{inhom} + h_B + h_{Cm} + h_{Cs} \quad (1)$$

wherein h_B represents the effective longitudinal diffusion (which is the only remaining source of band broadening when the flow is arrested), wherein h_{Cm} and h_{Cs} arise from the finite time needed for the mass transfer between the interstitial space and the particles, and wherein h_{inhom} groups all band broadening contributions arising from the heterogeneities of the velocity field of the bed. According to the general plate height model, the way in which h varies with the reduced interstitial velocity ν_i is, apart from the bed geometry, fully determined by the value of the zone retention factor k″ defined above and the ratio between the porous zone and the mobile zone diffusion coefficient (D_{pz}/D_{mol}) [20,25]. In the present study, we have considered two widely differing values for this ratio, one corresponding to a value that, at least for the case of small molecular weight compounds in reversed phase LC, can be considered as very large ($D_{pz}/D_{mol} = 0.5$) and one very small ($D_{pz}/D_{mol} = 0.1$).

2. Geometries and numerical methods

2.1. Geometries and flow, retention and diffusion parameters

Fig. 1 shows an axial cut of the simulation geometries used in the present study for each of the three different particle types: fully porous (Fig. 1a), CS particles with conventional (i.e., isotropic) diffusion (Fig. 1b) and CS-ROM particles (Fig. 1c). The default domain length was 153 μm but was extended to 307 μm for those cases (typically at high reduced velocity) where the standard length was too short to reach the long-time limit plate height value (see Section 2.3). The color pattern in overlay represents the species distribution recorded at a given moment in time.

The flow domain was composed of a 2D ordered arrangement of disks (representing the cross-section of cylindrical pillars with an infinite height) with an outer diameter $d_o = 2$ μm. Their centers were arranged on the vertices of a tile pattern made up of equilateral triangles. The flow direction was perpendicular to one of the sides of these triangles. During the calculation of the velocity and the species distribution fields, the sidewalls were put at symmetry, to mimic an infinitely wide domain. To account for the presence of an impermeable core, the core-shell disks contained a smaller concentric disk (radius $r_i = 1.26$, relative radius = 0.63) that was made impermeable to the species.

2.2. Simulation Methods

All simulations were performed with Ansys® Workbench version 16.2 from Ansys, Inc., purchased from Ansys Benelux, Wavre, Belgium. Within this software platform all flow domains were drawn with Ansys® Design Modeler and meshed with Ansys® Meshing. All simulations were performed with Ansys® Fluent.

2.2.1. Mesh

The shortest flow domains (153 μm) were divided in 5×10^5 mesh cells, the longer domains (307 μm) contained twice as many cells. Mainly quadrilateral cells were used, with a small fraction (less than 0.2%) of triangular cells. Mesh inflation layers were imposed on the disk walls on both sides (in the mobile zone as well as in the stationary zone) to capture the steepest velocity- and concentration gradients. Fifteen layers with a thickness growth rate of 1.1, resulting in a cumulative thickness of 0.17 μm was used. To check mesh independency, a mesh containing cells half the original size, resulting in a quadruple cell count, was used. At $\nu_i = 16$, the difference in plate height recorded with this finer mesh was only 0.15% smaller than in the original mesh. Therefore it was concluded the original mesh yields sufficient accuracy.

2.2.2. Solver

First, the velocity fields were computed solving the Navier-Stokes equations using the segregated pressure-based steady-state solver. For spatial discretization, the least squares cell based method was used to calculate gradients, the SIMPLE scheme for pressure-velocity coupling, the second order interpolation scheme for pressure and second order upwind scheme for momentum. Boundary conditions were set to symmetry (for the side walls) and the in- and outlet planes were put at a fixed pressure, respectively at 112487.39 Pa and 101325.00 Pa. The outer walls of the disks were set to the no-slip condition. Material properties in the mobile zone were those of water.

Subsequently, the outer wall of the disks was set to interior, to allow diffusion of the species from the mobile zone to the stationary zone and vice versa. The transient solver, with second order implicit temporal discretization and second order upwind scheme for spatial discretization, was then used to solve the convection diffusion equation yielding the transient concentration field of tracer band migrating through the flow domain. A fixed time stepping method with 500–3000 steps of size 5.10–5 s was used. The tracer was assigned the same properties as the water it was dissolved in.

Diffusion in the mobile zone was always isotropic and was characterized by the diffusion coefficient D_{mol}. Its value was tuned to produce different values of ν_i. The diffusion in the stationary zone was either put at $D_{pz}/D_{mol} = 0.5$ or at $D_{pz}/D_{mol} = 0.1$. To mimic the special case of the radial-only diffusion in the CS-ROM particles, the diffusion in the disks was made anisotropic, using user defined functions to assign each disk its proper anisotropic diffusion tensor (Cartesian coordinates), resulting in diffusion only in the radial direction of the respective disk.

2.2.3. Retention

In all considered cases, the zone retention factor of the analytes was put at $k'' = 8$, which, assuming a typical value for the intraparticle porosity $\varepsilon_{pz} = 0.35$, corresponds to a phase retention factor

of $k' = 4.9$ for the fully-porous particles and to a phase retention factor of $k' = 5.8$ for both core-shell types. Both can be considered as very typical for an LC separation.

2.2.4. Hardware

All simulations were performed on Dell Power Edge R210 Rack Servers each equipped with an Intel Xeon x3460 processor (clock speed 2,8 GHz, 4 cores) and 16 Gb, 1333 MHz ram memory, running on Windows server edition 2008 R2 (64-bit). Simulations of the steady-state velocity field in the aforementioned geometries took about 1 h, while the transient species concentration field simulations took about 24 h.

2.3. Determination of plate heights

Plate heights were determined by following the variance of a tracer band migrating through the flow domain. The initial species concentration of this band was defined by implementing a Gaussian distribution curve ($\sigma_x = 1\ \mu m$) near the inlet of the domain. Depending on the reduced velocity, the position of this band was adapted to be far enough downstream to avoid any tracer leaking from the inlet (going from 7 μm from the inlet at high ν_i to 50 μm at low ν_i).

At the end of each time step the 0th, 1st and 2nd order non-central moments (μ_0, μ_1 and μ_2) of the tracer concentration as function of the x-coordinate (flow direction) were reported. These were used to calculate the band's variance σ_x^2 [26,27]. After each time step, a local plate height was calculated by dividing the difference with the variance at the preceding time by the elapsed distance during this time step.

The resulting local plate height is then followed as a function of the band's position. After a sufficient distance this curve reaches an asymptotic value, which is then reported as the plate height representative for the studied condition.

2.4. Determination the effective diffusion coefficient (B-term constant)

The diffusion-only component of the band broadening was also computed independently. This was done by carrying out the same type of diffusion-only simulations as already described in [28]. In brief, this method consists of assigning fixed, but different values for the tracer concentration at the inlet and outlet of a flow domain containing only one representative unit cell. Subsequently, the steady-state concentration field is calculated in the absence of any fluid motion by solving the diffusion equation. Reporting the value of the species flux at either the inlet or outlet plane then allows to directly calculate the effective diffusion coefficient.

3. Results and discussion

3.1. Plate height data and analysis

Fig. 1 shows images of the species distribution at the moment when the band has moved to some intermediate position in the bed for the case of a reduced interstitial velocity of 16 ($\nu_i = 16$). As can be seen from the axial width of the color distribution, as well as from the C_{max}-values in the caption to Fig. 1, the amount of band broadening decreases significantly going from the fully porous (Fig. 1a), to the CS (Fig. 1b) and finally to the CS-ROM particles (Fig. 1c).

Fig. 2 summarizes and quantifies the results from all conducted band broadening simulations. Confirming the images in Fig. 1, the three considered particle types lead to important differences in reduced plate height. According to the general plate height model, the differences between the different particle types observed in Fig. 2 should be exclusively due to the differences in the intra-particle geometry, because all simulations have been carried out for the same particle arrangement, as well as the same zone retention factor k'' and the same values for the diffusion coefficients D_{pz} and D_{mol}. Considering the strong emphasis this field has always been putting on packing uniformity and external mass transfer when discussing column efficiency, much more than on the intra-particle properties, the observed differences are impressively large.

Whereas the conventional CS particles already have a h_{min}-value that is, depending on the D_{pz}/D_{mol}-ratio, between 0.28 and 0.41 h-units smaller than the fully porous particles, the CS-ROM particles display h_{min}-values that are yet significantly smaller than the conventional CS particles, between 0.48 and 0.22 h-units (again depending on the D_{pz}/D_{mol}-ratio). Interesting to note is the fact that the CS-ROM particles have clearly lower h-values in the B-term dominated region than conventional CS particles and at the same time this is not penalized by a steeper C-term, as the CS-ROM curve always remains below the conventional CS curve, even up till the highest ν_i (in practice columns are not operated much higher than $\nu_i = 15$ to 20).

Obviously, the relative position of the curves in Fig. 2a–b depends on the relative magnitude of the intra-particle diffusion coefficient. When D_{pz}/D_{mol} is large (cf. Fig. 2a), the difference between the curves for the conventional CS and the CS-ROM particles is larger than the difference between the fully porous and the conventional CS particles. When D_{pz}/D_{mol} is small (cf. Fig. 2b), the strongest difference in plate height curve is observed when going from the fully porous particles to the conventional CS particles, whereas the difference between the conventional CS and the CS-ROM particles is smaller here. This is further analyzed and explained in below sections.

3.2. B-term contribution and modelling

As is evident from Fig. 2, the h,ν_i-curves of the different particle types most strongly differ in their B-term dominated part (i.e., to the left of the optimum). In this velocity range, the band broadening is essentially dominated by the effective longitudinal diffusion coefficient D_{eff}. In this nomenclature, the word "effective" relates to the fact that D_{eff} is to be considered as the weighted contribution of two diffusion paths, one through the interstitial (=mobile) zone and the other through the porous particle zone (see Fig. 4 further on). The required weighing factor is not a straightforward value, but can be calculated to a very high degree of accuracy using the effective medium theory [29]. This has been introduced in the area of chromatography in [30,31].

The separate numerical diffusion experiments that were conducted in the present study (see Sections 2.3 and 2.4) provided independent values for D_{eff}. Given the speed with which this type of calculations can be run, a broad range of different zone retention factors was considered. In addition, we also considered one extra value for the relative porous zone diffusion coefficient ($D_{pz}/D_{mol} = 0.3$). The results are plotted in Fig. 3a in a dimensionless format, i.e., as $\gamma_{eff} = D_{eff}/D_{mol}$.

Considering first the series for the fully-porous and the conventional CS particles, the perfect coincidence between the data points and the dashed model curve readily shows that these particles produce D_{eff}-values that can be perfectly fitted by the effective medium expressions established in Ref. [29]. This agreement reflects the high accuracy of the model as well as of our computations. The effect of the relative porous zone diffusion coefficient (D_{pz}/D_{mol}) on the D_{eff}-curves for the fully-porous and the conventional CS particles is also quite straightforward, as the curves are arranged following the order of the D_{pz}/D_{mol}-value (higher means higher effective diffusion). The difference between the fully-porous and

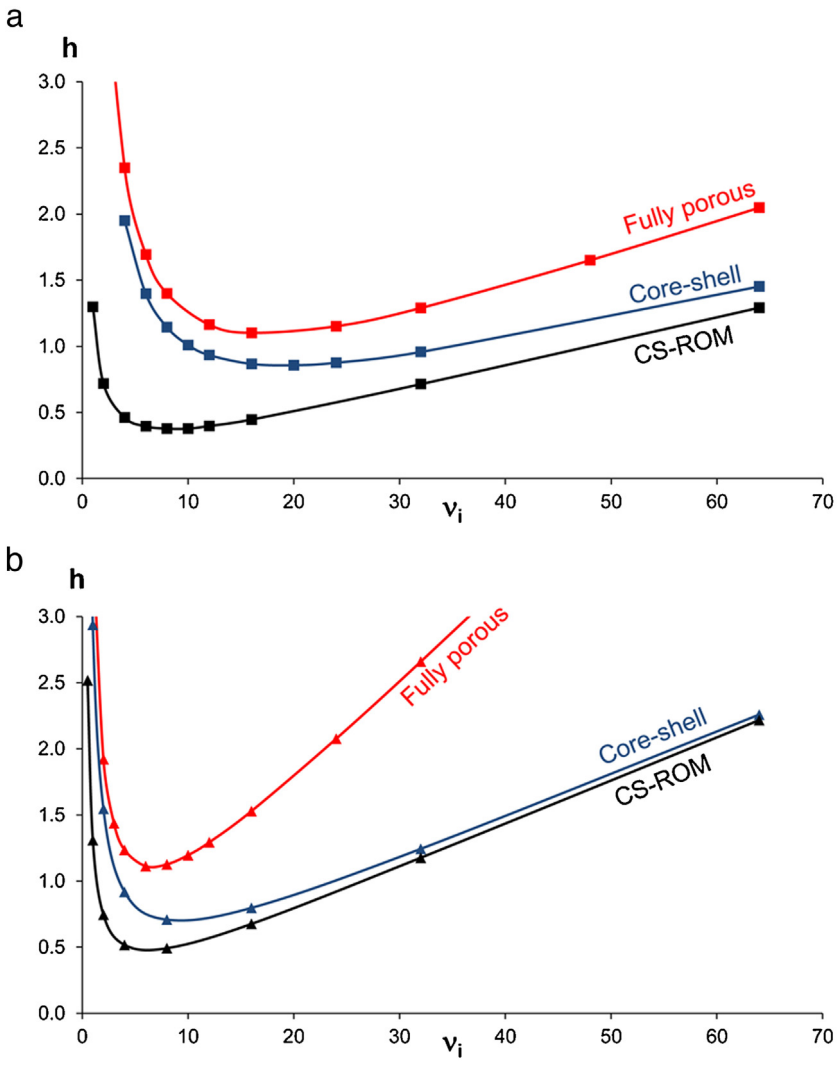

Fig. 2. Reduced plate height values h versus ν_i for the different (2D) particle types and the two considered D_{pz}/D_{mol}-values: (**a**) $D_{pz}/D_{mol} = 0.5$ and (**b**) $D_{pz}/D_{mol} = 0.1$.

the conventional CS particles for the same D_{pz}/D_{mol}-value reflects the obstructive effect of the core on the effective diffusion [9,30,31].

Turning now to the CS-ROM particles, it is first of all striking to observe that, unlike for the two other materials, the data points for the different D_{pz}/D_{mol}-value all fall on the same curve. This curve also decreases in a much steeper way with the zone retention factor k'' than the curves for the two other particles, where the porous zone diffusion is isotropic.

It is a well-established fact from the theory of chromatography that the B-term band broadening part of the reduced plate height h is given by [30,32]:

$$h_B = B/\nu_i, \text{ with} B = 2.\gamma_{eff}.(1 + k'') \quad (2)$$

Using Eq. (2), the γ_{eff} -values shown in Fig. 3a transform into the B-values shown in Fig. 3b. This figure readily reveals an important property of the CS-ROM particles: i.e., their B-term band broadening is fully independent of the retention factor, and remains at its minimal level, i.e., the one obtained at zero retention. This is in contrast with the two other particle types, where B quite strongly increases with k'', reflecting the fact that, although γ_{eff} drops with increasing k'' (cf. Fig. 3a), this drop is not sufficiently strong to outweigh the multiplication with $(1 + k'')$ in the expression for h_B. According to Eq. (2), the constant B-value observed for the CS-ROM particles automatically implies that γ_{eff} should vary inversely proportional with $(1 + k'')$. Since the observed γ_{eff} should equal that of a packed bed of fully solid particles at zero zone retention (i.e., when the particles are non-porous and $k'' = 0$), we can readily express the effective diffusion in a bed of CS-ROM particles by the following simple law:

$$\gamma_{eff,CS\text{-}ROM} = \gamma_{eff,non\text{-}porous}/(1 + k'') \quad (3)$$

As can be witnessed from the good agreement between the computed data points and the solid line curve added to Fig. 3a–b, this expression indeed perfectly describes the observed effective diffusion in CS-ROM particles.

Physically, the form of Eq. (3) can be understood as follows. According to the general effective medium theory, D_{eff} is a mix of series and parallel connection effects of the diffusion paths through the mobile zone and the stationary zone [30]. In Fig. 4, these are represented respectively by arrows (1) and (2). Since the longitudinal contribution of the diffusion path through the particles (path 2) is completely blocked in the CS-ROM particles, this only leaves path (1) as the only remaining diffusion route (cf. Fig. 4b). This route is the same as the one that would be followed when the particles would be non-porous (in which case $\gamma_{eff} = \gamma_{eff,non\text{-}porous}$). However, since the CS-ROM particles can effectively take up species, and since these species have a zero contribution to the longitudinal diffusion when residing in that state, the net effective diffusion should be weighed by a factor $1/(1 + k'')$ to express that the species are only effectively diffusing along path (1) during a fraction $1/(1 + k'')$ of

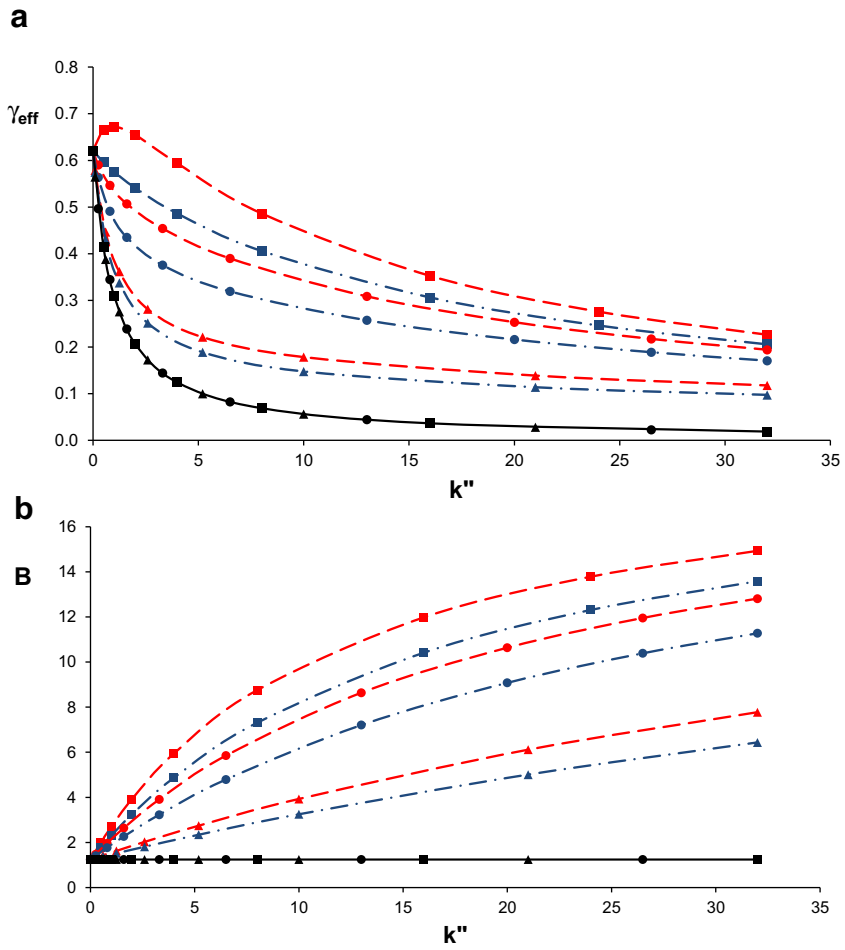

Fig. 3. Results of the numerical diffusion experiments, represented as (**a**) a plot of $\gamma_{eff} = D_{eff}/D_{mol}$ versus k″ and (**b**) a plot of B versus k″ for the 3 different (2D) particle types and the three considered D_{pz}/D_{mol}-values (squares $D_{pz}/D_{mol} = 0.5$, circles 0.3 and triangles 0.1). Solid curve represents Eq. (3), modelling the CS-ROM stacking. Dashed and dash-dotted curves calculated using Eq. (31) of Ref. [30], modelling the fully porous and core-shell stacking respectively.

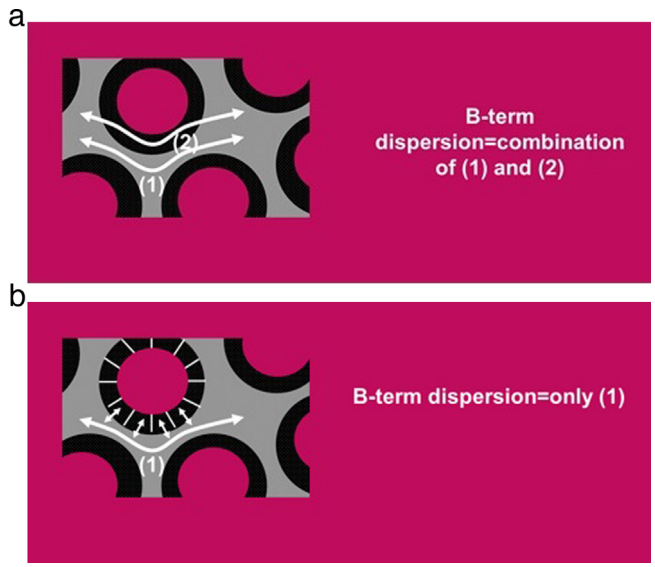

Fig. 4. Schematic difference between the diffusion paths in a core-shell particle with (**a**) random diffusion and (**b**) one with radial-only diffusion. Arrows (1) and (2) are discussed in the text. The radial lines added to the shell in (b) schematically represent the blockage of the diffusion in the circumferential direction.

the time they spend in the column. During the remainder of the time (fraction k″/(1 + k″)), they have a zero net diffusion in the longitudinal direction.

Returning now to Fig. 3, and considering the conditions used to obtain the reduced plate height data shown in Fig. 2, it can readily be verified that, for the $D_{pz}/D_{mol} = 0.5$-case, the CS-ROM particles produce a B-term contribution that is 7.05 times lower than that of the fully porous and 5.89 times lower than the conventional core-shell particles. For the $D_{pz}/D_{mol} = 0.1$-case, the values are respectively 2.78 and 2.32 times smaller.

3.3. *Detailed analysis of the relative magnitude of the different plate height contributions*

To understand the impact of the differences in B-term band broadening observed in the previous Section, Fig. 5 revisits the data of Fig. 2, but now after subtracting the h_B-contribution.

As can be noted, the conventional CS and the CS-ROM curves now produce nearly perfectly coinciding curves. This clearly demonstrates that the extra gain in efficiency one can expect by going from a CS particle with isotropic diffusion to one with radial-only diffusion can be fully attributed to the (large) difference in B-term band broadening (all other parameters are the same). There is however still a significant difference between (h-h_B)-curve for the fully-porous and the CS particles, reflecting that the difference in band broadening between a CS and a fully-porous particle is not only due to the difference in B-term band broadening.

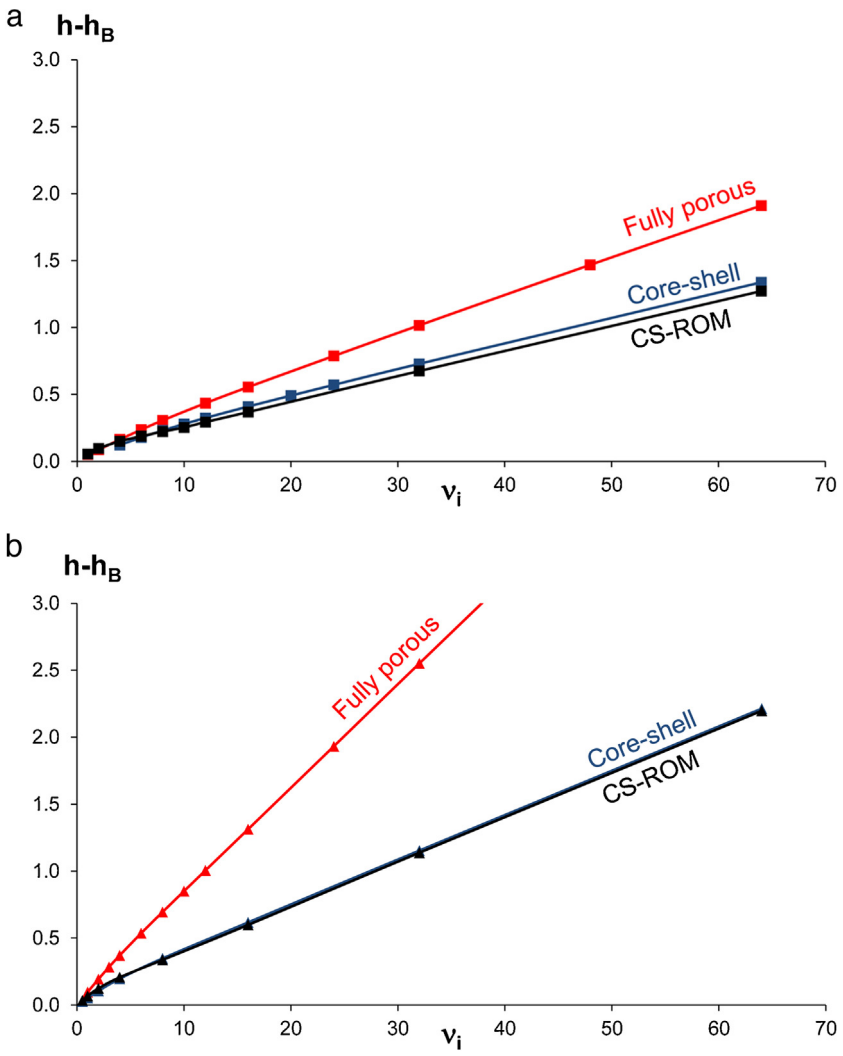

Fig. 5. Plot of h-h_B versus ν_i using the h-values shown in Fig. 2 and the h_B-values shown in Fig. 3b. (**a**) $D_{pz}/D_{mol} = 0.5$ and (**b**) $D_{pz}/D_{mol} = 0.1$.

Obviously, the explanation for this remaining difference is to be found in the difference in mass transfer resistance inside the particles (cf. the h_{Cs}-term). As was shown in [33], this contribution can, for the considered case of 2-D cylindrical particles, be written as:

$$h_{C_S} = \frac{k''}{(1+k'')^2} \cdot \frac{\nu_i}{2Sh_{pz}\frac{D_{pz}}{D_{mol}}} \tag{4}$$

with

$$Sh_{pz} = \frac{1-\rho^2}{\frac{1}{8} - \frac{1}{2}\rho^2 + \frac{3}{8}\rho^4 - \frac{\rho^4}{2}\ln\rho} \tag{5}$$

wherein ρ is the ratio of the solid core to the total cylinder radius. For the fully porous case, ρ = 0 and hence $Sh_{pz} = 8$. For the presently considered CS-geometry, ρ = 0.63, and Eq. (5) returns a value of $Sh_{pz} = 27.35$. This implies the CS particles can be expected to approximately have a 3.4 times smaller h_{Cs}-term than the fully porous. Since the theory [33–35] underlying the above expressions does not distinguish between isotropic and radial diffusion, this 3.4-fold lower h_{Cs}-contribution applies to both the conventional CS as well as to the CS-ROM particles, at least according to the theory underlying the general plate height model (see end of Section for some moderating comments).

To account for the difference in h_{Cs}-contribution between the fully porous and the CS particles, Fig. 6 shows the plate height values remaining after subtracting the h_{Cs}-contribution from the (h-h_B)-curves shown in Fig. 5a–b. As can be noted, all particle types now produce nearly perfectly coinciding (h-h_B-h_{Cs})-curves. This confirms that the only important remaining difference between the fully-porous and the CS particles in Fig. 5 is indeed due to the difference in h_{Cs}-term.

Since we consider a perfectly ordered system, without heterogeneities at the multi-particle level, the h_{Cs}-contribution is the only remaining contribution in Fig. 5 that depends on the D_{pz}/D_{mol}-ratio according to the general plate height model. This, together with the identical packing structure for the three different particle types, explains the (near-perfect) agreement between the (h-h_B-h_{Cs})-curves for both D_{pz}/D_{mol}-ratio's. This also explains why we opted to represent the two data sets in Fig. 6 in the same graph.

As a side note, it should be remarked that the reason why the h_{Cs}-term appears more dominant in our simulations than in real world experiments on real columns (see for example the strong difference in h-curves between the $D_{pz}/D_{mol} = 0.5$- and 0.1-cases in Figs. 2 and 5) is that the simulations relate to a perfectly ordered system. In real packed beds, the contribution of the eddy dispersion is so large that it makes the h_{Cs}-contribution much less important.

The fact that the (h-h_B-h_{Cs})-curves in Fig. 6 still display some small subtle differences (which are largest in the $D_{pz}/D_{mol} = 0.5$-case) is not due to any simulation inaccuracies. This was checked by going to extreme high computational cell densities and low time

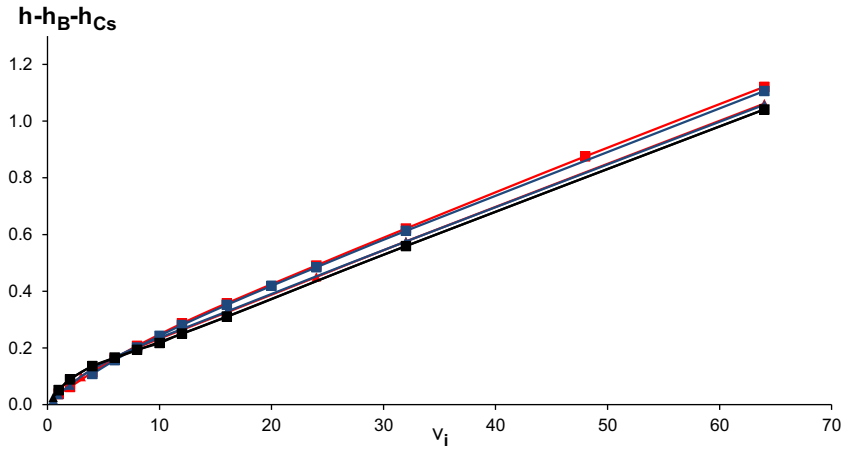

Fig. 6. Plot of $h-h_B-h_{Cs}$ versus ν_i using the h-values shown in Fig. 2 and the h_B-values shown in Fig. 3b. (squares D_{pz}/D_{mol} = 0.5 and triangles 0.1).

steps and finding that this did not affect the position of the curves. The differences are anyhow relatively small, on the order of some h = 0.05-reduced plate height units, and are hence not really relevant for real packed bed columns where they are overshadowed by the other contributions. The observed differences can be attributed to the fact that the mass transfer phenomena inside and outside the particles are not completely independent of each other in a packed bed medium, such that the pure additivity of the different band broadening sources in the general plate height model (as expressed in Eq. (1)) is not 100% accurate (as was already demonstrated in [36]). The strict independence and additivity in fact only holds in coated capillary systems, where the mobile and the stationary zone remain uniform in thickness all along the x-coordinate. As a consequence of the mutual influence the different mass transfer processes have on each other, the D_{pz}/D_{mol}-ratio and the presence or absence of the core have a small effect on how the mass transfer inside the particles (h_{Cs}-contribution) interacts with the mass transfer outside the particles (h_{Cm}-contribution). As a result, the different cases in Fig. 6 do not yield perfectly coinciding ($h-h_B-h_{Cs}$)-curves, despite they all relate to the same bed geometry, velocity field and zone retention factor.

3.4. *Extrapolations of the results to the performance of real packed beds and practical considerations*

Whereas the degree of simplification of the bed geometry is very high, the insights from the present study are sufficiently general to conclude that any bed of CS-ROM particles (be it 2D or 3D, and be it ordered or disordered) will always have the advantage to produce a very low B-term band broadening (remaining at the minimal value of $h_B = 2.\gamma_{eff,non\text{-}porous}$, independently of the retention factor), without affecting the speed of the C-term mass transfer. This implies that for the separation of (large) molecules with a small molecular diffusion coefficient and accompanying lower B-term contribution this advantage will be smaller, except of course if these separations would not be run at normal flow rates, but at or near the corresponding optimal flow rate.

Given the above, the magnitude of the corresponding drop in h_{min} observed in the present study is certainly also indicative for the potential gain in real packed beds, provided this drop is considered in absolute terms (drop of 0.22–0.48 in reduced plate height units compared to the regular core-shell particles), rather than in relative terms. Because in real packed beds, the total reduced plate height values are higher due to the significant eddy-dispersion. It could be that the latter will be somewhat larger for CS-ROM particles, because of their lower permeability and the correspondingly smaller multi-particle radial velocity equilibration. Nevertheless, the presently observed gains in h_{min} are very similar in absolute values compared to that in the Wei et al. study [17].

Another important remark is that, whereas the comparison in the graphs shown in Fig. 2 assumes the three particle types have the same D_{pz}/D_{mol}-value, it can be inferred that the straight running mesopores of the CS-ROM particles will lead to higher D_{pz}-values than can ever be expected in the random pore networks of conventional particles. This might lead to a further reduction of the h_{Cs}-contribution. Maybe this could also counter the above mentioned possibility of a slightly higher eddy-dispersion.

The fact that the B-term contribution of CS-ROM particles remains at the minimal value of $h_B = 2.\gamma_{eff,non\text{-}porous}$ for any value of k'', while B and hence also h_B rather strongly increase with the retention factor for particles with an isotropic internal diffusion (cf. Fig. 3b) also allows to conclude that the advantage of CS-ROM particles will be largest for components eluting with high retention factors (which is unfortunately the region where the h_{Cs}-contribution becomes ever and ever smaller such that the above mentioned advantage of higher D_{pz}-values of CS-ROM particles would vanish likewise).

The fact that the lower h_{min} of the CS-ROM particles is obtained via a lower B-term also implies the optimal velocity shifts to lower velocities. This is also observed in the Wei et al. study [17]. This obviously has a consequence on the achievable maximal speed, although the kinetic advantage is clear over the entire range of velocities (see the kinetic plot in Fig. 14 of Ref. [17]).

A drawback of the CS-ROM particles might be that they have yet a lower loadability than conventional CS particles, as they can maybe only be produced with a limited shell thickness. The nature of the pore network (parallel cylindrical versus randomly connected pores) furthermore also suggests a lower specific retention surface. Another potential issue could be their weaker mechanical strength, although no data are available to either support or contradict this.

4. Conclusions

Compared to conventional core-shell particles, core-shell particles with radially-oriented mesopores (CS-ROM particles) enable an additional strong reduction of the minimal plate height because their pore network produces the lowest possible B-term band broadening h_B, remaining at the minimal value of $h_B = 2.\gamma_{eff,non\text{-}porous}$ instead of increasing with the retention factor as is the case for particles with isotropic internal diffusion. This advantage is realized without affecting the speed of the C-term

mass transfer, such that the lower B-term band broadening is not penalized by an increase in C-term band broadening.

Comparing for the same zone retention factor ($k'' = 8$, corresponding to a phase retention factor of the order of 4.9–5.8), CS-ROM particles can be expected to produce a B-term which is between 2.32 ($D_{pz}/D_{mol} = 0.1$) and 5.89 ($D_{pz}/D_{mol} = 0.5$) times lower than that of a conventional core-shell particle with the same relative core, and between 2.78 ($D_{pz}/D_{mol} = 0.1$) and 7.05 ($D_{pz}/D_{mol} = 0.5$) times lower than for a fully porous particle.

In the perfectly ordered beds considered in the present simulation study, the CS-ROM particles displayed a h_{min}-value that was 0.76 and 0.48 h-units smaller than the ordinary fully porous and core-shell particles respectively for $D_{pz}/D_{mol} = 0.5$ and 0.63 and 0.22 h-units smaller in case $D_{pz}/D_{mol} = 0.1$. These values are of the same order as in the recent experimental study reported by Wei et al. [17].

Observing such large differences under conditions of identical packing quality suggests that column efficiency is also strongly determined by the intra-particle properties (diffusion, geometry,..), whereas the field of LC has always been more pre-occupied with packing uniformity and external mass transfer.

Acknowledgements

Deridder S. gratefully acknowledges a research grant from the Research Foundation – Flanders (FWO-Vlaanderen). The authors thank the Italian University and Scientific Research Ministry (Grant PRIN 2012ATMNJ_003).

References

[1] D.V. McCalley, Some practical comparisons of the efficiency and overloading behavior of sub-2 μm porous and sub-3 μm shell particles in reversed-phase liquid chromatography, J. Chromatogr. A 1218 (2011) 2887–2897.
[2] A.C. Sanchez, G. Friedlander, S. Fekete, J. Anspach, D. Guillarme, M. Chitty, T. Farkas, Pushing the performance limits of reversed-phase ultra high performance liquid chromatography with 1.3 μm core-shell particles, J. Chromatogr. A 1311 (2013) 90–97.
[3] F. Gritti, G. Guiochon, Speed-resolution properties of columns packed with new 4.6 μm Kinetex-C-18 core-shell particles, J. Chromatogr. A 1280 (2013) 35–50.
[4] G. Guiochon, F. Gritti, Shell particles trials, tribulations and triumphs, J. Chromatogr. A 1218 (2011) 1915–1938.
[5] S. Fekete, D. Guillarme, Kinetic evaluation of new generation of column packed with 1.3 μm core-shell particles, J. Chromatogr. A 1308 (2013) 104–113.
[6] V. González-Ruiz, A.I. Olives, M.A. Martín, Core-shell particles lead the way to renewing high-performance liquid chromatography, TrAC Trends Anal. Chem. 64 (2015) 17–28.
[7] D.S. Bell, R.E. Majors, Current state of superficially porous particle technology in liquid chromatography, LCGC North Am. 33 (2015) 386–395.
[8] C.G. Horváth, B.A. Preiss, S.R. Lipsky, Fast liquid chromatography – an investigation of operating parameters and separation of nucleotides on pellicular ion exchangers, Anal. Chem. 39 (1967) 1422–1428.
[9] A. Liekens, J. Denayer, G. Desmet, Experimental investigation of the difference in B-term dominated band broadening between fully porous and porous-shell particles for liquid chromatography using the Effective Medium Theory, J. Chromatogr. A 1218 (2011) 4406–4416.
[10] F. Gritti, G. Guiochon, Facts and legends about columns packed with sub-3-μm core-shell particles, LCGC North Am. 30 (2012) 586–595.
[11] A. Felinger, Diffusion time in core-shell packing materials, J. Chromatogr. A 1218 (2011) 1939–1941.
[12] D. Cabooter, A. Fanigliulo, G. Bellazzi, B. Allieri, A. Rottigni, G. Desmet, Relationship between the particle size distribution of commercial fully porous and superficially porous high-performance liquid chromatography column packings and their chromatographic performance, J. Chromatogr. A 1217 (2010) 7074–7081.
[13] K. Horvath, D. Lukacs, A. Sepsey, A. Felinger, Effect of particle size distribution on the separation efficiency in liquid chromatography, J. Chromatogr. A 1361 (2014) 203–208.
[14] O.H. Ismail, M. Catani, L. Pasti, A. Cavazzini, A. Ciogli, C. Villani, D. Kotoni, F. Gasparrini, D.S. Bell, Experimental evidence of the kinetic performance achievable with columns packed with new 1.9 mm fully porous particles of narrow particle size distribution, J. Chromatogr. A (2016), http://dx.doi.org/10.1016/j.chroma.2016.05.038.
[15] M. Catani, O.H. Ismail, A. Cavazzini, A. Ciogli, C. Villani, L. Pasti, C. Bergantin, D. Cabooter, G. Desmet, F. Gasparrini, D.S. Bell, Rationale behind the optimum efficiency of columns packed with new 1.9 mm fully porous particles of narrow particle size distribution, J. Chromatogr. A (2016), http://dx.doi.org/10.1016/j.chroma.2016.05.037.
[16] K. Broeckhoven, G. Desmet, The future of UHPLC: Towards higher pressure and/or smaller particles? TrAC Trends Anal. Chem. 63 (2014) 65–75.
[17] T.-C. Wei, A. Mack, W. Chen, J. Liu, M. Dittmann, X. Wang, W.E. Barber, Synthesis characterization, and evaluation of a superficially porous particle with unique, elongated pore channels normal to the surface, J. Chromatogr. A 1440 (2016) 55–65.
[18] J.J. van Deemter, F.J. Zuiderweg, A. Klinkenberg, Longitudinal diffusion and resistance to mass transfer as causes of nonideality in chromatography, Chem. Eng. Sci. 5 (1956) 271–289.
[19] J.H. Knox, Band dispersion in chromatography – a new view of A-term dispersion, J. Chromatogr. A 831 (1999) 3–15.
[20] J.C. Giddings, Dynamics of Chromatography Part 1, Marcel Dekker, New York, 1965.
[21] L. Lapidus, N.R. Amundson, Mathematics of adsorption in beds. VI. The effect of longitudinal diffusion in ion exchange and chromatographic columns, J. Phys. Chem. 56 (1952) 984–988.
[22] E. Kucera, Contribution to theory of chromatography linear non-equilibrium elution chromatography, J. Chromatogr. 19 (1965) 237–248.
[23] H.W. Haynes, P.N. Sarma, Model for application of gas-chromatography to measurements of diffusion in bidisperse structured catalysts, AIChE J. 19 (1973) 1043–1046.
[24] F. Gritti, G. Guiochon, The van Deemter equation: assumptions, limits, and adjustment to modern high performance liquid chromatography, J. Chromatogr. A 1302 (2013) 1–13.
[25] G. Desmet, K. Broeckhoven, Equivalence of the different C_m- and C_s-Term expressions used in liquid chromatography and a geometrical model uniting them, Anal. Chem. 80 (2008) 8076–8088.
[26] K. Broeckhoven, G. Desmet, Approximate transient and long time limit solutions for the band broadening induced by the thin sidewall-layer in liquid chromatography columns, J. Chromatogr. A 1172 (2007) 25–39.
[27] A.L. Berdichevsky, U.D. Neue, Nature of the eddy dispersion in packed beds, J. Chromatogr. 535 (1990) 189–198.
[28] S. Deridder, A. Vanmessen, K. Nakanishi, G. Desmet, D. Cabooter, Experimental and numerical validation of the effective medium theory for the B-term band broadening in 1st and 2nd generation monolithic silica columns, J. Chromatogr. A 1351 (2014) 46–55.
[29] S. Torquato, Random Heterogeneous Materials, Springer Science & Business Media, New York, 2002.
[30] G. Desmet, S. Deridder, Effective medium theory expressions for the effective diffusion in chromatographic beds filled with porous, non-porous and porous-shell particles and cylinders. Part I: Theory, J. Chromatogr. A 1218 (2011) 32–45.
[31] S. Deridder, G. Desmet, Effective medium theory expressions for the effective diffusion in chromatographic beds filled with porous, non-porous and porous-shell particles and cylinders. Part II: Numerical verification and quantitative effect of solid core on expected B-term band broadening, J. Chromatogr. A 1218 (2011) 46–56.
[32] J.H. Knox, H.P. Scott, B and C terms in the Van Deemter equation for liquid chromatography, J. Chromatogr. A 282 (1983) 297–313.
[33] W. De Malsche, H. Gardeniers, G. Desmet, Experimental study of porous silicon shell pillars under retentive conditions, Anal. Chem. 80 (2008) 5391–5400.
[34] J.C. Giddings, The role of lateral diffusion as a rate-controlling mechanism in chromatography, J. Chromatogr 5 (1961) 46–60.
[35] C. Horváth, S.R. Lipsky, Column design in high pressure liquid chromatography, J. Chromatogr. Sci. 7 (1969) 109–116.
[36] D. De Wilde, F. Detobel, J. Deconinck, G. Desmet, A numerical study of the assumptions underlying the calculation of the stationary zone mass transfer coefficient in the general plate height model of chromatography in two-dimensional pillar arrays, J. Chromatogr. A 1217 (2010) 1942–1949.

PAPER IV

Analytical and Bioanalytical Chemistry
https://doi.org/10.1007/s00216-017-0842-4

TRENDS

New frontiers and cutting edge applications in ultra high performance liquid chromatography through latest generation superficially porous particles with particular emphasis to the field of chiral separations

Martina Catani[1] · Simona Felletti[1] · Omar H. Ismail[2] · Francesco Gasparrini[2] · Luisa Pasti[1] · Nicola Marchetti[1] · Chiara De Luca[1] · Valentina Costa[1] · Alberto Cavazzini[1]

Received: 30 October 2017 / Revised: 5 December 2017 / Accepted: 15 December 2017

Abstract
About ten years after their introduction to the market (happened in 2006), the so-called second generation superficially porous particles (SPPs) have undoubtedly become the benchmark as well as, very often, the preferred choice for many applications in liquid chromatography (LC), when high efficiency and fast separations are required. This trend has interested practically all kinds of separations, with the only exception of chiral chromatography (at least so far). The technology of production of base SPPs is advanced, relatively simple and widely available. The deep investigation of mass transfer mechanisms under reversed-phase (RP) and normal-phase (NP) conditions for achiral separations has shown the advantages in the use of these particles over their fully porous counterparts. In addition, it has been demonstrated that SPPs are extremely suitable for the preparation of efficient packed beds through slurry packing techniques. However, the research in this field is in continual evolution. In this article, some of the most advanced concepts and modern applications based on the use of SPPs, embracing in particular ultrafast chiral chromatography and the design of SPPs with engineered pore structures or very reduced particle diameter, are revised. We describe modern trends in these fields and focus on those aspect where further innovation and research will be required.

Keywords Superficially porous particles (SPPs) · Sub-2 µm SPPs · 2.0 µm chiral SPPs · Highly ordered radially oriented mesopore SPPs · Highly efficient ultrafast (chiral) separations

Introduction

One of the main challenges facing chromatographers is developing high efficient and fast separation methods. A fundamental aspect of this process is the choice of the liquid-chromatography (LC) column, in particular regarding the physico-chemical and geometric characteristics of packing particles. Their size and morphology (either fully or superficially porous) indeed dramatically affect the kinetic performance of columns not only by modifying the volume available for the diffusion of molecules but also through the "quality" of the resulting packed bed [1–3].

As a matter of fact, for a long time, the main approach followed by column manufacturers to improve the efficiency of separation has been to prepare columns made of particles with smaller and smaller diameter. Sub-2 μm spherical fully porous particles (FPPs) are nowadays widely commercialized and routinely employed. The downside of this approach is in the very high pressure required to use these columns at their full potential (up to 1200-1500 bars or more) [4], since pressure drop along the column increases by a square function of the inverse of particle size [5].

In 2006, the so-called second generation superficially porous particles (SPPs) – alternatively named core-shell, fused-core^{TM} or porous shell particles – were launched [6]. Since then, columns packed with SPPs invaded the market,

✉ Martina Catani
martina.catani@unife.it

✉ Alberto Cavazzini
cvz@unife.it

[1] Department of Chemistry and Pharmaceutical Sciences, University of Ferrara, via L. Borsari 46, 44121 Ferrara, Italy

[2] Department of Drug Chemistry and Technology, "Sapienza" University of Rome, P.le Aldo Moro 5, 00185 Rome, Italy

Published online: 16 January 2018

representing an effective and concrete alternative to sub-2 μm FPPs in terms of efficiency and speed of separation, but orignating much less back pressure [7]. As an example, columns packed with C_{18} 2.7 μm SPPs provide efficiencies close to those of columns of the same geometry packed with 1.7 μm fully porous C_{18} particles but operating at a backpressure that is 50-75% smaller than that of FP particles [8, 9].

Second-generation SPPs are made of a nonporous solid silica core surrounded by a porous silica shell, exactly as the pellicular particles introduced in the sixties by Horváth and Lipsky [10]. The main advantage of these particles with respect to first generation ones is their higher loading capacity achieved thanks to a specific design, where the porous zone occupies roughly 3/4 of the total particle volume [11].

The rationale behind the introduction of a solid core into the particle was not only to improve solid-liquid mass transfer (c_s-term of the van Deemter equation) by shortening the diffusion path length across the particle but also to reduce the contribution of longitudinal diffusion (b-term of the van Deemter equation) by decreasing the pore volume accessible to analyte molecules [8, 12–14]. Later on, it turned out that SPPs are characterized by very low eddy diffusion (a-term of the van Deemter equation, accounting for any kind of flow inhomogeneity and unevenness in the packed bed), which largely contributes to the overall efficiency of a column [8, 15].

A countless number of papers and reviews have been published describing the fundamentals, developments and applications of SPPs in areas as different as food chemistry, biological applications, environmental chemistry, "omics" sciences, bi-dimensional chromatography, etc. [8, 11, 16–24]. Readers interested in these topics are addressed to specific literature.

On the other hand, in this paper, we focus on some of the most interesting solutions and ideas proposed to push further the limits of performance and the field of applications of SPPs. These innovations embrace different fields and sectors of activities. First of all, they pertain to high efficient and ultrafast chiral chromatography, where results that were unimaginable even only a few years ago have been recently achieved [16, 25–28]. For instance, several examples of chiral separations performed in less than one second with chiral SPPs as stationary phases have been published. Even if some fundamental aspects need further understanding [16, 25], these works represent the turning point between an old concept of chiral separations by LC and a new one based on columns exhibiting perfomance (in terms of efficiency and speed of separation) very similar to those of chips employed for high-speed enantioseparations [29]. We may reasonably expect in the next few years the appearence on the market of many chiral stationary phases based on these concepts, since the technology of production of chiral SPP particles is mature enough to find its way into commercial products.

In other less fortunate cases, very innovative and promising concepts of SPPs are still at the level of prototypes. Among these, it is worth to mention the so-called highly ordered radially oriented mesopore (ROM) SPPs [30, 31]. Engineered to achieve superior kinetic performance thanks to their highly ordered mesopore network, these SPPs have however exhibited some issues in terms of chemical and long term stability, limiting the extensive evaluation of their potential for high efficient separations. Another remarkable example of precursors is represented by SPPs of very reduced diameter (down up to 1.1 μm) and porous layer thickness. In this case, the major barrier to large scale production and commercialization has been essentially practical, coming from actual limits of even state-of-art instrumentation, whose extra column void volume is incompatible with the efficiency of these particles. Admittedly, also the slurry packing of smallest SPPs (1.1 μm) into very narrow tubes presents important difficulties [32, 33].

Chiral SPPs: the future of high efficient and ultrafast enantioseparations?

The employment of high efficient particles – either sub-2 μm fully porous or second-generation superficially ones – in chiral LC has been relatively recent. This delay, with respect to achiral separations, depends on different reasons. They include both practical issues and theoretical problems. Among the former, the most relevant ones are the difficulty to adapt in some cases pre-existing methods in use for the functionalization of larger chiral FPPs to very small particles; particle agglomeration during synthesis; the non uniform coating of chiral particles. On the other hand, from a theoretical viewpoint, the lack of complete understanding of the complex mass transfer phenomena in chiral chromatography is a relevant limitation to the development of very efficient chiral particles [1, 16, 34]. Last but not least, conservative commercial strategies by the most important producers of chiral columns may also be advocated to explain the delay.

As a matter of fact, until 2011, SPPs were not used as base material for the preparation of chiral stationary phases (CSPs) [35, 36] (for the sake of information completeness, the first report on the use of 1.9 μm fully porous chiral particles is dated 2010 [37, 38]). Since then, different classes of CSPs have been produced as porous shell materials and the debate about pros and cons of chiral SPPs over FPPs has begun. Chankvetadze and his group were most active in the preparation of polysaccharide-based

superficially porous CSPs [39, 40]. Their studies about the comparison of kinetic performance between these CSPs and their fully porous counterparts of comparable content of chiral selector and particle size led to the conclusion that SPP chiral columns can provide higher separation factors, higher efficiency and flatter van Deemter curves.

The most complete works on the evaluation of the performance of SPPs in chiral chromatography are those from Armstrong's group [28, 41–46]. Armstrong and coworkers have evaluated, from a kinetic viewpoint, a wide class of chiral selectors prepared on 2.7 μm SPPs including cyclofructan-6 and β-cyclodextrin, macrocyclic antibiotics (teicoplanin, teicoplanin aglycone and vancomycin) and quinine-based ones. In agreement with Chankvetadze's findings, they also have demonstrated that chiral SPPs perform systematically better than fully porous ones under RP, NP, hydrophilic interaction (HILIC) and polar organic mode LC. Remarkably, the employment of very short columns (5 mm long) packed with chiral SPPs and operated at a very high flow rate, permitted to achieve ultrafast enantioseparations (sub-second timescale) [27]. At the same time, also Gasparrini and coworkers reported about the possibility of performing sub-second separations by using SPPs functionalized with Whelk-O1 chiral selector [1, 16]. As an example, Fig. 1 shows some remarkable cases where – thanks to the use of high flow rates (up to 8 ml/min) and very short columns (length 5-10 mm) packed with latest generation chiral particles – separations of enantiomers in less than one second were achieved (see figure caption for details).

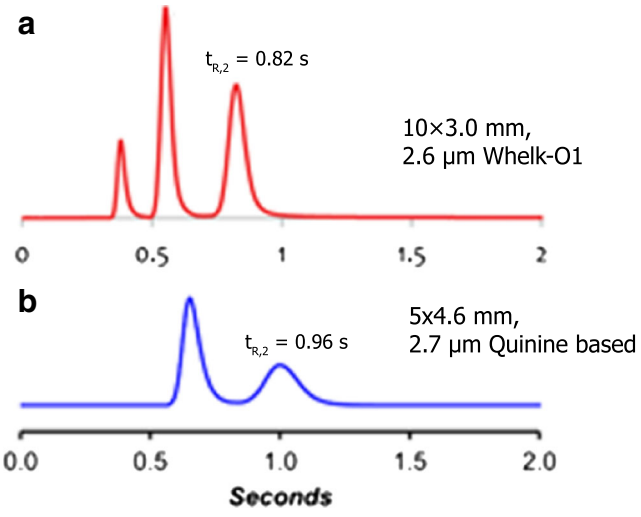

Fig. 1 Ultrafast enantioseparations of **a** *trans*-stilbene oxide enantiomers on a 10×3.0 mm column packed with 2.6 μm Whelk-O1 SPPs, MP: hexane/ethanol 90:10 %(v/v)+1% methanol, flow rate: 8 mL/min; **b** N-(3,5-dinitrobenzoyl)- DL-leucine enantiomers on a 5×4.6 mm column packed with 2.7 μm Quinine based SPPs, MP: acetonitrile/20 mM ammonium formate 70:30%(v/v), flow rate: 5 mL/min. (Modified with permissions from Refs. [16] and [27], respectively)

These proof-of-concept experiments demonstrate the state of the art of chiral LC and allow to predict a great future for this technology in the field of ultrafast enantioseparations. However, in spite of these very promising results, it is the opinion of the authors of this paper that there are still some fundamental aspects that require a deeper investigation to truly understand the potential and limits of these particles. They concern essentially two interconnected aspects. The first one is about the importance of the adsorption-desorption kinetics on the performance of modern, ultra-high effient chiral LC columns [47, 48]. In particular, questions such as:

- if (and how) the adsorption-desorption kinetics varies by changing the surface density of chiral selector;
- if (and how) the surface density of chiral selector varies across the particle diameter (this is particularly important when considering the comparison between chiral SPPs and FPPs);
- if (and how) the chemical environment surrounding the chiral moiety anchored to the surface affects the adsorption-desorption kinetics (physico-chemical properties of bare silicas can be very different);

need serious consideration. To date these points have been only marginally addressed in the literature.

The other aspect that needs more fundamental work is about the very complex problem of evaluating the contribution of eddy dispersion to band broadening and the factors on which it depends [49]. It concerns, clearly, also the study of packing of particles into chromatographic columns and how it possibly changes depending on the surface characteristics of particles themselves [50]. According to the experience of the authors of this work, packing apolar or polar particles (such as chiral ones), be they FPPs or SPPs, [16, 25] can be intrinsically different. Even the most advanced approaches to study mass transfer in chiral chromatography, indeed, cannot provide independent estimations of contributions to band broadening coming from eddy dispersion and adsorption-desorption kinetics [51].

These considerations show that the apparently obvious statement according to which columns packed with chiral SPPs must outperform those made of chiral FPPs in terms of efficiency (in agreement with what happens in achiral RP LC) [43, 44], must be taken with great caution. Indeed, some experimental facts showing that the above mentioned generalization cannot be always applied have been reported. Ismail et al. [1], for instance, compared the efficiency of chiral columns for ultrafast high-efficient separations packed with both Whelk-O1 SPPs (2.6 μm) and FPPs (1.8 and 2.5 μm). Contrary to initial expectations they found that, especially for the more retained enantiomer, the efficiency of the column packed with SPPs was worse than

that of the 1.8 μm FPP column and quasi-comparable to that of the column made of 2.5 μm FPPs [16]. The authors reported about the possible combination of both a slower adsorption-desorption kinetics and a larger eddy dispersion in the column packed with chiral SPPs as the reasons to explain this behavior. On the one hand, they correlated the unusual low perfomance of SPPs to the larger surface density of chiral selector found on the SPPs (+ 20%) with respect to the fully porous ones (even if particles were prepared under identical experimental conditions) and, on the other hand, to the empirical difficulties encountered during the packing of chiral SPPs.

Quite recently, the same group pushed beyond the limit of high efficient chiral particles, by featuring the first example of a (teicoplanin-based) CSP prepared on 2.0 μm SPPs [26]. The kinetic performance of the column packed with this new particles was compared to that of other two columns packed with 2.7 μm SPPs and 1.9 μm FPPs of narrow particle size distribution (Titan^{TM} particles), functionalized with the same chiral selector. At the minimum of the van Deemter curve, the new 2.0 μm SPP CSP was found to overcome the other two for the separation of both achiral and chiral compounds in HILIC conditions, with efficiency close to 300,000 plates/meter. On the opposite, at higher flow rates, even with the new 2.0 μm teicoplanin-based SPP column a significant loss of performance (especially for the second eluted enantiomer) was observed. This finding is consistent with the observation made with Whelk-O1 CSPs (see before).

To conclude this paragraph, Fig. 2 reports another extraordinary example, in addition to those given in Fig. 1, of the outstanding results that can be achieved with the new 2.0 μm teicoplanin-based SPPs. This figure shows the separation of a mixture of haloxyfop and ketorolac enantiomers in about 8 seconds with a resolution larger than 2.0 (see figure caption for details) [26]. Incidentally, we mention here that teicoplanin and teicoplanin-based derivatives have been for a long time considered "slow" selectors, unsuitable for high efficient and ultrafast separations.

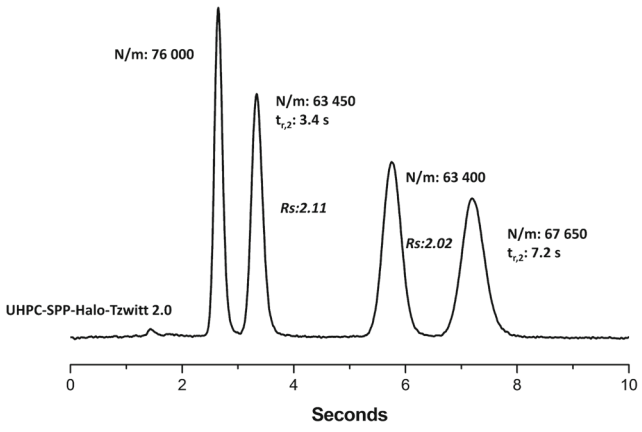

Fig. 2 Ultrafast enantioseparation of a racemic mixture containing haloxyfop (firstly eluted pair of peaks) and ketorolac (secondly eluted pairs of peaks) on a 20×4.6 mm (L×I.D.) column packed with 2.0 μm teicoplanin SPPs. Modified with permission from [26]

Highly ordered radially oriented mesopore SPPs: reaching unexplored efficiency limits through engineered particles

In 2016, an innovative approach named pseudomorphic transformation (PMT) micelle templating has been described to produce a new type of SPPs characterized by: (i) narrower particle size; (ii) thinner porous layer with high surface area; and, most importantly, (iii) a pore network made of highly ordered radially oriented mesopores [30]. PMT process is based on the dispersion of non-porous silica particles (which will form the core) in a silica-dissolving alkaline solution with self-organizing surfactant molecules. Fig. 3 reports SEM images of ROM-SPPs (squares *a* and *c*) and traditional SPPs (squares *b* and *d*). Cross-section views (Fig. 3c and d) show how the presence of ROM limits diffusion only to the radial direction. This is thus fundamentally different from the randomly distributed and tortuous diffusion pathways in conventional SPPs (Fig. 3d). Prototype columns packed ROM-SPPs with an overall diameter of 5 μm have been demonstrate to produce minimum reduced plate height values about 0.5-1 units lower than those achievable with fully porous and traditional SPPs of the same particle size, respectively. This represents the lowest value reported for analytical columns [30].

In a remarkable theoretical study by Deridder et al. [31], computational fluid dynamics (CFD) was used to compare mass transfer properties and band broadening in perfectly ordered beds made of: ROM-SPPs; traditional SPPs; and, finally, FPPs. To allow for a fair comparison, the same particle arrangement, the same values for the mobile zone and porous zone diffusion coefficients, as well as the same retention factor have been assumed for the three particle types. The results of this study can be summarized with the help of Fig. 4, where the theoretical van Deemter curves obtained for the three types of particles are reported. The advantage in terms of mass transfer given by ROM-SPPs is evident. The ordered pore structure allow these particles to outperform the others, thanks to a dramatic reduction of the *b*-term contribution.

Deridder et al. demonstrated the longitudinal diffusion to be independent of the retention factor. It remained at its minimal value (corresponding to that of unretained molecules) instead of increasing with retention, as it happens for particles with isotropic internal diffusion. This depends on the fact that when retained molecules reside in the porous layer of ROM-SPPs, their diffusion in the

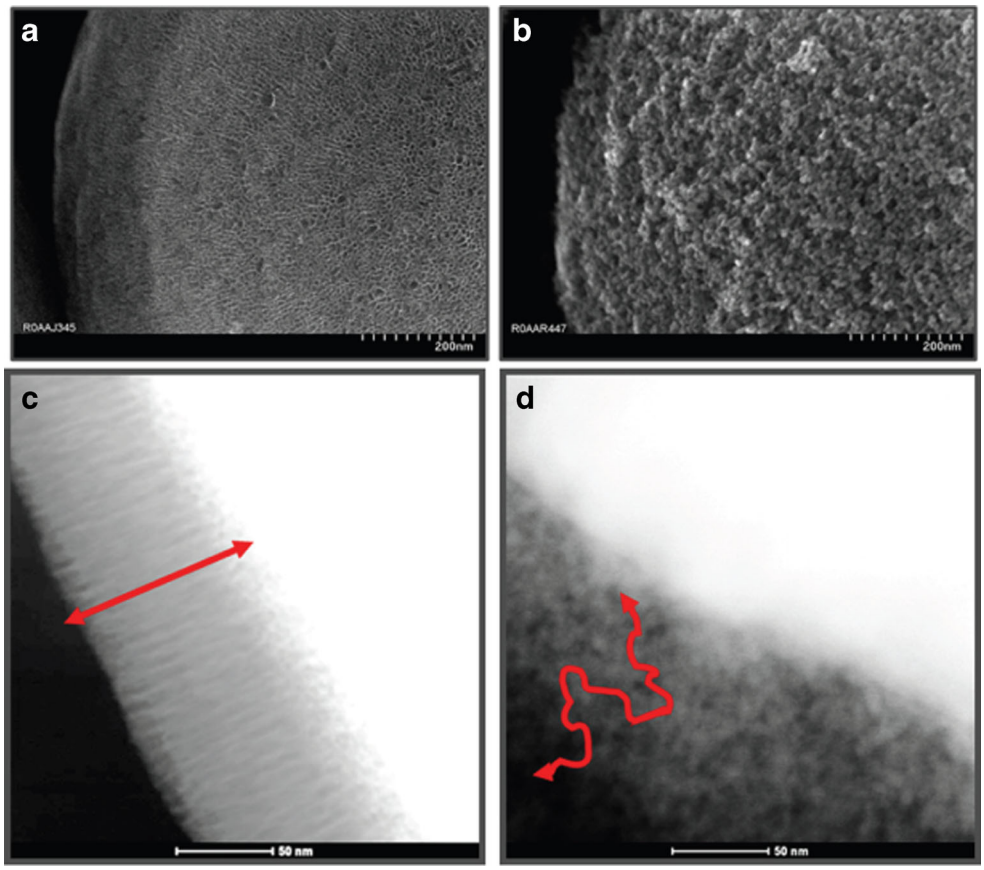

Fig. 3 High resolution SEM images of a ROM-SPP (**a**, **c**) and a SPP (**b**, **d**). Pictures (**c**) and (**d**) are cross-section views of the mesoporous network, showing the differences between the diffusion pathways in the two types of particles. Taken with permission from [30]

circumferential direction is completely blocked. Therefore, the only remaining route available for diffusion is the interstitial volume between particles. This advantage in the *b*-term is achieved without affecting the c_s-term, which does not increase, as it should be expected. Another important aspect that would affect the performance of ROM-SPPs is the geometrical shape of mesopores. From a theoretical point of view, Gritti has demonstrated that conical shaped mesopores would produce roughly 80% lower c_s-term than cylindrical ones [52].

In spite of these important advantages, the development of ROM-SPPs apparently is not any longer supported, due to (no better specified) both chemical stability problems and low mechanical resistance.

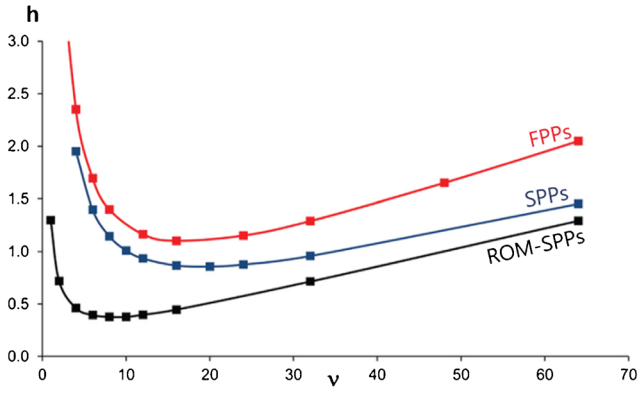

Fig. 4 Theoretical reduced van Deemter curves (h vs. ν, being h the reduced plate height and ν the reduced interstitial velocity) for packed beds made of FPPs (red data), traditional SPPs (blue data) and ROM-SPPs (black data). Modified with permission from [31]

Sub-2 μm SPPs: when instrumental constraints are the bottleneck to reaching highest efficiency

The reduction of the particle size to increase efficiency and favour faster separation has been pursued also with SPPs. Already a few years after the introduction of second generation SPPs in the format of 2.7 μm (Halo^{TM} particles), sub-2 μm SPPs were produced and commercialized. Very high efficiency and reduced analysis times were found by several authors by using columns packed with 1.7 μm SPPs [7, 17, 53–55]. Later on, the particle diameter of SPPs has been further decreased to 1.3 μm, which represents the smallest dimension of SPPs available to date in the market. Fekete et al. characterized columns packed with these particles from a kinetic viewpoint [4, 56]. They found exceptionally low reduced plate heights and high

peak capacities with cutting edge applications, especially in the field of fast separation of peptides. However, it appeared evident that instrumental constraints of even state of the art equipments prevent the full deployment of particle technology.

Figure 5 compares the van Deemter curves of Kinetex^{TM} SPPs of different sizes (including 1.3 μm ones). As it can be evinced from this plot, the minimum of the van Deemter curve for 1.3 μm particles is barely reached. This depends on the back-pressure limitations of commercial UHPLC equipments, which are not able to supply the pressure needed to push, through beds made of very small particles, the mobile phase at reasonably high linear velocities. As a matter of fact, for the current operating pressure limit, these particle format look advantageous only for the separation of large molecules (having a lower optimal velocity range than that of small molecules) both in isocratic and gradient elution mode [4, 56].

The reasearch was pushed forward by Blue and Jorgenson who featured the first example of 1.1 μm SPPs, the smallest SPP ever produced, through an innovative layer-by-layer synthetic approach [32, 33]. The information contained in Fig. 5 let us glimpse the highest potential of this material. Indeed, one might expect the van Deemter curve of 1.1 μm SPPs to be significantly lower than those of the other particle formats, potentially permitting to achieve incredibly high efficiency.

However, the expectation was not satisfied. Blue and Jorgenson report about the importance not only of an extremely precise control of experimental conditions for the synthesis of these particles but also of the slurry packing procedure, which can have a major impact on the efficiency of the column, in their case made of a 30 μm I.D. capillary. This last aspect, in particular, was claimed to be responsible for the performance observed with their capillaries, significantly lower than the theoretical values predictable for 1.1 μm particles.

In addition, the other very important instrumental factor limiting the development of this technology comes from the contribution to efficiency given by band broadening in the extra-column void volume (including injector, connections, column frits, detector, etc.) of modern UHPLC equipments, which is larger than that produced by particles of these intrinsic characteristics [57]. Finally, it is worth to mention that a practical problem of columns packed with very small particles is that they can behave as traps for particulate matter dissolved in the eluent, with important consequences on the lifetime of these columns if mobile phases and samples are not carefully filtered prior analysis.

Outlook

The technology not only of production but also of functionalization of SPPs to prepare very small particles with extremely enhanced properties in terms of mass transfer has come a long way. With the remarkable exception of RP achiral separations for particle not smaller than 1.7 μm, however, the potential of latest generation SPPs remains still largely unexplored due to a series of limitations, mainly instrumental ones, which have impeded the development of techniques and methods based on them.

The further advancement of the field requires an important contribution by LC instrument manufacturers for the production of equipments suitable to provide very large back pressure and, simultaneously, characterized by extremely low extra-column volume through innovative designs for detectors, injectors, column fittings, etc. This is particularly important (see below) for supercritical fluid chromatography (SFC), where the development of enhanced instrumentation is particularly necessary. Column manufacturers, on the other hand, should develop the technology to prepare very short columns with optimized

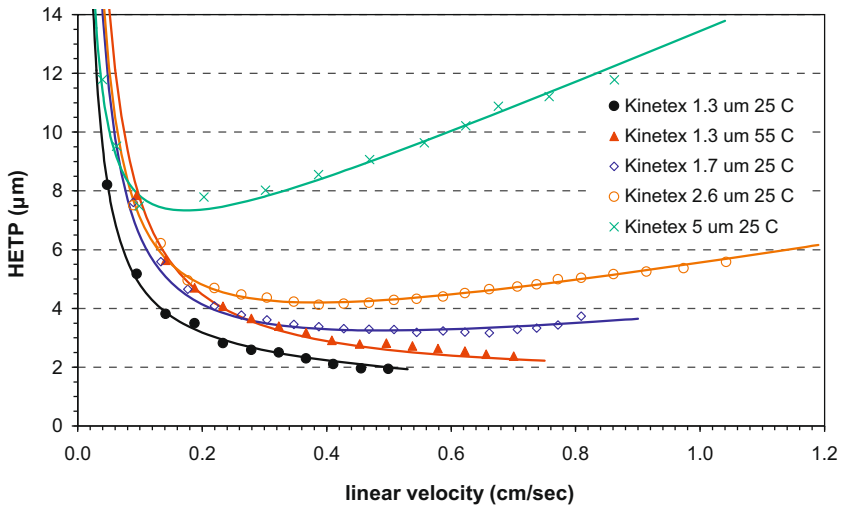

Fig. 5 Experimental van Deemter curves of butylparaben in reversed-phase conditions measured on columns packed with Kinetex 1.3, 1.7, 2.6 and 5 μm SPPs. Taken with permission from [4]

hardware (including column frits) to reduce extra-column band broadening. Advancement in 3D printing technology and CFD studies are fundamental to drive this change.

From a more theoretical viewpoint, an extension of our understanding of the packing process of slurry suspensions into chromatographic columns is necessary, by focusing in particular on the factors (including the rheology of particles, slurry density, etc. [49]) that affect it and which could have an impact on the performance of the resulting packed bed (e.g., through the a-term of the van Deemter equation).

In parallel, the investigation of the fundamentals of mass transfer is expected to provide information that will help the design of SPPs with still more advanced kinetic properties. For instance, the study of adsorption-desorption kinetics in chiral chromatography might suggest important indications on how to functionalize particles (e.g., in terms of density of chiral selector) for optimum performance.

It is precisely in the field of enantioseparations by LC that, in the nearest future, we can expect a real revolution thanks to the use of chiral SPPs of latest generation. Over the year, this field has fallen behind compared to achiral RP separations as regards ultrafast and high efficient separations. However, new developments in chiral particle technology let us predict an inversion of this trend. The market of chiral technology is already a very important one but it is expected to remarkably grow thanks to the new technology. In particular, extraordinary results and very fast enantioseparations are expected by the employment of latest generation chiral particles in SFC [58]. Moreover, chiral stationary phases made on SPPs could be suitable, thanks to their high efficiency, in the case of challenging enantiomeric separations (e.g., chiral impurity profiling), where an extremely low concentration of one enantiomer has to be detected [59].

Another field where chiral SPPs will find application is 2D-chromatography. Very short columns packed with SPPs can be efficiently used as second dimension for very fast separations in comprehensive applications [22].

Acknowledgements The authors thank Dr. Ercolina Bianchini of the University of Ferrara for technical support.

Compliance with Ethical Standards

Conflict of interests The authors declare that they have no conflict of interest.

References

1. Ismail OH, Catani M, Pasti L, Cavazzini A, Ciogli A, Villani C, et al. Experimental evidence of the kinetic performance achievable with columnspacked with new 1.9 μm fully porous particles of narrow particle size distribution. J Chromatogr A. 2016;1454:86–92.
2. Catani M, Ismail OH, Cavazzini A, Ciogli A, Villani C, Pasti L, et al. Rationale behind the optimum efficiency of columns packed with the new 1.9 μm fully porous particles of narrow particle size distribution. J Chromatogr A. 2016;1454:78–85.
3. Gritti F, Bell DS, Guiochon G. Particle size distribution and column efficiency. An ongoing debaterevived with 1.9 μm titan-C_{18} particles. J Chromatogr A. 2014;1355:179–92.
4. Fekete S, Guillarme D. Kinetic evaluation of new generation of column packed with 1.3 μm core-shell particles. J Chromatogr A. 2013;1308:104–13.
5. Neue UD. HPLC Columns: theory, technology and practice. Wiley-VCH. 1997.
6. Kirkland JJ, Langlois TJ. US Patent application 20070189944 a1. 2007.
7. Gritti F, Leonardis I, Shock D, Stevenson P, Shalliker A, Guiochon G. Performance of columns packed with the new shell particles, kinetex-C_{18}. J Chromatogr A. 2010;1217:1589–603.
8. Guiochon G, Gritti F. Shell particles, trials, tribulations and triumphs. J Chromatogr A. 2011;1218:1915–38.
9. Cavazzini A, Gritti F, Kaczmarski K, Marchetti N, Guiochon G. Mass-transfer kinetics in a shell packing materials for chromatography. Anal Chem. 2007;79:5972–79.
10. Horváth CG, Preiss BA, Lipsky SR. Fast liquid chromatogrpahy: an investigation of operating parameters and the separation of nucleotides on pellicular ion exchangers. Anal Chem. 1967;39:1422–28.
11. González-Ruiz V, Olives AI, Martín MA. Core-shell particles lead the way to renewing high-performance liquid chromatography. TrAC. 2015;64:17–28.
12. Guiochon G, Gritti F. Theoretical investigation of diffusion along columns packed with fully and superficially porous particles. J Chromatogr A. 2011;1218:3476–88.
13. van Deemter JJ, Zuiderweg FJ, Klinkenberg A. Longitudinal diffusion and resistance to mass transfer as causes of nonideality in chromatography. Chem Eng Sci. 1956;5:271–83.
14. Gritti F, Cavazzini A, Marchetti N, Guiochon G. Comparison between the efficiencies of columns packed with fully and partially porous C_{18}-bonded silica materials. J Chromatogr A. 2007;1157:289–303.
15. Daneyko A, Hlushkou D, Baranau V, Khirevic S, Seidel-Morgenstern A, Tallarek U. Computational investigation of longitudinal diffusion, eddy dispersion, and trans-particle mass transfer in bulk, random packings of core-shell particles with varied shell thickness and shell diffusion coefficient. J Chromatogr A. 2015;1407:139–56.
16. Catani M, Ismail OH, Gasparrini F, Antonelli M, Pasti L, Marchetti N, et al. Recent advancements and future directions of superficially porous chiral stationary phases for ultrafast high-performance enantioseparations. Analyst. 2017;142:555–66.
17. Gritti F, Leonardis I, Abia J, Guiochon G. Physical properties and structure of fine core-shell particles used as packing materials for chromatography. Relationship between particle characteristics and column performance. J Chromatogr A. 2010;1217:3819–43.
18. Preti R. Core-shell columns in high-performance liquid chromatography: food analysis applications. International Journal of Analytical Chemistry. 2016;2016:1–9.
19. Gritti F, Guiochon G. Speed-resolution properties of columns packed with new 4.6 μm kinetex-C_{18} core-shell particles. J Chromatogr A. 2013;1280:35–50.
20. Oláh E, Fekete S, Fekete J, Ganzler K. Comparative study of new shell-type, sub-2 μm fully porous and monolith stationary phases, focusing on mass transfer resistance. J Chromatogr A. 2010;1217:3642–53.
21. Hayes R, Ahmed A, Edge T, Zhang H. Core-shell particles: preparation, fundamentals and applications in high performance liquid chromatography. J Chromatogr A. 2014;1357:36–52.

22. Jandera P, Hàjek T, Staňkovà M. Monolithic and core-shell columns in comprehensive two-dimensional HPLC: a review. Anal Bioanal Chem. 2016;407:139–51.
23. Marchetti N, Guiochon G. High peak capacity separations of peptides in reversed-phase gradient elution liquid chromatography on columns packed with porous shell particles. J Chromatogr A. 2007;1176:206–16.
24. Marchetti N, Guiochon JNFG. High peak capacity separations of peptides in reversed-phase gradient elution liquid chromatography on columns packed with porous shell particles. Anal Chem. 2008;80:2756–67.
25. Ismail OH, Pasti L, Ciogli A, Villani C, Kocergin J, Anderson S, et al. Pirkle-type chiral stationary phase on core–shell and fully porousparticles: are superficially porous particles always the better choice toward ultrafast high-performance enantioseparations? J Chromatogr A. 2016;1466:96–104.
26. Ismail OH, Antonelli M, Ciogli A, Villani C, Cavazzini A, Catani M, et al. Future perspectives in high efficient and ultrafast chiral liquid chromatography through zwitterionic teicoplanin-based 2-μm superficially porous particles. J Chromatogr A. 1520;2017:91–102.
27. Patel DC, Wahab MF, Armstrong DW, Breitbach ZS. Salient sub-second separations. Anal Chem. 2016;88:8821–26.
28. Patel DC, Breitbach ZS, Wahab MF, Barhate CL, Armstrong DW. Gone in seconds: praxis, performance and peculiarities of ultrafast chiral liquid chromatography with superficially porous particles. Anal Chem. 2015;87:9137–48.
29. Thurmann S, Lotter C, Heiland JJ, Chankvetadze B, Belder D. Chip-based high-performance liquid chromatography for high-speed enantioseparations. Anal Chem. 2015;87:5568–76.
30. Wei TC, Mack A, Chen W, Liu J, Dittmann M, Wang X, et al. Synthesis, characterization and evaluation of a superficially porous particle with unique, elongated pore channels normal to the surface. J Chromatogr A. 2016;1440:55–65.
31. Deridder S, Catani M, Cavazzini A, Desmet G. A theorethical study on the advantage of core-shell particles with radially-oriented mesopores. J Chromatogr A. 2016;1456:137–44.
32. Blue LE, Jorgenson JW. 1.1 μm superficially porous particles for liquid chromatography. Part I: synthesis and particle structure characterization. J Chromatogr A. 2011;1218:7989–95.
33. Blue LE, Jorgenson JW. 1.1 μm superficially porous particles for liquid chromatography. Part II: column packing and chromatographic performance. J Chromatogr A. 2015;1380:71–80.
34. Cavazzini A, Pasti L, Massi A, Marchetti N, Dondi F. Recent applications in chiral high performance liquid chromatography: a review. Anal Chim Acta. 2011;706:205–22.
35. Reischl RJ, Hartmanova L, Carrozzo M, Huszar M, Frühauf P, Lindner W. Chemoselective and enantioselective analysis of proteinogenic ammino acids utilizing N-derivatization and 1-D enantioselective anion-exchange chromatography in combination with tandem mass spectrometry. J Chromatogr A. 2011;1218:8379–87.
36. Lai X, Tang W, Ng SC. Novel cyclodextrin chiral stationary phases for high performance liquid chromatography enantioseparation: Effect of cyclodextrin type. J Chromatogr A. 2011;1218:5597–601.
37. Cancelliere G, Ciogli A, D'Acquarica I, Gasparrini F, Kocergin J, Misiti D, et al. Transition from enantioselective high performance to ultra-high performance liquid chromatography: a case study of a brush-type chiral stationary phase based on sub-5-micron to sub-2-micron silica particles. J Chromatogr A. 2010;1217:990–9.
38. Cavazzini A, Marchetti N, Guzzinati R, Pierini M, Ciogli A, Kotoni D, et al. Enantioseparation by ultra-high-performance liquid chromatography. TrAC. 2014;63:95–103.
39. Lomsadze K, Jibuti G, Farkas T, Chankvetadze B. Comparative high-performance liquid chromatography enantioseparations on polysaccharide based chiral stationary phases prepared by coating totally porous and core-shell silica particles. J Chromatogr A. 2012;1234:50–55.
40. Kharaishvili Q, Jibuti G, Farkas T, Chankvetadze B. Further proof to the utility of polysaccharide-based chiral selectors in combination with superficially porous silica particles as effective chiral stationary phases for separation of enantiomers in high-performance liquid chromatography. J Chromatogr A. 2016;1467:163–8.
41. Spudeit DA, Dolzan MD, Breitbach ZS, Barber WE, Micke GA, Armstrong DW. Superficially porous particles vs. fully porous particles for bonded high performance liquid chromatography chiral stationary phases: isopropyl cyclofructan 6. J Chromatogr A. 2014;1363:89–95.
42. Barhate CL, Breitbach ZS, Pinto EC, Regalado EL, Welch CJ, Armstrong DW. Ultrafast separation of fluorinated and desfluorinated pharmaceuticals using highly efficient and selective chiral selectors bonded to superficially porous particles. J Chromatogr A. 2015;1426:241–7.
43. Patel DC, Wahab MF, Armstrong DW, Breitbach ZS. Advances in high-throughput and high-efficiency chiral liquid chromatographic separations. J Chromatogr A. 2016;1467:2–18.
44. Patel DC, Wahab MF, Armstrong DW, Breitbach ZS. Superficially porous particles vs. fully porous particles for bonded high performance liquid chromatographic chiral stationary phases: isopropyl cyclofructan 6. J Chromatogr A. 2014;1365:124–30.
45. Wimalasinghe RM, Weatherly CA, Breitbach ZS, Armstrong DW. Hydroxypropyl beta cyclodextrin bonded superficially porous particlebased HILIC stationary phases. J Liq Chromatogr Rel Tech. 2016;39:459–64.
46. Patel DC, Breitbach ZS, Yu J, Nguyen KA, Armstrong DW. Quinine bonded to superficially porous particles for high-efficiency and ultrafast liquid and supercritical fluid chromatography. Anal Chim Acta. 2017;963:164–74.
47. Pasti L, Marchetti N, Guzzinati R, Catani M, Bosi V, Dondi F, et al. Microscopic models of liquid chromatography: from ensemble-averaged information to resolution of fundamental viewpoint at single-molecule level. TrAC. 2016;81:63–68.
48. Dondi F, Cavazzini A, Remelli M. The stochastic theory of chromatography. Adv Chromatogr. 1998;38:51–74.
49. Bruns S, Franklin EG, Grinias JP, Godinho JM, Jorgenson JW, Tallarek U. Slurry concentration effects on the bed morphology and separation efficiency of capillaries packed with sub-2 μm particles. J Chromatogr A. 2013;1318:189–97.
50. Wahab MF, Patel DC, Wimalasinghe RM, Armstrong DW. Fundamental and practical insights on the packing of modern high-efficiency analytical and capillary columns. Anal Chem. 2017;89:8177–91.
51. Gritti F, Guiochon G. Mass transfer mechanism in chiral reversed phase liquid chromatography. J Chromatogr A. 2014;1332:35–45.
52. Gritti F. Impact of straight, unconnected, radially-oriented, and tapered mesopores on column efficiency: a theoretical investigation. J Chromatogr A. 1485;2017:70–81.
53. Fekete S, Ganzler K, Fekete J. Efficiency of the new sub-2 μm core-shell (Kinetex^{TM}) column in practice, applied for small and large molecule separation. J Pharm Biomed Anal. 2011;54:482–90.
54. Omamogho JO, Hanrahan JP, Tobin J, Glennon JD. Structural variation of solid core and thickness of porous shell of 1.7 μm core–shell silica particles on chromatographic performance: narrow bore columns. J Chromatogr A. 2011;1218:1942–53.

55. Gritti F, Guiochon G. Mass transfer resistance in narrow-bore columns packed with 1.7 μm particles in very high pressure liquid chromatography. J Chromatogr A. 2010;1217:5069–83.
56. Sanchez AC, Friedlander G, Fekete S, Anspach J, Guillarme D, Chitty M, et al. Pushing the performance limits of reversed-phase ultra high performance liquid chromatography with 1.3 μm core-shell particles. J Chromatogr A. 2013;1311:90–97.
57. Broeckhoven K, Desmet G. The future of UHPLC: towards higher pressure and/or smaller particles? TrAC. 2014;63:65–75.
58. Sciascera L, Ismail OH, Ciogli A, Kotoni D, Cavazzini A, Botta L, et al. Expanding the potential of chiral chromatography for high-throughput screening of large compound libraries by means of sub-2 μm Whelk-O 1 stationary phase in supercritical fluid conditions. J Chromatogr A. 2015;1383:160–8.
59. Mazzoccanti G, Ismail OH, D'Acquarica I, Vilani C, Manzo C, Wilcox M, et al. Cannabis through the looking glass: chemo- and enantio-selective separation of phytocannabinoids by enantioselective ultra high performance supercritical fluid chromatography. Chem Commun. 2017;53:12262–5.

PAPER V

Journal of Chromatography A, 1466 (2016) 96–104

Contents lists available at ScienceDirect

Journal of Chromatography A

journal homepage: www.elsevier.com/locate/chroma

Pirkle-type chiral stationary phase on core–shell and fully porous particles: Are superficially porous particles always the better choice toward ultrafast high-performance enantioseparations?

Omar H. Ismail[a], Luisa Pasti[b], Alessia Ciogli[a], Claudio Villani[a], Jelena Kocergin[c], Scott Anderson[c], Francesco Gasparrini[a,*], Alberto Cavazzini[b,*], Martina Catani[b]

[a] Dept. of Drug Chemistry and Technology, "Sapienza" Università di Roma, P.le A. Moro 5, 00185 Roma, Italy
[b] Dept. of Chemistry and Pharmaceutical Sciences, University of Ferrara, via L. Borsari 46, 44121 Ferrara, Italy
[c] Regis Technologies, Inc., 8210 Austin Avenue, Morton Grove, IL 60053, USA

ARTICLE INFO

Article history:
Received 29 July 2016
Received in revised form 31 August 2016
Accepted 1 September 2016
Available online 3 September 2016

Keywords:
Whelk-O1 superficially porous chiral stationary phase
Ultrafast enantioseparations
Mass transfer kinetics
Sub-second separation
Normal phase mode

ABSTRACT

Pirkle-type Whelk-O1 chiral stationary phase (CSP) was prepared on 2.6 μm superficially porous particles (SPPs). The chromatographic behavior of columns packed with this new CSP was compared with that of columns packed respectively with 1.8 and 2.5 μm Whelk-O1 fully porous particles (FPPs). In the comparison, both thermodynamic and kinetic aspects were considered. Contrary to initial expectations, chiral columns packed with 2.6 μm SPPs were quasi-comparable to those packed with 2.5 μm FPPs, apparently due to larger contributions to band broadening from both eddy dispersion and, especially for the second eluted enantiomer, adsorption–desorption kinetics. These findings raise the question if SPPs, in spite of the undeniable advantages of their morphology to speed up mass transfer, are always the best choice for high-efficient ultrafast chiral separations. The last part of the work focuses on the use of short columns (10 mm long) and very high flow rates to realize the separation of the enantiomers of *trans*-stilbene oxide (TSO) in normal phase mode in less than 1 s.

1. Introduction

Last generation superficially-porous particles (SPPs) [1,2], referred to also as core–shell, fused-core or solid-core particles, are made of a non-porous fused silica core surrounded by a porous shell, whose volume is usually 60–75% of particle volume. In terms of mass transfer, core–shell structure offers some advantages over that of a fully porous particle (FPP) since the contributions to band broadening from both the longitudinal diffusion due to the relaxation of axial gradient concentration along the column (the so-called *B*-term of the van Deemter equation) and the solid–liquid mass transfer resistance due to the diffusion across the particle (*C*-term of the van Deemter equation) are reduced by the presence of the inaccessible core. In addition, columns packed with C_{18}-SPPs have been demonstrated to be extremely efficient also thanks to the very low eddy diffusion, which comes from flow unevenness in the interstitial zone of the column (*A*-term of the van Deemter equation) [3–5]. Even though the explanation of the low *A*-term for columns packed with C_{18} SPPs remains to a large extent unknown, the most accepted hypothesis is that roughness of core–shell particles limits particle slipping after releasing the high pressure employed for the preparation of the packed bed by slurry-packing, therefore reducing radial bed heterogeneity [1,2]. The reason of the great success of SPPs is that they have provided a reasonable compromise between two opposite tendencies. Indeed, the tendency to improve analytical throughputs by means of columns packed with smaller and smaller particles and reduced dimensions is limited by instrumental factors, such as the extremely high pressures needed to operate these columns at high flow rates, on the one hand, and the effect of system extra-column volume on peak broadening, on the other. As a matter of fact, columns packed with 2.7 μm SPPs are able to provide essentially the same efficiency as columns packed with sub 2-μm FPPs (keeping constant column dimensions and experimental conditions), but at operating pressures similar to those of columns packed with 3 μm FPPs [6,7].

Surprisingly, the employment of SPPs in chiral chromatography is relatively recent [8]. The first work describing the use of SPPs in chiral HPLC dates 2011, when Lindner and coworkers prepared [9] a cinchona alkaloid based anion exchanger CSP by using

* Corresponding authors.
E-mail addresses: francesco.gasparrini@uniroma1.it (F. Gasparrini), cvz@unife.it (A. Cavazzini).

http://dx.doi.org/10.1016/j.chroma.2016.09.001
0021-9673/

2.7 μm fused-core particles as base material. The column was successfully employed for the enantioseparation of amide type amino acid derivatives, even if the authors do not mention the possible advantages given by this typology of CSP. Chankvetadze et al. [10] firstly compared the kinetic performance of CSPs prepared on polysaccharide-coated FPPs and SPPs. They mentioned some of the benefits of chiral SPPs over their fully porous counterparts, such as an higher enantioselectivity at comparable content of chiral selector, a limited dependence of plate height on mobile phase flow rate and a larger enantioresolution per analysis time, with obvious benefits for high-throughput screening of chiral compounds [10]. By using 4.6 mm I.D. × 250 mm columns, they demonstrated that columns packed with SPPs outperform those packed with FPPs in terms of efficiency and speed of analysis. Fanali and coworkers [11,12] employed the same polysaccharide-based chiral particles used in [10] to pack capillary columns (75 μm I.D. × 25 cm) for nano-liquid chromatography and electrochromatography experiments. They report about the difficulty to efficiently operate these capillaries. They conclude that, without further optimization, this column format does not allow to reach useful efficiency for high-performance separation. Even if the authors do not discuss in detail the reason of the poor performance of these packed capillaries, more than on the kinetic performance of particles themselves, this could depend either on the difficulty of efficiently packing chiral core–shell particles (and thus to the contribution of eddy dispersion to peak broadening) or on the overall difficulty in getting efficient SPP columns at the capillary scale [13–19].

The most systematic work on the comparison between chiral FPPs and SPPs has been done by Armstrong's group [20–22]. With the aim of investigating the potential of chiral SPPs for ultrafast enantioseparations, Armstrong and coworkers characterized a wide variety of bonded brush-type CSPs prepared on 2.7 μm SPPs, including cyclofructan-6 based, β-cyclodextrin and macrocyclic antibiotics (in particular, teicoplanin, teicoplanin aglycone and vancomycin) [20]. The concept that emerges from these studies is that chiral SPPs outperform their FPP counterparts in any chromatographic mode, namely, reversed-phase (RP), normal phase (NP), polar organic and HILIC.

In the first part of this paper, we report about the synthesis of novel Pirkle-type Whelk-O1 2.6 μm chiral SPPs and the kinetic characterization of columns packed with these particles. To this scope, a comparison between the performance of these columns and those of columns packed with both 2.5 and 1.8 μm FPPs functionalized with identical chiral selector [23,24] was performed by using *trans*-stilbene oxide (TSO) enantiomers as probes. In the second part of the work, the potential of Whelk-O1 CSPs for ultrafast enantioseparations on the second/sub-second time-scale is investigated by means of short columns (10 mm packed with both FFPs and SPPs) operated at very high flow rates (up to 8 mL/min).

2. Experimental

2.1. Columns and materials

All solvents and reagents employed in this work were purchased from Sigma–Aldrich (St. Louis, MI, USA). Kromasil silica (1.8 and 2.5 μm particle size, 100 Å pore size, 323 m^2/g specific surface area) was from Akzo-Nobel (Bohus, Sweden). Whelk-O1 selector was generously donated by Regis Technologies Inc. (Morton Grove, IL, USA). Accucore silica (2.6 μm particle size, 80 Å pore size, 130 m^2/g specific surface area, 0.5 μm shell thickness) was from Thermo Fisher Scientific (Waltham, MA, USA). 150 and 100 mm × 4.6 mm empty stainless steel columns were from IsoBar Systems by Idex (Erlangen, Germany), while 10 mm × 4.6 mm and 10 mm × 3.0 mm ones (including their holders) were fully developed and produced in-house. Fourteen polystyrene standards (from Supelco Sigma–Aldrich, Milan, Italy) with molecular weights 500, 2000, 2500, 5000, 9000, 17,500, 30,000, 50,000, 156,000, 330,000, 565,000, 1,030,000, 1,570,000, and 2,310,000 were employed for inverse size exclusion chromatography (ISEC).

2.2. Equipment

Two chromatographic equipments were employed in this work. Unless differently specified, the UHPLC chromatographic system used for 150 and 100 mm columns was an UltiMate 3000 RS system from Thermo Fisher Dionex (Whaltam, MA, USA) consisting of a dual gradient RS pump (flow rates up to 8.0 mL/min; pressure limit 800 bar under NP conditions), an in-line split loop Well Plate Sampler, a thermostated RS Column Ventilated Compartment and a diode array detector (UV Vanquish) with a low dispersion 2.5 μL flow cell. Detection wavelength was 214 nm (constant filter time: 0.002 s; data collection rate: 100 Hz; response time: 0.04 s). To reduce the extra-column contributions two 350 mm × 0.10 mm I.D. Viper capillaries were used to connect the injector to the column and the column to the detector. The extra-column peak variance (calculated through peak moments) was 5.5 μL^2 in Hex/EtOH 90:10 + 1% MeOH at a flow rate of 1.0 mL/min (extra-column volume: 12.2 μL). Data acquisition, data handling and instrument control were performed by Chromeleon (vers. 6.8) software.

An UPLC Acquity Waters system (Milford, MA, USA), equipped with a binary solvent manager (2 mL/min maximum flow rate; pressure limit 1000 bar), an auto-sampler with a 5 μL injection loop, a thermostated column compartment (operated in still air conditions [5]), a diode array detector with a 500 nL flow cell, 80 Hz acquisition rate (resolution 4.8 nm; no filter time constant) was employed. Two Viper capillaries (250 mm × 0.100 mm and 350 mm × 0.100 mm $L \times$ I.D.) were used as inlet and outlet connectors. The extra-column peak variance (through peak moments) was only 0.91 μL^2 at 1.0 mL/min. An updated version of Empower software was used in order to measure the second central time moments of the recorded concentration profiles. For the 10 mm columns, a modified version of the UPLC was used (Fig. S1 of Supplementary Data shows some images of the experimental arrangement). The programmable auto-sampler was replaced with an external in-house modified sample injector from VICI, Houston, TX, USA (model C74U). Essentially, this modification allowed for an electronic and fine control of the switching time (1.10 s) from injection to loading position and back. The injector is equipped with a 50 nL internal injection loop and a micro-electric actuator (Valco instruments, Houston, TX, USA). The sample solution was introduced through a 25 μL syringe. This arrangement ensured consistent reduction of tailing effect and high reproducibility between injections. The standard inlet and outlet connecting tubes were replaced by two PEEK tubings of, respectively, 50 and 60 mm length × 63.5 μm I.D. With this configuration, the extra-column peak variance (through peak moments) was only 0.14 μL^2 at 1.0 mL/min.

2.3. Synthesis of Whelk-O1 SPPs and preparation of columns

Whelk-O1 SPPs were synthesized according to the procedure described by Pirkle and co-workers in 1992 [25,26], which has been also employed for the synthesis of Whelk-O1 FPPs [27–29].

CHN elemental analysis for the different silica types functionalized in this work returned the following values: 6.28% C, 0.84% H and 0.73% N for 2.6 μm SPPs; 13.41% C, 1.73% H and 1.39% N for 1.8 μm FPPs; 13.30% C, 1.73% H and 1.38% N for 2.5 μm FPPs. Calculated bonding densities (based on N) are reported in Table 1. Details on how these calculations were performed can be found in

Table 1
Geometrical characteristics of Whelk-O1 columns: particle type (FP: fully porous, SP: superficially porous); column dimensions; particle diameter (d_p); specific surface area (A_s); pore size; bonding density (given both as μmol per gram of bare silica and μmol per square meter).

Particle type	Dimensions	d_p	A_s	Pore size	Bonding density	
	($L \times$ I.D., mm)	(μm)	(m^2/g)	(Å)	(μmol/g)	(μmol/m^2)
FP	150 × 4.6	2.5	323	100	391.2	1.21
FP	100 × 4.6	1.8	323	100	394.6	1.22
SP	150 × 4.6	2.6	130	80	189.8	1.46

reference [30]. FT-IR (KBr) of Whelk-O1 were: 2924, 2864, 1675, 1627, 1548, 1513, 1344, and 1078 cm^{-1}.

All columns were slurry packed with a pneumatically driven Haskel pump (P_{max} = 1000 bar). The slurry solution (10% (w/v) of Whelk-O1 particles in acetone) was pushed into the column by using a mixture of hexane/2-propanol 90:10 (%, v/v) as pushing solvent. The pressure was increased from 400 bar up to 1000 bar. 100 mL of pushing solvent were pumped into the column at 1000 bar to consolidate the bed. Decompression until atmospheric pressure was gradually performed.

2.4. van Deemter curve measurements

The kinetic performance of Whelk-O1 columns was evaluated in NP conditions. The mobile phase was a mixture of hexane/ethanol 90:10 (%, v/v) + 1% methanol. Injection volumes were 0.1–0.5 μL. Temperature was set at 35 °C. Retention time (t_R) and column efficiency (number of theoretical plates, N) of eluted peaks were automatically processed by the Chromeleon and Empower 3 software (using peak width at half height, according to European Pharmacopeia). N values were not corrected by extra-column contribution. The flow rates employed for studying the dependence of height equivalent to a theoretical plate H (=L/N, being L the column length) on the mobile phase velocity started from 0.1 mL/min up to maximum respectively of 4.0 mL/min (for 100 and 150 mm long columns; equipment: Dionex 3000RS) and 2.0 mL/min (for 10 mm long columns; equipment: Waters Acquity), with constant steps of 0.1 mL/min. van Deemeter curves were plotted as H vs. interstitial velocity, u_{int}. u_{int} was calculated according to the well known equation:

$$u_{\text{int}} = \frac{F_v}{\pi r^2 \epsilon_e} \tag{1}$$

being F_v the flow rate, r the radius of the column and ϵ_e the interstial porosity. ϵ_e was calculated by ISEC experiments, as described below.

2.5. ISEC measurements, estimation of interstitial and total porosity and retention factor evaluation

ISEC measurements were performed by using tetrahydrofuran as mobile phase [31]. Injection volume, flow rate and detection wavelength were, respectively, 2 μL, 0.1 mL/min and 254 nm. For ISEC plots, retention volumes were corrected for the extra-column contribution before being plotted against the cubic root of the molecular weight (M_W). The interstitial volume, V_e, was derived from the extrapolation to M_W = 0 of the linear regression calculated for the volumes of the totally excluded polystyrene samples [32]. From this, the estimation of external column porosity, ϵ_e, is straightforward (being $\epsilon_e = V_e/V_{col}$, with V_{col} the geometric volume of the column). The ISEC estimation of the thermodynamic void volume, V_0, was based on the retention volume of benzene. Through this, the total porosity ϵ_t can be calculated ($\epsilon_t = V_0/V_{col}$).

The retention factor for the ith enantiomer, k_i, was calculated by:

$$k_i = \frac{t_{R,i} - t_0}{t_0} \tag{2}$$

where $t_{R,i}$ is the retention time of the ith enantiomer (i = 1, 2) and t_0 the void time calculated by using carbon tetrachloride (CCl_4) as marker.

2.6. Specific permeability and Kozeny–Carman constant

The specific permeability of each column was calculated according to the traditional equation [33,34]:

$$k_0 = \frac{u\eta L}{\Delta P} \tag{3}$$

where $u = F_v/\pi r^2$ is the superficial velocity and η the viscosity of the eluent (0.46 cP for THF at 25 °C [35]). ΔP is the difference between the total pressure drop, P_{tot}, and the system pressure drop (without the column), P_{ex}. P_{ex} was measured by replacing the column with a zero-volume connector. Experimentally, k_0 can be estimated by the slope of ΔP vs. u plot [36].

The Kozeny–Carman constant K_c was estimated by [33]:

$$K_c = \frac{\epsilon_e^3}{(1-\epsilon_e)^2}\frac{d_p^2}{k_0} \tag{4}$$

where d_p is the particle size (nominal d_ps given by manufacturer were used in this work in place of the more correct Sauter diameter value [5]).

3. Results and discussion

The preparation of SPPs was performed by following the same experimental protocol described in [27–29] for the functionalization of sub-2 μm FPPs. The synthesis is particularly advantageous and reproducible even on SPPs, since phenomena such as particle aggregation and clogging or the non-uniform/excessive selector coating, frequently encountered with other chiral selectors, do not represent an issue with Whelk-O1 selector. Table 1 lists the characteristics of the particles employed in this work in terms of dimension, specific surface area, pore size (data from manufacturers) and chiral-selector loading (see Section 2). Surface coverage is given both as μmol per gram of bare silica (column 6 of Table 1) and μmol per square meter (column 7). Several things can be observed from this table. The first is that the synthesis of FPPs of different dimensions is extremely reproducible (practically the same loading of chiral selector, about 390 μmol/g or 1.2 μmol/m^2, was found on the 1.8 and 2.5 μm FPPs). The second is that, by keeping constant the experimental conditions, functionalization of bare silica leads to significantly larger surface coverage of chiral selector (+20%) on SPPs (1.5 μmol/m^2) than on fully porous ones (1.2 μmol/m^2). This could be due to different reasons such as larger accessibility of external layers of particles, different surface chemistry of base silica FPPs and SPPs, etc. However, it is difficult to generalize these findings. They are indeed consistent with previous reports by Armstrong and coworkers [21,20], but contrast with other data from

the same group [37]. Obviously, since the specific area per gram of FPPs is larger than that of SPPs, the total amount of chiral selector bounded per gram of base silica is also greater on the former type of particles than on fused-core ones.

The common understanding is that the larger the amount of chiral-selector tethered to the surface, the larger the loadability of the phase (which is definitely important in preparative applications [38–40]) and the larger the retention factor. On the other hand, the relationship between enantioselectivity and surface coverage of chiral selector is not straightforward, since this last could impact also on the adsorption–desorption kinetics and thus on the separation efficiency. The resolution, R_s, of two chromatographic peaks (defined by the peak separation divided by the mean peak width) can be indeed expressed as [41]:

$$R_s = \frac{\sqrt{N}}{2}\frac{\alpha - 1}{\alpha + 1}\frac{\bar{k}}{1 + \bar{k}} \quad (5)$$

where N is the number of theoretical plates, and $\bar{k}$ and α are, respectively, the average retention factor (i.e., the average of retention factors of the two enantiomers) and the selectivity, defined by [42]:

$$\alpha = \frac{k_2}{k_1} \quad (6)$$

According to Eq. (5), one observes that resolution not only depends on the fact that solutes must be retained ($\bar{k} \neq 0$) and that they must be retained at different extent ($\alpha \neq 1$), but also on the efficiency of the column, with higher efficiencies giving better resolution.

Fig. 1 shows the chromatograms recorded for the separation of TSO enantiomers on, respectively, the 150 mm × 4.6 mm I.D. column packed with 2.5 μm FPPs (top), the 100 mm × 4.6 mm I.D. one packed with 1.8 μm FPPs (middle) and, finally, the 150 mm × 4.6 mm I.D. column packed with 2.6 μm SPPs (bottom). On each column, the flow rate (see figure caption) at which the chromatogram was recorded corresponds to the optimal flow rate, that is where the van Deemter curve presents its minimum (see later on). For the sake of comparison between different columns, the x-axis is expressed as retention factor (in place of the traditional retention time). Retention factors were calculated by using CCl_4 as the void volume marker (see Section 2). As it can be noticed from Fig. 1, on the two columns packed with 2.5 μm and 1.8 μm FPPs, TSO enantiomers are characterized by the same retention factors (k_1 = 0.69 and k_2 = 1.72), with α equal to 2.49. On the other hand, on the column packed with 2.6 μm SPPs, retention of both enantiomers is smaller (k_1 = 0.50 and k_2 = 1.27) but α is slightly larger (2.54). On the same figure the efficiency (N/m) of each peak has also been reported. N was calculated as described in Section 2. In all cases, very large values were observed. In particular, on the 100 mm × 4.6 mm I.D. column packed with 1.8 μm FPPs (middle chromatogram), an efficiency as large as 292,000 and 271,000 N/m was obtained respectively for the first and the second eluted enantiomer. As a marginal remark, it can be observed that these values are typical of efficient RP systems [36,5]. The resolution of columns, estimated by Eq. (5), resulted very large as well. R_s is 19.6 on the column packed with 1.8 μm FPPs, 20.2 for the column packed with 2.5 μm FPPs and 17.3 on the column packed with core–shell particles. Therefore, the column packed with SPPs has the lowest R_s, even if the surface density of chiral-selector measured on these particles was the highest (Table 1). However, the overall much higher surface area for FPPs can outweigh this feature and explain this fact. The difference in R_s between columns packed with FPPs could reflect not only the difference in column length and thus in the total N per column (Fig. S2 of Supplementary Data graphically shows this concept by reporting, for the three columns, N per column as a function of velocity) but also the impact of particle size (1.8 vs. 2.5 μm) on the measured efficiency. On the other hand, to explain the smallest R_s measured on the core–shell column one has to consider that the very favorable contribution of α is ruled out by both the effect of efficiency and retention.

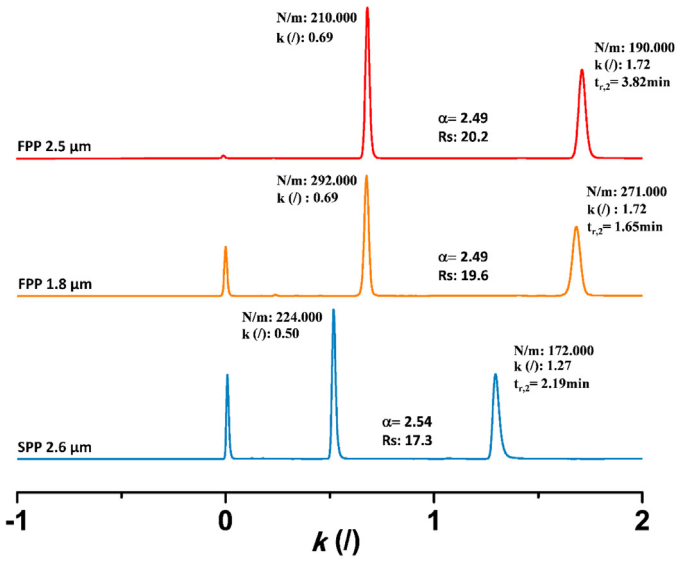

Fig. 1. Chromatograms showing the separation of TSO enantiomers on the three columns employed in this work. Carbon tetrachloride was used as dead time marker. Top: 150 mm × 4.6 mm column packed with Whelk-O1 2.5 μm FPPs; middle: 100 mm × 4.6 mm column packed with Whelk-O1 1.8 μm FPPs; bottom: 150 mm × 4.6 mm column packed with Whelk-O1 2.6 μm SPPs. Chromatograms were recorded at the flow rate corresponding to the minimum of the van Deemter curve (they were, from top to bottom, respectively 1.2, 1.8 and 1.5 mL/min). For the sake of comparison, x-axis is given in terms of retention factor instead of retention time. Close to each peak, efficiency (N/m), retention factor (k) and retention time (t_R) are indicated. Instrument employed for measurements: UPLC Waters Acquity.

Table 2 reports some of the physico-chemical parameters in use to assess the quality of column packing, at least from a qualitative viewpoint, such as the external porosity, ϵ_e, and the Kozeny–Carman constant (see Eq. (4)). For well packed columns, ϵ_e is roughly 0.4 [1,43] and 0.37 [44,5] respectively for beds made of core–shell and fully porous particles and the K_c constant is close to 180 [33]. As it can be seen from this table, for all columns ϵ_e was about 40%. However, while the columns packed with FPPs have K_c equal to 180, for the one packed with SPPs K_c is only 160. For the sake of completeness, in Table 2, the total porosities, ϵ_t, of columns are also reported (see Section 2 for details). Their values are close to typical values for columns packed with fully porous (0.65–0.7) and core–shell (0.52–0.55) particles [32,39,45].

The other important information that can be derived from Table 2 is about the permeability (see Eq. (3)) of columns. As expected, the column packed with 1.8 μm FPPs is characterized by the smallest k_0 value, 2.95×10^{-11} cm^2, which reflects the difficulty of delivering a flow in a bed made of very fine particles. Surprisingly, the column packed with 2.6 SPPs results to be about 25% more permeable than that packed with 2.5 FPPs, even tough their ϵ_e are very similar. This could suggest a less dense packing of SPPs that, together with the already discussed low value of K_c, could affect the kinetic performance of the column.

Table 2
Physico-chemical properties of Whelk-O1 columns: particle type (FP: fully porous, SP: superficially porous); total porosity (ϵ_t); external porosity (ϵ_e); Kozeny–Carman constant (K_c); permeability (k_0).

Particle type	ϵ_t	ϵ_e	K_c	$k_0 \times 10^{11}$ (cm^2)
FP	0.670	0.412	180	7.06
FP	0.644	0.393	180	2.95
SP	0.524	0.413	160	8.60

When the van Deemter equation is employed in chiral chromatography, in addition to the traditional terms describing longitudinal diffusion (B), eddy dispersion (A) and solid–liquid mass transfer kinetics (C_S), an additional term taking into account the slow adsorption–desorption kinetics (C_{ads}), which frequently characterizes enantiorecognition phenomena, is also added [4,46]. The dependence of H on the mobile phase velocity is therefore written as:

$$H = A(u) + \frac{B}{u} + C_S u + C_{ads} u \quad (7)$$

Fig. 2 shows the van Deemter curves of TSO enantiomers measured, respectively, on the 150 mm × 4.6 mm column packed with 2.5 μm FPPs (top), on the 150 mm × 4.6 mm one packed with 2.6 μm SPPs (middle) and on the 100 mm × 4.6 mm column packed with 1.8 μm FPPs (bottom). Diamonds (green) refer to the first enantiomer and circles (blue) to the second one. The height equivalent to a theoretical plate has been plotted against the interstitial velocity, u_{int} (Eq. (1)), which represents the true linear velocity of the mobile phase (since the fluid flows around and between the particles, not through them). These plots suggest some considerations. First, one may observe that the longitudinal diffusion of the two enantiomers in each column is the same. This is demonstrated by the overlapping of their van Deemter curves at low flow rates (where the B-term is dominant). Then, under the assumption of the same eddy dispersion for the two enantiomers in a given column [47], the conclusion is reached that the difference in the van Deemter curves (already evident at relatively low linear velocity, starting at u_{int} roughly 0.3 cm/s) is essentially due to a slow adsorption–desorption process. This is particularly evident for the column packed with 2.6 μm SPPs (middle plot). Another interesting observation coming from Fig. 2 is that the slope of the C-branch of the van Deemter equation is markedly steeper for the column packed with 1.8 μm FPPs (bottom part of the figure) than for columns packed with both 2.5 μm FPPs (top) and 2.6 μm SPPs (middle). This is due to frictional heating generated by the stream of mobile phase against the packed bed of the column through which it percolates under significant pressure gradient [48–50]. For instance, at u_{int} = 0.8 cm/s, the backpressure generated by the 1.8 μm column was 5300 psi and, at u_{int} = 1.0 cm/s, it reached 6750 psi. The heat produced locally is dissipated in both the radial and longitudinal direction of the column. This generates longitudinal and radial temperature gradients, whose amplitude depends on the degree of thermal insulation of the column (either adiabatic or isothermal). The column compartment of the Dionex UHPLC equipment used for the measurement of the van Deemter curves with these columns (see Section 2) can only work in the so-called forced-air mode (quasi-isothermal conditions), where it is well known that radial temperature gradients degrade the efficiency of column [51–53].

With the purpose of comparing the behavior of the three columns, in Fig. 3 van Deemter curves of the first and the second TSO enantiomer are overlapped. Curves on top of this figure are those for the less retained enantiomer, while on the bottom there are the van Deemter curves relative to the second enantiomer. The kinetic behavior of the first enantiomer looks very similar on all columns, in consequence of the very low retention (see Fig. 1) of this compound that does not allow to draw any significant conclusion on mass transfer phenomena. The only minor difference is around the minimum of van Deemter curves, where the core–shell column is the less efficient (see later on).

By considering the second enantiomer (bottom part of Fig. 3), very different kinetic behaviors can be observed, depending on column. Unexpectedly, the column packed with Whelk-O1 2.6 μm SPPs (circles, purple), no matter the flow rate, is characterized by the worst performance, even worse than its 2.5 μm fully porous counterpart (diamonds, cyan). This is a surprising result that

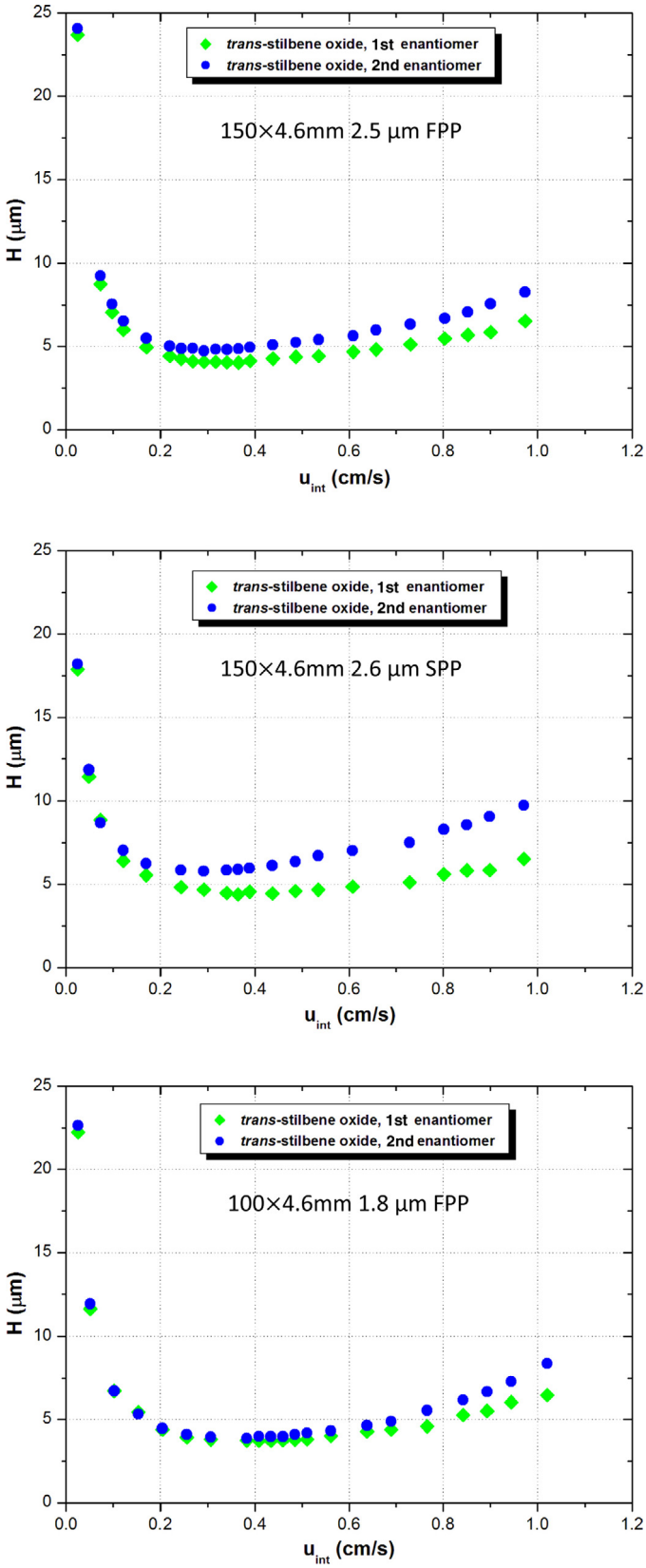

Fig. 2. van Deemter curves for TSO enantiomers measured on Whelk-O1 columns (same geometries as in Fig. 1) packed with, respectively, 2.5 μm FPPs (top), 2.6 μm SPPs (middle) and 1.8 μm FPPs (bottom). Instrument employed for measurements: Dionex 3000RS. (For interpretation of the references to color in the text, the reader is referred to the web version of the article.)

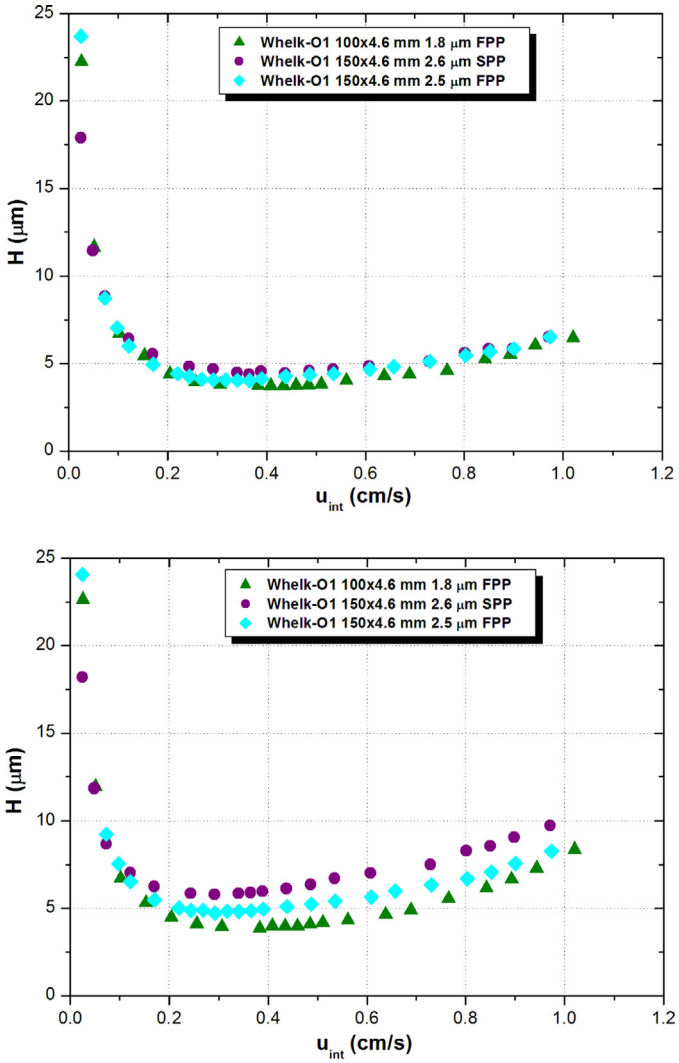

Fig. 3. Overlapped van Deemter curves measured on the three Whelk-O1 columns (same geometries as in Fig. 1), respectively for the first (top) and the secondly (bottom) eluted TSO enantiomers. Diamonds: column packed with 2.5 µm FPPs; circles: column packed with 2.6 µm SPPs; triangles: column packed with 1.8 µm FPPs. Instrument employed for measurements: Dionex 3000RS. See text for details. (For interpretation of the references to color in the text, the reader is referred to the web version of the article.)

contrasts with the commonly observed performance of columns packed with C_{18} SPPs [6,7]. It can be explained by considering the contribution to band broadening coming from either eddy dispersion or slow adsorption–desorption kinetics or a combination of both. The first statement, about the importance of eddy dispersion in columns packed with SPPs, is counter intuitive at least according to literature data that demonstrate how packed beds made of SPPs are expected to be more efficient than those of FPPs (see before). It can be however suggested by the experimental difficulties encountered during the slurry packing of Whelk-O1 SPPs. By considering their characteristics, first of all that these particles are polar, however it does not seem weird that they behave differently from hydrophobic C_{18} ones during the slurry packing [19,54]. As a matter of fact, not only the achievement of stable slurry suspensions was more difficult with very polar SPPs than with Whelk-O1 fully porous ones but also, e.g., the time needed to compress the bed (by high-pressure flushing) did not follow any expected trend and could not be optimized. In conclusion, the impression is that one of the most important characteristics of hydrophobic core–shell particles, i.e. their ability to generate very efficient packed beds, could not be easily reproducible with very polar Whelk-O1 SPPs. Further investigation is needed to assess this point, in particular on rheological characteristics of Whelk-O1 SPPs. In agreement with [11,12], it should be concluded that the efficient preparation of packed beds of polar SPPs still requires a long way to go. This essentially needs the optimization of all steps of packing protocol, without which the full potential of polar chiral SPPs can be barely reached.

As mentioned before, on the 2.6 µm Whelk-O1 core–shell column the contribution to band broadening coming from a slow mass transfer process seems to be particularly evident. Since the solid–liquid mass transfer term (C_s) should be lower on core–shell than on fully porous particles (due to the presence of the inaccessible core), the conclusion is that the adsorption–desorption kinetics must be slower on core–shell particles (higher C_{ads} term in Eq. (7)) than on the fully porous ones. An explanation could be the different surface density of chiral selector between core–shell and FPPs. Table 1 shows that this surface density is about 20% larger on SPPs than on fully porous ones. In literature there are practically no studies which have attempted to assess if and how chiral recognition is modified by changing the amount of chiral selector tethered to the surface and how this could impact on the chromatographic performance [12]. On the other hand, this is a very important subject that needs more experimental and theoretical work to be fully understood.

Finally, by still looking at the bottom part of Fig. 3, it is evident that the column packed with 1.8 µm FPPs (triangles, green) outperform the other two in terms of kinetic behavior but it is also clear that, at high flow rates, where the effect of frictional heating on efficiency is dominant, this column does not offer any advantage over the one packed with 2.5 µm FPPs. Indeed, at u_{int} slightly larger than 1 cm/s, the *C*-branch of the 1.8 µm fully porous column merges to that of the column packed with 2.5 µm FPPs.

Fig. 4 (top) shows the gain in analysis time that can be obtained by moving from both the columns packed with 2.5 µm FPPs and 2.6 µm SPPs to that packed with 1.8 µm FPPs. The necessary premise to discuss this figure – whose meaning is merely practical – is that the length of commercially available columns packed with 2.5–2.7 µm particles (no matter if fully porous or pellicular) is usually 150 mm, while that of columns packed with sub-2 µm particles is only 100 mm or less. This justifies the direct comparison presented in Fig. 4, where column length is not accounted for. Having acknowledged this, and by referring for each column to condition of maximum efficiency (indeed chromatograms presented in Fig. 4 were recorded at the optimum flow rate, see figure caption for details), one observes that the column packed with 1.8 µm FPPs permits to decrease analysis time (here simply calculated as the retention time of the second eluted enantiomer) more than 50 and 30% with respect to the 2.5 µm fully porous column and the 2.6 µm core–shell one. The practical advantage achievable with the 100 mm column packed with sub-2 µm particles, becomes still more evident by considering, in addition to analysis time, also the resolution of columns (see before). Thus, the ratio between resolution and analysis time [55], graphically given as bar chart in the bottom part of Fig. 4, is strongly favorable for the 1.8 µm column packed with FPPs (it is indeed 11.9 on this column vs. 5.3 and 7.9 on, respectively, the 2.5 µm fully porous and the 2.6 µm core–shell column). Incidentally, the gain of $R_s/t_{R,2}$ ratio observed for the 2.6 µm core–shell column over that packed with 2.5 µm FPPs comes from the reduction of retention time in the former column (due to a much lower total surface area per column) and not from an increase of R_s (which actually is larger on the 2.5 µm fully porous column).

The last part of this study briefly reports on the use of short columns, packed with both Whelk-O1 FPPs and SPPs, to realize ultrafast enantioseparations. In this proof-of-concept study, 10 mm columns of different I.D. (3.0 and 4.6 mm) were employed. These columns were in-house designed and developed.

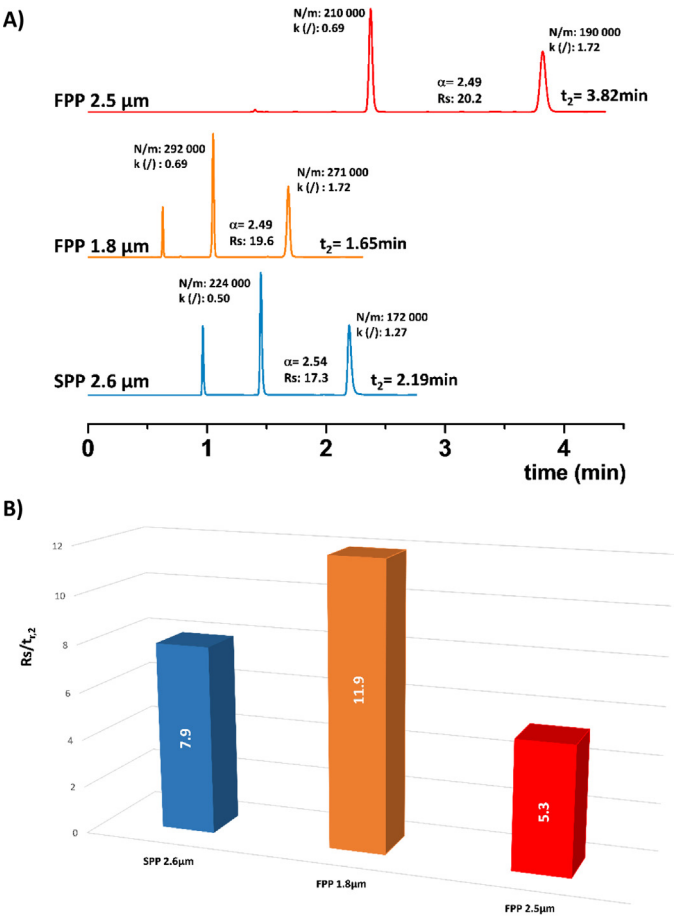

Fig. 4. (A) Same chromatograms as in Fig. 1, showing the separation of TSO enantiomers on the three columns employed in this work, but with the *x*-axis given in retention time. Carbon tetrachloride was used as dead time marker. B) Bar chart showing the ratio between resolution and retention time for the 2.6 μm core–shell column (first bar on the left, blue color), the 1.8 μm fully porous column (middle bar, orange) and, finally, the 2.5 μm fully porous column (last bar on the right, red). Ratios were calculated on the second eluted enantiomer. Instrument employed for measurements: UPLC Waters Acquity. (For interpretation of the references to color in this figure legend, the reader is referred to the web version of the article.)

Fig. S3 of Supplementary Data shows a picture of the 10 mm column and holder. They were packed by following the same protocol also used for longer columns. Table 3 has some information that helps to characterize these columns, in particular the optimal flow rate (i.e., the flow rate corresponding to the minimum of van Deemter curve), the corresponding interstitial linear velocity and the maximum efficiency (in *N*/m). With the purpose of performing ultrafast enantioseparations, these columns were operated at the maximum flow achievable by instrumentation (8 mL/min).

Table 3
Kinetic performance (in *N*/m) of short columns (10 mm) of different diameter. $F_{v,opt}$ and $u_{int,opt}$ represent, respectively, the optimum flow rate (that is the flow rate corresponding to the minimum of the van Deemter curve) and the optimum interstial velocity; N_{max} is the number of theoretical plates per column, when the column was operated at 8 mL/min (see text for more details). In all cases, *N* has been calculated as the average value of *N*s of the two TSO enantiomers. Particle type: FP, fully porous; SP, superficially porous). Instruments employed for measurements: UPLC Waters Acquity for van Deemter curves; Dionex 3000RS for ultrafast enantioseparations (evaluation of N_{max}).

Particle type	L × I.D. (mm)	$F_{v,opt}$ (mL/min)	$u_{int,opt}$ (cm/s)	*N*/m	N_{max}
FP	10 × 4.6	1.7	0.43	190,000	1220
SP	10 × 4.6	1.5	0.36	140,000	850
FP	10 × 3.0	0.7	0.42	180,000	520

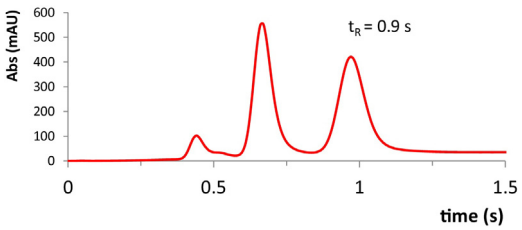

Fig. 5. Example of ultrafast enantioseparation thanks to the use of short column and high flow rate. In this particular case, a 10 × 3.0 mm column packed with 1.8 μm FPPs was operated at 8 mL/min (u_{int} = 4.8 cm/s) for the separation of TSO enantiomers. Carbon tetrachloride was used as dead time marker. Note the time scale in seconds. Instrument employed for measurements: Dionex 3000RS. See text for details.

Accordingly, the Thermo Dionex equipment (see Section 2) was employed, even though its extra-column variance is not negligible with respect to that of first and second eluted enantiomers (respectively, roughly 11.2 and 28 μL^2). In the last column of Table 3, the number of theoretical plates per column measured at the highest flow rate is reported. As an example, Fig. 5 shows the chromatogram recorded with the 10 mm × 3.0 mm column packed with 1.8 μm FPPs. As it can be seen, the separation of TSO enantiomers was performed in less than 1 s, with R_S = 2.2. This represents an extraordinary result, unimaginable only a few years ago in chiral liquid chromatography, which is even comparable with that of chiral separations on microchip platforms [56].

4. Conclusions

The investigation of the kinetic performance of columns packed with Whelk-O1 fully porous and core–shell particles of similar diameter (2.5 μm for FPPs vs. 2.6 μm for core–shell ones) has surprisingly revealed that FPPs outperform SPPs. This depends, in part, on the faster mass-transfer adsorption–desorption kinetics observed (especially on the second eluted enantiomer) on the FPPs and, in part, on the smaller eddy dispersion contribution to band broadening on the column packed with FPPs. The slower mass-transfer adsorption–desorption process is most likely due to the larger surface density of chiral selector on the SPPs. Indeed, even though the same experimental conditions were maintained during functionalization of SPPs and FPPs, the outcome was different. The surface density of Whelk-O1 selector on SPPs was indeed 20% larger than that of FPPs. These results suggest that, at least for the case considered in this work, the higher the surface coverage, the lower the adsorption–desorption process but with the information in our possession no generalization can be made. Fundamental studies aimed at investigating the relationship between mass transfer kinetics and surface density of chiral selector are needed.

On the other hand, the empirical difficulty to pack Whelk-O1 core–shell particles explains the important eddy dispersion contribution to band broadening in columns packed with these particles. Different attempts have been done to improve the packing process, by varying many experimental variables (slurry composition, consolidation time, etc.) during the packing, but without success. These findings show that packing polar SPPs is significantly different from packing hydrophobic SPPs (such as C_{18} particles), for which a large amount of information and expertise has been collected over the years. One of the most significant characteristics of beds made of C_{18} core–shell particles is their extremely low eddy dispersion term. This, however, seems to be difficult to achieve with Whelk-O1 SPPs. The investigation of rheological properties of these particles can help to understand their different behavior with respect to fully porous particles so to optimize the packing protocol and, thus, the kinetic performance of columns made of polar Whelk-O1 SPPs.

Acknowledgments

The authors thank the Italian University and Scientific Research Ministry (Grant PRIN 2012ATMNJ_003) and the Laboratory Terra&Acqua Tech, member of Energy and Environment Cluster, Technopole of Ferrara of Emilia-Romagna High Technology Network. Dr. Valentina Costa from the University of Ferrara is acknowledged for technical support. The authors thank Thermo Fisher for providing Accucore 2.6 μm SPP silica.

Appendix A. Supplementary data

Supplementary data associated with this article can be found, in the online version, at http://dx.doi.org/10.1016/j.chroma.2016.09.001.

References

[1] G. Guiochon, F. Gritti, Shell particles, trials, tribulations and triumphs, J. Chromatogr. A 1218 (2011) 1915–1938.
[2] R. Hayes, A. Ahmed, T. Edge, H. Zhang, Core–shell particles: preparation, fundamentals and applications in high performance liquid chromatography, J. Chromatogr. A 1357 (2014) 36–52.
[3] F. Gritti, T. Farkas, J. Heng, G. Guiochon, On the relationship between band broadening and the particle-size distribution of the packing material in liquid chromatography: theory and practice, J. Chromatogr. A 1218 (2011) 8209–8221.
[4] F. Gritti, G. Guiochon, Mass transfer kinetics, band broadening and column efficiency, J. Chromatogr. A 1221 (2012) 2–40.
[5] M. Catani, O.H. Ismail, A. Cavazzini, A. Ciogli, C. Villani, L. Pasti, D. Cabooter, G. Desmet, F. Gasparrini, D.S. Bell, Rationale behind the optimum efficiency of columns packed with the new 1.9 μm fully porous particles Titan c_{18}, J. Chromatogr. A 1454 (2016) 78–85.
[6] R.W. Brice, X. Zhang, L.A. Colón, Fused-core, sub-2 micron packings, and monolithic HPLC columns: a comparative evaluation, J. Sep. Sci. 32 (2009) 2723–2731.
[7] F. Gritti, I. Leonardis, D. Shock, P. Stevenson, A. Shalliker, G. Guiochon, Performance of columns packed with the new shell particles Kinetex-C_{18}, J. Chromatogr. A 1217 (2010) 1589–1603.
[8] A. Cavazzini, L. Pasti, A. Massi, N. Marchetti, F. Dondi, Recent applications in chiral high performance liquid chromatography: a review, Anal. Chim. Acta 706 (2011) 205–222.
[9] R.J. Reischl, L. Hartmanova, M. Carrozzo, M. Huszar, P. Frühauf, W. Lindner, Chemoselective and enantioselective analysis of proteinogenic amino acids utilizing N-derivatization and 1-D enantioselective anion-exchange chromatography in combination with tandem mass spectrometric detection, J. Chromatogr. A 1218 (2011) 8379–8387.
[10] K. Lomsadze, G. Jibuti, T. Farkas, B. Chankvetadze, Comparative high-performance liquid chromatography enantioseparations on polysaccharide based stationary phases prepared by coating totally porous and core–shell silica particles, J. Chromatogr. A 1234 (2012) 50–55.
[11] S. Fanali, G. D'Orazio, T. Farkas, B. Chankvetadze, Comparative performance of capillary columns made with totally porous and core–shell particles coated with a polysaccharide-based chiral selector in nano-liquid chromatography and capillary electrochromatography, J. Chromatogr. A 1269 (2012) 136–142.
[12] S. Rocchi, S. Fanali, T. Farkas, B. Chankvetadze, Effect of content of chiral selector and pore size of core–shell type silica support on the performance of amylose tris(3,5-dimethylphenylcarbamate)-based chiral stationary phases in nano-liquid chromatography and capillary electrochromatography, J. Chromatogr. A 1363 (2014) 363–371.
[13] J.W. Treadway, K.D. Wyndham, J.W. Jorgenson, Highly efficient capillary columns packed with superficially porous particles via sequential column packing, J. Chromatogr. A 1422 (2015) 345–349.
[14] J.P. Grinias, R.T. Kennedy, Evaluation of 5 μm superficially porous particles for capillary and microfluidic LC columns, Chromatography 2 (2015) 502–514.
[15] Z. Aturki, L. Mondello, S. Fanali, Analysis of polyphenols and methylxantines in tea samples by means of nano-liquid chromatography utilizing capillary columns packed with core–shell particles, J. Chromatogr. A 1234 (2012) 38–44.
[16] G. D'Orazio, S. Rocchi, S. Fanali, Nano-liquid chromatography coupled with mass spectrometry: separation of sulfonamides employing non-porous core–shell particles, J. Chromatogr. A 1255 (2012) 277–285.
[17] S. Bruns, D. Stoeckel, B.M. Smarsly, U. Tallarek, Influence of particle properties on the wall region in packed capillaries, J. Chromatogr. A 1268 (2012) 53–63.
[18] J.W. Jorgenson, 1.1 μm superficially porous particles for liquid chromatography: Part II: Column packing and chromatographic performance, J. Chromatogr. A 1380 (2015) 71–80.
[19] S. Bruns, E.G. Franklin, J.P. Grinias, J.M. Godinho, J.W. Jorgenson, U. Tallarek, Slurry concentration effects on the bed morphology and separation efficiency of capillaries packed with sub-2 m particles, J. Chromatogr. A 1318 (2013) 189–197.
[20] D.C. Patel, Z.S. Breitbach, M.F. Wahab, C.L. Barhate, D.W. Armstrong, Gone in seconds: praxis, performance and peculiarities of ultrafast chiral liquid chromatography with superficially porous particles, Anal. Chem. 87 (2015) 9137–9148.
[21] D.A. Spudeit, M.D. Dolzan, Z.S. Breitbach, W.E. Barber, G.A. Micke, D.W. Armstrong, Superficially porous particles vs. fully porous particles for bonded high performance liquid chromatographic chiral stationary phases: isopropyl cyclofructan 6, J. Chromatogr. A 1363 (2014) 89–95.
[22] C.L. Barhate, Z.S. Breitbach, E. Costa Pinto, E.L. Regalado, C.J. Welch, D.W. Armstrong, Ultrafast separation of fluorinated and desfluorinated pharmaceuticals using highly efficient and selective chiral selectors bonded to superficially porous particles, J. Chromatogr. A 1426 (2015) 241–247.
[23] A. Cavazzini, N. Marchetti, R. Guzzinati, M. Pierini, A. Ciogli, D. Kotoni, I. D'Acquarica, C. Villani, F. Gasparrini, Enantioseparation by ultra-high-performance liquid chromatography, Trends Anal. Chem. 63 (2014) 95–103.
[24] L. Sciascera, O. Ismail, A. Ciogli, D. Kotoni, A. Cavazzini, L. Botta, T. Szczerba, J. Kocergin, C. Villani, F. Gasparrini, Expanding the potential of chiral chromatography for high-throughput screening of large compound libraries by means of sub-2 μm Whelk-O1 stationary phase in supercritical fluid conditions, J. Chromatogr. A (2015) 160–168.
[25] B.L.W.H. Pirkle, C.J. Welch, Design, synthesis, and evaluation of an improved enantioselective naproxen selector, J. Org. Chem. 57 (1992) 3854–3860.
[26] W.H. Pirkle, P.G. Murray, An instance of temperature-dependent elution order of enantiomers from a chiral brush-type HPLC column, J. High Resolut. Chromatogr. 16 (1993) 285–288.
[27] D. Kotoni, A. Ciogli, C. Molinaro, I. D'Acquarica, J. Kocergin, T. Szczerba, H. Ritchie, C. Villani, F. Gasparrini, Introducing enantioselective Ultrahigh-Pressure Liquid Chromatography (eUHPLC): theoretical inspections and ultrafast separations on a new sub-2-μm Whelk-O1 stationary phase, Anal. Chem. 84 (2012) 6805–6813.
[28] D. Kotoni, A. Ciogli, I. D'Acquarica, J. Kocergin, T. Szczerba, H. Ritchie, C. Villani, F. Gasparrini, Enantioselective ultra-high and high performance liquid chromatography: a comparative study of columns based on the Whelk-O1 selector, J. Chromatogr. A 1269 (2012) 226–241.
[29] I. D'Acquarica, D. Kotoni, A. Ciogli, M. Pierini, J. Kocergin, H. Ritchie, C. Villani, F. Gasparrini, The evolution of chiral stationary phases from HPLC to UHPLC, LC/GC Europe 27 (2014) 128–137.
[30] A. Cavazzini, L. Pasti, R. Greco, V. Costa, D. Solera, F. Dondi, N. Marchetti, A. Laganà, F. Gasparrini, Geometric characterization of straight-chain perfluorohexylpropyl adsorbents for high performance liquid chromatography, J. Chromatogr. A 1286 (2013) 47–54.
[31] I. Halász, K. Martin, Pore size of solids, Angew. Chem. Int. Ed. Engl. 17 (1978) 901–908.
[32] A. Cavazzini, F. Gritti, K. Kaczmarski, N. Marchetti, G. Guiochon, Mass-transfer kinetics in a shell packing material for chromatography, Anal. Chem. 79 (2007) 5972–5979.
[33] U.D. Neue, HPLC Columns: Theory, Technology and Practice, Wiley-VCH, 1997.
[34] J.C. Giddings, Dynamics of Chromatography, Marcel Dekker, New York, 1965.
[35] A. Villares, P. Cea, C. Lafuente, Densities and viscosities of the binary mixtures of tetrahydrofuran with isomeric chlorobutanes at 298.15 K and 303.15 K, J. Chem. Eng. Data 51 (2006) 1321–1325.
[36] O.H. Ismail, M. Catani, L. Pasti, A. Cavazzini, A. Ciogli, C. Villani, D. Kotoni, F. Gasparrini, D.S. Bell, Experimental evidence of the kinetic performance achievable with columns packed with the new 1.9 μm fully porous particles Titan c_{18}, J. Chromatogr. A 1454 (2016) 86–92.
[37] M.D. Dolzan, D.A. Spudeit, Z.S. Breitbach, W.E. Barber, G.A. Micke, D.W. Armstrong, Comparison of superficially porous and fully porous silica supports used for a cyclofructan 6 hydrophilic interaction liquid chromatographic stationary phase, J. Chromatogr. A 1365 (2014) 124–130.
[38] I. Quiñones, A. Cavazzini, G. Guiochon, Adsorption equilibria and overloaded band profiles of basic drugs in a reversed-phase system, J. Chromatogr. A 877 (2000) 1–11.
[39] K. Kaczmarski, A. Cavazzini, P. Szabelski, D. Zhou, X. Liu, G. Guiochon, Application of the general rate model and the generalized Maxwell–Stefan equation to the study of the mass transfer kinetics of a pair of enantiomers, J. Chromatogr. A 962 (2002) 57–67.
[40] A. Felinger, A. Cavazzini, F. Dondi, Equivalence of the microscopic and macroscopic models of chromatography: stochastic-dispersive versus lumped kinetic model, J. Chromatogr. A 1043 (2004) 149–157.
[41] J.P. Foley, Resolution equations for column chromatography, Analyst 116 (1991) 1275–1279.
[42] Fundamentals and applications of chromatography and related differential migration methods. Part A, in: E. Heftmann (Ed.), Chromatography, 5th ed., Elsevier, 1992 (Chapter 1).
[43] F. Gritti, I. Leonardis, J. Abia, G. Guiochon, Physical properties and structure of fine core–shell particles used as packing materials for chromatography: relationships between particle characteristics and column performance, J. Chromatogr. A 1217 (2010) 3819–3843.
[44] V. Baranau, U. Tallarek, Random-close packing limits for monodisperse and polydisperse hard spheres, Soft Matter 10 (2014) 3826–3841.
[45] F. Gritti, G. Guiochon, Speed-resolution properties of columns packed with new 4.6 μm Kinetex-c_{18} core–shell particles, J. Chromatogr. A 1280 (2013) 35–50.

[46] F. Gritti, G. Guiochon, Possible resolution gain in enantioseparations afforded by core–shell particle technology, J. Chromatogr. A 1348 (2014) 87–96.
[47] F. Gritti, G. Guiochon, Mass transfer mechanism in chiral reversed phase liquid chromatography, J. Chromatogr. A 1332 (2014) 35–45.
[48] H. Lin, C. Horváth, Viscous dissipation in packed beds, Chem. Eng. Sci. 36 (1981) 47–55.
[49] C. Horváth, H.J. Lin, Band spreading in liquid chromatography. General plate height equation and a method for the evaluation of the individual plate height contributions, J. Chromatogr. 149 (1978) 43–70.
[50] H. Poppe, J.C. Kraak, J.F.K. Huber, J.H.M.v. Berg, Temperature gradients in HPLC columns due to viscous heat dissipation, Chromatographia 14 (1981) 515–523.
[51] F. Gritti, M. Martin, G. Guiochon, Influence of viscous friction heating on the efficiency of columns operated under very high pressures, Anal. Chem. 81 (2009) 3365–3384.
[52] A. de Villiers, H. Lauer, R. Szucs, S. Goodall, P. Sandra, Influence of frictional heating on temperature gradients in ultra-high-pressure liquid chromatography on 2.1 mm I.D. columns, J. Chromatogr. A 1113 (2006) 84–91.
[53] F. Gritti, G. Guiochon, Comparison of heat friction effects in narrow-bore columns packed with core–shell and totally porous particles, Chem. Eng. Sci. 65 (2010) 6310–6319.
[54] A.E. Reising, J.M. Godinho, K. Hormann, J.W. Jorgenson, U. Tallarek, Larger voids in mechanically stable, loose packings of 1.3 μm frictional, cohesive particles: their reconstruction, statistical analysis, and impact on separation efficiency, J. Chromatogr. A 1436 (2016) 118–132.
[55] E.L. Regalado, A.A. Makarov, R. McClain, M.P.C.J. Welch, Search for improved fluorinated stationary phases for separation of fluorine-containing pharmaceuticals from their desfluoro analogs, J. Chromatogr. A 1380 (2015) 45–54.
[56] S. Thurmann, C. Lotter, J.J. Heiland, B. Chankvetadze, D. Belder, Chip-based high-performance liquid chromatography for high-speed enantioseparations, Anal. Chem. 87 (2015) 5568–5576.

PAPER VI

http://www.americanpharmaceuticalreview.com/Featured-Articles/339730-Pirkle-Type-Chiral-Stationary-Phases-for-Ultra-High-Performance-Ultra-Fast-Enantioseparations/

New Whelk-O1 Pirkle-type chiral stationary phases for ultra-high performance ultra-fast enantioseparations

Martina Catani[(a) *]; Omar H. Ismail[(b) *]; Simona Felletti[(a)]; Francesco Gasparrini[(b)]; Luisa Pasti[(a)]; Valentina Costa[(a)]; Alberto Cavazzini[(a)]

a) Department of Chemistry and Pharmaceutical Sciences, University of Ferrara, via L. Borsari 46, 44121 Ferrara, Italy
b) Department of Drug Chemistry and Technology, "Sapienza" University of Rome, P.le A. Moro 5, 00185 Rome, Italy

[*]corresponding authors. E-mail addresses: martina.catani@unife.it; omar.ismail@uniroma1.it

Abstract

During the last decade, column manufacturers have put much effort into the design and preparation of materials (e.g., sub-2 micron fully porous and core-shell particles) suitable for highly efficient and fast separations in ultra high-performance liquid chromatography (UHPLC). It is a matter of fact that this advancement has so far only partially touched the field of chiral liquid chromatography. This delay has been essentially due to the lack of understanding of mass transfer processes in chiral chromatography, on the one hand, and to practical difficulties in the preparation of small chiral particles. Recently, Pirkle-type chiral stationary phases (CSPs) have been prepared by using both sub-2 micron fully porous and 2.6 micron core-shell silica particles as base materials. This report describes the employment of these CSPs to achieve not only very high performance but also ultrafast (less than one second) chiral separations in different chromatographic modes.

Introduction

In the last decade the field of chiral separations has been affected by a radical transformation. The attention of scientists and manufacturers has indeed moved from the research of novel CSPs with enhanced enantioselectivity to the preparation of new versions of already known CSPs prepared on kinetically highly efficient silica particles, such as the sub-2 micron fully porous particles (FPPs) and the 2.6 micron superficially porous ones (SPPs). Pressing requirements especially by pharmaceutical and medicinal industries – e.g., for the screening of large libraries of chiral molecules or, in general, for high-throughput analysis [1] – have indeed pushed towards the development of increasingly faster and efficient chiral separations, which could not be achieved on CSPs developed on typical 3-5 micron FPPs.

This new trend has had a tremendous impact on the analysis time. If indeed, until only ten years ago, several tens of minutes were the standard time required to perform chiral separations, [2] today the scenario has completely changed. [3] Many examples of chiral separations performed in few minutes, or even on sub-minute scale, have been reported thanks to the use of the above mentioned silica particles, be they FPPs [4, 5] or SPPs [6, 7,8, 9]. This report describes the employment of novel Pirkle-type Whelk-O1 CSPs in ultra-high performance chiral chromatography (UHPLC) for fast and ultra-fast (less than one second) enantioseparations.

New Whelk-O1 Pirkle-type CSPs for ultra-high performance, ultra-fast enantioseparations

Pirkle-type (even referred to generically as brush-type) CSPs were the first ones employed for the preparation of sub 2 micron chiral particles. [10] The choice of this selector for the transition from enantioselective high performance liquid chromatography (e-HPLC) to e-UHPLC finds its rationale in the ease to prepare sub-2 micron particles (absence of particle aggregation and clogging during their synthesis) [10] and on the supposed fast mass transfer kinetics proper of CSPs based on this class of selectors [9].

The first Pirkle type eUHPLC CSP was prepared in 2010 by Cancelliere et al. They functionalized 1.9 micron FPPs with DACH-DNB selector [5]. Kinetic performance of columns packed with this CSP was compared to that of columns packed with 4.3 and 2.6 micron DACH-DNB FPPs. The sub-2 micron column displayed both significant efficiency gain and reduced analysis times (see **Figure 1**) with respect of the other two particle formats by simultaneously maintaining comparable selectivity and improving the resolution (due to higher efficiency).

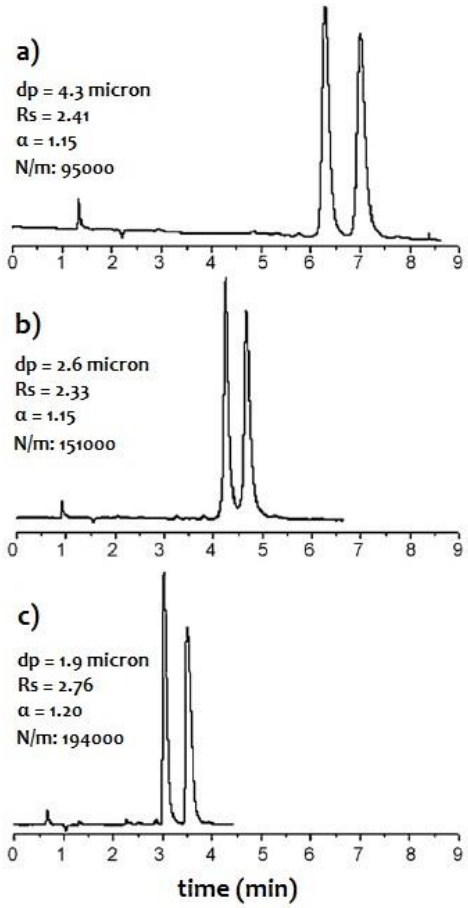

Figure 1: Chromatograms showing the separations of enantiomers of 2-methoxyphenyl methyl sulfoxide on columns packed with DACH-DNB FPPs at constant L/d_p (length/particle diameter) ratio: a) 150×4.1 mm, d_p = 4.3 micron, L/d_p = 35; b) 100×4.1 mm; d_p = 2.6 micron, L/d_p = 38; c) 75×4.1 mm; d_p = 1.9 micron, L/d_p = 39. Resolution (*Rs*), selectivity (α) and efficiency (number of theoretical plates per meter, *N/m*) are reported close to each chromatogram. Adapted from ref. 5 (D. Kotoni et al., *Anal. Chem.* 2012;84:6805-6813). Copyright (2012) American Chemical Society.

A few years later, the Whelk-O1 chiral selector (see **Figure 2**), probably the most popular and versatile one among the Pirkle-types, was employed to functionalize sub 2-micron FPPs [4, 8, 11, 12].

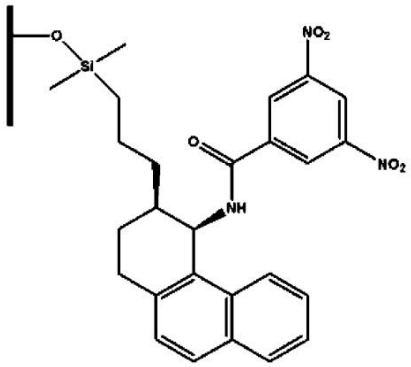

Figure 2: Schematic structure of (*R,R*)-Whelk-O1 CSP.

Whelk-O1 selector is well known for being able to discriminate a broad range of chiral compounds and for its stability at high pressure and temperature. Whelk-O1 CSPs can be used in normal phase (NP), polar organic mode (POM), reversed-phase (RP) and supercritical fluid chromatography (SFC) conditions. As shown as an example in **Figure 3**, this CSP allowed to achieve excellent chromatographic performance, with very large resolution and very symmetrical and thin peak shapes in ultrafast separations. [4]

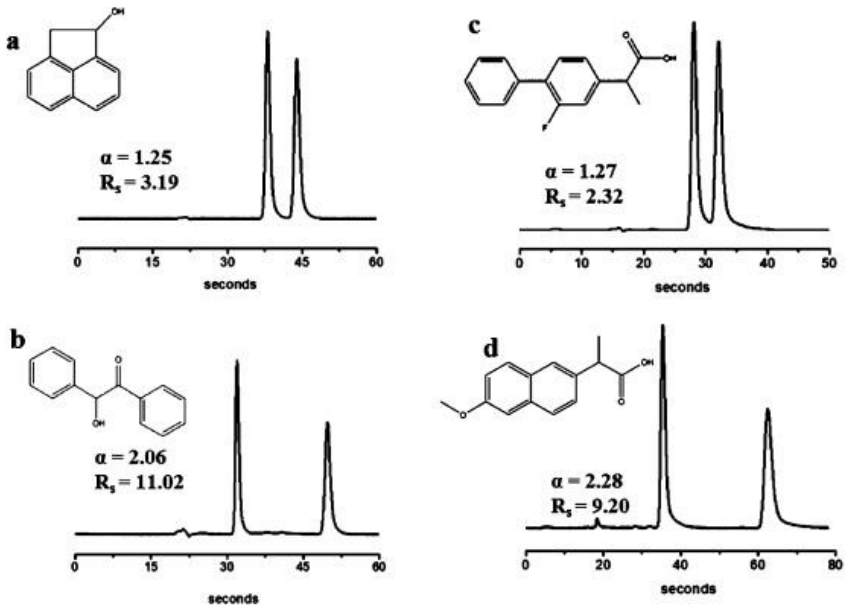

Figure 3: Examples of ultrafast enantioseparations performed on a 50 × 4.6 mm ID column packed with sub-2 micron Whelk-O1 particles. Acenaphtenol (a) and benzoin (b) separated in NP mode (mobile phase: hexane/ethanol 70:30 (% v/v), flow rate: 2 mL/min); flurbiprofen (c) and naproxen (d) separated in POM (mobile phase: acetonitrile + 0.2% acetic acid + 0.07% dietilamine (%v/v), flow rate: 2.5 mL/min). Selectivity (α) and resolution (R_s) are indicated close to each chromatogram. Reprinted with permission from ref. 4.

Short columns (5 cm) packed with sub 2-micron Whelk-O1 FPPs were successfully employed for the fast screening of a library of 129 racemic compounds (**Figure 4**) with significantly different physico-chemical properties (including organic acids, β-blockers, antidepressants, agrochemicals) in SFC. [2]

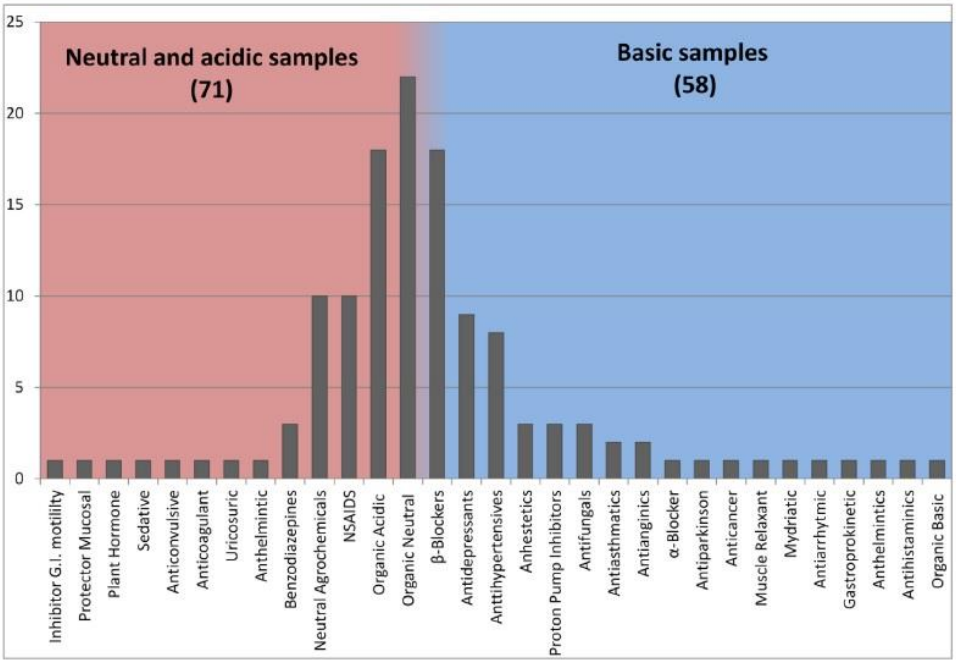

Figure 4: Classification of chiral compounds separated on a sub-2micron Whelk-O1 column in SFC. Reprinted with permission from Ref. 2.

The overall screening was carried out in less than 24 hours under fast gradient elution (9 minute total analysis time, including column reconditioning) by using a mixture of CO_2/methanol as mobile phase. The sub-2 micron fully porous Whelk-O1 CSP was found to be able to resolve even basic racemic mixtures, which are not traditionally easily separated on Whelk-O1 CSPs prepared on larger particles. Under NP conditions, these new columns exhibited kinetic performance comparable to those typical of achiral separations with efficiency in the order of 300,000 plates/meter (**figure 5**).
These efficiencies were even difficult to imagine only a few years ago in chiral chromatography. In 2016, Whelk-O1 chiral selector was employed also for the preparation of 2.6 micron SPPs. [8]

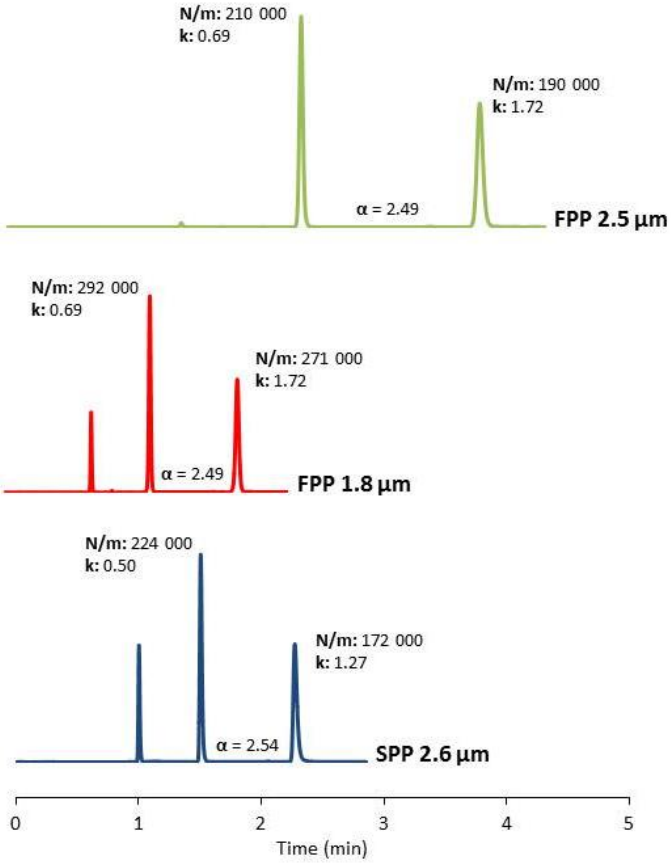

Figure 5: Chromatograms showing the separation of *trans*-stilbene oxide enantiomers on the three columns at the flow rate corresponding to the minimum of the van Deemter curve (from top to bottom, respectively, 1.2, 1.8 and 1.5 mL/min). CCl_4 was used as dead volume marker. For each peak retention factor (k) and efficiency as number of theoretical plates per meter (N/m) are reported.

With Whelk-O1 CSPs prepared on these highly performance particles, extraordinary results in terms of ultrafast enantioseparations were obtained thanks to the use of short columns (1 cm) and high flow rates. For instance, by employing 10 × 0.3 cm (length × I.D.) columns at a flow rate of 8 mL/min, the two enantiomers of *trans*-stilbene oxide were separated in less than one second on both the SPP and FPP columns (see **figure 6**).

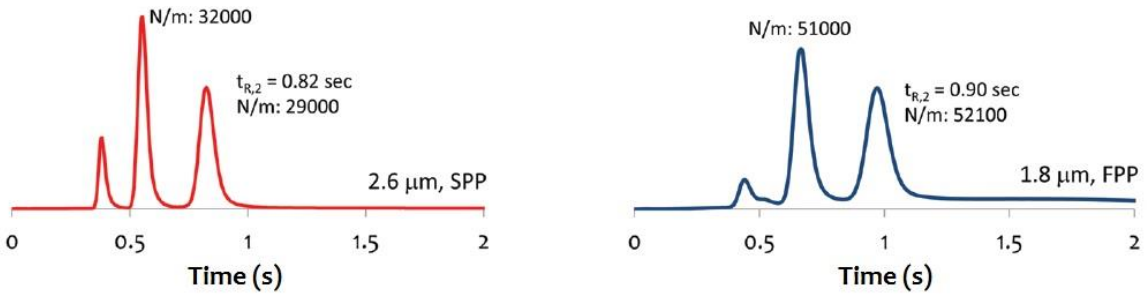

Figure 6: Ultrafast enantioseparation of *trans*-stilbene oxide enantiomers on 10 × 3.0 mm columns packed with Whelk-O1 SPP 2.6 µm (left) and Whelk-O1 FPP 1.8 µm (right). Adapted with permission from ref. 9 with permission from The Royal Society of Chemistry.

Conclusions

The transition from traditional e-HPLC to e-UHPLC has started and will continue in the future.
Whelk-O1 Pirkle-type chiral selectors definitely represent one of the successful examples of the enormous advantages that can be achieved, also in the field of chiral separations, by employing small silica particles with enhanced characteristics in terms of mass transfer. The issues in the preparation of small chiral particles seem to be overtaken. On the other hand, slurry packing of small particles (including core-shell ones) [13] has tremendously improved in the last years to the point that modern techniques of packing allow to obtain very efficient packed beds. Nowadays, CSPs able to perform as efficiently as typical reversed-phase stationary phases (with efficiency in the order of 300,000 theoretical plates per meter or more) have been already prepared and tested in laboratory, even if they are not yet commercially available. These phases can be operated in very different chromatographic modes and they are suitable for very high-pressure regimes. The future of chiral separations via liquid chromatography is strictly connected to the development of these new CSPs and will be characterized by very fast and efficient separations on columns of reduced length and diameter.

Bibliography

1. Mangelings D, Heyden YV. Screening approaches for chiral separations. In: E. Grushka NG, ed. *Advances in chromatography*. Vol 46. New York: CRC Press; 2007.

2. Sciascera L, Ismail OH, Ciogli A, et al. Expanding the potential of chiral chromatography for high-throughput screening of large compound libraries by means of sub-2 um Whelk-O1 stationary phase in supercritical fluid conditions. *J. Chromatogr. A*. 2015;1383:160-168.

3. Patel DC, Breitbach ZS, Wahab MF, Barhate CL, Armstrong DW. Gone in seconds: praxis, performance, and peculiarities of ultrafast chiral liquid chromatography with superficially porous particles. *Anal. Chem.* 2015;87:9137–9148.

4. Kotoni D, Ciogli A, Molinaro C, et al. Introducing enantioselective Ultrahigh-Pressure Liquid Chromatography (eUHPLC): Theoretical inspections and ultrafast separations on a new sub-2um Whelk-O1 stationary phase. *Anal. Chem.* 2012;84:6805-6813.

5. Cancelliere G, Ciogli A, D'Acquarica I, et al. Transition from enantioselective high performance to ultra-high performance liquid chromatography: A case study of a brush-type chiral stationary phase based on sub-5-micron to sub-2-micron silica particles. *J. Chromatogr. A*. 2010;1217:990-999.

6. Wahab MF, Wimalasinghe RM, Wang Y, Barhate CL, Patel DC, Armstrong DW. Salient sub-second separations. *Anal. Chem.* 2016;88:8821-8826.

7. Wimalasinghe RM, Weatherly CA, Breitbach ZS, Armstrong DW. Hydroxypropyl beta cyclodextrin bonded superficially porous particle-based HILIC stationary phases. *J. Liq. Chromatogr. Relat. Technol.* 2016;39:459-464.

8. Ismail OH, Pasti L, Ciogli A, et al. Pirkle-type chiral stationary phase on core-shell and fully porous particles: Are superficially porous particles always the better choice toward ultrafast high-performance enantioseparations? *J. Chromatogr. A*. 2016;1466:96-104.

9. Catani M, Ismail OH, Gasparrini F, et al. Recent advancements and future directions of superficially porous chiral stationary phases for ultrafast high-performance enantioseparations. *Analyst*. 2017;142:555-566.

10. Cavazzini A, Marchetti N, Guzzinati R, et al. Enantioseparation by ultra-high performance liquid chromatography. *TrAC, Trends Anal. Chem.* 2014;63:95-103.

11. Kotoni D, Ciogli A, D'Acquarica I, et al. Enantioselective ultra-high and high performance liquid chromatography: A comparative study of columns based on the Whelk-O1 selector. *J. Chromatogr. A*. 2012;1269:226-241.

12. Gasparrini F, Ciogli A, Pierini M, et al. The Evolution of Chiral Stationary Phases from HPLC to UHPLC. *LC/GC Eur.* 2014;27:128-137.

13. Patel DC, Breitbach ZS, Yu J, Nguyen KA, Armstrong DW. Quinine bonded to superficially porous particles for high-efficiency and ultrafast liquid and supercritical fluid chromatography. *Anal. Chim. Acta*. 2017;963:164-174.

PAPER VII

Analyst

CRITICAL REVIEW

View Article Online
View Journal | View Issue

Cite this: *Analyst*, 2017, **142**, 555

Recent advancements and future directions of superficially porous chiral stationary phases for ultrafast high-performance enantioseparations

Martina Catani,[a] Omar H. Ismail,[b] Francesco Gasparrini,[b] Michela Antonelli,[b] Luisa Pasti,[a] Nicola Marchetti,[a] Simona Felletti[a] and Alberto Cavazzini*[a]

Received 24th November 2016,
Accepted 20th December 2016

DOI: 10.1039/c6an02530g

rsc.li/analyst

This review focuses on the use of superficially porous particles (SPPs) as chiral stationary phases for ultra-high performance liquid enantioseparations. In contrast to what happened in achiral separations where core–shell particles invaded the market, the introduction of SPPs in chiral liquid chromatography (LC) has been relatively recent. This is due in part to the technical difficulties in the preparation of these phases, and in part to scarce understanding of mass transfer phenomena in chiral chromatography. As a matter of fact, nowadays, the development of superficially porous CSPs is still in its infancy. This paper covers the most recent advancements in the field of core–shell technology applied to chiral separations. We review the kinds of chiral selectors that have been used for the preparation of these phases, by discussing the advantages of chiral SPPs over their fully-porous counterparts for high efficient high throughput enantioseparations. Notwithstanding the apparently obvious advantages in terms of the mass transfer of chiral SPPs, some critical aspects that could impact their development are presented.

1. Introduction

In 2006 Kirkland introduced the so-called second generation superficially porous particles (SPPs),[1,2] also referred to as core–shell, solid–core, Fused-Core™ or pellicular particles. Prepared by a proprietary nanoparticle technology, these 2.7 μm C_{18}

[a]*Dept. of Chemistry and Pharmaceutical Sciences, University of Ferrara, via L. Borsari 46, 44121 Ferrara, Italy. E-mail: cvz@unife.it; Fax: +39 0532 240709; Tel: +39 0532 455331*
[b]*Department of Drug Chemistry and Technology, "Sapienza" Università di Roma, P.le A. Moro 5, 00185 Roma, Italy*

Martina Catani

Martina Catani was born in 1989. She received a master's degree in Chemistry in 2013 from the University of Ferrara. Since 2014 she has been a PhD student at the same university under the supervision of Prof. Alberto Cavazzini. Her research activity focuses around the investigation of the thermodynamics and the kinetics of separations in liquid chromatography with different kinds of stationary phases, including C_{18}, perfluorinated and chiral ones. During her PhD program, she spent periods of study in the groups of Prof. Gert Desmet (Brussels) and Prof. Attila Felinger (Pécs).

Omar H. Ismail

Omar H. Ismail was born in 1989. He has a master's degree in Medicinal Chemistry from the Sapienza University of Rome, and, currently, is a PhD student in Pharmaceutical Sciences at the same university. His scientific studies are focused on the theoretical evaluation of the new generation of sub-2 μm C_{18} columns in RP-ultra-high performance chromatography (RP-UHPLC). In addition, his research includes the development of sub-2 μm chiral stationary phases, using Pirkle/brush-type selectors, starting from the optimization of the synthetic strategies to the kinetic/thermodynamic evaluation of the columns packed with those CSPs. He is the co-author of 10 publications in peer-reviewed international scientific journals.

spherical particles were made of a 1.7 μm solid core surrounded by a 0.5 μm porous shell. The advantage of a porous zone occupying roughly three-quarters of the total volume of the particle is that it allows for a higher loading than the first generation core–shell particles developed in the late 1960s, which were made of a 50 μm solid core surrounded by a porous layer of only 1–2 μm.[3,4] Second generation core–shell particles have represented a breakthrough innovation into the market of chromatographic columns, providing efficiencies very similar to those of columns packed with 1.7 μm spherical fully porous particles but at a significantly lower back-pressure.[5–8] Since their introduction, a very large number of core–shell particles have been commercialized by different manufacturers with specific processes of preparation, surface chemistries and functionalization.[9–13]

The employment of SPPs in chiral liquid chromatography (LC) is more recent.[14–16] To the best of our knowledge, the first report about the use of chiral SPPs in LC is by Lindner's group in 2011.[17] They reported about the enantioseparation of amide type amino acid derivatives on a cinchona alkaloid-based anion exchanger CSP prepared on 2.7 μm fused-core particles. In this study, however, not much emphasis was given to the novelty of the CSP, nor to the advantages of the core–shell technology for efficient chiral separations.

Chankvetadze and his group[18] were the first to investigate the characteristics of a pellicular CSP from a fundamental viewpoint. They used a polysaccharide-based CSP obtained by coating 2.6 μm pellicular particles. Following these authors, the principal advantages in using chiral SPPs compared to (chiral) fully porous particles (FPPs) lie in a higher enantioselectivity at a comparable content of the chiral selector, a limited dependence of the plate height on the mobile phase flow rate and a larger enantioresolution per analysis time.[18,19]

The most comprehensive work aimed at evaluating the performance of chiral SPPs for high-efficiency and high-throughput enantioseparations has been done by Armstrong and coworkers.[20–23] They have studied a wide variety of bonded brush-type CSPs prepared on 2.7 μm SPPs, including cyclofructan-6 based, β-cyclodextrin and macrocyclic antibiotics (among which are, in particular, teicoplanin, teicoplanin aglycone and vancomycin).[20] The emerging concept from these studies is that chiral SPPs outperform, in terms of kinetic performance, their FPP counterparts practically in all modes of chromatography, *i.e.*, reversed-phase (RP), normal phase (NP), polar organic and HILIC.[20–24] Thanks to the employment of very short columns (5 cm) packed with chiral SPPs operated at high flow rates, Armstrong and colleagues have very recently obtained striking results in the field of ultra-fast chiral chromatography. By carefully reducing the extra-column volume of the equipment used in their measurements, they have indeed performed the sub-second separation of several enantiomers on various stationary phases (quinine- and teicoplanin-based) and under a variety of chromatographic modes.[25,26]

Looking at these extraordinary results, it would seem difficult to think about different approaches to achieve ultra-fast chiral separations *via* LC. However, at the same time as Armstrong's group, Ismail *et al.*[27] published the first example of a sub-second enantioseparation performed on chiral FPPs. In particular, they report about the separation of *trans*-stilbene oxide enantiomers on a 10 × 3.0 mm column packed with 1.8 μm Pirkle-type Whelk-O1 FPPs in 0.9 seconds (retention factor of the more retained enantiomer is about 1.7). Furthermore, in this study, some of the above-mentioned advantages theoretically provided by SPPs over FPPs towards ultrafast chiral chromatography have been challenged. Essentially, on the one hand, these authors point out about

Francesco Gasparrini

Francesco Gasparrini, born in 1945, earned a Laurea in Chemistry in 1969 (University of Camerino). He has been a Professor of Organic Chemistry since 1986 at the Sapienza University of Rome; he was the Co-Chairman of the 2nd ISCD (1991) and of the 16th ISCD (2005). Awards: from the Italian Chemical Society (2001, "Structure Determination and Molecular Interactions" and 2011, award in the memory of Prof. Piero Pino); from the Analytical Chemistry Division of the Italian Chemical Society (2013, Arnaldo Liberti medal). He is the author of ca. *210 peer-reviewed papers and 15 patents (3 new CSPs are commercially available: DACH-DNB by Regis, USA; Chirobiotig-TAG and P-CAP by Sigma Aldrich, USA).*

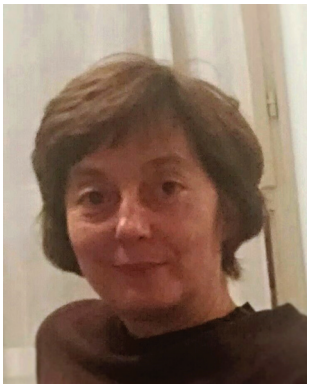

Luisa Pasti

Luisa Pasti was born in 1964, and she has a master's degree in Chemistry and a PhD in Chemical Sciences from the University of Ferrara. She was a research fellow at the Vrije Universiteit Brussel, in the group of Prof. Désiré L. Massart from 1996 to 1998. She was employed in the Enichem Research Center. In 2007 she became an Assistant Professor at the University of Ferrara, until 2014 when she became an Associate Professor of Analytical Chemistry. Her research is concerned with both the theoretical and experimental development of chromatography and chromatography-like techniques. Practical applications of this research include the characterization of microporous and mesoporous materials.

the difficulty of achieving highly efficient packed beds by a slurry packing of polar SPPs (such as the chiral ones). On the other hand, they mention the importance of a deeper investigation of if and how the kinetics of adsorption–desorption depends on the surface density of chiral ligands. Not only could this be very important to understand how the resolution, selectivity and loading of chiral ligands are connected, but it is also fundamental to compare the performance of chiral SPPs and FPPs of similar particle sizes. The chemical functionalization of these particles (even if performed under identical experimental conditions) has been indeed shown to lead to different results in terms of the surface density of the chiral selector.[21,24,27] Following these authors, the assumption that chiral SPPs are the only support suitable to prepare chiral columns for ultrafast enantioseparations is therefore possibly premature.

The scope of this review is to provide an overview of the most important achievements in the field of fast and ultrafast chiral separations permitted by the use of core–shell technology. In doing so, the different CSPs that have been prepared in a pellicular format have been described; the fundamentals of mass transfer in chiral chromatography have been discussed; a critical comparison of the pros and cons of chiral SPPs and FPPs for ultrafast enantioseparations has been proposed by focussing on some critical aspects that, in our opinion, need to be further investigated for the successful implementation of core–shell technology in chiral separations.

2. Mass transfer in chiral chromatography

In this section, the fundamentals of mass transfer in chiral chromatography are shortly summarized. The equation from which this discussion starts from is the well-known van Deemter equation,[28] which correlates the height equivalent to a theoretical plate, H (or its adimensional form, $h = H/d_p$, where d_p is the particle diameter) to the mobile phase velocity. Since there is no flow inside the mesoporous silica employed in LC, the right velocity to refer to is the interstitial velocity, u_e, *i.e.* the velocity of the mobile phase moving between particles:[29]

$$u_e = \frac{F_v}{\pi r_c^2 \varepsilon_e} \quad (1)$$

or, in reduced coordinates:

$$\nu = \frac{u_e d_p}{D_m}. \quad (2)$$

In eqn. (1) and (2), F_v is the flow rate, r_c the inner column radius, D_m the bulk molecular diffusion coefficient and ε_e the external column porosity, defined as:

$$\varepsilon_e = \frac{V_e}{V_{col}} \quad (3)$$

with V_{col} and V_e, respectively, the geometric and the external volume of the column. V_e can be determined, *e.g.*, through inverse size exclusion chromatography (ISEC) or pore blocking.[28,30–32] Under the hypothesis that the different mass transfer phenomena are independent of each other, the van Deemter equation, in reduced coordinates, is written as:

$$h = a(\nu) + \frac{b}{\nu} + c_s\nu + c_{ads}\nu + h_{heat} \quad (4)$$

where $a(\nu)$ is the eddy dispersion, b represents the longitudinal diffusion term, c_s is the mass transfer resistance across the stationary phase and c_{ads} is a term accounting for slow adsorption–desorption kinetics. This term is usually omitted in achiral RP LC, owing to the very fast adsorption–desorption process under these conditions (unless the separation of very

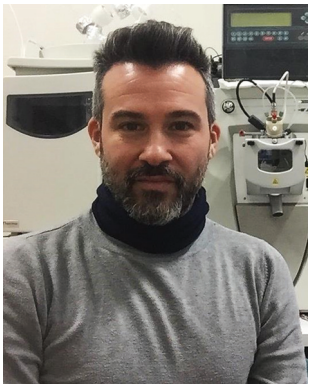

Nicola Marchetti

Nicola Marchetti was born in 1976. He has a master's degree in Chemistry and received his PhD in Chemical Sciences from the University of Ferrara in 2005. He was a post-doctoral research fellow at the University of Tennessee (Knoxville, TN, USA) from 2006 to 2008, in the group of Prof. Georges Guiochon. Then he returned to Italy and was appointed as a fixed-term Assistant Professor at the University of Ferrara from 2010. Now, he is a senior temporary Assistant Professor and his research activities focus on LC-MS and sample extraction, particularly the qualitative–quantitative analytical characterization of complex matrices of environmental, biological and food origin.

Alberto Cavazzini

Alberto Cavazzini (1970) has a master's degree in Chemistry and received his PhD in Chemical Sciences from the University of Ferrara in 2000. He was a research fellow at the University of Tennessee (Knoxville, TN, USA) and Oak Ridge National Laboratories (Oak Ridge, TN, USA) from 2000 to 2002, in the group of Prof. Georges Guiochon. In 2002 he returned to Italy after accepting an Assistant Professor position at the University of Ferrara, which he held until 2014 when he became a Professor of Analytical Chemistry. His research activities focus on separation science, particularly on liquid chromatography and chromatographic-like techniques.

large molecules, such as proteins, is considered). In chiral LC, on the other hand, the adsorption–desorption kinetics can be significantly slow also for low molecular-weight compounds and, particularly, for the second eluted enantiomer.[33] The term h_{heat} in eqn (4) accounts for the frictional heating due to the stream of the mobile phase against the bed under significant pressure. This contribution must be considered with columns packed with very fine particles, irrespective of whether they are chiral or achiral.[20,23,31,34]

The study of mass transfer in porous media has tremendously advanced in the last few years. Nowadays an accurate and independent evaluation of the individual factors contributing to peak broadening in LC is possible.[28,35–39] Conversely, the approach based on the nonlinear fitting of the experimental h data collected at different flow rates – traditionally employed for the estimation of van Deemter's equation coefficients – is to be avoided leading to parameters that are not physically meaningful.[40]

The longitudinal (or axial) diffusion term describes the band broadening due to the relaxation of the axial concentration gradient through the porous particles and the interstitial volume, in the absence of a flow. Since this is the only contribution to the band broadening when the flow is switched off, it is the best estimated through peak parking experiments. These consist of: (1) taking at a constant, arbitrary linear velocity as a sample zone somewhere in the middle of the chromatographic column; (2) suddenly stopping the flow; (3) leaving the band free to diffuse during a certain parking time, t_p; (4) resuming the flow rate to move the band out of the column. The variance (in length units) of the eluted peak, σ_x^2, is measured ($\sigma_x^2 = L^2/N$, where L is the column length and N the number of theoretical plates) and the procedure is repeated (keeping the flow rate constant) for different parking times. The slope of the σ_x^2 *vs.* t_p plot gives an estimate of the D_{eff}, being:[34,41]

$$D_{eff} = \frac{1}{2}\frac{\Delta\sigma_x^2}{\Delta t_p}. \quad (5)$$

Through D_{eff}, the longitudinal diffusion term can be calculated. In reduced coordinates, it is:

$$b = 2(1 + k_1)\frac{D_{eff}}{D_m} = 2(1 + k_1)\gamma_{eff} \quad (6)$$

where γ_{eff} ($= D_{eff}/D_m$) is the dimensionless effective diffusion coefficient and k_1 is the zone retention factor, defined as:

$$k_1 = \frac{t_R - t_e}{t_e} \quad (7)$$

t_R being the retention time and t_e is the time spent by a species molecule in the interstitial volume. By invoking the ergodic hypothesis,[42–44] it is straightforward to show that:

$$k_1 \equiv \frac{n_{part}}{n_e} = \frac{1 - \varepsilon_e}{\varepsilon_e}\left[\varepsilon_p + (1 - \varepsilon_p)K_a\right](1 - \rho^3) \quad (8)$$

where n_{part} and n_e represent the number of molecules in the particle volume and in the interstitial volume, respectively,

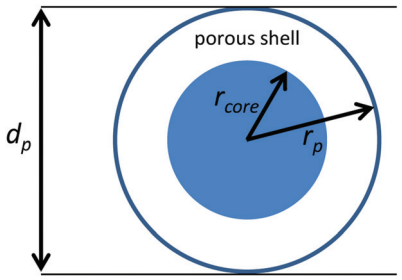

Fig. 1 Structure of a core–shell particle. d_p: particle diameter; r_p: particle radius; r_{core}: inaccessible core radius.

K_a is the distribution coefficient (equilibrium constant) of the sample between the porous zone and the eluent (see Fig. 1), $\rho = r_{core}/r_p$ is the ratio between the radius of the core and that of the whole particle (ρ is thus 0 for fully porous particles and 1 for non-porous ones) and ε_p is the particle porosity, *i.e.* the fraction of the particle volume that is occupied by pores:

$$\varepsilon_p = \frac{V_{pores}}{V_{part}} \quad (9)$$

V_{pores} and V_{part} being the pore and the particle volume, respectively. For core–shell particles, ε_p can be calculated as:[45]

$$\varepsilon_p = \frac{\varepsilon_t - \varepsilon_e}{(1 - \varepsilon_e)(1 - \rho^3)} \quad (10)$$

where ε_{tot} ($= V_0/V_{col}$, being V_0 the void volume) is the total column porosity.[46]

Finally, k_1 is connected to the more often employed phase retention factor, $k(= \frac{t_R - t_0}{t_0}$, t_0 being the void time), *via*:

$$k_1 = \frac{(1 + k)\varepsilon_{tot}}{\varepsilon_e} - 1. \quad (11)$$

Eqn (11) directly originates from the fact that the migration velocity of a retained component, u_R, can be referred to as either the migration velocity of an unretained compound, u_0, or as the interstitial velocity, *i.e.*:[47]

$$u_R = \frac{u_0}{1 + k} = \frac{u_e}{1 + k_1}. \quad (12)$$

The c_s term appearing in eqn (4) describes the solid–liquid mass transfer resistance due to the diffusion across the particle. Since there is an absence of flow inside the particles, this term is velocity-independent, which makes it easier to establish a theoretically-sound expression for this contribution. Following Kaczmarski,[48] for superficially porous spherical particles, this term can be written as:

$$c_s = \frac{1}{30}\frac{\varepsilon_e}{1 - \varepsilon_e}\left[\frac{k_1}{1 + k_1}\right]^2 \frac{1 + 2\rho + 3\rho^2 - \rho^3 - 5\rho^4}{(1 + \rho + \rho^2)^2} \frac{D_m}{D_{pz}\left(\varepsilon_p + (1 - \varepsilon_p)K_a\right)} \quad (13)$$

where D_{pz} is the diffusion coefficient in the porous zone, which can be estimated from D_{eff}, once a model of diffusion

through the porous medium has been defined.[28,35,36] For instance, in the simplest case of the so-called parallel or time-averaged model proposed by Knox (where all mass fluxes inside and outside the particle are considered additives),[49] D_{pz} is simply given by:

$$D_{pz} = \frac{(1 + k_1)D_{eff} - \gamma_e D_m}{k_1} \quad (14)$$

γ_e being the so-called obstructive geometrical factor. For a randomly packed column of impermeable spheres with a porosity of about 0.4, γ_e is approximatively 0.65 (ref. 50) (otherwise γ_e can be experimentally estimated through pore blocking[30]).

The expression of the term associated with a slow adsorption–desorption kinetics obtained by the Laplace transformation of the general rate model of chromatography,[45,51] is written in the case of superficially porous particles:[48,52,53]

$$c_{ads} = 2\frac{\varepsilon_e}{1-\varepsilon_e}\frac{1}{1-\varepsilon_p}\frac{1}{1-\rho^3}\left(\frac{k_1}{1+k_1}\right)^2\left(\frac{k_p}{1+k_p}\right)^2\frac{D_m}{k_{ads}{d_p}^2} \quad (15)$$

where k_p is:

$$k_p = \frac{1-\varepsilon_p}{\varepsilon_p}K_a \quad (16)$$

and k_{ads} is the kinetic adsorption constant. eqn (15) reveals that the calculation of c_{ads} requires the independent estimation of k_{ads} that – as will be discussed in the following – makes the estimation of this term *via* LC nontrivial.

The eddy dispersion term, $a(\nu)$ in eqn (4), is caused by the erratic flow profile in the through-pores of the packed bed. It includes *trans*-channel eddy dispersion, short-range inter-channel eddy dispersion, and *trans*-column eddy dispersion. Despite the fundamental work of Giddings that culminated in the well-known coupling theory,[42] there is still considerable debate in the literature regarding the values of the geometrical parameters needed to describe the complex structures of packed beds. Much work in this direction has been done by Tallarek and coworkers, who proposed a sophisticated approach based on the morphological reconstruction of the stationary phase structure and the calculation of the transport properties in the reconstructed materials.[38,39,54] In achiral systems, where the contribution of c_{ads} is negligible, the experimental estimation of $a(\nu)$ can be achieved by subtracting, from accurately measured h values (eqn (4)), both the longitudinal diffusion and the mass transfer terms (estimated, respectively, by eqn (6) and (13)).[28] In chiral systems, in contrast, this approach cannot be pursued since c_{ads} cannot be neglected. By ignoring frictional heating, indeed, the subtraction of b and c_s terms from h values, leads to

$$a(\nu) + c_{ads}\nu = h - \frac{b}{\nu} - c_s\nu \quad (17)$$

showing that an independent evaluation of the $a(\nu)$ and c_{ads} terms is not possible with this approach. Either $a(\nu)$ or c_{ads} must be estimated by different routes. As it was mentioned before, $a(\nu)$ can be quantified by the theoretical estimation of *trans*-channel, short-range, inter-channel and *trans*-column eddy dispersions.[33] Otherwise, $a(\nu)$ could be measured by employing achiral compounds eluted on the chiral column under investigation. Both approaches have some limitations. In the former case, the theoretical estimation of single terms of eddy dispersion, and thus $a(\nu)$, is difficult to assess. In the second case, one assumes that the eddy dispersion for achiral compounds is the same as for chiral ones, which could not be even in the case when they have similar retention factors.[55]

On the other hand, the determination of c_{ads} could be made by the microscopic model of chromatography, such as the so-called stochastic theory of chromatography.[42–44] This model focuses on the behavior of a single molecule during its chromatographic migration through the column. This erratic process is described as the sum of a random number of (random) events corresponding to visits in the stationary phase and movements in the mobile phase between two successive adsorptions. Accordingly, the time spent by a molecule inside the column is the sum of the times spent by the molecule in the stationary phase and those elapsed in the mobile phase between two successive adsorptions.[44,56–60] From the analysis of the peak shape, the stochastic model allows for the estimation of both the average adsorption time, τ_s, and the flying time, as well as of the number of adsorption–desorption steps. Thus, from the average adsorption time, the estimation of k_{ads} is possible, as follows:[42]

$$k_{ads} = \frac{1}{\tau_s}. \quad (18)$$

The difficulty of accurately measuring the adsorption–desorption kinetics has definitely slowed down the developments of high-efficiency, high-throughput enantioseparations, independent of whether core–shell or fully porous particles are employed.

3. Advantages and drawbacks of core–shell and fully-porous chiral particles for ultrafast high-efficiency enantioseparations

It is well known that core–shell particles offer some important advantages to speed up mass transfer compared to FPPs. The contributions to band broadening coming from both longitudinal diffusion (b-term of the van Deemter equation) and solid–liquid mass transfer resistance (c_s-term of the van Deemter equation) are indeed reduced by the presence of the inaccessible core. But, possibly, an even more important advantage of SPPs is that packed beds made of these particles are claimed to be more efficient than those packed with FPPs, even if admittedly this has been so far demonstrated only for hydrophobic C_{18} SPPs. It turned out that indeed columns packed with C_{18} SPPs are extremely efficient owing to their very low eddy dispersion.[32,34,61] Granted that the explanation of

this remains to a large extent unknown, the most accepted hypothesis is that the roughness of the C_{18} core–shell particles limits particle slipping after the release of the high pressure employed for the preparation of the packed bed by slurry-packing. This should basically reduce the bed heterogeneity in the radial direction and thus $a(\nu)$.[9,11]

The design and preparation of chiral SPPs has reflected the aim of exploiting the above mentioned advantages also in the field of chiral separations *via* LC. Recently, the proof-of-concept demonstration of ultrafast chiral separations on chiral SPPs was presented by Armstrong's group. In a series of publications, Armstrong and coworkers described several examples of subsecond enantioseparations performed on core–shell based CSPs.[20–23]

For all these reasons, core–shell CSPs have been considered the best candidate for the transition from traditional chiral-high performance LC (HPLC) to fast or ultrafast chiral ultra-high performance LC (UHPLC).

In spite of these very promising results, some of the authors of this review[27] have recently pointed out that to draw a definitive conclusion on whether SPPs are the only (or, possibly, the best) option towards the realization of high-efficiency, high-throughput CSPs, a deeper investigation of some aspects is necessary. In their study, Ismail *et al.*[27] compared the kinetic behavior of Whelk-O1 CSPs prepared on 2.6 μm core–shell particles and on both 2.5 and 1.8 μm FPPs. Two critical issues were identified. The first is about the experimental difficulty in the preparation, through high-pressure slurry packing, of efficient packed beds made of polar SPPs (in their case chiral Whelk-O1 SPPs). The second is the lack of information regarding the kinetics of adsorption–desorption on CSPs and, in particular, if and how the surface density of a chiral selector may affect it.

The difficulty to efficiently pack a chromatographic bed impinges on the kinetic performance of the column, basically through the *a*-term of the van Deemter equation. Following Ismail *et al.*, the slurry packing of polar SPPs is more difficult than that of C_{18} ones.[28,31,32] However, it is complicated to understand which are the critical factors determining the quality of the packing of chiral core–shell particles. Not only is the preparation of stable slurry suspensions of polar core–shell particles something that can create problems, but also the fine control of the experimental conditions of packing appears difficult to optimize, not to say, to standardize. Quite unpredictable results were obtained by changing some experimental conditions that are commonly varied to improve the quality of packing. For instance, it was observed that the kinetic performance (estimated through the minimum of the van Deemter curves) of chiral core–shell columns, otherwise packed under identical experimental conditions, changed dramatically by changing the time of compression of the bed.[27] However, this did not follow a clearly decipherable pattern. For instance, it was not possible to find any correlation between the compression time and column efficiency. On the other hand, these issues were not observed during the preparation of columns packed with fully porous chiral particles. These findings suggest that much work has still to be done to improve the packing of polar SPPs to get the maximum benefit in terms of column efficiency.

The second consideration by Ismail *et al.*[27] concerns the adsorption–desorption kinetics and, mainly, if and how it depends on the surface density of the chiral selector. While in achiral chromatography the kinetics of adsorption–desorption is practically never an issue (unless the separation of very large molecules is considered), in chiral chromatography even low molecular-weight molecules can exhibit slow adsorption–desorption. This can be particularly evident for the more retained enantiomer, which is often characterized by a strongly tailed peak.[18] However, there are no systematic studies in the literature aimed at investigating these features, while more attention has been paid to the dependence of thermodynamics (*e.g.*, the enantioselectivity) on the amount of the chiral selector bound to the surface.[18,19]

This is, however, particularly important as several research groups have independently reported about the experimental difficulty to obtain the same surface coverage (μmol m^{-2}) of the chiral selector on superficially and fully porous particles, even if the functionalization of both kinds of particles was carried out under identical experimental conditions.[21,24,27] Incidentally, these conditions are such that the amount of the chiral selector is always in a large excess with respect to the estimated number of reactive surface silanols. For instance, Ismail *et al.*[27] found that the functionalization of base SPPs leads to a significantly larger surface coverage of the chiral selector (roughly +20%) than that of native fully porous silica particles. They suggested that this could be due to different reasons, including a larger accessibility of the external layers of particles (with respect to the inner ones) or a different surface chemistry of base silica FPPs and SPPs. Both Spudeit *et al.*[21] and Patel *et al.*[20] reported very similar findings. On the other hand, Dolzan *et al.*[24] found the opposite behavior, the surface coverage of chiral selectors being larger on fully- than on superficially-porous particles. Obviously, since the specific surface area (m^2 g^{-1}) of FPPs is larger than that of SPPs, the total amount of the chiral selector bound per gram of base silica is always greater on FPPs than on SPPs. In light of these aspects, it is fundamental to know how the adsorption–desorption kinetics is affected by the surface density of the chiral selector. If the adsorption–desorption kinetics depended on the surface density of chiral selectors, this last one would possibly become one of the most important parameters to be considered during the preparation of high efficiency CSPs for ultrafast separations.

One last aspect that is worth discussing in this paragraph is regarding the effect of frictional heating. This is generated by the stream of the mobile phase against the packed bed of the column through which it percolates under a significant pressure gradient.[62–64] It can happen in RP as well as in NP, even though in the latter mode it is less evident due to a smaller back pressure under these conditions.[20] The heat produced locally is dissipated in both the radial and longitudinal directions of the column. This generates longitudinal and

radial temperature gradients, whose amplitude depends on the degree of thermal insulation of the column (either adiabatic or isothermal).[65–67] It is evident that, in this respect, chiral core–shell particles offer, at least theoretically, a significant advantage over fully porous ones exactly as it happens in achiral chromatography.

4. Chiral selectors prepared on SPPs

In this section, the classes of chiral selectors that have been prepared on superficially porous particles are briefly reviewed. Their structures are schematically represented in Fig. 2. Simultaneously, some of the applications for which they have been employed are described.

4.1 Polysaccharide-based CSPs

The first report about polysaccharide-based CSPs made on SPPs is that by Lomsadze *et al.* in 2012.[18] 2.6 μm SPPs were coated with cellulose tris(4-chloro-3-methylphenylcarbamate). These particles were used to prepare a packed column (250 × 4.6 mm, *L* × ID), whose chromatographic behavior was compared to that of the other two columns, namely, (i) a home-made 250 × 4.6 mm column packed with 3 μm FPPs functionalized in house with the same chiral selector and (ii) a commercial 250 × 4.6 mm Lux Cellulose-4 (from Phenomenex), also packed with 3 μm FPPs coated with cellulose tris(4-chloro-3-methylphenylcarbamate). The difference between the last two columns (apart from the packing) is the loading of the chiral selector that was almost four times larger on the commercial phase than on the home-made one. The authors concluded that the SPP column outperformed the FPP ones in terms of the plate number, resolution per unit time and optimal flow rate range. On the other hand, they observed that the commercial FPP column showed the highest selectivity, by virtue of a larger amount (in the paper by Lomsadze *et al.*,[18] this is the total amount per gram of base silica and not the surface density) of the chiral selector. Thus, this observation contrasts with that by Ismail *et al.*[27] who found a larger selectivity on the core–shell CSP with respect to the fully porous counterpart, in spite of a significantly smaller total amount of the chiral selector on the SPPs. The authors also mentioned about the difficulty of preparing polysaccharide-based CSPs on small silica particles due to the formation of numerous particle aggregates. The same CSPs were used by Fanali and co-workers to pack capillary columns for capillary chromatography and electrochromatography.[68,69] The authors encountered several difficulties to adequately operate these capillaries most likely owing to their inefficient packing.

In a recent paper,[19] Chankvetadze's group prepared two other polysaccharide-based CSPs on SPPs, by respectively coating cellulose tris(3,5-dimethylphenylcarbamate) on 2.8 μm particles and amylose tris(3,5-dimethylphenylcarbamate) on 3.6 μm particles. This study was aimed at demonstrating the potential of polysaccharide-based SPP CSPs to perform fast chiral separations. Indeed some interesting examples of enantioseparations performed in less than half a minute were reported by Chankvetadze's group (see Fig. 3), even though admittedly there is not enough information to evaluate the real kinetic performance of these CSPs.

4.2 Pirkle-type CSPs

By using a layer-by-layer self-assembly approach, Wu *et al.* synthetized SPPs with *trans*-(1*R*,2*R*)-diaminocyclohexane (DACH). These particles were tested as CSPs for LC towards the separation of several couples of enantiomers including binaphthol, bromo-substituted binaphthol and biphenantrol.[70] In a very basic approach (apparently based on the comparison of only two chromatograms, in addition to being recorded under different experimental conditions), these authors compared the performance of this column with that of a column packed with DACH-functionalized periodic mesoporous silica, by concluding that the SPP version of the CSP allows for a better performance and shorter analysis times than the FPP one.

The Whelk-O1 chiral selector was used by Ismail *et al.*[27] to functionalize 2.6 μm SPPs. The performance of a column packed with these particles was compared, under NP conditions, to that of the other two columns packed with 2.5 μm and 1.8 μm FPPs. Contrary to the initial expectations, the performance of the column packed with SPPs was worse than that of the column packed with 1.8 μm FPPs and quasi-comparable to that of the column packed with 2.5 μm FPPs. As it was widely discussed in previous paragraphs, this was presumably due to the combined effect of a slower adsorption–desorption kinetics and a greater contribution of eddy dispersion on the Whelk-O1 SPPs than on the FPPs. A series of chromatograms showing the ultrafast enantioseparation of *trans*-stilbene oxide enantiomers on two columns (10 × 4.6 mm and 10 × 3.0 mm, *L* × ID) packed with 2.6 μm SPP and 1.8 μm FPP Whelk-O1 particles are reported in Fig. 4. See the figure caption for details.

4.3 Macrocyclic antibiotic CSPs

Macrocyclic antibiotics including teicoplanin, teicoplanin aglycone (TAG) and vancomycin were employed by Armstrong and co-workers to prepare 2.7 μm core–shell CSPs.[20] Columns of different geometrical characteristics (either 10 or 5 mm long with a 4.6 mm I.D.) were slurry packed with these CSPs. The ultrafast separation (<30 s) of a wide range of amino acids was performed with teicoplanin and TAG CSPs.

The performance of a 10 × 4.6 mm vancomycin SPP column was compared to that of the commercial Chirobiotic V column of the same dimensions by Barhate and colleagues.[22] The former column exhibited better peak shapes, greater performance and a higher resolution for the separation of fluorinated and desfluorinated pharmaceuticals.

Finally, macrocyclic antibiotic SPP-based columns were employed for the sub-minute[20] and sub-second[25] screening of achiral and chiral compounds in various chromatographic modes. Some remarkable examples of sub-second enantioseparations are reported in Fig. 5. See the figure caption for more details.

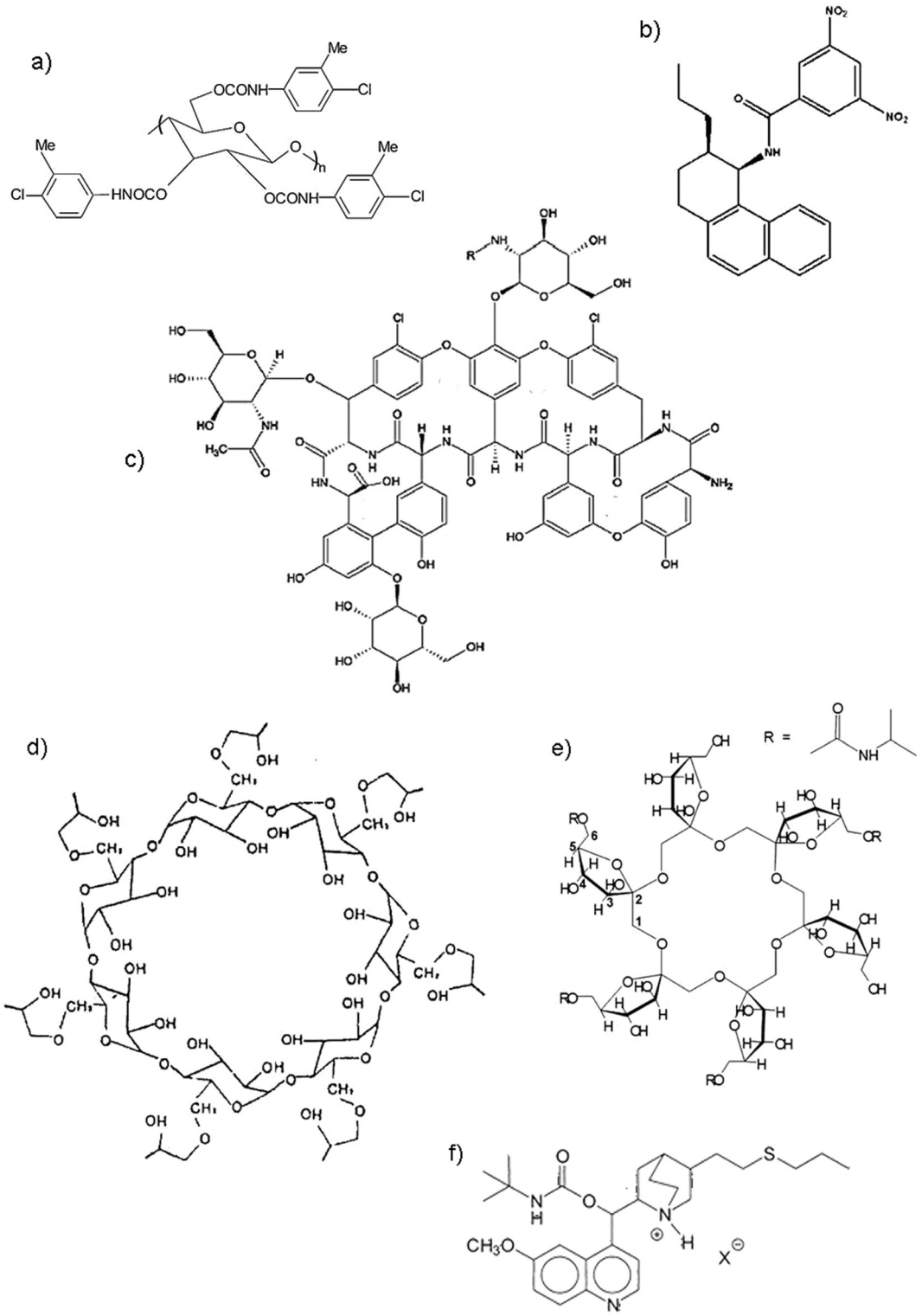

Fig. 2 Chemical structures of chiral selectors employed for the preparation of core–shell CSPs. (a) Cellulose tris(4-chloro-3-methylphenylcarbamate); (b) Whelk-O1; (c) teicoplanin; (d) cyclodextrin; (e) cyclofructan functionalized with the isopropyl carbamate group (CF6-P); (f) quinine carbamate derivative.

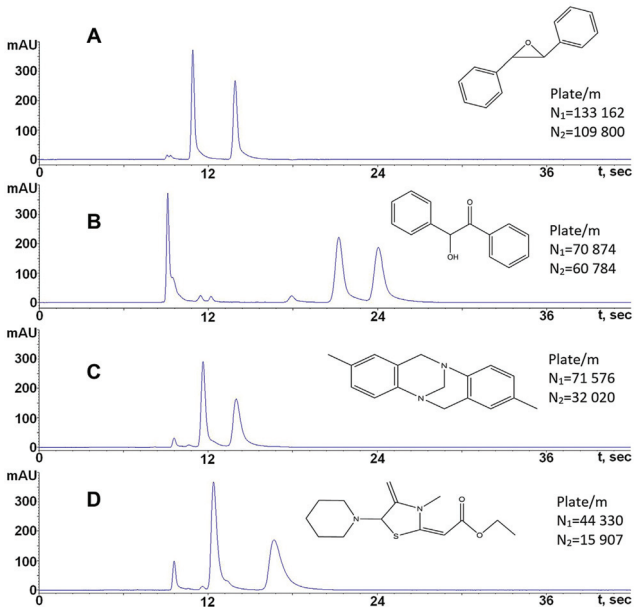

Fig. 3 Fast enantioseparations of the enantiomers of *trans*-stilbene oxide (A), benzoin (B), Tröger's base (C), and etozoline (D) performed on a 100 × 4.6 mm column packed with 3.6 μm SPPs functionalized with amylose tris(3,5-dimethylphenylcarbamate). Mobile phase: hexane/2-propanol 90 : 10 (case A and B) and methanol (case C and D). Flow rate: 5 mL min^{-1}. Reprinted with permission from ref. 19.

4.4 Cyclodextrin CSPs

Hydroxypropyl-β-cyclodextrin was used by Armstrong and co-workers to functionalize 2.7 μm SPPs, whose performance was compared to that of the two columns packed with 5 and 3 μm FPPs functionalized with the same chiral selector.[26] Small polar molecules such as nucleic acid bases, nucleotides, water soluble vitamins, β-blockers and salicylic acids were separated in the HILIC mode. Compared to FPP-based columns, the chiral SPP one exhibited better selectivities. No remarkable loss of efficiency was observed when the core–shell column was operated at high flow rates. Ultrafast separations were performed in less than 1 min.

This SPP-based CSP was also employed by Barhate and co-workers[22] to perform the ultrafast separation (analysis times <1 min) of fluorinated and desfluorinated pharmaceuticals.

4.5 Derivatized cyclofructan CSPs

Spudeit *et al.*[21] chemically bonded isopropyl cyclofructan 6 (CF6-P) to 2.7 μm SPPs. The column packed with this CSP was compared with other two FPP columns (5 and 3 μm particle sizes) with the same chemistry. The columns were operated under polar organic and normal phase modes for the separation of four pairs of enantiomers, including those of amlodipine and fipronil. The three columns showed comparable enantiomeric selectivity under constant mobile phase conditions, even though the SPP column was characterized by a higher surface density of the chiral selector. In contrast, the resolution measured on the SPP column was noticeably larger than that on the FPP columns. Shorter analysis times and wider optimal flow rates were achievable on the SPP-based column. Moreover, following these authors, the efficiency was enhanced thanks to a good packing quality. However, in the paper there is apparently not enough experimental

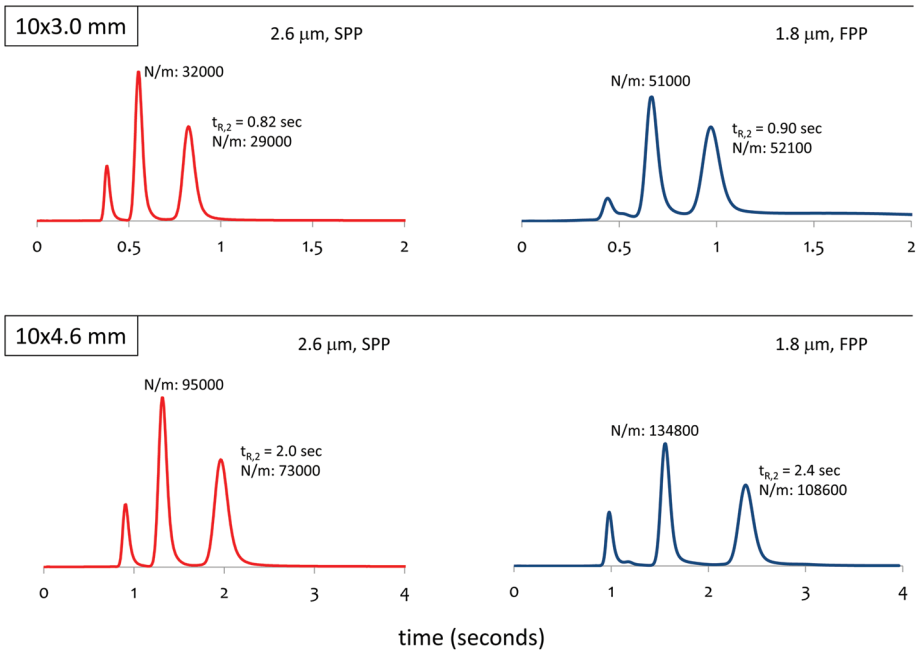

Fig. 4 Ultrafast enantioseparations on 10 × 3.0 mm (top) and 10 × 4.6 mm columns (bottom) packed with both 1.8 μm fully porous and 2.6 μm core–shell Whelk-O1 particles. Mobile phase 90 : 10, Hex/EtOH + 1% MeOH. Flow rate: 8 mL min^{-1}. The number of theoretical plates per meter and the retention time of the more retained enantiomer are indicated in each chromatogram. Unpublished data from ref. 27.

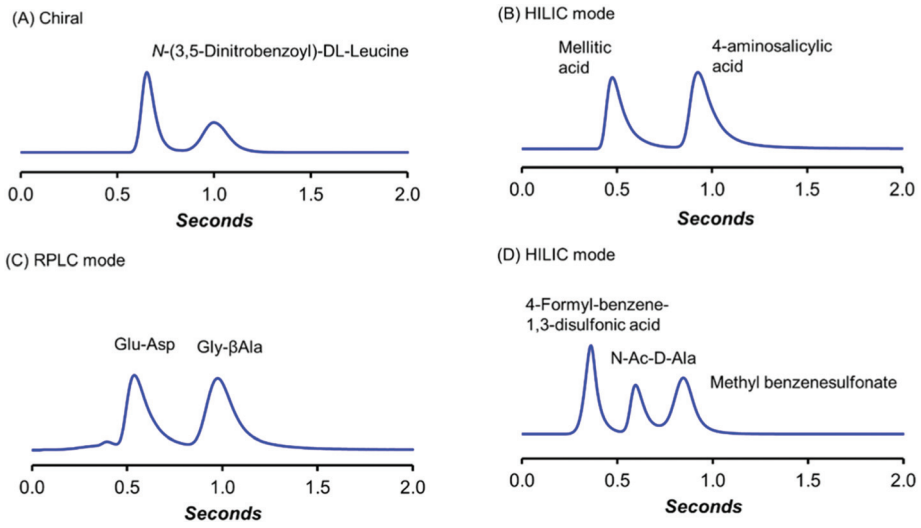

Fig. 5 Sub-second chromatography on various stationary phases using 50 × 4.6 mm I.D. columns: (A) SPP quinine (mobile phase 70 : 30, ACN/20 mM NH_4CO_2H, flow rate: 5 mL min^{-1}); (B) SPP silica (are indicated 94 : 6, ACN/15 mM $NH_4CH_3CO_2$, flow rate: 5 mL min^{-1}); (C) SPP teicoplanin (mobile phase 42 : 58, ACN/20 mM NH_4CO_2H, flow rate 5 mL min^{-1}); (D) SPP teicoplanin (mobile phase 70 : 30 ACN/water, flow rate 5 mL min^{-1}). Reprinted with permission from ref. 25.

information to support this hypothesis. The SPP-based CF6-P CSP was efficiently employed to perform the ultrafast separation of fluorinated and desfluorinated pharmaceuticals.[22]

Native cyclofructan 6 was employed as the chiral selector bonded to 2.7 μm SPP by Dolzan *et al.*[24] The performance of the column packed with these particles was evaluated under HILIC conditions and compared with that of the two FPP columns packed with 5 and 3 μm particles functionalized with the same chiral selector. This is the work where the functionalization of SPPs was found to lead to a lower surface density of the chiral selector than that of FPPs. The chiral core–shell column performed well in terms of analysis times and exhibited both higher optimal flow rates and efficiency than fully porous columns. However, the van Deemter curve measured on the 2.7 μm SPP column showed a comparable slope at high flow rates as that of the 3 μm FPP one, indicating that mass transfer was not advantageous on the former column. Following the authors, this was most likely due to a slow adsorption/desorption kinetics in the adsorbed water multilayer (typical of the HILIC mode).

Cyclofructan SPP-based CSPs were successfully employed to perform ultrafast separations (some of these in the sub-second domain) of achiral and chiral small molecules in different chromatographic modes.[20,25]

4.6 Ion and ligand exchange CSPs

The first ever report on SPP-based CSPs was that of Lindner and coworkers in 2011.[17] They reported about the preparation of a cinchona alkaloid based anion exchanger CSP on 2.7 μm SPPs. The column was employed for the separation of amide type amino acid derivatives.

A quinine-based CSP on 2.7 μm SPPs was employed by Armstrong and coworkers to perform sub-second separations of amino acid derivatives.[25]

5. Future directions

The reason for the great success of SPPs in achiral LC is that they have provided a reasonable compromise between two opposite tendencies. It is indeed well known that the tendency to improve analytical throughputs by using columns packed with smaller and smaller particles is limited by technical constraints, such as the very high pressures needed to operate these columns and the system extra-column volume. The future development of SPPs, even the chiral ones, towards particles of smaller diameters will necessarily require the availability of equipment with minimal extra-column volumes, that is also able to provide a very high back-pressure in the normal mode.

Another field where the development of a highly efficient chiral stationary phase for ultrafast separations is expected to have a tremendous impact is in supercritical fluid chromatography (SFC). Unlike what happened in LC, the technological advancement of SFC equipment has been much slower. The technical specifications of most of the instruments available nowadays on the market for SFC (*e.g.*, extra-column volume, maximum back-pressure/maximum flow-rate achievable, *etc.*) are indeed significantly worse than those for the instrumentation routinely employed in LC. Admittedly, with the packing particles already available, minor improvements in the characteristics of SFC equipment (for instance, a reduction in the volume of the detector cell that in many commercial instruments is excessively large) would permit the immediate achievement of extraordinary results in the direction of highest throughputs and ultrafast chiral separations.[71]

6. Conclusions

Chiral SPPs represent one of the most interesting advancements in the field of high-throughput ultrafast enantioseparations.

They were introduced as CSPs for LC more than five years ago. The scope was to exploit, in chiral liquid separations also, the advantages offered by core–shell particles and widely demonstrated in the literature (in particular, for the *b*- and *c*-terms of the van Deemter equation). Since then, different research groups all over the world have contributed to the development of these phases, to the resolution of many issues in their preparation and to the understanding of their properties in chiral separations.

It follows that the idea of using chiral core–shell particles for the preparation of highly efficient chiral columns is not a new one. Several research teams have been devoted to making pioneering publications in the field of chiral chromatography, as it has been mentioned in the present publication. It should also be mentioned that most recently a patent in this area has been filed, including selectors already described in some of the previous publications.[72]

The consistent employment of chiral SPPs for the fast separation of several classes of compounds is more recent. It culminated in the latest demonstration by Armstrong's group of sub-second chiral separations achieved on chiral SPPs of a different nature.

However, to conclude from all this that SPPs are the ideal (or, possibly, the only) support to prepare highly efficient CSPs for ultrafast enantioseparations is in our opinion not obvious. To fully exploit the intrinsic advantages of SPPs even in the field of chiral separations some not trivial practical and theoretical aspects need further investigation. In particular, the achievement of efficient packed beds of polar SPPs, by high-pressure slurry packing, is significantly more difficult than that of hydrophobic C_{18} core–shell particles. Thus, one of the greatest advantages (possibly the greatest one) of C_{18} core–shell particles – namely, their ability to give extraordinarily well packed beds – is not said to be a characteristic of polar SPPs too.

In addition, in our opinion it is necessary to deeply understand if and how the surface density of a chiral selector impinges on the kinetics of adsorption–desorption, especially by considering that the chemical functionalization of chiral SPPs is apparently inherently different from that of FPPs.

The impact of both an inefficient packing and a slow adsorption–desorption kinetics on the column efficiency can be extremely negative in terms of the column performance especially at high flow rates.

As a conclusive remark, we point out that without this information the comparison of the kinetic performance of the chiral core–shell and fully porous particles lacks any scientifically sound basis. This becomes particularly important when the comparison is used to generalize concepts beyond the performance analysis of the application explicitly executed.

Acknowledgements

The authors thank the Italian University and Scientific Research Ministry (Grant PRIN 2012ATMNJ_003) and the Laboratory Terra&Acqua Tech, member of the Energy and Environment Cluster, Technopole of Ferrara of Emilia-Romagna High Technology Network. Dr Valentina Costa from the University of Ferrara is acknowledged for technical support.

References

1 J. J. Kirkland, J. J. DeStefano and T. J. Langlois, *Am. Lab.*, 2007, 18–21.
2 J. J. DeStefano, S. A. Schuster, J. M. Lawhorn and J. J. Kirkland, *J. Chromatogr., A*, 2012, **1258**, 76–83.
3 C. G. Horváth, B. A. Preiss and S. R. Lipsky, *Anal. Chem.*, 1967, **39**, 1422–1428.
4 J. J. Kirkland, F. A. Truszkowski, C. H. Dilks Jr. and G. S. Engel, *J. Chromatogr., A*, 2000, **890**, 3–13.
5 A. Cavazzini, F. Gritti, K. Kaczmarski, N. Marchetti and G. Guiochon, *Anal. Chem.*, 2007, **79**, 5972–5979.
6 N. Marchetti, A. Cavazzini, F. Gritti and G. Guiochon, *J. Chromatogr., A*, 2007, **1163**, 203–211.
7 F. Gritti, A. Cavazzini, N. Marchetti and G. Guiochon, *J. Chromatogr., A*, 2007, **1157**, 289–303.
8 N. Marchetti and G. Guiochon, *J. Chromatogr., A*, 2007, **1176**, 206–216.
9 G. Guiochon and F. Gritti, *J. Chromatogr., A*, 2011, **1218**, 1915–1938.
10 F. Gritti, I. Leonardis, J. Abia and G. Guiochon, *J. Chromatogr., A*, 2010, **1217**, 3819–3843.
11 R. Hayes, A. Ahmed, T. Edge and H. Zhang, *J. Chromatogr., A*, 2014, **1357**, 36–52.
12 P. Jandera, T. Hàjek and M. Staňkovà, *Anal. Bioanal. Chem.*, 2016, **407**, 139–151.
13 N. Tanaka and D. V. McCalley, *Anal. Chem.*, 2016, **88**, 279–298.
14 A. Cavazzini, N. Marchetti, R. Guzzinati, M. Pierini, A. Ciogli, D. Kotoni, I. D'Acquarica, C. Villani and F. Gasparrini, *Trends Anal. Chem.*, 2014, **63**, 95–103.
15 L. Sciascera, O. Ismail, A. Ciogli, D. Kotoni, A. Cavazzini, L. Botta, T. Szczerba, J. Kocergin, C. Villani and F. Gasparrini, *J. Chromatogr., A*, 2015, 160–168.
16 A. Cavazzini, L. Pasti, A. Massi, N. Marchetti and F. Dondi, *Anal. Chim. Acta*, 2011, **706**, 205–222.
17 R. J. Reischl, L. Hartmanova, M. Carrozzo, M. Huszar, P. Frühauf and W. Lindner, *J. Chromatogr., A*, 2011, **1218**, 8379–8387.
18 K. Lomsadze, G. Jibuti, T. Farkas and B. Chankvetadze, *J. Chromatogr., A*, 2012, **1234**, 50–55.
19 Q. Kharaishvili, G. Jibuti, T. Farkas and B. Chankvetadze, *J. Chromatogr., A*, 2016, **1467**, 163–168.
20 D. C. Patel, Z. S. Breitbach, M. F. Wahab, C. L. Barhate and D. W. Armstrong, *Anal. Chem.*, 2015, **87**, 9137–9148.
21 D. A. Spudeit, M. D. Dolzan, Z. S. Breitbach, W. E. Barber, G. A. Micke and D. W. Armstrong, *J. Chromatogr., A*, 2014, **1363**, 89–95.
22 C. L. Barhate, Z. S. Breitbach, E. Costa Pinto, E. L. Regalado, C. J. Welch and D. W. Armstrong, *J. Chromatogr., A*, 2015, **1426**, 241–247.

23 D. C. Patel, M. F. Wahab, D. W. Armstrong and Z. S. Breitbach, *J. Chromatogr., A*, 2016, **1467**, 2–18.
24 M. D. Dolzan, D. A. Spudeit, Z. S. Breitbach, W. E. Barber, G. A. Micke and D. W. Armstrong, *J. Chromatogr., A*, 2014, **1365**, 124–130.
25 M. F. Wahab, R. M. Wimalasinghe, Y. Wang, C. L. Barhate, D. C. Patel and D. W. Armstrong, *Anal. Chem.*, 2016, **88**, 8821–8826.
26 R. W. Wimalasinghe, C. A. Weatherly, Z. S. Breitbach and D. W. Armstrong, *J. Liq. Chromatogr. Relat. Technol.*, 2016, **39**, 459–464.
27 O. H. Ismail, L. Pasti, A. Ciogli, C. Villani, J. Kocergin, S. Anderson, F. Gasparrini, A. Cavazzini and M. Catani, *J. Chromatogr., A*, 2016, **1466**, 96–104.
28 F. Gritti and G. Guiochon, *J. Chromatogr., A*, 2012, **1221**, 2–40.
29 U. D. Neue, in *HPLC Columns: Theory, Technology and Practice*, Wiley-VCH, 1997.
30 D. Cabooter, F. Lynen, P. Sandra and G. Desmet, *J. Chromatogr., A*, 2007, **1157**, 131–141.
31 O. H. Ismail, M. Catani, L. Pasti, A. Cavazzini, A. Ciogli, C. Villani, D. Kotoni, F. Gasparrini and D. S. Bell, *J. Chromatogr., A*, 2016, **1454**, 86–92.
32 M. Catani, O. H. Ismail, A. Cavazzini, A. Ciogli, C. Villani, L. Pasti, D. Cabooter, G. Desmet, F. Gasparrini and D. S. Bell, *J. Chromatogr., A*, 2016, **1454**, 78–85.
33 F. Gritti and G. Guiochon, *J. Chromatogr., A*, 2014, **1332**, 35–45.
34 F. Gritti and G. Guiochon, *J. Chromatogr., A*, 2012, **1221**, 2–40.
35 G. Desmet, K. Broeckhoven, J. De Smet, S. Deridder, G. V. Baron and P. Gzil, *J. Chromatogr., A*, 2008, **1188**, 171–188.
36 G. Desmet and S. Deridder, *J. Chromatogr., A*, 2011, **1218**, 32–45.
37 S. Deirdder, M. Catani, A. Cavazzini and G. Desmet, *J. Chromatogr., A*, 2016, **1456**, 137–144.
38 S. Bruns, T. Müllner, M. Kollmann, J. Schachtner, A. Höltzel and U. Tallarek, *Anal. Chem.*, 2010, **82**, 6569–6575.
39 S. Bruns and U. Tallarek, *J. Chromatogr., A*, 2011, **1218**, 1849–1860.
40 A. Cavazzini, G. Nadalini, V. Malanchin, V. Costa, F. Dondi and F. Gasparrini, *Anal. Chem.*, 2007, **79**, 3802–3809.
41 K. Miyabe, Y. Matsumoto and G. Guiochon, *Anal. Chem.*, 2007, **79**, 1970–1982.
42 J. C. Giddings, *Dynamics of Chromatography*, Marcel Dekker, New York, 1965.
43 F. Dondi, A. Cavazzini and M. Remelli, *Adv. Chromatogr.*, 1998, **38**, 51–74.
44 A. Cavazzini, M. Remelli, F. Dondi and A. Felinger, *Anal. Chem.*, 1999, **71**, 3453–3462.
45 G. Guiochon, A. Felinger, D. G. Shirazi and A. M. Katti, *Fundamentals of Preparative and Nonlinear Chromatography*, Academic Press, Elsevier, 2nd edn, 2006.
46 I. Quiñones, A. Cavazzini and G. Guiochon, *J. Chromatogr., A*, 2000, **877**, 1–11.
47 G. Desmet, *LC GC Eur.*, 2008, **21**, 310–317.
48 K. Kaczmarski, *J. Chromatogr., A*, 2011, **1218**, 951–958.
49 J. H. Knox and H. P. Scott, *J. Chromatogr.*, 1983, **282**, 297–313.
50 J. H. Knox and L. McLaren, *Anal. Chem.*, 1964, **36**, 1477–1482.
51 K. Kaczmarski, A. Cavazzini, P. Szabełski, D. Zhou, X. Liu and G. Guiochon, *J. Chromatogr., A*, 2002, **962**, 57–67.
52 K. Miyabe, *Anal. Sci.*, 2011, **27**, 1007–1017.
53 F. Gritti and G. Guiochon, *J. Chromatogr., A*, 2014, **1348**, 87–96.
54 S. Bruns, J. P. Grinias, L. E. Blue, J. W. Jorgenson and U. Tallarek, *Anal. Chem.*, 2012, **84**, 4496–4503.
55 F. Gritti and G. Guiochon, *J. Chromatogr., A*, 2010, **1217**, 6350–6365.
56 A. Cavazzini, F. Dondi, A. Jaulmes, C. Vidal-Madjar and A. Felinger, *Anal. Chem.*, 2002, **74**, 6269–6278.
57 A. Felinger, A. Cavazzini, M. Remelli and F. Dondi, *Anal. Chem.*, 1999, **71**, 4472–4479.
58 P. Jandera, V. Bačkovská and A. Felinger, *J. Chromatogr., A*, 2001, **919**, 67–77.
59 L. Pasti, N. Marchetti, R. Guzzinati, M. Catani, V. Bosi, F. Dondi, A. Sepsey, A. Felinger and A. Cavazzini, *TrAC, Trends Anal. Chem.*, 2016, 63–68.
60 M. C. Pietrogrande, A. Cavazzini and F. Dondi, *Rev. Anal. Chem.*, 2000, **19**, 124–154.
61 F. Gritti, T. Farkas, J. Heng and G. Guiochon, *J. Chromatogr., A*, 2011, **1218**, 8209–8221.
62 H. Lin and C. Horváth, *Chem. Eng. Sci.*, 1981, **36**, 47–55.
63 C. Horváth and H. J. Lin, *J. Chromatogr.*, 1978, **149**, 43–70.
64 H. Poppe, J. C. Kraak, J. F. K. Huber and J. H. M. v. Berg, *Chromatographia*, 1981, **14**, 515–523.
65 F. Gritti, M. Martin and G. Guiochon, *Anal. Chem.*, 2009, **81**, 3365–3384.
66 A. de Villiers, H. Lauer, R. Szucs, S. Goodall and P. Sandra, *J. Chromatogr., A*, 2006, **1113**, 84–91.
67 F. Gritti and G. Guiochon, *Chem. Eng. Sci.*, 2010, **65**, 6310–6319.
68 S. Rocchi, S. Fanali, T. Farkas and B. Chankvetadze, *J. Chromatogr., A*, 2014, **1363**, 363–371.
69 S. Fanali, G. D'Orazio, T. Farkas and B. Chankvetadze, *J. Chromatogr., A*, 2012, **1269**, 136–142.
70 X. Wu, L. You, W. Hao, M. Su, Y. Gu and L. Shen, *J. Chromatogr., A*, 2013, **1299**, 78–84.
71 E. L. Regalado and C. J. Welch, *J. Sep. Sci.*, 2015, **38**, 2826–2832.
72 D. W. Armstrong and Z. S. Breitbach, New ultrahigh efficiency, superficially porous particle chiral phases for liquid chromatography, *WO* 20160/11425, (PCT/US2015/041026), 2016.

PAPER VIII

Journal of Chromatography A, 1520 (2017) 91–102

Contents lists available at ScienceDirect

Journal of Chromatography A

journal homepage: www.elsevier.com/locate/chroma

Future perspectives in high efficient and ultrafast chiral liquid chromatography through zwitterionic teicoplanin-based 2-μm superficially porous particles

Omar H. Ismail [a,*], Michela Antonelli [a], Alessia Ciogli [a], Claudio Villani [a], Alberto Cavazzini [b], Martina Catani [b], Simona Felletti [b], David S. Bell [c], Francesco Gasparrini [a,*]

[a] Dipartimento di Chimica e Tecnologie del Farmaco, "Sapienza" Università di Roma, P. le Aldo Moro 5, 00185 Roma, Italy
[b] Dipartimento di Scienze Chimiche e Farmaceutiche, Università di Ferrara, via L. Borsari 46, 44121 Ferrara, Italy
[c] MilliporeSigma/Supelco, 595 North Harrison Road, Bellefonte, PA 16823, USA

ARTICLE INFO

Article history:
Received 21 July 2017
Received in revised form 1 September 2017
Accepted 4 September 2017
Available online 6 September 2017

Keywords:
UHPC-Tzwitt
Superficially porous particles CSP
Very-high efficiency column
Ultra-fast/ultra-high performance chromatography

ABSTRACT

With the aim of pushing forward the limits of high efficient and ultrafast chiral liquid chromatography, a new Chiral Stationary Phase (CSP) has been prepared by covalently bonding the teicoplanin selector on 2.0 μm Superficially Porous Particles (SPPs). An already validated bonding protocol, which permits to achieve teicoplanin-based CSPs exhibiting zwitterionic behaviour, has been employed to prepare not only the 2.0 μm version of the CSP but also two other analogous CSPs based, respectively, on 2.7 μm SPPs and 1.9 μm Fully Porous Particles (FPPs). The kinetic performance of these CSPs has been compared through the analysis of both van Deemter curves and kinetic plots by employing in-house packed columns of 4.6 mm internal diameter and different lengths (20, 50 and 100 mm). In particular on the columns packed with 2.0 μm SPPs, extremely large efficiencies were observed for both achiral (>310,000 theoretical plates/meter, *N*/m; h_r: 1.61) and chiral compounds (>290,000 *N*/m; h_r: 1.72) in HILIC conditions. Thanks to their efficiency and enantioselectivity, these CSPs were successfully employed in ultrafast chiral separations. As an example, the enantiomers of haloxyfop were baseline resolved in about 3 s, with a resolution higher than 2.0, (flow rate: 8 mL/min) on a 2 cm long column packed with the 2.0 μm chiral SPPs.

1. Introduction

In the last decades, the technological progress and the continuous research of higher and higher column efficiency has led, on the one hand, to the development of stationary phases made of sub 2-μm fully porous particles (FPPs) and, since their introduction into the market in 2007 [1], to the employment of so-called second-generation superficially porous particles (SPPs, even referred to as core-shell or pellicular particles). Second-generation SPPs are made of a solid core surrounded by a porous layer which occupies about 75% of the overall particle volume. They have a particle diameter generally either 2.6 or 2.7 μm, depending on manufacturer [1–7]. In both approaches, the rationale is to decrease the contribution to band broadening due to intraparticle dispersion. As a consequence in achiral reversed-phase (RP) liquid chromatography, nowadays, the efficiency of modern chromatographic columns (be they packed with sub 2-μm FPPs or second-generation SPPs) easily reaches 300,000–350,000 theoretical plates per meter (*N*/m).

As a matter of fact, this extraordinary improvement of performance has instead only partially touched the field of chiral separations. Essentially up to 2010 [8], CSPs were prepared on FPPs with particle diameter of 3–5 μm. Improvements in the preparation of high efficient CSPs have lagged behind due to (i) the difficulty to adapt traditional techniques of surface modification to the preparation of small particles; (ii) the tendency of small particles to aggregate during chemical modification with consequent inefficient/poor packing; (iii) the low mechanical resistance and long-term stability of particles functionalized with chiral selector at the high flow rates/high pressure required to drive the flow through the packed bed in ultra-high performance liquid chromatography (UHPLC); (iv) the lack of fundamental studies of mass transfer in CSPs [9].

* Corresponding authors.
E-mail addresses: omar.ismail@uniroma1.it (O.H. Ismail), francesco.gasparrini@uniroma1.it (F. Gasparrini).

http://dx.doi.org/10.1016/j.chroma.2017.09.008
0021-9673/

Starting from 2010, Gasparrini and coworkers firstly reported on the use of brush-type CSPs prepared on sub-2 μm FPPs for the high efficient separation of enantiomers in the second-time scale [8,10–12]. In 2011, thanks to the work by Lindner and coworkers, the first example on the use of second-generation SPPs for the preparation of a weak anion-exchanger CSP was presented [13]. The first work aimed at evaluating the kinetic performance of chiral SPPs and FPPs dates 2012, when Chankvetadze et al. compared polysaccharide-based CSPs prepared on both kinds of particles [14]. The conclusion of this work was that columns packed with SPPs exhibited not only higher enantioselectivity (at comparable selector loading), but also both better kinetic performance at high flow-rate and larger enantioresolution than those made of FPPs. The systematic study of the performance of chiral SPPs and FPPs has been performed by Armstrong and coworkers who characterized many different types of CSPs (such as, cyclodextrins, cyclofructan-6, macrocyclic antibiotics, etc.) prepared on both supports [15–20]. In agreement with the conclusions drawn by Chankvetadze et al. [14], in these studies chiral SPPs were found to be more efficient from a kinetic viewpoint and thus more suitable for the transition to ultrafast chiral separations than their FPP counterparts. In principle the same basic concepts for which achiral hydrophobic SPPs outperform the fully porous ones (incidentally, a better packing quality, a reduced longitudinal diffusion and a smaller solid liquid mass transfer resistance), have been considered at the base of the better behavior of chiral SPPs.

More recently, some of the authors of this work, partially challenged this vision [21]. Basically, they tackled the idea that chiral SPPs exhibit superior performance, from the kinetic point of view, than fully porous ones. Unexpected results were indeed found by comparing the behavior of brush-type Whelk-O1 CSPs made on 2.6 μm SPPs, on the one hand, with that of both 1.8 and 2.5 μm FPPs, on the other [21]. In their study, Ismail et al. found the columns packed with FPPs to exhibit better performance than those made of SPPs, especially for the second eluted enantiomer. Following these authors, therefore, a deeper investigation of the effect of several factors on the chromatographic performance is needed to assess the superiority of either particle type. In particular, Ismail et al. mention the need to carefully investigate the effect of chiral selector surface density on the adsorption/desorption kinetics [8,21]. The latter observation seems particularly important since, as reported by many authors [15,18,21], significant differences in the surface density of chiral selectors were observed during functionalization of SPPs and FPPs even if the same experimental protocol was employed in both cases. Nevertheless, this effect has never been systematically investigated.

In this work, a deep evaluation of the kinetic and thermodynamic performance of three columns prepared respectively on 2.0 μm Halo® SPPs (here referred to as UHPC-SPP-Halo-Tzwitt 2.0), 2.7 μm Halo® SPPs (UHPC-SPP-Halo-Tzwitt 2.7) and 1.9 μm monodispersed Titan® FPPs (UHPC-FPP-Titan-Tzwitt 1.9) [22] is presented. In all cases, the teicoplanin selector was bonded to the particle so to guarantee to the CSP a zwitterionic character. The comparison between the three columns is based on the evaluation of both van Deemter curves and kinetic plots.

2. Theory

The efficiency of a column is usually evaluated through the well-known van Deemter equation (1), which correlates the plate height, H, to the interstitial velocity μ_{int} (i.e., the velocity of the fluid truly moving inside the column). In its basic formulation [23,24], the van Deemter equation is written as:

$$H = A + B/\mu_{int} + C\mu_{int} \quad (1)$$

Table 1
Physical properties of columns packed with zwitterionic teicoplanin-based CSPs (SPP-2.0, 2.7 μm and FPP-1.9 μm).

	SPP-Halo 2.0	SPP-Halo 2.7	FPP-Titan 1.9
L.xI.D. (mm)	100 × 4.6 20 × 4.6	100 × 4.6	100 × 4.6 20 × 4.6
d_p (μm)	2.0	2.7	1.9
Pore size (Å)	90	90	120
Surface area (m^2)	125	123	282
Selector loading (μmol/m^2)	0.45	0.47	0.27
Total porosity (ε_t)	0.54	0.53	0.65

where A represents the eddy dispersion, B the longitudinal diffusion and C the solid-liquid mass transfer resistance. The interstitial velocity is defined by:

$$\mu_{int} = \frac{\Phi}{\pi r^2 \varepsilon_e} \quad (2)$$

being Φ the flow rate, r the column radius and ε_e the external porosity ($\varepsilon_e = \frac{V_e}{V_{col}}$, with V_e the interstitial volume and V_{col} the geometrical volume of the column).

In addition to van Deemter plots, the kinetic performance of columns can be also evaluated through the kinetic plots. They provide the highest plate number, N, achievable in the shortest time possible while working at the maximum pressure of the system, ΔP_{max} [25]. Hold up time, t_0, versus N plots can be used to quickly estimate which column offers the fastest separation for a fixed efficiency or the highest N value that can be obtained in a given analysis time. Other forms of kinetic plots can be used to correlate either the column length, L, or the retention time, t_R, to N.

The following equations are employed for the conversion of experimentally determined linear velocity μ_0:

$$\mu_0 = \frac{L}{t_0} \quad (3)$$

and H values in kinetic plots:

$$N = \frac{\Delta P_{max}}{\eta}\left[\frac{K_0}{\mu_0 H}\right] \quad (4)$$

$$t_0 = \frac{\Delta P_{max}}{\eta}\left[\frac{K_0}{\mu_0^2}\right] \quad (5)$$

$$t_R = \frac{t_0}{(k' + 1)} \quad (6)$$

being η the viscosity of the mobile phase, K_0 the column permeability and k' the retention factor.

ΔP_{max} values were set at 600 bar for the UHPC-SPP-Halo-Tzwitt 2.7 column and to 1000 bar for both the UHPC-SPP-Halo-Tzwitt 2.0 and UHPC-FPP-Titan-Tzwitt 1.9 columns.

3. Experimental

3.1. Materials and chemicals

All chemicals were purchased from Sigma-Aldrich (St. Louis, Mo, USA). HPLC gradient grade solvents were filtered before use on 0.2 μm Omnipore filters (Merck Millipore, Darmstadt, Germany). Chiral samples were from Sigma-Aldrich (St. Louis, Mo, USA). Titan® monodispersed silica (pore size 120 Å, particle size 1.9 μm and specific surface area 282 $m^2\ g^{-1}$), Halo® 2.0 and 2.7 μm (90 Å, 125 and 123 m^2/g, respectively) and teicoplanin selector were provided by Merck Sigma–Aldrich (St. Louis, MO, USA). All physical properties of CSPs were summarized in Table 1. Empty stainless steel columns, 20, 50 and 100 mm × 4.6 mm (L × I.D.), were from IsoBar Systems by Idex (Wertheim-Mondfeld, Germany).

3.2. Instruments

The UHPLC chromatographic system used for all achiral tests in HILIC was an UltiMate 3000 RS system (Thermo Fisher Dionex Sunnyvale, California), equipped with a dual gradient RS pump, an in-line split loop Well Plate Sampler, a thermostatted RS Column Ventilated Compartment (temperature range 5–110 °C) and a diode array detector (Vanquish detector) with a low dispersion 2.0 μL flow cell. In addition, a second DAD detector with a 2.5 μL flow cell was employed for flow-rates higher than 4.0 mL/min. Vanquish and DAD detector, both, were set at a filter time constant of 0.002 s, a data collection rate of 100 Hz and a response time of 0.04 s. Inlet and outlet viper tubes (2 × 350 mm × 0.10 mm I.D.) were employed. Data acquisition and processing were performed with Chromeleon 6.8 software from Thermo Fisher. The extra-column peak variance (calculated through peak moments) was 3.94 μL^2 at a flow-rate of 1.0 mL/min. Data acquisition, data handling and instrument control were performed by Chromeleon software.

3.3. Preparation of chiral stationary phases

All columns were packed with CSPs synthesized according to the same Supelco proprietary bonding protocol immobilizing teicoplanin selector onto SPP-Halo 2.0 μm and 2.7 μm and monodispersed FPP-Titan-120 1.9 μm silica particles, leading to the zwitterionic chiral stationary phases named UHPC-SPP-Halo-Tzwitt 2.0, UHPC-SPP-Halo-Tzwitt 2.7 UHPC-FPP-Titan-Tzwitt 1.9, respectively. UHPC-FPP-Titan-Tzwit 1.9 μm silica particles were prepared by adjusting the synthetic procedure (medium density selector) in order to achieve comparable retention as the SPP CSPs. All CSPs were slurry packed with a pneumatically driven Haskel pump (roughly ΔP_{max} 950 bar) into stainless steel columns. Elemental analysis (C, H, N) of the different CSPs were used to extract values of selector loading and surface coverage. UHPC-SPP-Halo-Tzwitt 2.0 particles: 5.75%C, 0.74%H and 0.63%N, corresponding to 56 μmol of selector per gram of silica and to 0.45 μmol of selector per m^2 (based on N); UHPC-SPP-Halo-Tzwitt 2.7 particles: 6.05%C, 0.79%H and 0.66%N, corresponding to 59 μmol of selector per g of silica and to 0.47 μmol of selector per m^2 (based on N); UHPC-FPP-Titan-Tzwitt 1.9 particles: 8.19%C, 1.06%H and 0.92%N, corresponding to 85 μmol of selector per g of silica and to 0.27 μmol of selector per m^2 (based on N). As expected, the two SPP CSPs showed a lower loading (μmol/g) of selector but a higher surface density of teicoplanin (μmol/m^2) in comparison with the 1.9 μm FPPs (Table 1).

3.4. Methodology

All separations were performed in Hydrophilic Interaction Liquid Chromatography (HILIC) conditions by using a mobile phase made by ACN/H_2O 85:15 + 20 mM $HCOONH_4$ (^spH = 7.5). Injected volumes were 0.5-1.0 μL. For data evaluation, the values of resolution (R_s) and efficiency (N/m) were calculated according to the European Pharmacopeia using peak width at half height ($w_{0.5}$). Hold up time was estimated by injection of naphthalene. All data were processed with Origin 8.0.

3.4.1. Pycnometry measurement

Thermodynamic hold-up volume (V_0^{pyc}) was determined by static pycnometry:

$$V_0^{pyc} = \frac{w_{CHCl3} - w_{THF}}{\rho_{CHCl3} - \rho_{THF}} \quad (7)$$

where w and ρ are the mass of the column and the solvent density, respectively [26,27].

3.4.2. ISEC measurement

Inverse size exclusion chromatography (ISEC) was performed to determine both external, ε_e, and ε_p particle porosity, wide range of polystyrene standards (molecular weight between 500 and 3.6×10^6 Da) was injected into the columns, using neat THF as the mobile phase [28,29]. Total porosity, ε_t, was calculated as the ratio V_{col} between V_0^{pyc} and

Results of ISEC measurements are reported in Table 1S.

3.4.3. Frictional heating effect

For the sake of completeness, the column inlet and outlet temperatures were measured at the maximum flow-rates employed: 6.0 and 8.0 mL/min on the 5 and 2-cm long columns, respectively, by using thermocouples (accuracy: 0.1 °C) placed at the column inlet and outlet. The temperature of the ventilated column oven was set at 35 °C (the same temperature used for all the experiments reported in the paper). A ΔT of 7.5 and 3.2 °C on the 5 and 2-cm long columns, respectively, was recorded. These ΔTs are not dramatic (due to the very reduced length of columns employed in these experiments), and their effects on column performance are very reduced.

4. Results and discussion

4.1. Physical and geometric characterization of columns

In order to have a complete characterization of columns, the specific and the column permeability (K_{sf} and K_0, respectively) were calculated from the linear velocity vs. ΔP_{col} linear plots (Fig. 1). For this study, 100 × 4.6 mm (L × I.D.) columns were employed. As known, the linear velocity μ_0 and pressure drop ΔP_{col} are correlated by the Darcy's law with the equation: $K_0 = \frac{\mu_0 \eta L}{\Delta P}$ [30]. The column permeability (K_0) was 0.499, 0.500 and 1.00×10^{-14} m^2 for the UHPC-Halo-SPP-Tzwitt 2.0, the UHPC-Titan-FPP-Tzwitt 1.9 and the UHPC-Halo-SPP-Tzwitt 2.7 column, respectively (Fig. 1A). As expected, the column packed with 2.7 μm SPPs showed the highest K_0 value due to the larger particle diameter. This means that this column generates, at the same flow rate, a lower back-pressure (almost twice smaller) than the other two (Fig. 1B). Finally, the total porosity (ε_t) of columns was calculated through ISEC analysis. The two columns packed with SPPs, as expected, exhibited very similar ε_t values, consistently lower than the UHPC-Titan-FPP-Tzwitt 1.9 column. These data are summarized into Table 1S.

4.2. van Deemter analysis of achiral samples

All analysis, including van Deemter plots, were made on a Dionex Ultimate 3000RS with flow rates ranging from 0.2 mL/min up to 4.0 mL/min with a maximum operating pressure of 550 bar. This wide range of flow rates has permitted to achieve a complete view on the kinetic performance of the whole set of columns. The first evaluation was made using a mixture of the achiral solutes naphthalene (hold-up volume marker), thiourea, uracil and adenosine. In this work, all H values were not corrected for the extra-column variance since its contribution to band broadening was found to be negligible. van Deemter plots have been expressed as H as a function of μ_{inter} (Fig. 2), μ_0 (Fig. 1S) or flow rate depending on need; μ_{inter}, which takes into account the external porosity of each column, was used to have a correct comparison between columns packed with SPP and FPP CSPs. In Fig. 2A, the van Deemter plots of thiourea (k': 0.62–0.65) on the three columns are shown. Clearly, the column packed with UHPC-SPP-Halo-Tzwitt 2.0 CSP provides the best efficiency with more than 311,000 N/m, corresponding to a plate height H = 3.21 μm (h_r: 1.60) at a flow rate of 1.5 mL/min (μ_{inter} = 3.63 mm/s). Also

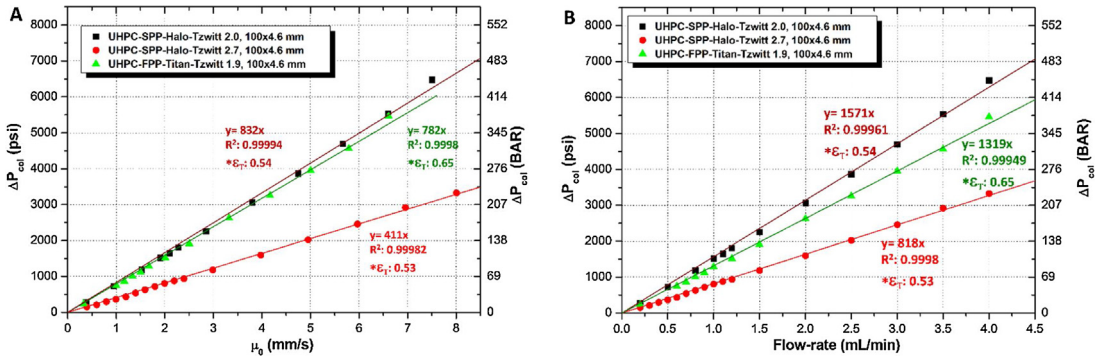

Fig. 1. A) Backpressure ΔP_{col} vs. flow-rate plots on UHPC-SPP-Halo-Tzwitt 2.0 μm (Black square), UHPC-SPP-Halo-Tzwitt 2.7 μm (Red circle) and UHPC-FPP-Titan-Tzwitt 1.9 μm (Green triangle). B) Backpressure ΔP_{col} vs. μ_0 plots on the UHPC-SPP-Halo-Tzwitt 2.0 μm (Black square), UHPC-SPP-Halo-Tzwitt 2.7 μm (Red circle) and UHPC-FPP-Titan-Tzwitt 1.9 μm (Green triangle). Eluent: ACN/H_2O 85:15 + 20 mM $HCOONH_4$, η: 0.41 × 10^{-3} Pa s, T: 35 °C. (For interpretation of the references to colour in this figure legend, the reader is referred to the web version of this article.)

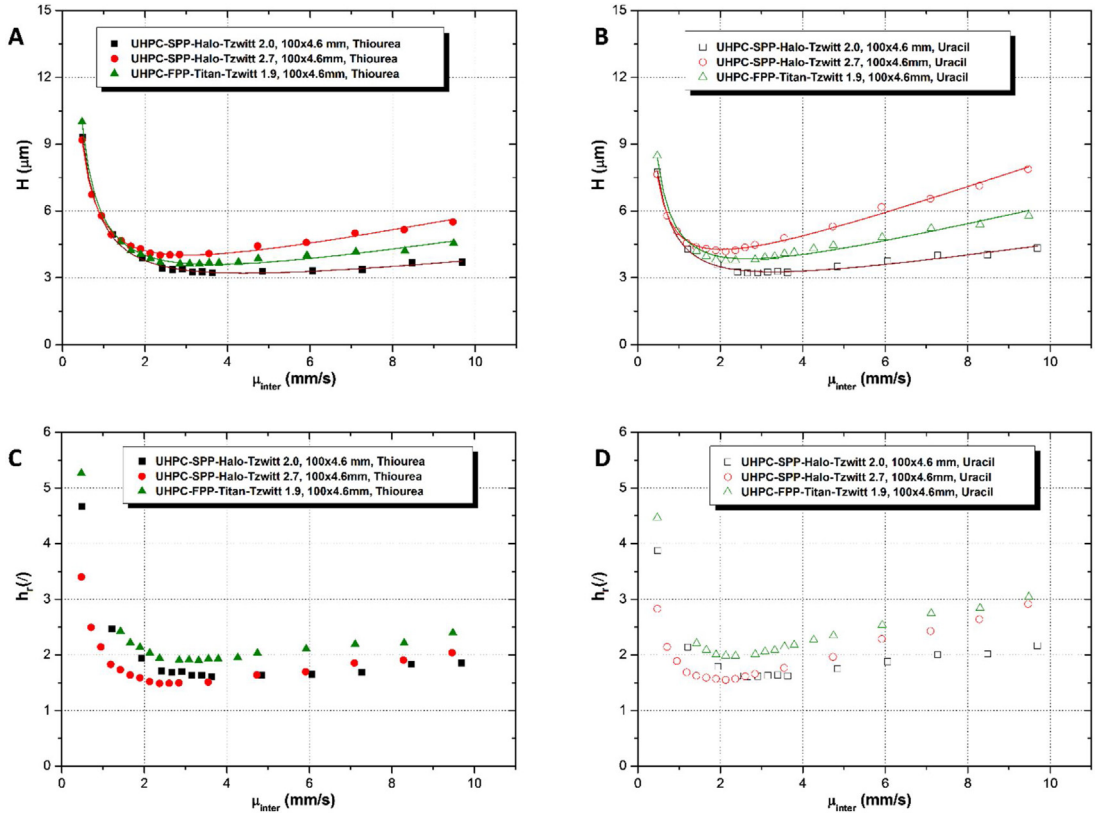

Fig. 2. A) and B) van Deemter plots (H vs μ_{inter}) for thiourea (k' = 0.6) and uracil (k' = 1.0), respectively, on the UHPC-SPP-Halo-Tzwitt 2.0 μm (Black square), UHPC-SPP-Halo-Tzwitt 2.7 μm (Red circle) and UHPC-FPP-Titan-Tzwitt 1.9 μm (Green triangle). C) and D) Plots of the reduced plate height, h_r vs. μ_{inter} on thiourea and uracil, respectively. Eluent: ACN/H_2O 85:15 + 20 mM $HCOONH_4$, T: 35 °C. (For interpretation of the references to colour in this figure legend, the reader is referred to the web version of this article.)

the column packed with UHPC-FPP-Titan-Tzwitt 1.9 CSP showed remarkable efficiency, with 277,000 N/m (H = 3.61 μm, h_r: 1.90) at a flow rate of 1.4 mL/min (μ_{inter} = 3.32 mm/s). The lowest efficiency was observed on the column packed with UHPC-SPP-Halo-Tzwitt 2.7 CSP, with less than 250,000N/m (H = 4.03 μm, h_r: 1.49) at a flow rate of 1.1 mL/min (μ_{inter} = 2.60 mm/s) (Table 2). Moreover, looking at the shape of plots, it can be observed that the C-branch of the van Deemter curve for the 2.0 μm SPP column is lower than both those of the 1.9 μm FPP and the 2.7 μm SPP columns. This characteristic is of fundamental importance for UHPLC separations since a flatter C-branch permits to increase the flow rate without significant loss of efficiency. Indeed, moving from the optimal flow rate to 3.0 mL/min, efficiency drops were 4.7%, 25% and 15% respectively for the UHPC-SPP-Halo-Tzwitt 2.0, the UHPC-SPP-Halo-Tzwitt 2.7 and UHPC-FPP-Titan-Tzwitt 1.9 columns. The van Deemter curves on the three columns for a test probe with a moderate retention (uracil, k': 0.99–1.03) are reported in Figs. 2B, 1SA and 1SC. Also in this case, at a flow rate of 1.2 mL/min, 311,000 N/m were recorded on the UHPC-SPP-Halo-Tzwitt 2.0 column, resulting in significantly higher efficiency than on both the UHPC-SPP-Halo-Tzwitt 2.7 column (30%) and the UHPC-FPP-Titan-Tzwitt 1.9 one (15%), respectively.

Considering a molecule with an higher retention factor, such as adenosine (k': 1.82–2.07) (see Fig. 1SB and D), the gap in terms of optimal flow rate becomes even larger in favor of the UHPC-SPP-Halo-Tzwitt 2.0 column, which shows an optimal flow rate

Table 2
Experimental van Deemter analysis data under Hilic conditions on UHPC-SPP-Halo-Tzwitt 2.0 μm, UHPC-SPP-Halo-Tzwitt 2.7 μm and UHPC-FPP-Titan-Tzwitt 1.9 μm. Eluent: ACN/H_2O 85:15 + 20 mM $HCOONH_4$, T: 35 °C.

UHPC-SPP-Halo-Tzwitt 2.0							
Sample	k' (/)	H_{min} (μm)	h_{min} (/)	N/m	$\mu_{0,opt}$ (mm/s)	$\mu_{inter,opt}$ (mm/s)	Flow-rate$_{opt}$ (mL/min)
Thiourea	0.62	3.21	1.60_5	311 280	2.85	3.63	1.5
Uracil	0.99	3.22	1.61	310 660	2.28	2.91	1.2
Adenosine	1.82	3.71	1.85	269 750	2.28	2.91	1.2
UHPC-SPP-Halo-Tzwitt 2.7							
Sample	k' (/)	H_{min} (μm)	h_{min} (/)	N/m	$\mu_{0,opt}$ (mm/s)	$\mu_{inter,opt}$ (mm/s)	Flow-rate$_{opt}$ (mL/min)
Thiourea	0.62	4.03	1.49	248 090	2.20	2.60	1.1
Uracil	0.99	4.19	1.55	238 920	1.59	1.89	0.8
Adenosine	1.93	4.50	1.67	222 040	1.00	1.18	0.5
UHPC-FPP-Titan-Tzwitt 1.9							
Sample	k' (/)	H_{min} (μm)	h_{min} (/)	N/m	$\mu_{0,opt}$ (mm/s)	$\mu_{inter,opt}$ (mm/s)	Flow-rate$_{opt}$ (mL/min)
Thiourea	0.66	3.61	1.90	276 780	2.34	3.32	1.4
Uracil	1.06	3.77	1.98	265 220	1.68	2.37	1.0
Adenosine	2.10	4.20	2.21	238 300	1.34	1.90	0.8

respectively 1.5 and 2.4 times higher than those of the UHPC-FPP-Titan-Tzwitt 1.9 and the UHPC-SPP-Halo-Tzwitt 2.7 columns. In Figs. 2C, D, 1SC and D, the reduced van Deemter plots are reported. Reduced plate height $h_r \left(= \frac{H}{d_p}\right)$ permits to properly evaluate the kinetic performance of columns packed with silica particles of size. Extremely low h_r values were found with thiourea (1.49, 1.60 and 1.90 on the UHPC-SPP-Halo-Tzwitt 2.7, the UHPC-SPP-Halo-Tzwitt 2.0 and the UHPC-FPP-Titan-Tzwitt 1.9 columns, respectively), proving the goodness of the packing process obtained for all columns.

4.3. Kinetic performance (achiral compounds)

The kinetic plot method was used to have a complete overview of the kinetic performance limits of all columns. This method shows the highest efficiency achievable by a column in the shortest time, working at the maximum pressure reachable by the instrument. Kinetic plots method is the best choice to have a clear and proper comparison of kinetic performance of different columns (also with different geometries) in various analytical conditions (HPLC, UHPLC or SFC). The t_0 *vs. N* kinetic plot is the original one introduced by Giddings in 1965 [31]. This is the starting point for other forms of kinetic plots, such as the so-called Poppe plot [32,33]. This plot permits to have a clearer view on the C-term of van Deemter equation. In this work, for the preparation of kinetic plots, the maximum operating pressure was set at 600 bar for columns packed with 2.7 μm SPP CSP (silica pressure limit) and 1000 bar (maximum operative pressure in most common UHPLC systems) for those packed with 2.0 μm SPP and 1.9 μm FPP CSPs. In Fig. 3, the kinetic plots for the three columns are reported. Fig. 3A (t_0 *vs N*) shows that the use of the UHPC-SPP-Halo-Tzwitt 2.0 column is worthwhile up to 190,000 plates. After this value, the best choice would be the UHPC-FPP-Titan-Tzwitt 1.9 column and beyond $N = 226{,}000$ the UHPC-SPP-Halo-Tzwitt 2.7 column gives the best kinetic performance, due to its very high permeability and low operating pressure. The same trend is observed in the Poppe plot (t_0/N *vs N*, Fig. 3B) and t_R*vs N* plot, on uracil, (Fig. 3C), where the column packed with the 2.0 μm SPP CSP overcomes the columns packed with the other two CSPs in the bottom left corner of the graph, which represents the maximum separation speed with realistic column length. In these two plots, where the data of uracil (*k'*: 0.99-1.03) are reported, it is evident how the UHPC-Halo-Tzwitt 2.0 column exceeds, in terms of kinetic performance, the other two columns in every area of the plot thanks to its low C-term (1.8 and 2.1 times lower than that of the UHPC-FPP-Titan-Tzwitt 1.9 and the UHPC-SPP-Halo-Tzwitt 2.7 columns, respectively). *L* vs *N* plots (Fig. 3D) confirm the same trend. Indeed, by assuming an efficiency of 45,000 plates as the target value, one sees that a 18 cm long column packed with 2.0 μm SPPs can be used (at 1000 bar) against the 24 cm required by the UHPC-FPP-Titan-Tzwitt 1.9 column and the 28 cm of the UHPC-SPP-Halo-Tzwitt 2.7 one (but at 600 bar). Finally, the same kinetic behavior was observed, considering adenosine (*k'*: 1.82–2.07) as the probe (Fig. 2S). In this case, the C-term critically affects kinetic plots. Indeed the UHPC-SPP-Halo-Tzwitt 2.7 column seems to be the less efficient from the kinetic point of view. On the other hand, the UHPC-SPP-Halo-Tzwitt 2.0 column performs better than the other two columns across the entire range of these plots.

Chromatograms showing the separation of a mixture of achiral probes naphthalene (hold-up volume marker), thiourea, uracil and adenosine, on all the three columns at their optimal flow rate (on thiourea) are shown in Fig. 4A. Since the optimal flow rate of the UHPC-SPP-Halo-Tzwitt 2.0 column is higher than those of the other columns, a reduction of almost 40% of analysis time could be achieved with this column. Fig. 4B and C shows the same chromatographic separations at higher flow rates (2.0 and 2.5 mL/min). The column packed with 2.0 μm SPPs exhibits the lower drops in efficiency and resolution when compared with the other two columns as a confirmation of the flat C-branch of its van Deemter curve. Indeed, by considering thiourea, moving from the optimal flow-rate to 2.5 mL/min produced efficiency loss of 3%, 10% and 12% respectively on the UHPC-SPP-Halo-Tzwitt 2.0, the UHPC-FPP-Titan-Tzwitt 1.9 and UHPC-SPP-Halo-Tzwitt 2.7 columns. If one considers adenosine, the efficiency drop became even more evident, going from 23% to 27% and then to 42% for the three columns (considered in the same order as before). This efficiency loss is reflected in corresponding resolution values, which decrease in the same order (Table 3). In Fig. 4D all chromatograms are reported as a function of *k'*. As it can be noticed, analytes have almost the same retention factors on the two SPP CSPs, while they are 6–10% higher on the FPP one (see above).

4.4. van Deemter analysis of chiral compounds

The kinetic profile of the different columns was completed by measuring van Deemter plots of the racemic chiral molecule 2-(4-chloro-phenoxy)-propionic acid (Fig. 5). The column packed with UHPC-SPP-Halo-Tzwitt 2.0 particles showed outstanding perfor-

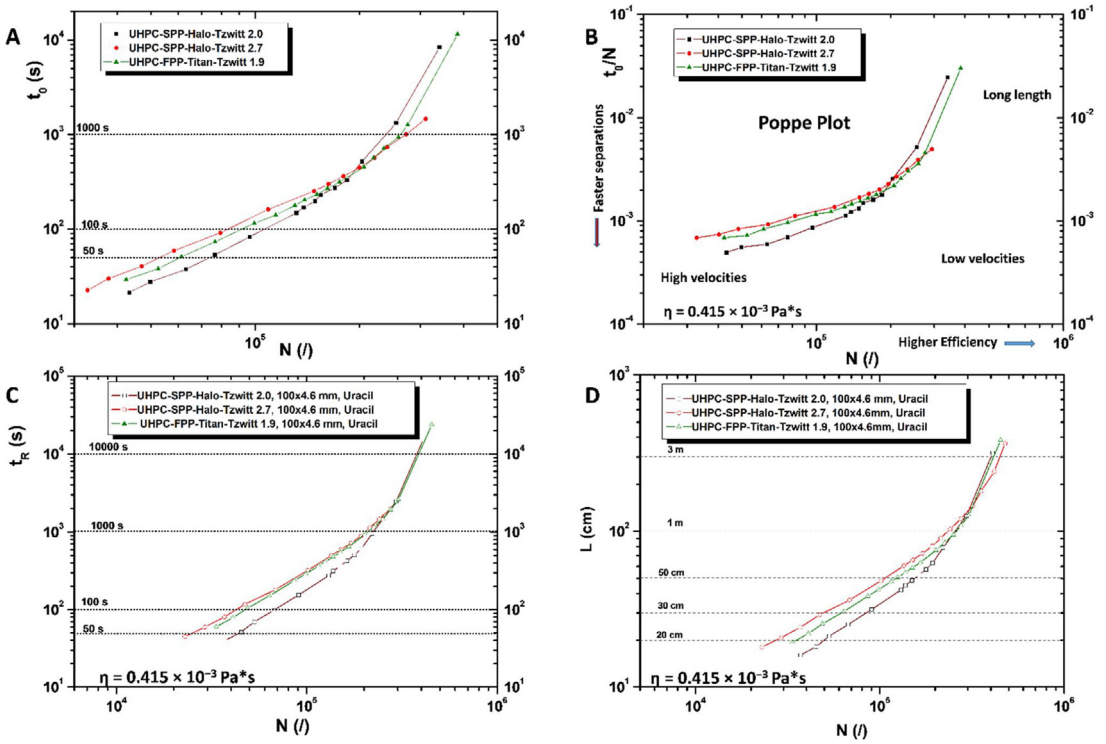

Fig. 3. Kinetic plots showing a comparison of the three different columns under HILIC conditions, mobile phase: ACN/H_2O 85:15 + 20 mM $HCOONH_4$; $\eta = 0.41 \times 10^{-3}$ Pa s; $T = 35\,^{\circ}C$. (A) t_0 vs N plot, (B) t_0/N vs Nplot, (C) Uracil t_R vs N plot and (D) L vs N plot on uracil. $\Delta P_{max} = 1000$ bar was set for the UHPC-SPP-Halo-Tzwitt 2.0 μm (Black square) and UHPC-FPP-Titan-Tzwitt 1.9 μm (Green triangle), but a $\Delta P_{max} = 600$ bar was used for the UHPC-SPP-Halo-Tzwitt 2.7 μm (Red circle). (For interpretation of the references to colour in this figure legend, the reader is referred to the web version of this article.)

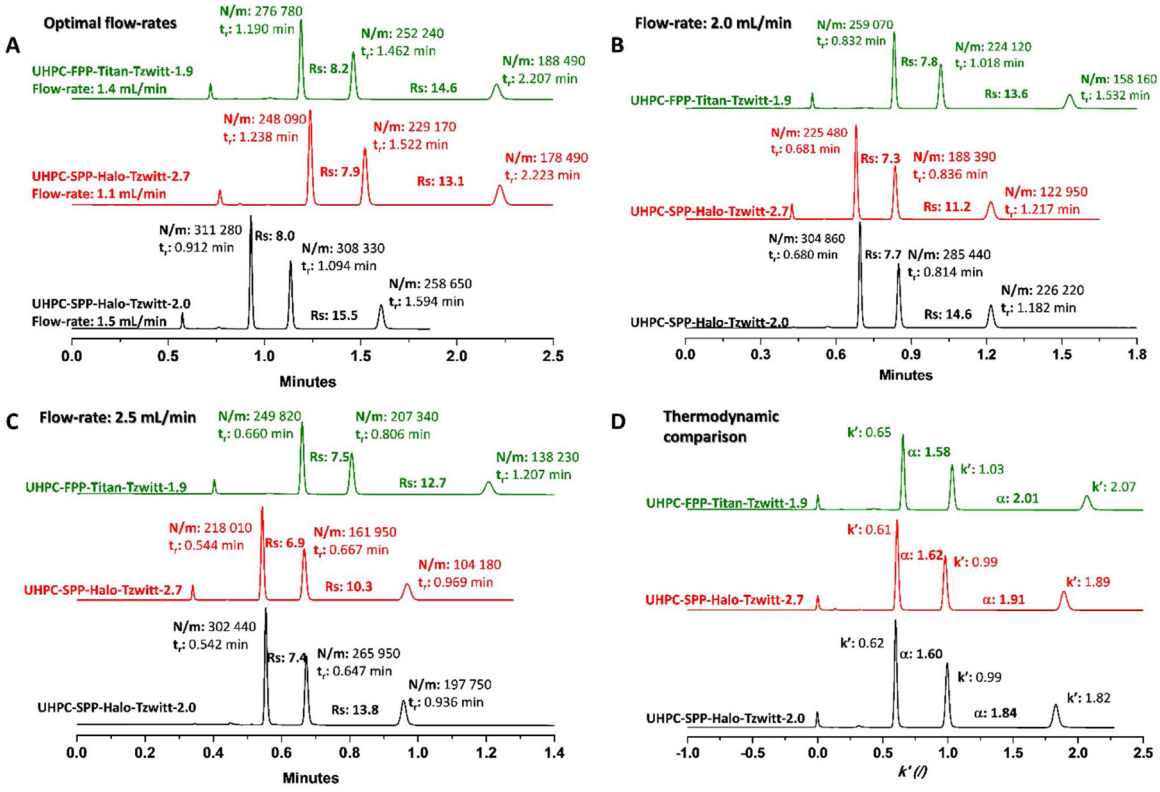

Fig. 4. Separations of the achiral probes naphthalene (hold-up volume marker), thiourea, uracil and adenosine on the UHPC-SPP-Halo-Tzwitt 2.0 μm (Black line), UHPC-SPP-Halo-Tzwitt 2.7 μm (Red line) and UHPC-FPP-Titan-Tzwitt 1.9 μm (Green line) at their optimal flow-rates (A), at flow-rate: 2.0 mL/min (B) and at 2.5 mL/min (C). Graph (D) shows the same chromatograms as a function of the retention factor (k'). Eluent: ACN/H_2O 85:15 + 20 mM $HCOONH_4$, T: 35 °C. (For interpretation of the references to colour in this figure legend, the reader is referred to the web version of this article.)

Table 3
Percentage of efficiency and resolution loss moving from the optimal flow-rate of each column up to flow-rate = 2.5 mL/min.

Column	Efficiency loss% [Φ_{opt} vs Φ 2.5 mL/min]			Resolution loss% [Φ_{opt} vs Φ 2.5 mL/min]	
	N/m Thiourea	N/m Uracil	N/m Adenosine	$Rs_{[Thiourea-Uracil]}$	$Rs_{[Uracil-Adenosine]}$
UHPC-SPP-Halo-Tzwitt 2.0	−3%	−14%	−23%	−7%	−11%
UHPC-SPP-Halo-Tzwitt 2.7	−12%	−30%	−42%	−13%	−21%
UHPC-FPP-Titan-Tzwitt 1.9	−10%	−18%	−27%	−9%	−13%

mance. Almost 300,000 N/m (H = 3.42 μm, h_r = 1.71) were recorded for the first eluted enantiomer and roughly 280,000 plates/m for the second one, at optimal flow rates of 0.9 and 0.7 mL/min, respectively. The column packed with 1.9 μm FPPs generated more than 260,000 N/m (H = 3.82 μm, h_r = 2.01) at 0.7 mL/min for the first eluted enantiomer. As expected, the column packed with the UHPC-SPP-Halo-Tzwitt 2.7 particles was the less efficient, by producing 211,000 N/m for the first eluted enantiomer (H = 4.74 μm, h_r = 1.76) at a flow rate of 0.5 mL/min. This gap in terms of efficiency is clearly pointed out in Fig. 5B and C, where N/m is reported as a function of flow rates for both enantiomers for each column. An efficiency gain of about 11% and more than 40% on the second eluted enantiomer is achievable with the UHPC-SPP-Halo-Tzwitt 2.0 column if compared to the UHPC-FPP-Titan-Tzwitt 1.9 and UHPC-SPP-Halo-Tzwitt 2.7 ones (Fig. 5C), respectively. Moreover, the UHPC-SPP-Halo-Tzwitt 2.0 column still exhibits a flatter C-branch also for the separation

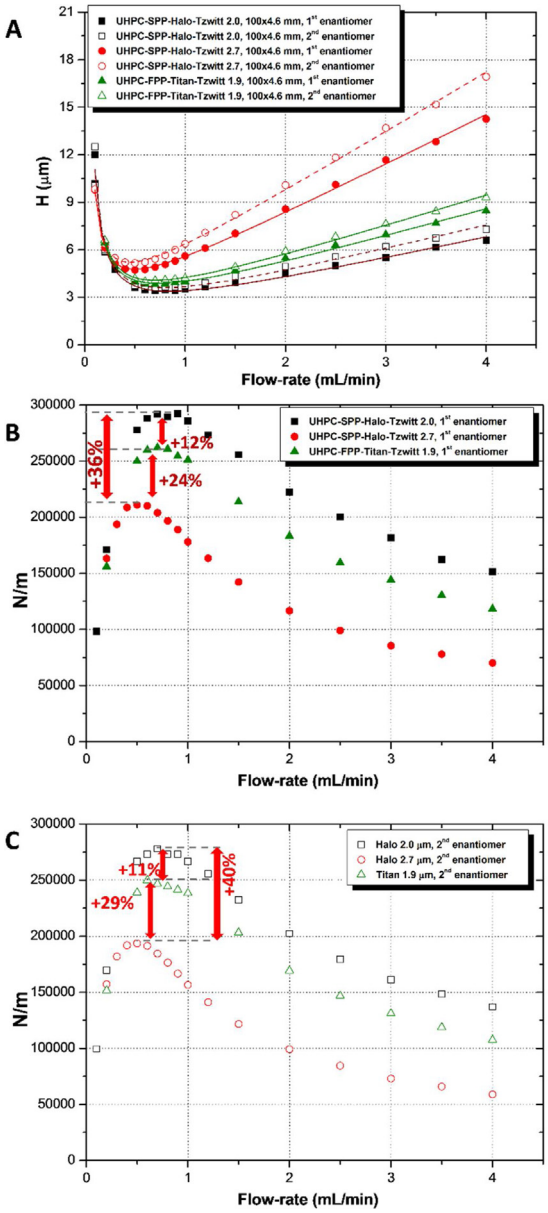

UHPC-SPP-Halo-Tzwitt 2.0

Sample	k' (/)	H_{min} (μm)	h_{min} (/)	N/m	Flow-rate$_{opt}$ (mL/min)
1° enantiomer	2.21	3.42	1.71	292 220	0.9
2° enantiomer	2.80	3.60	1.80	278 060	0.7

UHPC-SPP-Halo-Tzwitt 2.7

Sample	k' (/)	H_{min} (μm)	h_{min} (/)	N/m	Flow-rate$_{opt}$ (mL/min)
1° enantiomer	2.09	4.74	1.76	211 060	0.5
2° enantiomer	2.88	5.16	1.91	193 720	0.5

UHPC-FPP-Titan-Tzwitt 1.9

Sample	k' (/)	H_{min} (μm)	h_{min} (/)	N/m	Flow-rate$_{opt}$ (mL/min)
1° enantiomer	2.61	3.82	2.01	261 950	0.7
2° enantiomer	3.29	4.00	2.11	249 900	0.6

Fig. 5. A) van Deemter plots of 1st (solid lines) and 2nd (dashed lines) eluted enantiomers of 2-(4-chloro-phenoxy)-propionic acid on the UHPC-SPP-Halo-Tzwitt 2.0 μm (Black square), UHPC-SPP-Halo-Tzwitt 2.7 μm (Red circle) and UHPC-FPP-Titan- Tzwitt 1.9 μm (Green triangle). B) N/m of the 1st eluted enantiomer vs. flow-rate plots on the three columns. C) N/m of the 2nd eluted enantiomer vs. flow-rate plots on the three columns Eluent: ACN/H_2O 85:15 + 20 mM $HCOONH_4$, T: 35 °C. (For interpretation of the references to colour in this figure legend, the reader is referred to the web version of this article.)

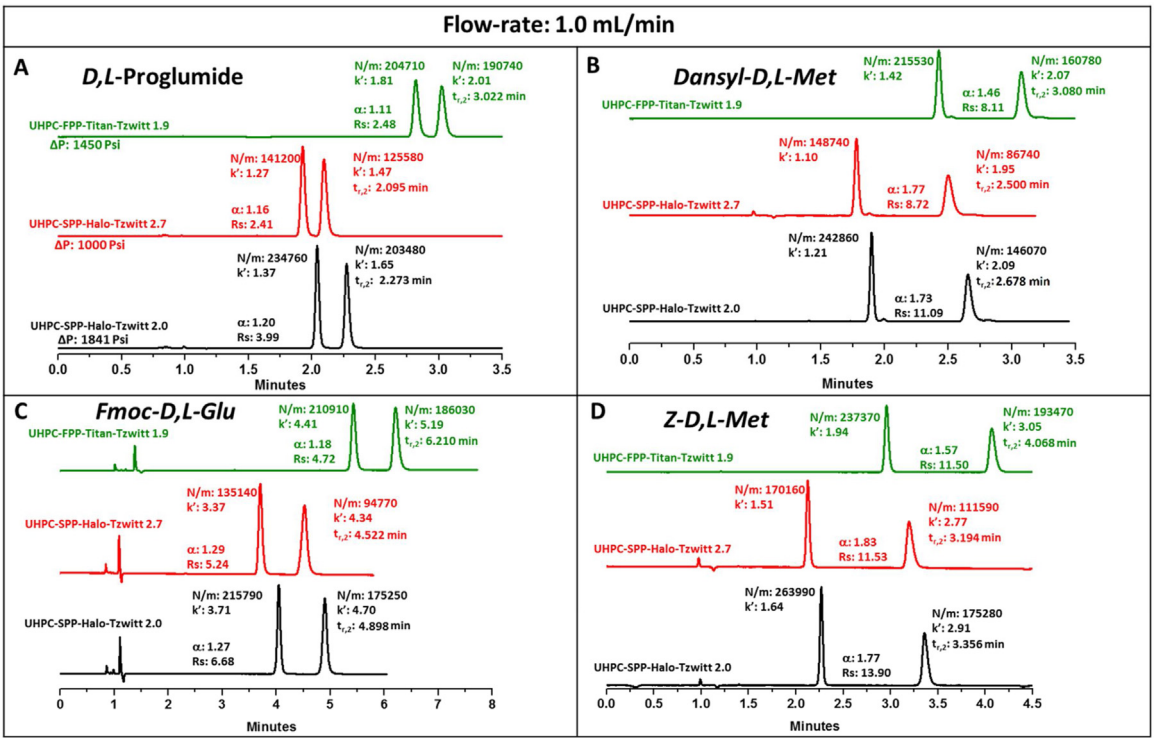

Fig. 6. Separations of the racemic analytes on the UHPC-SPP-Halo-Tzwitt 2.0 μm (Black line), UHPC-SPP-Halo-Tzwitt 2.7 μm (Red line) and UHPC-FPP-Titan-Tzwitt 1.9 μm (Green line) at flow-rate: 1.0 mL/min. (A) D,L-Proglumide, (B) Dansyl-D,L-Methionine, (C) Fmoc-D,L-Glutamine, (D) *Z*-D,L-Methionine. Eluent: ACN/H_2O 85:15 + 20 mM $HCOONH_4$, *T*: 35 °C. (For interpretation of the references to colour in this figure legend, the reader is referred to the web version of this article.)

of chiral samples. This is an essential advantage of this column for UHPLC enantioseparations, as it will be shown in the following.

4.5. Applications to chiral compounds

4.5.1. Kinetic performance (chiral compounds)

After evaluation of physical and kinetic properties, all columns were tested for practical applications. A broad range of chiral compounds (including N-derivatized amino acids, agrochemical and drugs or drug-like molecules) was employed under HILIC conditions. All kinetic data are summarized in Table 2S and Fig. 3S. As expected, the most efficient column was the UHPC-SPP-Halo-Tzwitt 2.0, followed by the UHPC-FPP-Titan-Tzwitt 1.9 and the UHPC-SPP-Halo-Tzwitt 2.7. Indeed, looking at the bar plot in Fig. 3S, an average 35% loss of efficiency for the first eluted enantiomer was observed on the UHPC-SPP-Halo-Tzwitt 2.7 column in comparison to the UHPC-SPP-Halo-Tzwitt 2.0 one.

Chromatograms of four different chiral samples recorded at 1.0 mL/min on the three columns are shown in Fig. 6. Roughly 265,000 *N*/m were recorded on the UHPC-SPP-Halo-Tzwitt 2.0 column for the first eluted enantiomer of *Z*-D,L-Met (Fig. 6D). Smaller efficiencies were observed on the UHPC-FPP-Titan-Tzwitt 1.9 column (−10%) and UHPC-SPP-Halo-Tzwitt 2.7 one (−36%).

Moreover in Fig. 3S, *N*/m values for 15 pairs of racemic samples recorded at a flow rate of 1.0 mL/min are reported as a bar plot. In most cases, the column packed with 2.0 μm particles provides the highest efficiency for the first eluted enantiomer (see Fig. 3S A). On the opposite, the UHPC-FPP-Titan-Tzwitt 1.9 column has shown larger efficiency for the second eluted enantiomer (see Fig. 3S B). The effect is more pronounced for the N-derivatized amino acids with medium-high retention factors. These findings seem to suggest the existence of different adsorption/desorption kinetics on the two columns, which could be correlated to the different surface density of chiral selector on particles (see above). However, further experimental and theoretical investigations are necessary to explain this behavior and to deeply understand the adsorption mechanism occurring on both SPP and FPP CSPs.

4.5.2. Thermodynamics and resolution (R_S)

Retention and enantioselectivity values for several chiral probes on the three CSPs are listed in Table 4 and Fig. 4S. From these data it is evident that the two SPP CSPs have similar retention behavior, while the UHPC-FPP-Titan-Tzwitt 1.9 column showed higher retention factors. Very similar enantioselectivity was observed on the two SPP CSPs (average value about 1.5). They were about 10% higher than those observed on the FPP CSP (Fig. 4S). This difference could be related to the higher density of the teicoplanin selector on the two SPP silica in comparison to the fully porous one (see above).

As far as resolution is concerned, the UHPC-SPP-Halo-Tzwitt 2.0 column showed the highest resolution values for 12 out of 15 samples (Fig. 7A). For instance, the UHPC-SPP-Halo-Tzwitt 2.0 column exhibited a resolution value of about 4.0 for D,L-Proglumide (Fig. 6A), which is 40% and 37% higher than those observed on the UHPC-SPP-Halo-Tzwitt 2.7 and UHPC-FPP-Titan-Tzwitt 1.9 columns, respectively. In Fig. 7B, the ratio between resolution values and retention times of the second eluted enantiomers is reported. This plot clearly shows the very high resolution power of the UHPC-SPP-Halo-Tzwitt 2.0 column in comparison to both the UHPC-SPP-Halo-Tzwitt 2.7 and the UHPC-FPP-Titan-Tzwitt 1.9 columns.

4.6. Very/ultra-high speed and ultra-high performance chiral separations

van Deemter analysis revealed the ability of these columns to work easily at flow rates higher than optimal ones. The behavior of these CSPs was thus investigated up to 6.0 mL/min flow rate (so-called very-high speed regime), by employing 50 × 4.6 mm in house

Table 4
Chromatographic data for chiral separations obtained on UHPC-SPP-Halo-Tzwitt 2.0 (Col. 1), UHPC-SPP-Halo-Tzwitt 2.7 (Col. 2) and UHPC-FPP-Titan-Tzwitt 1.9 (Col. 3) at flow-rate: 1.0 mL/min. Column geometry: 100 × 4.6 mm L.xI.D. Eluent: ACN/H_2O 85:15 + 20 mM $HCOONH_4$, T: 35 °C.

Sample	k'$_2$ (/)			α (/)			Rs (/)		
Name	Col. 1	Col. 2	Col. 3	Col. 1	Col. 2	Col. 3	Col. 1	Col. 2	Col. 3
N-Fmoc-D-L-Ala	3.18	2.83	2.96	1.61	1.57	1.39	7.73	6.37	6.75
N-Fmoc-D-L-Phe	1.31	1.33	1.46	1.15	1.27	1.15	2.67	3.45	2.91
N-Fmoc-D-L-Glu	4.70	4.34	5.19	1.27	1.29	1.18	6.68	5.24	4.72
N-Fmoc-D-L-Leu	1.22	1.29	1.42	1.40	1.29	1.42	5.84	5.65	5.34
N-BOC-D-L-Met	1.99	1.89	2.14	1.42	1.45	1.30	8.50	7.13	6.21
Dansyl-D-L-Met	2.09	1.95	2.07	1.73	1.77	1.46	11.09	8.72	8.11
Dansyl-D-L-Phe	1.33	1.24	1.52	1.15	1.17	1.11	2.72	2.30	2.08
Z-D,L-Phe	1.91	1.88	2.21	1.19	1.30	1.20	4.24	4.88	4.46
Z-D,L-Met	2.91	2.77	3.05	1.77	1.83	1.57	13.90	11.53	11.50
Z-D,L-Ala	4.33	4.02	4.47	1.54	1.65	1.44	12.54	10.38	10.12
Mandelic Acid	11.44	9.65	11.90	2.97	2.73	2.38	27.82	21.96	24.99
D,L-4,5-Dihydro orotic Acid	25.53	20.59	25.80	1.42	1.34	1.29	11.78	8.71	8.87
D,L-Proglumide	1.65	1.47	2.01	1.20	1.16	1.11	3.99	2.41	2.48
Haloxyfop	1.46	1.20	1.42	1.78	1.67	1.39	11.58	7.50	6.72
Ketorolac	4.80	4.30	4.44	1.40	1.37	1.26	9.61	7.03	6.33

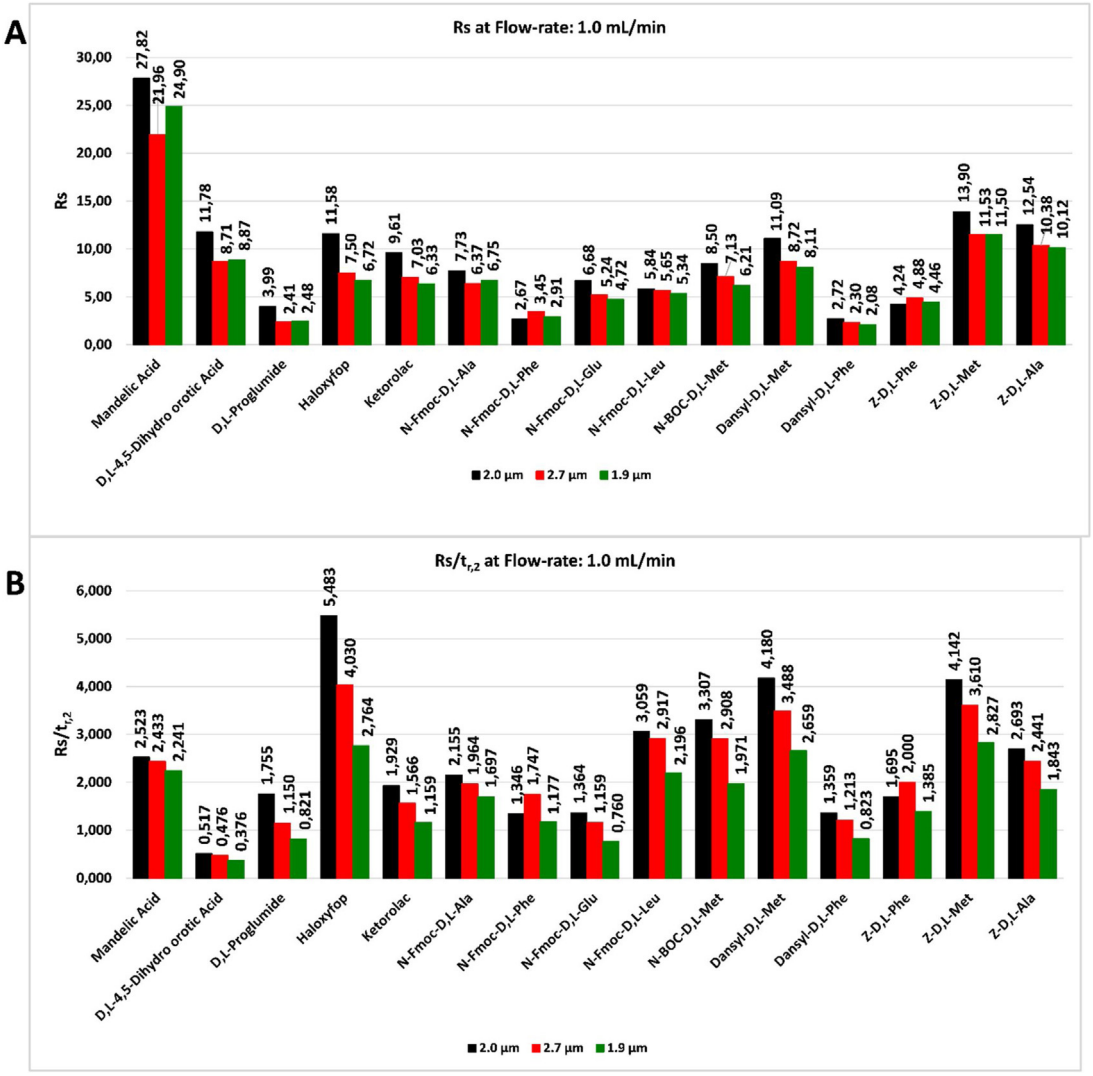

Fig. 7. Bar plots of resolution (R_s) and $R_s/t_{R,2}$ obtained for different analytes on the UHPC-SPP-Halo-Tzwitt 2.0 µm (Black), UHPC-SPP-Halo-Tzwitt 2.7 µm (Red) and UHPC-FPP-Titan-Tzwitt 1.9 µm (Green) at flow-rate: 1.0 mL/min. Eluent: ACN/H_2O 85:15 + 20 mM $HCOONH_4$, *T*: 35 °C. (For interpretation of the references to colour in this figure legend, the reader is referred to the web version of this article.)

packed columns and different chiral samples were tested (Fig. 5S). Fig. 8 shows the separation of a mixture of enantiomers of haloxyfop and ketorolac at flow rates ranging from 1.0 to 6.0 mL/min. The resolution drop was about 45% on both the UHPC-SPP-Halo-Tzwitt 2.0 and the UHPC-FPP-Titan-Tzwitt 1.9 columns and higher than 50% on the UHPC-SPP-Halo-Tzwitt 2.7 one (see Table 5). An average

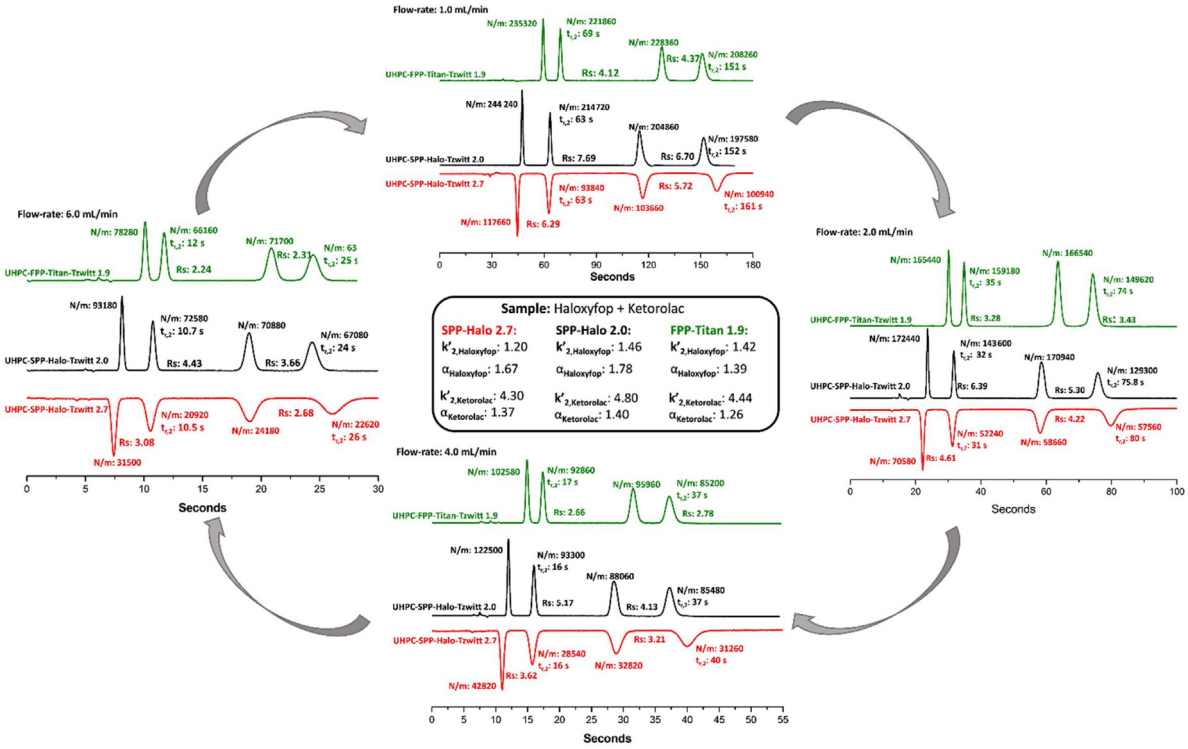

Fig. 8. Very-High speed/Ultra-High Performance separations of the enantiomers of Haloxyfop and Ketorolac, at different flow-rates, on UHPC-SPP-Halo-Tzwitt 2.0 μm (Black line), UHPC-SPP-Halo-Tzwitt 2.7 μm (Red line) and UHPC-FPP-Titan-Tzwitt 1.9 μm (Green line) packed in 50 × 4.6 mm columns. *k'* and α values reported in figure were calculated at flow-rate: 1.0 mL/min. Eluent: ACN/H_2O 85:15 + 20 mM $HCOONH_4$, *T*: 35 °C. (For interpretation of the references to colour in this figure legend, the reader is referred to the web version of this article.)

Table 5
Percentage of efficiency and resolution loss on 5-cm and 2-cm long columns (4.6 mm I.D.) moving from the flow-rate: 1.0 mL/min up to flow-rate: 6.0 (on the 50 × 4.6 mm) and 8.0 mL/min (on the 20 × 4.6 mm columns).

Flow-rate 1.0 mL/min vs. 6.0 mL/min (50 × 4.6 mm)/8.0 mL/min (20 × 4.6 mm)							
LxI.D.	CSP	Resolution drop (−%)		Efficiency drop (−%)			
		Haloxyfop	Ketorolac	1° enantiomer Haloxyfop	2° enantiomer Haloxyfop	1° enantiomer Ketorolac	2° enantiomer Ketorolac
50 × 4.6 mm	SPP-Halo 2.0	42	45	62	66	65	66
	SPP-Halo 2.7	51	53	73	78	77	78
	FPP-Titan 1.9	46	47	67	70	69	70
20 × 4.6 mm	SPP-Halo 2.0	44	52	61	69	74	72
	FPP-Titan 1.9	50	52	69	72	73	66

loss in efficiency of more than 60% was observed on both the UHPC-SPP-Halo-Tzwitt 2.0 and UHPC-FPP-Titan-Tzwitt 1.9 columns. On the other hand, a dramatic efficiency loss of about 80% was recorded on the UHPC-SPP-Halo-Tzwitt 2.7 column.

To further assess the potential of the two CSPs, exhibiting the best behavior under Ultra-High-Speed and Ultra-High-Performance regimes (namely, the UHPC-SPP-Tzwitt-Halo 2.0 and the UHPC-FPP-Tzwitt-Titan 1.9), two additional 20 × 4.6 mm columns were in house packed with these phases. Various chiral samples were tested, at flow rates as high as 8.0 mL/min (Fig. 6S). The separation of a mixture of haloxyfop and ketorolac is reported in Fig. 9. Ultra-fast separations were obtained on both columns. 73 s and 61 s were necessary to achieve the complete separation at 1.0 mL/min on the UHPC-FPP-Tzwitt-Titan 1.9 column and on the UHPC-SPP-Tzwitt-Halo 2.0 one, respectively, with efficiencies higher than 200,000 *N*/m and resolutions close to 4.0. Increasing the flow rate at 8.0 mL/min, the separation of the mixture was completed in roughly 8 s. Remarkably, by considering only the enantiomers of haloxyfop they were resolved in only 4.0 and 3.4 s on the UHPC-FPP-Titan-Tzwitt 1.9 and UHPC-SPP-Halo-Tzwitt 2.0 columns, respectively. High efficiency values close to 60,000 N/m were obtained also at this flow rate on the UHPC-FPP-Titan-Tzwitt 1.9 column, whereas the UHPC-SPP-Halo-Tzwitt 2.0 one showed about 76,000 *N*/m (Table 5). It is important to observe that the combination of high efficiency and high enantioselectivity allowed to maintain excellent R_s values also in ultrafast regimes. Indeed, the UHPC-FPP-Titan-Tzwitt 1.9 column showed R_s values of about 1.6 while the UHPC-SPP-Halo-Tzwitt 2.0 column exhibited R_s values higher than 2.0.

5. Conclusions

This work has demonstrated that the zwitterionic teicoplanin based CSP prepared on 2.0 μm SPPs is very promising towards the development of high efficient and ultrafast liquid chromatography. The columns packed with this CSP exhibited excellent performance (300,000 *N*/m), very close to that obtained in RP achiral chromatography. These columns were also characterized by extremely fast mass transfer (very flat C-branch of van Deemter equation). Therefore, they could be employed in ultrafast separation (up to 8 mL/min flow rate) without dramatically loosing performance. As a proof of concept example of the feasibility of ultrafast and high performance

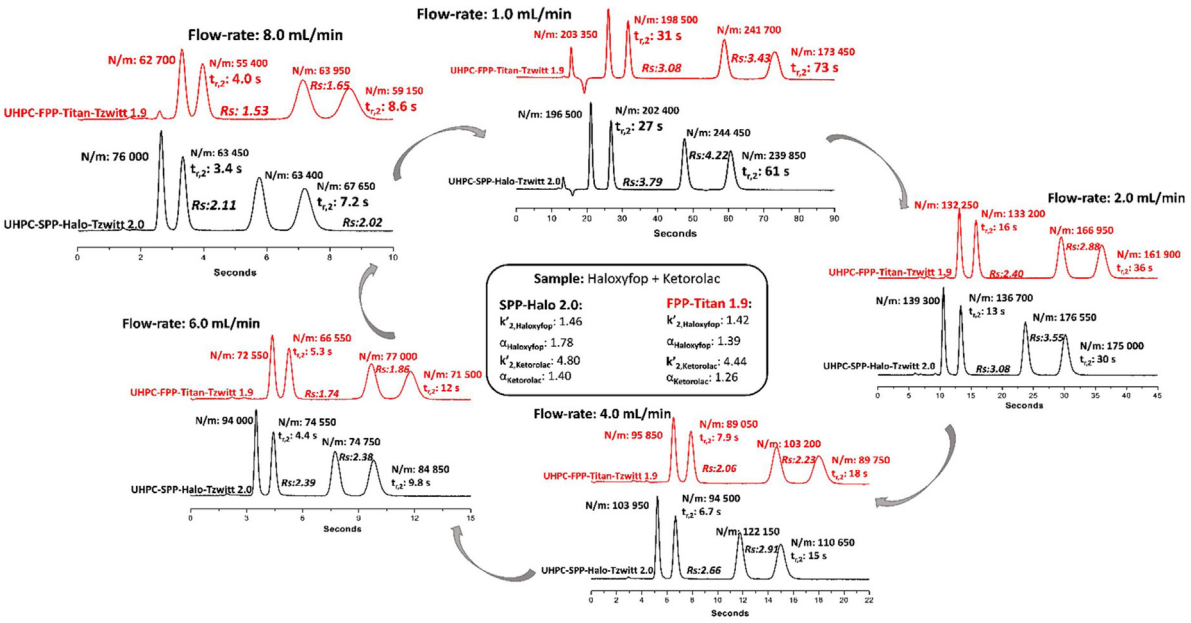

Fig. 9. Ultra-High speed/Ultra-High Performance separations of the enantiomers of Haloxyfop and Ketorolac, at different flow-rates, on UHPC-SPP-Halo-Tzwitt 2.0 μm (Black line) and UHPC-FPP-Titan-Tzwitt 1.9 μm (Green line) packed in 20 × 4.6 mm columns. *k'* and α values reported in figure were calculated at flow-rate: 1.0 mL/min. Eluent: ACN/H_2O 85:15 + 20 mM $HCOONH_4$, *T*: 35 °C. (For interpretation of the references to colour in this figure legend, the reader is referred to the web version of this article.)

chiral separations on these columns, haloxyfop enantiomers were baseline resolved (resolution equal to 2) in only 3 s.

In a forthcoming paper, the effect of chiral selector surface density on the adsorption/desorption kinetics will be investigated by preparing a series of chiral particles (both SPP and FPP) with the same base chemistry and different loading of chiral selector. In our opinion, indeed, this parameter has a dramatic effect on the efficiency of the chiral stationary phase and its optimization will allow to prepare CSPs significantly more efficient towards ultrafast applications.

Acknowledgements

This work was conducted with financial support from Sapienza University of Rome, Italy (DR n. 3210/16 of 16/12/2016). The authors thank Dr. E. Bianchini, Department of Chemistry and Pharmaceutical Sciences, University of Ferrara, for elemental analysis measurements.

Appendix A. Supplementary data

Supplementary data associated with this article can be found, in the online version, at http://dx.doi.org/10.1016/j.chroma.2017.09.008.

References

[1] J.J. Kirkland, J.J. DeStefano, T.J. Langlois, Characteristics of superficially-porous silica particles for fast HPLC: some performance comparisons with sub-2-μm particles, Am. Lab. (2007) 18–21.
[2] J.J. DeStefano, S.A. Schuster, J.M. Lawhorn, J.J. Kirkland, Performance characteristics of new superficially porous particles, J. Chromatogr. A 1258 (2012) 76–83.
[3] G. Guiochon, F. Gritti, Shell particles trials, tribulations and triumphs, J. Chromatogr. A 1218 (2011) 1915–1938.
[4] A. Cavazzini, F. Gritti, K. Kaczmarski, N. Marchetti, G. Guiochon, Mass-transfer kinetics in a shell packing material for chromatography, Anal. Chem. 79 (2007) 5972–5979.
[5] N. Marchetti, A. Cavazzini, F. Gritti, G. Guiochon, Gradient elution separation and peak capacity of columns packed with porous shell particles, J. Chromatogr. A 1163 (2007) 203–211.
[6] F. Gritti, A. Cavazzini, N. Marchetti, G. Guiochon, Comparison between the efficiencies of columns packed with fully and partially porous C18-bonded silica materials, J. Chromatogr. A 1157 (2007) 289–303.
[7] N. Marchetti, G. Guiochon, High peak capacity separations of peptides in reversed-phase gradient elution liquid chromatography on columns packed with porous shell particles, J. Chromatogr. A 1176 (2007) 206–216.
[8] G. Cancelliere, A. Ciogli, I. D'Acquarica, F. Gasparrini, J. Kocergin, D. Misiti, M. Pierini, H. Ritchie, P. Simone, C. Villani, Transition from enantioselective high performance to ultra-high performance liquid chromatography: a case study of a brush-type chiral stationary phase based on sub-5-micron to sub-2-micron silica particles, J. Chromatogr. A 1217 (2010) 990–999.
[9] M. Catani, O.H. Ismail, F. Gasparrini, M. Antonelli, L. Pasti, N. Marchetti, S. Felletti, A. Cavazzini, Recent advancements and future directions of superficially porous chiral stationary phases for ultrafast high-performance enantioseparations, Analyst 142 (2017) 555–566.
[10] D. Kotoni, A. Ciogli, C. Molinaro, I.D. Acquarica, J. Kocergin, T. Szczerba, H. Ritchie, C. Villani, F. Gasparrini, Introducing enantioselective ultrahigh-pressure liquid chromatography (eUHPLC): theoretical inspections and ultrafast separations on a new sub-2-μm whelk-O1 stationary phase, Anal. Chem. 84 (2012) 6805–6813.
[11] D. Kotoni, A. Ciogli, I. D'Acquarica, J. Kocergin, T. Szczerba, H. Ritchie, C. Villani, F. Gasparrini, Enantioselective ultra-high and high performance liquid chromatography: a comparative study of columns based on the Whelk-O1 selector, J. Chromatogr. A 1269 (2012) 226–241.
[12] A. Cavazzini, N. Marchetti, R. Guzzinati, M. Pierini, A. Ciogli, D. Kotoni, I. D'Acquarica, C. Villani, F. Gasparrini, Enantioseparation by ultra-high-performance liquid chromatography, TrAC – Trends Anal. Chem. 63 (2014) 95–103.
[13] R.J. Reischl, L. Hartmanova, M. Carrozzo, M. Huszar, P. Frühauf, W. Lindner, Chemoselective and enantioselective analysis of proteinogenic amino acids utilizing N-derivatization and 1-D enantioselective anion-exchange chromatography in combination with tandem mass spectrometric detection, J. Chromatogr. A 1218 (2011) 8379–8387.
[14] K. Lomsadze, G. Jibuti, T. Farkas, B. Chankvetadze, Comparative high-performance liquid chromatography enantioseparations on polysaccharide based chiral stationary phases prepared by coating totally porous and core-shell silica particles, J. Chromatogr. A 1234 (2012) 50–55.
[15] D.A. Spudeit, M.D. Dolzan, Z.S. Breitbach, W.E. Barber, G.A. Micke, D.W. Armstrong, Superficially porous particles vs. fully porous particles for bonded high performance liquid chromatographic chiral stationary phases: isopropyl cyclofructan 6, J. Chromatogr. A 1363 (2014) 89–95.
[16] M.D. Dolzan, D.A. Spudeit, Z.S. Breitbach, W.E. Barber, G.A. Micke, D.W. Armstrong, Comparison of superficially porous and fully porous silica supports used for a cyclofructan 6 hydrophilic interaction liquid chromatographic stationary phase, J. Chromatogr. A 1365 (2014) 124–130.
[17] C.L. Barhate, Z.S. Breitbach, E. Costa Pinto, E.L. Regalado, C.J. Welch, D.W. Armstrong, Ultrafast separation of fluorinated and desfluorinated pharmaceuticals using highly efficient and selective chiral selectors bonded to superficially porous particles, J. Chromatogr. A 1426 (2015) 241–247.
[18] D.C. Patel, Z.S. Breitbach, M.F. Wahab, C.L. Barhate, D.W. Armstrong, Gone in seconds: praxis, performance, and peculiarities of ultrafast chiral liquid

chromatography with superficially porous particles, Anal. Chem. 87 (2015) 9137–9148.
[19] D.C. Patel, M.F. Wahab, D.W. Armstrong, Z.S. Breitbach, Advances in high-throughput and high-efficiency chiral liquid chromatographic separations, J. Chromatogr. A 1467 (2016) 2–18.
[20] M.F. Wahab, R.M. Wimalasinghe, Y. Wang, C.L. Barhate, D.C. Patel, D.W. Armstrong, Salient sub-second separations, Anal. Chem. 88 (2016) 8821–8826.
[21] O.H. Ismail, L. Pasti, A. Ciogli, C. Villani, J. Kocergin, S. Anderson, F. Gasparrini, A. Cavazzini, M. Catani, Pirkle-type chiral stationary phase on core-shell and fully porous particles: are superficially porous particles always the better choice toward ultrafast high-performance enantioseparations? J. Chromatogr. A 1466 (2016) 96–104.
[22] O.H. Ismail, A. Ciogli, C. Villani, M. De Martino, M. Pierini, A. Cavazzini, D.S. Bell, F. Gasparrini, Ultra-fast high-efficiency enantioseparations by means of a teicoplanin-based chiral stationary phase made on sub-2μm totally porous silica particles of narrow size distribution, J. Chromatogr. A 2016 (1427) 55–68.
[23] F. Gritti, G. Guiochon, Mass transfer kinetics, band broadening and column efficiency, J. Chromatogr. A 1221 (2012) 2–40.
[24] M. Catani, O.H. Ismail, A. Cavazzini, A. Ciogli, C. Villani, L. Pasti, C. Bergantin, D. Cabooter, G. Desmet, F. Gasparrini, D.S. Bell, Rationale behind the optimum efficiency of columns packed with new 1.9 μm fully porous particles of narrow particle size distribution, J. Chromatogr. A 2016 (1454) 78–85.
[25] G. Desmet, D. Clicq, P. Gzil, Geometry-independent plate height representation methods for the direct comparison of the kinetic performance of LC supports with a different size or morphology, Anal. Chem. 77 (2005) 4058–4070.
[26] G. Gritti, Y. Kazakevich, G. Guiochon, Effect of the surface coverage of endcapped C18-silica on the excess adsorption isotherms of commonly used organic solvents from water in reversed phase liquid chromatography, J. Chromatogr. A 1169 (2007) 111–124.
[27] F. Gritti, Y. Kazakevich, G. Guiochon, Measurement of hold-up volumes in reverse-phase liquid chromatography: definition and comparison between static and dynamic methods, J. Chromatogr. A 1161 (2007) 157–169.
[28] M. Al-Bokari, D. Cherrak, G. Guiochon, Determination of the porosities of monolithic columns by inverse size-exclusion chromatography, J. Chromatogr. A 975 (2002) 275–284.
[29] O.H. Ismail, A. Pasti, A. Cavazzini, C. Ciogli, D. Villani, F. Kotoni, D.S. Bell, Experimental evidence of the kinetic performance achievable with columns packed with new 1.9 μm fully porous particles of narrow particle size distribution, J. Chromatogr. A 1454 (2016) 86–92.
[30] C.A. Cramers, J.A. Rijks, C.P.M. Schutjes, Factors determining flow rate in chromatographic columns, Chromatographia 14 (1981) 439–444.
[31] J.C. Giddings, Comparison of theoretical limit of separating speed in gas and liquid chromatography, Anal. Chem. 37 (1965) 60–63.
[32] U.D. Neue, Kinetic plots made easy, LC-GC Eur. 22 (2009) 570.
[33] H. Poppe, Some reflections on speed and efficiency of modern chromatographic methods, J. Chromatogr. A 778 (1997) 3–21.

PAPER IX

analytical chemistry

Article

pubs.acs.org/ac

Exploring Fluorous Affinity by Liquid Chromatography

Martina Catani,[†] Roberta Guzzinati,[†,‡] Nicola Marchetti,[†] Luisa Pasti,[†] and Alberto Cavazzini*[,†]

[†]University of Ferrara, Department of Chemistry and Pharmaceutical Sciences, Via L. Borsari, 46, 44121 Ferrara, Italy

[‡]Italian National Agency for New Technologies, Energy and Sustainable Economic Development (ENEA), R. C. Casaccia, Via Anguillarese, 301, S. Maria di Galeria, 00123, Roma, Italy

Supporting Information

ABSTRACT: Terms such as "fluorous affinity" and "fluorophilicity" have been used to describe the unique partition and sorption properties often exhibited by highly fluorinated organic compounds, that is molecules rich in sp^3 carbon−fluorine bonds. In this work, we made use of a highly fluorinated stationary phase and a series of benzene derivatives to study the effect of one single perfluorinated carbon on the chromatographic behavior and adsorption properties of molecules. For this purpose, the adsorption equilibria of α,α,α-trifluorotoluene, toluene, and other alkylbenzenes have been studied by means of nonlinear chromatography in a variety of acetonitrile/water eluents. Our results reveal that one single perfluorinated carbon is already enough to induce a drastic change in the adsorption properties of molecules on the perfluorinated stationary phase. In particular, it has been found that adsorption is monolayer if the perfluoroalkyl carbon is present but that, when this unit is missing, molecules arrange as multilayer stack structures. These findings can contribute to the understanding of molecular mechanisms of fluorous affinity.

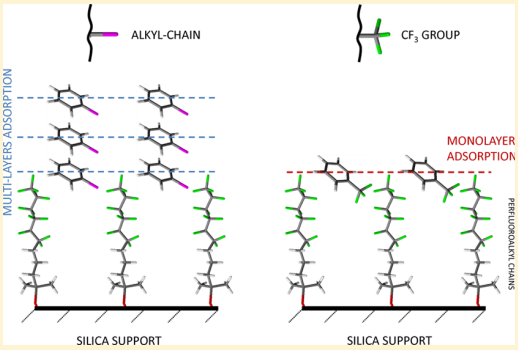

Fluorous affinity is the property that describes the capacity of highly (or heavily) fluorinated materials to selectively interact with each other by means of strong noncovalent fluorine−fluorine (F−F) interactions, in a sort of similar dissolves (or likes) similar principle. By definition, highly fluorinated materials are those where a relevant number of hydrogen atoms, typically from 7 to 20, attached to sp^3 carbon atoms are replaced with F atoms. This gives the molecules specific properties, different from those of their parent hydrocarbon analogues.[1]

Fluorophilicity has been extensively employed especially in organic chemistry for the purification of fluorous-tagged molecules from other mixture components by solid phase extraction over fluorous-functionalized silica gel (usually C_6F_{13}- or C_8F_{17}-perfluoro-functionalized silica gels[2,3]) and in fluorous-biphase technology to promote the high-temperature mixing of innately immiscible fluorous and organic phases as to conduct catalytic reactions efficiently under homogeneous conditions.[4]

The importance of fluorous-functionalized stationary phases has been increasingly more recognized by the analytical chemistry community that developed new methods, based on the concept of fluorous-tag and fluorinated chromatography, for highly sensitive and selective analyses of different classes of compounds from very complex matrixes. This is the case, for instance, of the determination of low-abundance proteins in complex biological mixtures, which represents one of the most relevant issues in bioanalytical applications.[5−7] These proteins, whose diagnostic potential is in general very relevant, are often remarkably difficult to detect in the presence of more abundant biological molecules (proteins/peptides) or contaminants due to a series of analytical problems, such as the masking presence of the high-abundance (e.g., serum) proteins, mass spectrometry signal suppression, etc.[8] Fluorous-based separation concepts proved to be fundamental for the solution of these problems.

Another important field where it is reasonable to believe there will be an increasing demand for efficient and selective fluorous-based analytical methods is the determination of perfluorinated compounds in the environment.[9,10] In addition to the well-known cases of perfluorooctanoic acid (PFOA) and perfluorooctanesulfonate (PFOS), there are indeed many other perfluorinated compounds potentially dangerous for humans, whose presence in the environment has been recently demonstrated, such as perfluoroalkane sulfinic acids and perfluoroalkyl phosphinic and phosphonic acids[11] or the class of fluorotelomers and fluorotelomer-based products.[12] For these compounds, however, fundamental studies focusing on their fate in the environment, their transport properties, how they degrade, where they (bio)accumulate, etc. are essentially still missing.

Previous investigations on perfluoro-based stationary phases[8,13−15] have shown that, when employed with aqueous/acetonitrile (ACN) binary eluents, they exhibit features very similar to traditional reversed-phase (RP) stationary phases,[10] such as C_{18}. This is so, for instance, regarding both the linear dependence of the logarithm of

Received: March 31, 2015
Accepted: June 5, 2015
Published: June 5, 2015

DOI: 10.1021/acs.analchem.5b01212
Anal. Chem. 2015, 87, 6854−6860

retention factor on the volume fraction of the organic modifier[9,10] and the preferential adsorption of ACN from ACN/water binary mixtures.[10,13] What differentiates perfluorinated and C_{18} stationary phases, instead, is their ability to discriminate between molecules differing by one single methylene or perfluomethylene group that is, in chromatographic terms, their methylene[17,18] or perfluoromethylene selectivity.[9,19] Experimentally, perfluoromethylene selectivity can be estimated by the dependence of the logarithm of retention factor on the number of CF_2 groups in homologous series of, e.g., perfluorinated acids.[9,10] When perfluorinated stationary phases are employed in these measurements, the Gibbs free energy of phase transfer for the passage of a perfluoroalkyl carbon from the mobile to the stationary phase can be considered a sort of direct measure of fluorous affinity.[9,10] As a consequence, by employing eluents of different composition, these experiments permit to establish how fluorous affinity varies with the composition of the eluent.[10]

The majority of models used to describe retention in RPLC are based on measurement performed under linear conditions, i.e., when the concentrations of solutes injected in the column are very low (ideally, infinite dilution conditions for the solute). To this category belong, for instance, the so-called linear free-energy relationships (LFER)[20] or the hydrophobic subtraction methods (HSM).[21,22] On the other hand, it has been pointed out, for example, by Fornstedt and co-workers[23] that an important limitation of these approaches is that the effects of different possible interactions between molecule and stationary phase are lumped in one single parameter (the retention factor), so that some fundamental aspects of the chromatographic process might be lost.[24] For instance, if the adsorption surface is energetically heterogeneous (i.e., composed of different kinds of adsorption sites), the retention factor cannot be used to distinguish between sites with different energy/abundance.[25−27] To gather this information, indeed, one needs to extend the adsorption measurements to the nonlinear range of the adsorption isotherm.[16,28]

In this work, the adsorption equilibria of α,α,α-trifluorotoluene and toluene on a straight-chain perfluorinated stationary phase have been studied with the purpose of investigating the effect of one single perfluorinated sp^3 carbon on the adsorption behavior of these molecules. The investigation has been carried on under a variety of experimental conditions, through linear and nonlinear chromatographic measurements. For the sake of comparison and to assess the possible effect of the alkyl-chain length on the adsorption process linear alkylbenzenes with alkyl chain lengths ranging from C_2 to C_6 have also been considered in our study. These investigations have shown that there is a drastic change in the adsorption properties of molecules due to the presence of one single CF_3 group. On the contrary, the adsorption mode was not found to be substantially influenced by the alkyl-chain length. These findings may contribute to the understanding of molecular mechanisms of fluorous affinity.

THEORY

For the sake of space, only a short overview of the theory and equations employed in this work is given. For a detailed discussion about theoretical aspects or how these equations can be derived, readers are referred to the literature (and to the Supporting Information) where these features are covered in detail.

Tracer Pulse Chromatography. The tracer pulse method has been extensively used for measuring excess surface isotherm of binary systems.[9,29−40] According to this theory, the operational definition of the excess volume of an isotopically labeled compound i, V_i^{exc}, is given by[30]

$$V_i^{exc} = (V_{R,i}^* - V_{R,j}^*)\theta_i^M\theta_j^M \quad (1)$$

where $V_{R,i}^*$ and $V_{R,j}^*$ are the elution volumes for each labeled component i and j of the binary system and θ_i^M and θ_j^M their volume fractions in the bulk mobile phase. On the other hand, V_0, the thermodynamic void volume (defined as the total volume of the eluent in the column, $V_0 = V_M + V_S$, being V_M and V_S the kinetic void volume and the stationary phase volume) is given by

$$V_0 = V_{R,i}^*\theta_i^M + V_{R,j}^*\theta_j^M \quad (2)$$

According to the method originally proposed by Nagy and Schay,[41] the capacity and thickness of the surface phase (needed to pass from excess to absolute adsorption[30,38,42]) can be estimated by the linear region of the excess isotherm, being

$$V_i^{exc} = V_i^S - V_S\theta_i^M \quad (3)$$

where V_i^S is the volume of i in the stationary phase.

Selectivity. The selectivity, α, is the ratio of the retention factor, k, of two solutes (here, 1 and 2):

$$\alpha = \frac{k_1}{k_2} \quad (4)$$

When alkyl homologues are employed for the evaluation of α, the so-called methylene selectivity is defined;[43] analogously, the perfluoromethylene selectivity is when perfluoroalkyl homologues are used to calculate α.[8,10,19] With a homologous series, in addition, α is best calculated by the slope of the plot of ln k vs the carbon number in the chain.[17] The natural logarithm of methylene or perfluoromethylene selectivity multiplied by the factor $-RT$ (being R the gas constant and T the temperature) gives the change of Gibbs free energy for the transfer, respectively, of a methylene or perfluoromethylene group from the mobile to the stationary phase, $\Delta G_{CX_2}^\circ$:

$$-RT \ln \alpha = \Delta G_{CX_2}^\circ \quad (5)$$

where X is either H (methylene selectivity) or F (perfluoromethylene selectivity).

Finally, following Martin,[44] the total free energy ΔG° for the transfer of a molecule from the mobile to the stationary phase can be calculated by assuming that each group g of the molecule is associated with its own unique change ΔG_g° in free Gibbs energy, independent of the presence of other groups, that is

$$\Delta G^\circ = \sum_g \Delta G_g^\circ \quad (6)$$

Inverse Method. The inverse method permits to determine adsorption isotherms in chromatography through a numerical procedure in which the parameters of an isotherm model are derived from overloaded (nonlinear) band profiles of compounds.[45,46] It is based on the nonlinear least-squares method. The numerical constants of the isotherm models are tuned so that the calculated and the measured band profiles match as much as possible. Calculated band profiles are derived by numerically solving the equilibrium-dispersive model of chromatography, once an isotherm model has been chosen to

DOI: 10.1021/acs.analchem.5b01212
Anal. Chem. 2015, 87, 6854−6860

correlate the concentration of the component in the mobile, C, and stationary, q, phases (more information is in the Supporting Information). In the equilibrium-dispersive model of chromatography, it is assumed instantaneous equilibrium between the stationary and the mobile phases, and an apparent dispersion term (D_a) accounts for both the axial dispersion and the finite rate of the mass transfer kinetics. The differential mass balance equation is written as

$$\frac{\partial C(z,t)}{\partial t} + F\frac{\partial q(z,t)}{\partial t} + u\frac{\partial C(z,t)}{\partial z} = D_a\frac{\partial^2 C(z,t)}{\partial z^2} \quad (7)$$

where z is the length, t the time, u the mobile phase linear velocity, and F the phase ratio (V_S/V_M). D_a is the apparent dispersion coefficient that can be calculated from the number of theoretical plates (N) determined by an analytical injection:

$$D_a = \frac{uL}{2N} \quad (8)$$

being L the column length. Initial and boundary conditions employed to solve eq 7 are reported in the Supporting Information.

EXPERIMENTAL SECTION

Column and Materials. A commercial 150 mm × 2.1 mm stainless steel column, packed with perfluorohexylpropylsiloxane-bonded silica, 5 μm particle size, 100 Å pore size (Fluophase-RP, Thermo Scientific) was used for all measurements. Toluene, ethylbenzene, propylbenzene, pentylbenzene, hexylbenzene, and α,α,α-trifluorotoluene were purchased from Sigma-Aldrich. Ultrahigh quality Milli-Q water was obtained by a Milli-Q water purification system (Millipore). ACN was LC−MS grade from Sigma-Aldrich. Deuterated water, D_2O, and deuterated ACN, D_3-ACN, were from Cambridge Isotope Laboratories Inc.

Equipment and Measurements. *Tracer Pulse Experiments.* The excess isotherm of ACN from binary water/ACN mixtures was measured through the tracer pulse technique by using a LC−MS/MS instrument made of a micro-HPLC (Finnigan Surveyor Plus) interfaced to a LTQ-XL linear ion trap MS detector (Thermo Scientific) through an APCI source. Ion source operational conditions are reported in the Supporting Information. The 5 μL injections of D_3-ACN and D_2O were done in the column equilibrated with different ACN aqueous solutions. The ACN concentration was varied with an increase of 10% in the range 0−80%. Between 80 and 100%, the following concentrations were prepared: 85, 90, 93, 95, 97, and 100%. The flow rate was 0.1 mL/min. Measurements were done in triplicate. Retention times of perturbations were determined through peak moments.[9]

In order to exclude the presence of the isotopic effect, the excess isotherm has been also measured through the perturbation on the plateau technique.[16] The results of this study are reported in the Supporting Information and show that the labeled and the unlabeled components have the same isotherm.

Linear and Nonlinear Measurements of Benzene Derivatives. A 1290 Infinity ultra high-performance liquid chromatography system (from Agilent Technologies) equipped with a degasser, binary pump, autosampler, column thermostat, and UV−vis diode array was employed. Under linear conditions, 1 μL of diluted solutions of benzene derivatives (0.02% v/v) were injected. Chromatograms were recorded at 214 nm. Four different binary water/ACN mobile phases were considered, with ACN ranging from 60 to 90% v/v (in increments of 10%). Peak retention times were estimated through peak moments.

High-concentration injections (needed for estimating the adsorption isotherm through the inverse method) of toluene, butylbenzene, and α,α,α-trifluorotoluene were performed at two different mobile phases, namely, 60/40 and 70/30% v/v ACN/water. The highest injected concentrations were close to the empirically evaluated solubility limits of the analytes in the actual mobile phase. In particular, at 60/40% v/v ACN/water, these were 13 g/L (toluene), 10 g/L (butylbenzene), and 20 g/L (α,α,α-trifluorotoluene). At 70/30% v/v ACN/water, on the other hand, we found solubilities of 35, 30, and 48 g/L, respectively, for toluene, butylbenzene, and α,α,α-trifluorotoluene. Large volume (up to 20 μL) injections were performed by using the available binary solvent delivery system. One channel was used to deliver the sample solution and the other to pump the pure mobile phase. The low volume (35 μL) of the jet-weaver mixer of the 1290 chromatograph allows for an efficient mixing of solvent streams without loss of performance (with the column employed in this work). Under nonlinear conditions, the detector was calibrated at 266 nm for butylbenzene and at 278 nm for toluene and α,α,α-trifluorotoluene.

All chromatographic measurements (including tracer pulse experiments) were performed at 0.1 mL/min at 25 ± 0.1 °C. Temperature was controlled by a digital contact thermometer (IKA Laboratory Equipment). All measurements were performed as triplicate determinations.

For the calculation of the simulated profiles, eq 7 was solved by using a finite difference scheme.[16,47] The isotherm parameters were optimized by using a super modified downhill simplex search routine.[45,48] All programs were written in Matlab.

RESULTS AND DISCUSSION

A rigorous description of thermodynamic equilibria in complex systems such as in RPLC would require simultaneously measuring the competitive isotherms of all the species in the system, that is both the eluent components and the analytes. These measurements, however, are very difficult to perform. Usually, therefore, the distribution isotherms of the eluent components are measured on the entire concentration range without regard to analytes (excess isotherms), while those of analytes are measured at a fixed mobile phase composition when a convention for the determination of the volume of the mobile and the stationary phase has been established (absolute isotherms). A common approach for fixing the position of the boundary between mobile and stationary phase (or, in other words, to define the position of the Gibbs dividing surface[49]) is by employing a purportedly unretained compound, from the retention time of which it is possible to estimate V_M. The very common example is uracile with traditional C_{18} silica gel in RP conditions. This is the so-called "component J not adsorbed" (JNA) convention, according to Riedo and Kováts.[50]

In this work, the determination of the stationary and mobile phase volumes has been done through an approach, originally proposed by Schay and Nagy,[41] which involves measuring the excess adsorption isotherm of ACN from water/ACN binary mixtures and the use of eqs 2 and 3. Briefly, eq 3 shows that the estimation of V_S can be obtained by considering the region of the excess isotherm where the excess of ACN decreases linearly with θ^M_{ACN} (i.e., the zone of saturation of the stationary phase by

DOI: 10.1021/acs.analchem.5b01212
Anal. Chem. 2015, 87, 6854−6860

ACN[30,41,51]); then, since V_0 can be calculated by eq 2, estimations of V_M ($V_M = V_0 - V_S$) and F (eq 7) are straightforward.

The excess isotherm of ACN is represented in the main part of Figure 1 in the form of excess volume of adsorbed ACN per

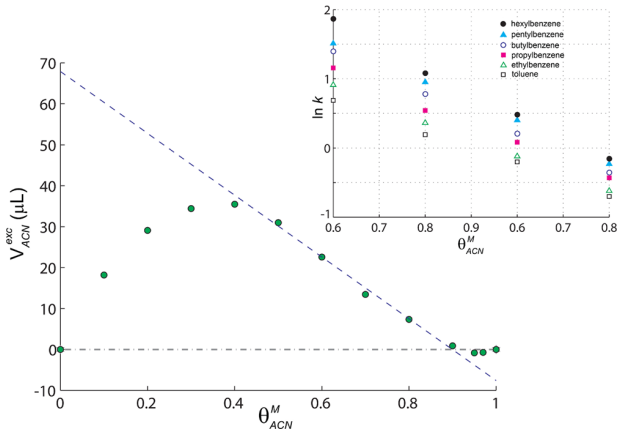

Figure 1. Main: excess adsorption isotherm of ACN (microliter per column) from binary water/ACN mixtures. Straight line: linear regression for the evaluation of V_S and V^S_{ACN}, according to eq 3. Inset: dependence of the logarithm of retention factor of alkylbenzenes on the volume fraction of acetonitrile in mobile phase: toluene (empty squares); ethylbenzene (empty triangles); propylbenzene (full squares); butylbenzene (empty circles); pentylbenzene (full triangles); hexylbenzene (full circles).

column. The excess volume increases gradually in the first part of the isotherm (roughly up to θ^M_{ACN} 0.4), it reaches a maximum and then it decreases quasi-linearly for $0.5 < \theta^M_{ACN} < 0.9$. For very organic-rich eluents, the excess of ACN becomes negative in consequence of a positive excess of adsorbed water. This is due to the presence of residual unreacted surface silanols that under these conditions have not been yet completely saturated by water molecules. The analysis of the linear region of the excess isotherm ($0.5 < \theta^M_{ACN} < 0.9$) by means of eq 3 leads to estimated values of V_S and V^S_{ACN} of 75 and 68 μL, respectively. In other words, at saturation, the stationary phase is made by more than 90% of ACN. Accordingly, being $V_0 = 351$ μL (from eq 2), the phase ratio was 0.27.

All measurements of benzene derivatives have been performed in this zone of the excess isotherm. Indeed, since retention in LC involves equilibria in both the stationary and the mobile phase, it is very important to work where these phases can be properly defined and characterized.[10,30,49] Initially, the dependence of ln k on θ^M_{ACN} for a series of six alkylbenzenes (namely, toluene, ethylbenzene, propylbenzene, butylbenzene, pentylbenzene, and hexylbenzene) has been investigated. The inset in the right upper part of Figure 1 shows the experimental data. From them it can be observed that, at a given mobile phase composition, retention increases as the hydrophobic portion of the molecule increases (thus with a typical RP behavior) and that, for all compounds, ln$k$ decreases linearly with θ^M_{ACN}. The linear fitting of experimental data, in fact, led to correlation coefficients R^2 larger than 0.99 in all cases (straight lines not shown to avoid overcrowding the figure). Therefore, these data can be used for the calculation of the methylene selectivity[17] and, by means of eq 5, of the free energy change for the transfer of a CH_2 unit from the mobile to the stationary phase. Calculated $\Delta G_{CH_2}^\circ$ values, in function of the eluent composition, are listed in the second column of Table 1 (more information in the Supporting Information).

Table 1. Gibbs Free Energy for the Transfer of Either a Methylene Group, $\Delta G_{CH_2}^\circ$, or a Perfluoromethylene Group, $\Delta G_{CF_2}^\circ$, from the Mobile to the Stationary Phase As a Function of the Mobile Phase Composition[a]

θ^M_{ACN}	$\Delta G_{CH_2}^\circ$	$\Delta G_{CF_2}^\circ$	$4 \times \Delta G_{CH_2}^\circ$
0.6	−562	−2006	−2248
0.7	−456	−1775	−1824
0.8	−359	−1677	−1436
0.9	−280	−1426	−1120

[a] $\Delta G_{CF_2}^\circ$s were taken from ref 8. Free energy values in J mol^{-1} (T = 298 K). See text for details.

By considering now the chromatographic behavior of α,α,α-trifluorotoluene, i.e., of a molecule that differs from toluene only for the aromatic ring substituent (a CF_3 vs a CH_3 group), some interesting results can be observed. Figure 2 reports the

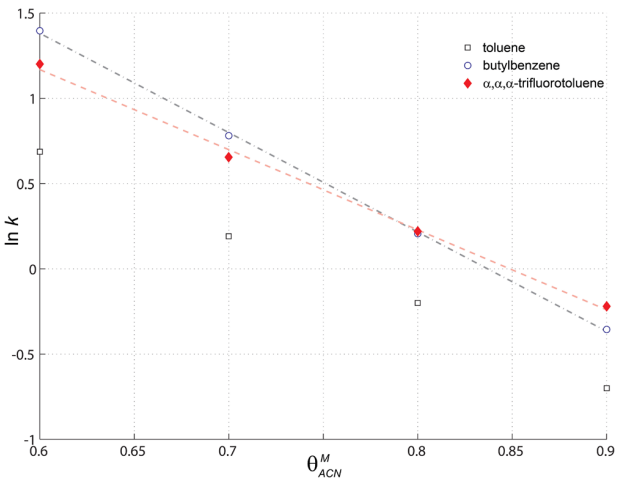

Figure 2. Dependence of the logarithm of the retention factor of benzene derivatives on the volume fraction of acetonitrile in the mobile phase: toluene (empty squares); butylbenzene (empty circles); α,α,α-trifluorotoluene (full diamond). Linear regressions have been shown to stress the inversion of the elution order between butylbenzene and α,α,α-trifluorotoluene as a function of θ^M_{ACN}.

dependence of ln$k$ on θ^M_{ACN} for α,α,α-trifluorotoluene in the same range of eluent compositions previously considered. For the sake of comparison, in the same plot also the data for toluene and butylbenzene (see later on) have been shown. By looking at these data, it is evident that the presence of the CF_3 group provokes a drastic change in the retention behavior of the molecule inducing an increase in retention of roughly 60% (compare retention of toluene and α,α,α-trifluorotoluene). This finding is still more significant by considering that solubility of α,α,α-trifluorotoluene in water/ACN mixtures is noticeably larger than that of toluene and that, in RP chromatography, retention is expected to decrease when the solubility in mobile phase increases.[16,43] As an example, at 70/30% v/v ACN/water, the experimentally measured solubility limit for α,α,α-trifluorotoluene was approximately 48 g/L vs only about 35

DOI: 10.1021/acs.analchem.5b01212
Anal. Chem. 2015, 87, 6854−6860

g/L for toluene. This is, however, only apparently in contrast with our understanding of retention in RP liquid chromatography. The explanation lies in the concept of fluorous affinity. From a thermodynamic viewpoint,[52−55] indeed, it is largely more favorable to transfer one CF_3 group from the aqueous/ACN mobile phase to the perfluorinated stationary phase than one CH_3 unit. This has been demonstrated, e.g., in ref 10 where $\Delta G_{CF_2}^{\circ}$s were evaluated, at different mobile phases, by using a series of perfluorinated acids. For the sake of comparison, the $\Delta G_{CF_2}^{\circ}$ values calculated in ref 10 have been reported in Table 1 (third column). They are indeed significantly more negative than the corresponding $\Delta G_{CH_2}^{\circ}$s.

Other information that can be derived from Figure 2 is that, since retention of α,α,α-trifluorotoluene is comparable to that of butylbenzene, in terms of energy transfer change, four methylene units should correspond to one single perfluoromethylene group. This comes directly from the application of the group additivity principle (eq 6) to these molecules, as shown in details in the Supporting Information. Indeed, by comparison, at each mobile phase composition, the free energy change for the transfer of the CF_2 group with four times the value of $\Delta G_{CH_2}^{\circ}$ (third column of Table 1), one observes that, within the limits of experimental errors and the simplification introduced by the model of additivity of the free energies per functional group, these values are reasonably comparable.

From a more fundamental viewpoint, however, the most relevant thing that can be observed in Figure 2 is probably the inversion of the elution order of α,α,α-trifluorotoluene and toluene induced by a change in the mobile phase composition (to emphasize this aspect, the linear regressions of experimental data have been represented in the figure). Indeed one may observe that, at organic-rich mobile phases, the former is more retained than the latter but, when the mobile phase becomes more polar, the opposite is true.

To further investigate these aspects, therefore, our study has been extended to the nonlinear range of the adsorption isotherm. Thus, the adsorption isotherm of toluene, butylbenzene, and α,α,α-trifluorotoluene have been measured, through the inverse method, at different mobile phase compositions. The results of the nonlinear investigation are surprising. They are summarized in Figures 3 and 4 where the overloaded band profiles recorded for toluene, butylbenzene, and α,α,α-trifluorotoluene, at the maximum injected concentrations and two different eluent compositions (70/30 and 60/40% v/v ACN/water), have been reported. As it can be seen, the shapes of the nonlinear peaks of alkylbenzenes (Figures 3 and 4, squares a and b) are remarkably different from those of α,α,α-trifluorotoluene (same figures, squares c). Indeed, in the former cases, the profiles present a diffuse boundary in their front and a shock in the rear. The opposite, instead, can be observed for α,α,α-trifluorotoluene, where the shock comes before the diffuse boundary. According to the theory of nonlinear chromatography,[16] we may conclude that for toluene and butylbenzene the isotherm should be convex downward (so-called anti-Langmuirian) while, on the contrary, for the perfluoro-substituted compound the isotherm must be convex upward, or Langmuirian. On the basis of this preliminary information, the adsorption isotherms were determined through the inverse method. The extended liquid−solid BET isotherm assumes that solute molecules can adsorb from the solution onto either the bare surface of the adsorbent or a layer of solute already adsorbed. It is written:

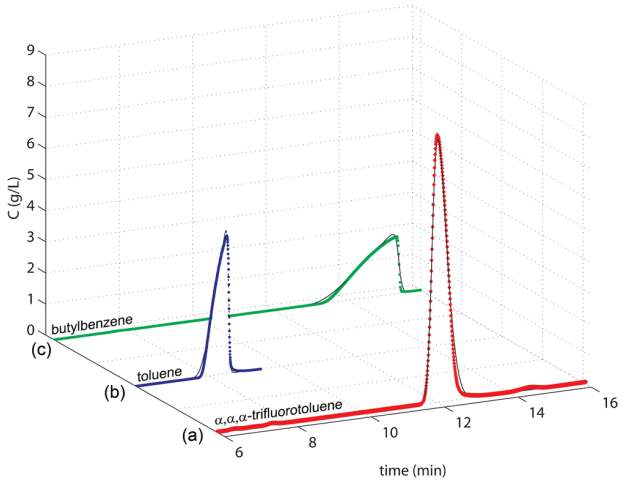

Figure 3. Comparison between experimental (points) and simulated (black continuous line) overloaded profiles. (a) α,α,α-trifluorotoluene (injected volume, 20 μL; injected concentration, 20 g/L); (b) toluene (20 μL; 13 g/L); (c) butylbenzene (20 μL; 10 g/L). Mobile phase: 60/40 ACN/water, v/v.

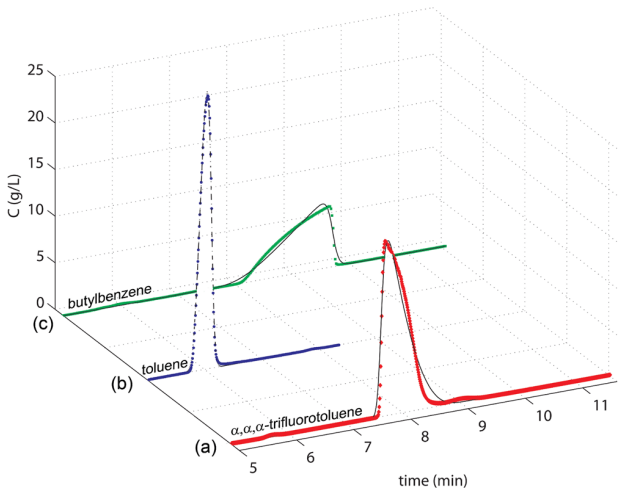

Figure 4. Comparison between experimental (points) and simulated (continuous line) overloaded profiles. (a) α,α,α-trifluorotoluene (injected volume, 20 μL; injected concentration, 48 g/L); (b) toluene (20 μL; 35 g/L); (c) butylbenzene (20 μL; 30 g/L). Mobile phase: 70/30 ACN/water, v/v.

$$q = \frac{q_s b_s C}{(1 - b_l C)(1 - b_l C + b_s C)} \tag{9}$$

where b_s and b_l are the equilibrium constants of adsorption of the compound on the bare surface and on a layer of adsorbate previously adsorbed and q_s the saturation capacity. On the other hand, for α,α,α-trifluorotoluene, we employed the Tóth isotherm, which has been often successfully employed to describe monolayer adsorption on heterogeneous surfaces:[16,56]

$$q = \frac{q_s K^{1/\nu} C}{[1 + (KC)^{\nu}]^{1/\nu}} \tag{10}$$

where ν is the so-called heterogeneity parameter, K the equilibrium constant (L/g), and q_s the saturation capacity (g/L).

DOI: 10.1021/acs.analchem.5b01212
Anal. Chem. 2015, 87, 6854−6860

The results of the inverse method calculations have been also represented in Figures 3 and 4, with continuous lines, overlaid to experimental profiles. These peaks have been obtained by solving eq 7 and using, as isotherm models, either eq 9 (alkylbenzenes) or eq 10 (α,α,α-trifluorotoluene), with the optimized isotherm parameters given by the inverse method (more details in the Supporting Information). Table 2 lists their values. Other comparisons between experimental and simulated peaks, for different injection volumes and concentrations, are given in the Supporting Information, where we have also reported the results of simulations for alkylbenzenes with other models of anti-Langmuirian isotherms, such as the quadratic model:[16]

Table 2. Best Isotherm Parameters Calculated According to the Inverse Method for Toluene and Butylbenzene (Extended Liquid−Solid BET Model, eq 9) and α,α,α-Trifluorotoluene (Tóth Model, eq 10)[a]

θ^{M}_{ACN}	toluene	butylbenzene	α,α,α-trifluorotoluene
0.6	q_s = 557 $b_s = 1.2 \times 10^{-2}$ $b_l = 1.0 \times 10^{-3}$	q_s = 358 $b_s = 4.0 \times 10^{-2}$ $b_l = 1.1 \times 10^{-5}$	q_s = 2472 K = 0.088 ν = 0.46
0.7	q_s = 3450 $b_s = 1.2 \times 10^{-3}$ $b_l = 8.5 \times 10^{-4}$	q_s = 514 $b_s = 1.4 \times 10^{-2}$ $b_l = 6.8 \times 10^{-3}$	q_s = 667 K = 0.076 ν = 0.57

[a]See text for details.

$$q = q_s \frac{b_1 C + 2b_2 C^2}{1 + b_1 C + b_2 C^2} \quad (11)$$

and the simplest convex downward isotherm represented by a Langmuir-type isotherm equation with a negative value of b:[16,57]

$$q = \frac{aC}{1 - bC} \quad (12)$$

(parameters a, b, b_1, and b_2 in eqs 11 and 12 are numerical coefficients).

In all cases, included those of Figures 3 and 4, the matching between calculated and empirical profiles has been satisfactory enough to conclude that the models proposed to describe the adsorption behavior of alkylbenzenes (eq 9) and α,α,α-trifluorotoluene (eq 10) take into account, within experimental error, the main features of the adsorption process. The differences between experimental and simulated profiles, especially in the diffuse boundaries of α,α,α-trifluorotoluene and butylbenzene at 70/30 ACN/water v/v (Figure 4) can be most likely due to kinetic effects not accounted for in the equilibrium-dispersive model of chromatography employed in calculations (eq 7).

Accordingly, the conclusion can be drawn that the adsorption nature of benzene derivatives on highly fluorinated stationary phases changes radically depending if the molecule bears a perfluorinated carbon or not. Indeed, for α,α,α-trifluorotoluene, adsorption leads to formation of Langmuir monolayers while, with alkylbenzenes, of multilayer stack structure. These data emphasize the importance of the F−F interaction to drive the adsorption process. The information and the approach proposed in this study might be useful for a better understanding not only of the specificity of the F−F interaction at a molecular level but also, more in general, of other properties of highly perfluorinated materials, such as the fact that they do not mix with most organic solvents or their tendency to bioaccumulate in body compartments high in protein content such as the liver, kidney, and blood.

CONCLUSIONS

The comparison between toluene and α,α,α-trifluorotoluene has evidenced that the presence of one single CF_3 group provokes a drastic change in the adsorption behavior of molecules on a highly perfluorinated stationary phase from water/ACN solutions. In particular, this study has revealed that α,α,α-trifluorotoluene molecules interact with the stationary phase to form a monolayer, while, on the contrary, the adsorption of toluene is likely multilayer. An analogous anti-Langmuirian adsorption behavior has been observed also for linear alkylbenzenes with longer alkyl chain. This information can contribute to the understanding, at a molecular level, of the nature of F−F interactions. The interaction was found to be effective already when one single fluorinated sp^3 carbon interacts with a highly perfluorinated moiety. This is interesting if one considers that, in the fluorous literature, a fluorous label or tag (i.e., that portion that properly introduced into a molecule, for example, as a part of a protecting group, "exerts primary control over the separability characteristics of the molecule in fluorous separation techniques"[1]) is defined to contain at least six fully fluorinated sp^3 carbons.

ASSOCIATED CONTENT

Supporting Information

APCI source conditions, methylene selectivity calculation, group-additivity principle of free energies, inverse method steps, initial and boundary conditions for the differential mass balance equation, comparison between tracer pulse and perturbation on the plateau methods for the evaluation of the excess isotherm, and other simulated cases. The Supporting Information is available free of charge on the ACS Publications website at DOI: 10.1021/acs.analchem.5b01212.

AUTHOR INFORMATION

Corresponding Author

*E-mail: cvz@unife.it. Phone: +39 0532 455331. Fax: +39 0532 240709.

Notes

The authors declare no competing financial interest.

ACKNOWLEDGMENTS

The authors thank the Italian University and Scientific Research Ministry (Grant PRIN 2012ATMNJ_003). N.M. thanks Laboratory Terra&Acqua Tech, member of Energy and Environment Cluster, Technopole of Ferrara of Emilia-Romagna High Technology Network.

REFERENCES

(1) *Handbook of Fluorous Chemistry*; Gladysz, J. A., Curran, D. P., Horváth, I. T., Eds.; Wiley-VCH: Weinheim, Germany, 2004.
(2) Curran, D. P.; Hadida, S.; He, M. *J. Org. Chem.* **1997**, *62*, 6714−6715.
(3) Curran, D. P.; Luo, Z. *J. Am. Chem. Soc.* **1999**, *121*, 9069−9072.
(4) Horváth, I. T.; Rábai, J. *Science* **1994**, *266*, 72−75.
(5) Brittain, S. M.; Ficarro, S. B.; Brock, A.; Peters, E. C. *Nat. Biotechnol.* **2005**, *23*, 463−468.

DOI: 10.1021/acs.analchem.5b01212
Anal. Chem. 2015, 87, 6854−6860

(6) Go, E. P.; Uritboonthai, W.; Apo, J. V.; Trauger, S. A.; Nordstrom, A.; O'Maille, G.; Brittain, S. M.; Peters, E. C.; Siuzdak, G. *J. Proteome Res.* **2007**, *6*, 1492−1499.
(7) Li, L.; Jiao, J.; Cai, Y.; Zhang, Y.; Lu, H. *Anal. Chem.* **2015**, *87*, 5125−5131.
(8) Marchetti, N.; Guzzinati, R.; Catani, M.; Massi, A.; Pasti, L.; Cavazzini, A. *Anal. Bioanal. Chem.* **2015**, *407*, 17−2.
(9) Marchetti, N.; Caciolli, L.; Laganà, A.; Gasparrini, F.; Pasti, L.; Dondi, F.; Cavazzini, A. *Anal. Chem.* **2012**, *84*, 7138−7145.
(10) Cavazzini, A.; Marchetti, N.; Guzzinati, R.; Pasti, L.; Ciogli, A.; Gasparrini, F.; Laganà, A. *Anal. Chem.* **2014**, *86*, 4919−4926.
(11) Kannan, K. *Environ. Chem.* **2011**, *8*, 333−338.
(12) Washington, J. W.; Naile, J. E.; Jenkins, T. M.; Lynch, D. G. *Environ. Sci. Technol.* **2014**, *48*, 5762−5769.
(13) Cavazzini, A.; Pasti, L.; Greco, R.; Costa, V.; Solera, D.; Dondi, F.; Marchetti, N.; Laganà, A.; Gasparrini, F. *J. Chromatogr. A* **2013**, *1286*, 47−54.
(14) Cavazzini, A.; Marchetti, N.; Pasti, L.; Greco, R.; Dondi, F.; Laganà, A.; Ciogli, A.; Gasparrini, F. *Anal. Chem.* **2013**, *85*, 19−22.
(15) Ciogli, A.; Simone, P.; Villani, C.; Gasparrini, F.; Laganà, A.; Capitani, D.; Marchetti, N.; Pasti, L.; Massi, A.; Cavazzini, A. *Chem.—Eur. J.* **2014**, *20*, 1−12.
(16) Guiochon, G.; Felinger, A.; Shirazi, D. G.; Katti, A. M. *Fundamentals of Preparative and Nonlinear Chromatography*, 2nd ed.; Academic Press: Boston, MA, 2006.
(17) Bhagwat, V.; Bereznitski, T.; Buszewski, B.; Jaroniec, M. *J. Liq. Chromatogr. Relat. Technol.* **1998**, *21*, 923−939.
(18) Sadek, P. C.; Carr, P. W.; Russo, M. J. *Anal. Chem.* **1987**, *59*, 1032−1039.
(19) Gilpin, R. K.; Jaroniec, M.; Lin, S. *Anal. Chem.* **1990**, *62*, 2092−2098.
(20) Kaliszan, R.; Wiczling, P.; Markuszewski, M. J.; Al-Haj, M. A. *J. Chromatogr. A* **2011**, *1218*, 5120−5130.
(21) Snyder, L. R.; Dolan, J. W.; Carr, P. W. *J. Chromatogr. A* **2004**, *1060*, 77−116.
(22) Snyder, L. R.; Maule, A.; Heebsh, A.; Cuellar, R.; Paulson, S.; Carrano, J.; Wrisley, L.; Chan, C. C.; Pearson, N.; Dolan, J. W.; Gilroy, J. J. *J. Chromatogr. A* **2004**, *1057*, 49−57.
(23) Undin, T.; Samuelsson, J.; Törncrona, A.; Fornstedt, T. *J. Sep. Sci.* **2013**, *36*, 1753−1761.
(24) Cavazzini, A.; Pasti, L.; Dondi, F.; Finessi, M.; Costa, V.; Gasparrini, F.; Ciogli, A.; Bedani, F. *Anal. Chem.* **2009**, *81*, 6735−6743.
(25) Cavazzini, A.; Remelli, M.; Dondi, F.; Felinger, A. *Anal. Chem.* **1999**, *71*, 3453−3462.
(26) Dondi, F.; Munari, P.; Remelli, M.; Cavazzini, A. *Anal. Chem.* **2000**, *72*, 4353−4362.
(27) Dondi, F.; Cavazzini, A.; Remelli, M. *Adv. Chromatogr.* **1998**, *38*, 51−74.
(28) Gritti, F.; Guiochon, G. *J. Chromatogr. A* **2005**, *1099*, 1−42.
(29) Wang, M.; Mallette, J.; Parcher, J. F. *J. Chromatogr. A* **2008**, *1190*, 1−7.
(30) Mallette, J.; Wang, M.; Parcher, J. F. *Anal. Chem.* **2010**, *82*, 3329−3336.
(31) Lindholm, J.; Forssen, P.; Fornstedt, T. *Anal. Chem.* **2006**, *78*, 2765−2771.
(32) Samuelsson, J.; Fornstedt, T. *J. Chromatogr. A* **2006**, *1114*, 53−61.
(33) Samuelsson, J.; Forssén, P.; Stefansson, M.; Fornstedt, T. *J. Chromatogr. A* **2006**, *1114*, 53−61.
(34) Arnell, R.; Fornstedt, T. *Anal. Chem.* **2006**, *78*, 4615−4623.
(35) Samuelsson, J.; Arnell, R.; Diesen, J. S.; Tibbelin, J.; Paptchikhine, A.; Fornstedt, T.; Sjöberg, P. J. R. *Anal. Chem.* **2008**, *80*, 2105−2112.
(36) Arnell, R.; Ferraz, N.; Fornstedt, T. *Anal. Chem.* **2006**, *78*, 1682−1689.
(37) Fornstedt, T. *J. Chromatogr. A* **2010**, *1217*, 792−812.
(38) Gritti, F.; Kazakevich, Y.; Guiochon, G. *J. Chromatogr. A* **2007**, *1161*, 157−169.
(39) Knox, J. H.; Kaliszan, R. *J. Chromatogr.* **1985**, *349*, 211−234.
(40) Peterson, D. L.; Helfferich, F. *J. Phys. Chem.* **1965**, *69*, 1283−1293.
(41) Schay, G.; Nagy, L. *J. Chim. Phys.* **1961**, *140*, 149−158.
(42) Ościk, J. *Adsorption*; Ellis Horwood Limited: Chichester, U.K., 1982.
(43) Snyder, L. R.; Kirkland, J. J.; Dolan, J. W. *Introduction to Modern Liquid Chromatography*, 3rd ed.; Wiley & Sons: Hoboken, NJ, 2010.
(44) Martin, A. J. P. *Biochem. Soc. Symp.* **1949**, *3*, 4−13.
(45) Cavazzini, A.; Felinger, A.; Guiochon, G. *J. Chromatogr. A* **2003**, *1012*, 139−149.
(46) Forssén, P.; Arnell, R.; Fornstedt, T. *Comput. Chem. Eng.* **2006**, *30*, 1381−1391.
(47) Rouchon, P.; Schonauer, M.; Valentin, P.; Guiochon, G. *Sep. Sci. Technol.* **1987**, *22*, 1793−1833.
(48) Morgan, E.; Burton, K. W. *Chemom. Intel. Lab. Syst.* **1990**, *8*, 97−107.
(49) Yun, K. S.; Zhu, C.; Parcher, J. F. *Anal. Chem.* **1995**, *67*, 613−619.
(50) Riedo, F.; Kováts, E. S. *J. Chromatogr.* **1982**, *239*, 1−28.
(51) Slaats, E. H.; Kraak, J. C.; Poppe, H. *J. Chromatogr.* **1978**, *149*, 519−533.
(52) Huang, M. R.; Peng, Q. Y.; Li, X. G. *Chem.—Eur. J.* **2006**, *12*, 4341−4350.
(53) Lü, Q. F.; Huang, M. R.; Li, X. G. *Chem.—Eur. J.* **2007**, *13*, 6009−6018.
(54) Li, X. G.; Liu, R.; Huang, M. R. *Chem. Mater.* **2005**, *17*, 5411−5419.
(55) Li, X. G.; Ma, X. L.; Sun, J.; Huang, M. R. *Langmuir* **2009**, *25*, 1675−1684.
(56) Marchetti, N.; Dondi, F.; Felinger, A.; Guerrini, R.; Salvadori, S.; Cavazzini, A. *J. Chromatogr. A* **2005**, *1069*, 162−172.
(57) Cavazzini, A.; Bardin, G.; Kaczmarski, K.; Szabelski, P.; Al-Bokari, M.; Guiochon, G. *J. Chromatogr. A* **2002**, *957*, 111−126.

DOI: 10.1021/acs.analchem.5b01212
Anal. Chem. 2015, 87, 6854−6860

PAPER X

Anal Bioanal Chem (2015) 407:17–21
DOI 10.1007/s00216-014-8198-5

TRENDS

New insights into perfluorinated adsorbents for analytical and bioanalytical applications

Nicola Marchetti · Roberta Guzzinati · Martina Catani · Alessandro Massi · Luisa Pasti · Alberto Cavazzini

Received: 27 June 2014 / Revised: 29 August 2014 / Accepted: 16 September 2014 / Published online: 31 October 2014

Abstract Perfluorinated (*F*-) adsorbents are generally prepared by bonding perfluoro-functionalized silanes to silica gels. They have been employed for a long time essentially as media for solid-phase extraction of *F*-molecules or *F*-tagged molecules in organic chemistry and heterogeneous catalysis. More recently, this approach has been extended to proteomics and metabolomics. Owing to their unique physicochemical properties, namely fluorophilicity and proteinophilicity, and a better understanding of some fundamental aspects of their behavior, new applications of *F*-adsorbents in the field of environmental science and bio-affinity studies can be envisaged. In this article, we revisit the most important features of *F*-adsorbents by focusing, in particular, on some basic information that has been recently obtained through (nonlinear) chromatographic studies. Finally, we try to envisage new applications and possibilities that *F*-adsorbents will allow in the near future.

Keywords HPLC · Perfluoroalkyl acids · Endocrine disruptors · Trace elements · Surfactants · Fluorous

Introduction

Highly fluorinated compounds (*F*-compounds) are characterized by the presence in their structure of a portion in which a substantial number of hydrogen atoms (typically 7 to 20) attached to carbon atoms are replaced with fluorine atoms. This gives the molecules specific properties that are different from those of their parent hydrocarbon analogs. In the terminology of fluorous chemistry a portion or domain of a molecule rich in sp^3 carbon–fluorine bonds is termed a fluorous label or tag (more specifically, if at least six fully fluorinated sp^3 carbons are present, the *F*-portion is referred to as a "ponytail") [1].

F-alkyl chains are bulkier and more rigid than alkyl chains (cross section of around 30 $Å^2$ vs. about 20 $Å^2$ for alkyl chains) and adopt a helical-like structure in place of the typical planar zigzag structure of alkyl chains. The stiffness of *F*-alkyl chains is claimed to be responsible, on the one hand, for their ordered stacking and, on the other, for their slower equilibration and exchange kinetics compared with those of alkyl chains [2–5].

F-alkyl chains are more hydrophobic than alkyl chains of similar length. According to the Hildebrand and Scott solubility scale, for instance, the solubility parameter (that strongly correlates with polarity) for *F*-alkanes is roughly 5 $cal^{1/2}$ $cm^{3/2}$, whereas it is 7 for *n*-alkanes (and 15 for water) [6]. In addition, *F*-alkyl chains possess a lipophobic character (sometimes referred to as oleophobicity [1]) and are less polarizable than the corresponding hydrocarbons, as indicated by their Kamlet–Taft dipolarity/polarizability parameters and by lower refractive indexes than hydrocarbons [7]. These characteristics, together with the strength of the C–F bond and the enhanced electroattracting character of fluorine (that reinforces the C–C backbone), explains the well-known chemical inertness and thermal stability of perfluorocarbons [1].

Perfluorocarbons have recently found important applications in many fields of research, including synthesis, catalyst technology, adsorption/purification processes, materials chemistry, and biomedical applications. Table 1 lists some of the most popular perfluorinated materials for applications in HPLC and fluorous solid-phase extraction (F-SPE).

N. Marchetti · R. Guzzinati · M. Catani · A. Massi · L. Pasti · A. Cavazzini (✉)
Department of Chemical and Pharmaceutical Sciences, University of Ferrara, 44121 Ferrara, Italy
e-mail: cvz@unife.it

R. Guzzinati
Italian National Agency for New Technologies, Energy and Sustainable Economic Development (ENEA), RC Casaccia via Anguillarese, 301, S.M. di Galeria, 00123 Roma, Italy

Table 1 Commercially available perfluorinated stationary phases for both HPLC and F-SPE applications

Brand name	Provider	Bonding phase	Particle size (μm)	Pore size (Å)	End-capped
Fluoro*Flash*	Fluorous Technologies Inc.	C_8F_{17}	5; 40	60	No
FluoroSep-RP Octyl	ES	C_8F_{17}	5	60	N/A
Fluofix	Wako	C_6F_{13}-branched	5	120; 300	No, yes
	Thermo	C_6F_{13}-branched	5	100; 300	Yes
Fluophase RP/WP	Thermo	C_6F_{13}	5	100; 300	Yes
Tridecafluoro	Silicycle	C_6F_{13}	40; 63	60	Yes
FluoroSep-RP Propyl	ES	C_3F_7	5	300	N/A
Fluorochrom	Silicycle	N/A	40; 63	60	No

N/A not available

Perfluorinated (*F*-) adsorbents

F-silica gels and fluorophilicity

F-silica gels have the general structure silica–O–$Si(Me)_2(CH_2)_n$ R_f, where n is either 2 or 3 and R_f is C_6F_{13} or C_8F_{17} [1]. Sometimes, pentafluorophenyl (PFP)-functionalized silica gels have been considered *F*-materials but, strictly speaking, they are not and will not be considered in this review.

Since their first appearance in the early 1980s, *F*-silica gels, thanks to their extreme hydrophobicity and low polarity, were claimed to be ideal candidates as adsorbents for the reversed-phase (RP) separation of large biomolecules under nondenaturating conditions (i.e., with minimum amount of organic modifier in the mobile phase) [8, 9]; however, the field has not been explored in depth and *F*-adsorbents have never actually been considered a real alternative to traditional RP phases, such as octyl- (C_8) or octadecyl-functionalized (C_{18}) silica gels. In contrast, *F*-silica gels have been applied as adsorbents for F-SPE and separation of fluorous molecules from non-fluorous ones and from each other [10, 11]. The unique ability of *F*-molecules to recognize other molecules possessing an *F*-portion is referred to as fluorous affinity or fluorophilicity. It arises from selective, strong noncovalent interactions between the perfluoroalkyl segments of molecules, in a sort of "like dissolves like" interaction.

On the basis of the concept of fluorophilicity, a series of cutting edge applications of *F*-adsorbents have appeared in recent years in the omics sciences [12, 13], food chemistry [14], environmental science [15], amongst others.

Perfluoro-selectivity through liquid chromatography studies

Fluorophilicity is generally quantified by fluorous/organic liquid/liquid partition coefficients [1]. High-performance liquid chromatography (HPLC) offers an alternative approach to evaluate fluorous phase affinity, when a perfluoroalkyl stationary phase is used.

Indeed, the dependence of the logarithm of the chromatographic retention factor (k) upon the number of perfluorocarbon units (n_{CF_2}) in the backbone chain of a perfluoroalkyl homologous series (at fixed mobile phase composition) permits the estimation of the change of Gibbs free energy, ΔG_{CF_2}, for the transfer from the mobile to the stationary phase of a perfluoromethylene group as follows [15–18]:

$$\Delta G_{CF_2} = -RT\frac{d\ln k}{dn_{CF_2}} = -RT\ln \alpha_{CF_2} \quad (1)$$

where α_{CF_2}, R and T, are the selectivity, the universal gas constant, and the absolute temperature, respectively. As an example of this approach, Fig. 1 shows how ln k changes by changing the amount of acetonitrile in the mobile phase for four perfluoroalkyl acids of environmental concern. In the region delineated by green points, ln k decreases quasi-linearly with increasing organic modifier. At each mobile phase composition, the slope of the ln k vs. n_{CF_2} plot gives the natural logarithm of the selectivity (for the sake of clarity, the case of 50 % acetonitrile in the mobile phase is illustrated in Fig. 1). Table 2 reports ΔG_{CF_2} values (calculated by this approach through Eq. 1) as a function of the mobile phase composition for two different stationary phases, a traditional octadecyl and a straight-chain perfluorinated one [17]. Even if the transfer of the CF_2 moiety from the mobile to the stationary phase is thermodynamically favorable on both phases at all mobile phase compositions (its value always being negative), the ability of the *F*-adsorbent to "recognize", and thus to stabilize, this moiety is markedly larger than that of the C_{18} phase. This is demonstrated by absolute values of ΔG_{CF_2}, on average much larger (+70 %) on the *F*-adsorbent than on the C_{18} one.

Another example of the improved selectivity of fluorinated stationary phases over hydrocarbon ones towards the separation of fluorinated solutes is given in Fig. 2, where chromatograms of the separation of benzene and five fluorinated analogues on the two phases are compared [19].

Adsorption of organic compounds from multicomponent mixtures on *F*-adsorbents

The adsorption of organic compounds from multicomponent mixtures on *F*-adsorbents can be measured by several techniques, including HPLC [20, 21]. When the adsorption isotherm is measured through chromatography, the information can be given either as the excess or absolute isotherm. The quantity directly measured in an adsorption experiment is the excess (usually indicated by Γ). It is defined as the excess of solute contained in the adsorption system (considered as a whole) compared to what would be present in a hypothetical system where solute concentration is uniform throughout the whole volume of the eluent and equal to the equilibrium concentration in the bulk phase of the real system [22–24]. On the other hand, the total adsorbed amount (q) is the amount of solute contained in an adsorbed layer of finite thickness. Clearly the definition of the adsorbed layer is arbitrary and needs the adoption of some convention [25, 26]. Figure 3 shows both types of isotherms measured for the adsorption of acetonitrile from water/acetonitrile binary mixtures on a straight-chain perfluorohexylethylsiloxane-bonded stationary phase [27]. Acetonitrile is strongly adsorbed by the *F*-phase with a saturation value of roughly 13 μmol of acetonitrile adsorbed per square meter of solid. The negative excess of acetonitrile at organic-rich mobile phase compositions corresponds to a positive excess of water on the surface. This is due to the adsorption by unreacted silanols, which remain on the silica surface after its functionalization, that, under these conditions, have not been saturated yet [27].

Adsorption isotherm data allow one to estimate several characteristic properties of the system under examination, including solvent fluorophilicity, interfacial tension at the solid/liquid interface, and wetting properties, which all have important implications for technological applications of catalysis, material engineering, environmental science, the fluorotelomer industry, pollution research, etc. as will be further discussed in the "Outlook" section.

Retention mechanisms in liquid chromatography with *F*-stationary phases

A recent study focusing on the chromatographic behavior of silica-based *F*-adsorbents revealed that, under typical RP conditions (with aqueous acetonitrile eluents), the major features described for these phases can be understood and rationalized in terms of traditional liquid–solid chromatographic models based (1) on the formation of a mixed stationary phase and (2) partitioning of solutes between the mobile and this stationary phase [17]. As an example, the so-called U-shape retention behavior of *F*-adsorbents (i.e., the U-shaped dependence of ln k with increasing amount of acetonitrile in the mobile phase, see Fig. 1), which in some cases has been described as a sort of

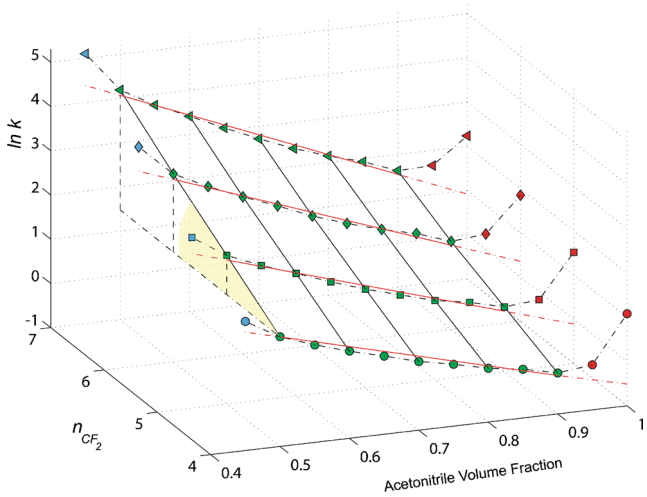

Fig. 1 3D plot showing the dependence of ln k on both the mobile phase composition (expressed as volume fraction of acetonitrile) and number of perfluorocarbon units in the backbone chain, n_{CF_2} . Sample, mixture of four perfluoroalkyl acids (perfluoropentanoic, $n_{CF_2} = 4$, perfluorohexanoic, $n_{CF_2} = 5$, perfluoroheptanoic, $n_{CF_2} = 6$, perfluorooctanoic $n_{CF_2} = 7$). Column, perfluorohexylpropylsiloxane-bonded silica (Fluophase-RP from Thermo Scientific); mobile phase, water/acetonitrile mixtures (+0.1% v/v formic acid); temperature, 298 K. Adapted from ref. [15]

peculiar characteristic of these materials [28], can be explained by considering a mixed-mode retention mechanism in which both fluorophilic (hydrophobic) and silanophilic (hydrophilic) interactions are simultaneously present (exactly as happens with C_{18} silica-based adsorbents) [17].

Although *F*-adsorbents certainly exhibit a different selectivity than traditional RP adsorbents (e.g., C_{18} or C_8), the true peculiarity of *F*-adsorbents is when they are used with *F*-compounds. Fluorophilicity can be thus modulated by careful choice of the eluent composition [15, 17]. With aqueous/acetonitrile mixtures, fluorophilicity can be maximized by maximizing the content of water in the mobile phase (to reduce the competitive adsorption of acetonitrile). It has been demonstrated, however, that to allow the complete wetting [29] of the (meso)porous structure of silica-based *F*-adsorbents, a minimum amount of organic (approx. 5–10 % in volume) is necessary in the eluent [30].

Outlook

In this section, we briefly present our views on the future of *F*-adsorbents by trying to anticipate new solutions and opportunities that, in our opinion, will be offered by these materials in several different fields of research.

The most important area in which we believe *F*-adsorbents will contribute to the advancement of knowledge and technical know-how is environmental chemistry. In particular, we

Table 2 Free-energy change, ΔG_{CF_2}, for the transfer from the mobile to the stationary phase of a CF_2 unit as a function of mobile phase (MP) composition (expressed as acetonitrile volume fraction) on an *F*- and an octadecyl stationary phase. *F*-alkyl, perfluorohexylpropylsiloxane-bonded silica, Fluophase-RP from Thermo Scientific; C_{18}, octadecylethyl-bridged hybrid organic/inorganic, BEH-C_{18} from Waters; temperature, 298 K. Adapted from ref. [17]

MP	*F*-alkyl (J/mol)	C_{18} (J/mol)
0.5	−2,239	−1,399
0.6	−2,008	−1,209
0.7	−1,777	−1,053
0.8	−1,679	−902
0.9	−1,427	−761

are thinking about the numerous classes of perfluoroalkyl and polyfluoroalkyl substances and their several homologues and isomers. Concern about the effects of *F*-compounds on the environment and human health has dramatically increased in recent years as these compounds are toxic, extremely resistant to degradation, bioaccumulate in food chains, and can have long half-lives in humans [31]. In spite of the complexity and variety of these compounds, the interest of the scientific community has focused almost exclusively on perfluoroalkylcarboxylic and perfluoroalkylsulfonic acids. Even though numerous studies have been published in the literature and much information has been gathered about the sources, fate, transport, and toxicity of these species, some fundamental aspects of their physicochemical properties and

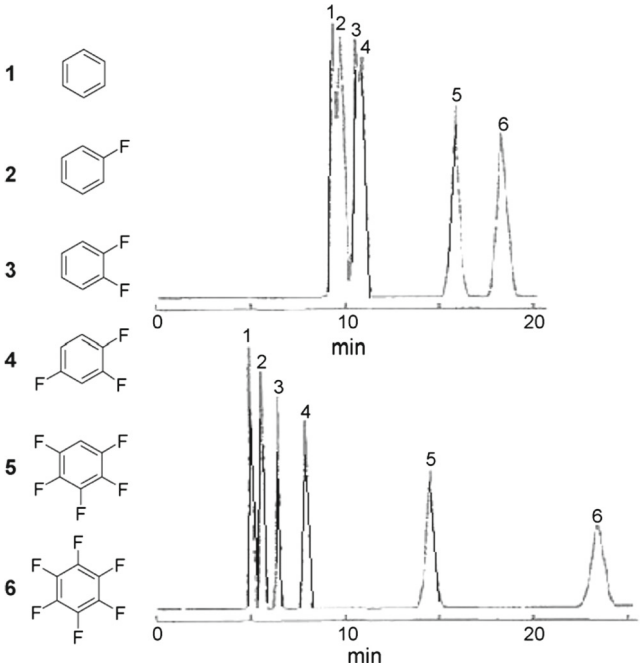

Fig. 2 Chromatographic separation of a mixture of benzene and five different fluorinated analogues on a C_{18} (*top*) and a C_8F_{17} (*bottom*) column. Taken with permission from ref. [19]

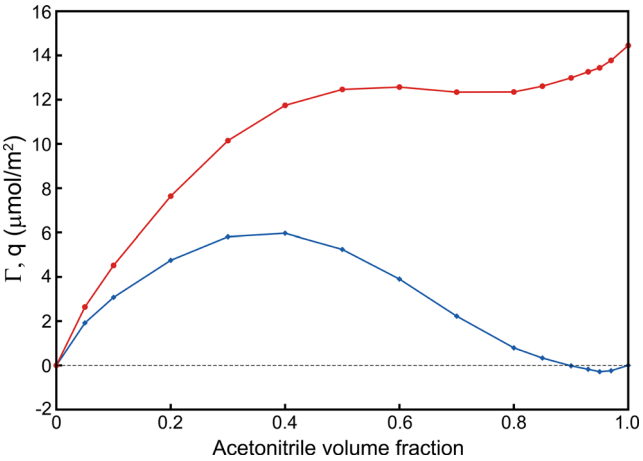

Fig. 3 Excess (*Γ*, *blue line*) and absolute (q, *red line*) adsorption isotherm of acetonitrile from water/acetonitrile binary mixtures on a straight-chain perfluorohexylethylsiloxane-bonded stationary phase. Temperature, 298 K. Adapted from ref. [27]

partitioning behavior are poorly understood and widely debated. As an example, the pK_a value of perfluorooctanoic acid is reported to vary from 0 (i.e., a strong acid) to about 4 (relatively weak acid) [32–34]. Since transport properties in the environment are strictly dependent on the chemical form of molecule (in this case ionic or neutral), and thus on pH, one understands how fundamental research in the field is still needed.

There are also many other *F*-compounds, whose presence in the environment has been recently demonstrated (e.g., perfluoroalkane sulfinic acids and perfluoroalkyl phosphinic and phosphonic acids [35]), for which the scenario is even worse because practically no studies have been performed on them.

Still another example is the class of fluorotelomers and fluorotelomer-based products recently brought into the spotlight [36]. This class includes, among others, many antistaining and antiwetting agents, which are widely employed in everyday life. Nevertheless, systematic studies about their stability and degree of exposure in both humans and the environment not only to them but also to their degradation products are substantially missing.

As is illustrated by these examples, many questions about *F*-compounds are unanswered and others will arise as more is learned about these ubiquitous anthropogenic substances [31]. In the near future, it is reasonable to anticipate that there will be an increasing demand by both the scientific community and control and regulatory agencies for efficient, selective, and easy-to-automate analytical methods and tools for the determination, monitoring, and removal of *F*-compounds in matrixes of different origin (including biological samples). In all these cases, the potential of *F*-adsorbents is evident. Owing to their intrinsic affinity towards *F*-compounds, *F*-adsorbents look like being the perfect counterpart for the separation and capture of these species [15, 29, 30].

Apart from the already demonstrated use in proteomics [12] and metabolomics [13] for the separation of fluorous-tagged molecules, another field where we consider the use of *F*-adsorbents to be potentially very useful is as stationary phases for bioaffinity chromatographic studies. This consideration comes from the evidence that *F*-compounds preferentially bioaccumulate in body compartments high in protein content (this property of *F*-compounds is known as proteinophilicity), such as the liver, kidney, and blood. For instance, it has been demonstrated that human serum albumin (HSA), the most abundant protein in blood plasma, binds through specific high affinity interactions with several *F*-compounds [37–39]. Thus, one might imagine using these adsorbents either directly as supports for binding studies of proteins by means of nonlinear chromatographic techniques [40] or as a sort of pre-fractionation system (possibly in-line) for proteome analysis of low-abundance proteins [41]. Indeed these proteins, whose diagnostic potential is very relevant, are often extremely difficult to detect because of the masking presence of high-abundance serum proteins.

Finally, another field of application where *F*-adsorbents can be useful is heterogeneous catalysis for investigating and designing new recovery strategies of fluorous catalysts and reagents without using fluorous solvents. This is strictly connected to the possibility of studying the affinity of different solvents, including supercritical CO_2, or multicomponent solvent mixtures towards *F*-materials through dynamic (chromatographic) adsorption studies.

Acknowledgments The authors thank the Italian University and Scientific Research Ministry (PRIN 2012ATMNJ_003). NM thanks Laboratory Terra&Acqua Tech, member of the Energy and Environment Cluster, Technopole of Ferrara of Emilia-Romagna High Technology Network.

References

1. Gladysz JA, Curran DP, Horváth IT (eds) (2004) Handbook of fluorous chemistry. Wiley-VCH, Weinheim
2. Barton SW, Goudot A, Bouloussa O, Rondelez F, Lin B, Novak F, Acero A, Rice SA (1992) J Chem Phys 96:1343–1351
3. Kondo Y, Miyazawa H, Sakai H, Yoshino N (2002) J Am Chem Soc 124:6516–6517
4. Kubo K, Moroi Y, Nomura K, Abe Y, Takahahi T (2002) Langmuir 18:8770–8776
5. Riess JG (2001) Chem Rev 101:2797–2920
6. Hildebrand JH, Scott RL (1964) The solubility of nonelectrolytes, 3rd edn. Dover, New York
7. Riddick JA, Bunger W, Sakano TK (1986) Organic solvents: physical properties and methods of purification, 4th edn. Wiley-Interscience, New York
8. Berendsen GE, Pikaart KA, de Galan L, Olleman C (1980) Anal Chem 52:1990–1993
9. Xindu G, Carr PW (1983) J Chromatogr 269:96–102
10. Curran DP, Hadida S, He M (1997) J Org Chem 62:6714–6715
11. Zhang W, Curran DP (2006) Tetrahedron 62:11837–11865
12. Brittain SM, Ficarro SB, Brock A, Peters EC (2005) Nat Biotechnol 23:463–468
13. Go EP, Uritboonthai W, Apo JV, Trauger SA, Nordstrom A, O'Maille G, Brittain SM, Peters EC, Siuzdak G (2007) J Proteome Res 6: 1492–1499
14. Hayama T, Sakaguchi Y, Yoshida H, Itoyama M, Todoroki K, Yamaguchi M, Nohta H (2012) Anal Chem 84:8407–8414
15. Marchetti N, Caciolli L, Laganà A, Gasparrini F, Pasti L, Dondi F, Cavazzini A (2012) Anal Chem 84:7138–7145
16. Bhagwat V, Bereznitski T, Buszewski B, Jaroniec M (1998) J Liq Chrom Rel Technol 21:923–939
17. Cavazzini A, Marchetti N, Guzzinati R, Pasti L, Ciogli A, Gasparrini F, Laganà A (2014) Anal Chem 86:4919–4926
18. Xu Z, Oleschuk RD (2014) J Chromatogr A 1329:61–70
19. Billiet HAH, Schoenmakers PJ, de Galan L (1981) J Chromatogr 218:443–454
20. Guiochon G, Felinger A, Shirazi DG, Katti AM (2006) Fundamentals of preparative and nonlinear chromatography, 2nd edn. Academic Press, Elsevier, New York
21. Bocian S, Vajda P, Felinger A, Buszewski (2009) Anal Chem 81: 6334–6346
22. Defay R, Prigogine I, Bellemans A, Everett DH (1966) Surface tension and adsorption. Longmans, London, Chap II
23. Gibbs JW (1928) The collected works of J. W. Gibbs, vol I. Longmans, Green and Co., New York, Chap III, p 219
24. Everett DH (1964) J Chem Soc Faraday Trans 60:1803–1813
25. Riedo F, Kováts ES (1982) J Chromatogr 239:1–28
26. Yun KS, Zhu C, Parcher JF (1995) Anal Chem 67:613–619
27. Ciogli A, Simone P, Villani C, Gasparrini F, Laganà A, Capitani D, Marchetti N, Pasti L, Massi A, Cavazzini A (2014) Chem Eur J 20:1–12
28. Zhang W (2008) J Fluor Chem 129:910–919
29. Cavazzini A, Marchetti N, Pasti L, Greco R, Dondi F, Laganà A, Ciogli A, Gasparrini F (2013) Anal Chem 85:19–22
30. Cavazzini A, Pasti L, Greco R, Costa V, Solera D, Dondi F, Marchetti N, Laganà A, Gasparrini F (2013) J Chromatogr A 1286:47–54
31. Lindstrom AB, Strynar MJ, Libelo EL (2011) Environ Sci Technol 45:7954–7961
32. Burns DC, Ellis DA, Li H, McMurdo CJ, Webster E (2008) Environ Sci Technol 42:9283–9288
33. Goss KU, Arp HPH (2009) Environ Sci Technol 43:5150–5151
34. Burns DC, Ellis DA, Webster E, McMurdo CJ (2009) Environ Sci Technol 43:5152–5154
35. Kannan K (2011) Environ Chem 8:333–338
36. Washington JW, Naile JE, Jenkins TM, Lynch DG (2014) Environ Sci Technol 48:5762–5769
37. Bischel HN, MacManus-Spencer LA, Luthy RC (2010) Environ Sci Technol 44:5263–5269
38. Bischel HN, MacManus-Spencer LA, Zhang C, Luthy RC (2011) Environ Toxicol Chem 30:2423–2430
39. Salvalaglio M, Muscionico I, Cavallotti C (2010) J Phys Chem B 114:14860–14874
40. Cavazzini A, Pasti L, Dondi F, Finessi M, Costa V, Gasparrini F, Ciogli A, Bedani F (2009) Anal Chem 81:6735–6743
41. Boschetti E, Righetti PG (2013) Low-abundance protein discovery as potential early biomarkers. Elsevier, Amsterdam

UNIVERSITÀ DEGLI STUDI DI FERRARA

Sezioni

Dottorati di ricerca

Il tuo indirizzo e-mail

martina.catani@unife.it

Oggetto:

Dichiarazione di conformità della tesi di Dottorato

Io sottoscritto Dott. (Cognome e Nome)

Catani Martina

Nato a:

Ferrara

Provincia:

Ferrara

Il giorno:

04/05/1989

Avendo frequentato il Dottorato di Ricerca in:

Scienze Chimiche

Ciclo di Dottorato

30

Titolo della tesi:

Mass transfer characteristics and thermodynamic properties of new generation porous particles for ultrafast, high-efficient separations in chiral and achiral liquid chromatography

Titolo della tesi (traduzione):

Studio dei fenomeni di trasferimento di massa e delle proprietà termodinamiche di particelle porose di nuova generazione per separazioni cromatografiche chirali e achirali ultrafast e ad alta efficienza

Tutore: Prof. (Cognome e Nome)

Cavazzini Alberto

Settore Scientifico Disciplinare (S.S.D.)

CHIM/01

Parole chiave della tesi (max 10):

Fenomeni di trasferimento di massa, isoterme d'adsorbimento, separazioni ultrafast, cromatografia liquida Mass transfer phenomena, adsorption isotherms, ultrafast separations, liquid chromatography

Consapevole, dichiara

CONSAPEVOLE: (1) del fatto che in caso di dichiarazioni mendaci, oltre alle sanzioni previste dal codice penale e dalle Leggi speciali per l'ipotesi di falsità in atti ed uso di atti falsi, decade fin dall'inizio e senza necessità di alcuna formalità dai benefici conseguenti al provvedimento emanato sulla base di tali dichiarazioni; (2) dell'obbligo per l'Università di provvedere al deposito di legge delle tesi di dottorato al fine di assicurarne la conservazione e la consultabilità da parte di terzi; (3) della procedura adottata dall'Università di Ferrara ove si richiede che la tesi sia consegnata dal dottorando in 2 copie di cui una in formato cartaceo e una in formato pdf non modificabile su idonei supporti (CD-ROM, DVD) secondo le istruzioni pubblicate sul sito: http://www.unife.it/studenti/dottorato alla voce ESAME FINALE – disposizioni e modulistica; (4) del fatto che l'Università, sulla base dei dati forniti, archivierà e renderà consultabile in rete il testo completo della tesi di dottorato di cui alla presente dichiarazione attraverso l'Archivio istituzionale ad accesso aperto "EPRINTS.unife.it" oltre che attraverso i Cataloghi delle Biblioteche Nazionali Centrali di Roma e Firenze; DICHIARO SOTTO LA MIA RESPONSABILITA': (1) che la copia della tesi depositata presso l'Università di Ferrara in formato cartaceo è del tutto identica a quella presentata in formato elettronico (CD-ROM, DVD), a quelle da inviare ai Commissari di esame finale e alla copia che produrrò in seduta d'esame finale. Di conseguenza va esclusa qualsiasi responsabilità dell'Ateneo stesso per quanto riguarda eventuali errori, imprecisioni o omissioni nei contenuti della tesi; (2) di prendere atto che la tesi in formato cartaceo è l'unica alla quale farà riferimento l'Università per rilasciare, a mia richiesta, la dichiarazione di conformità di eventuali copie; (3) che il contenuto e l'organizzazione della tesi è opera originale da me realizzata e non compromette in alcun modo i diritti di terzi, ivi compresi quelli relativi alla sicurezza dei dati personali; che pertanto l'Università è in ogni caso esente da responsabilità di qualsivoglia natura civile, amministrativa o penale e sarà da me tenuta indenne da qualsiasi richiesta o rivendicazione da parte di terzi; (4) che la tesi di dottorato non è il risultato di attività rientranti nella normativa sulla proprietà industriale, non è stata prodotta nell'ambito di progetti finanziati da soggetti pubblici o privati con vincoli alla divulgazione dei risultati, non è oggetto di eventuali registrazioni di tipo brevettale o di tutela. PER ACCETTAZIONE DI QUANTO SOPRA RIPORTATO

Firma del dottorando

Ferrara, li 02/02/2018 (data) Firma del Dottorando Martina Catani

Firma del Tutore

Visto: Il Tutore Si approva Firma del Tutore Alberto Cavazzini